Multifaceted Roles for the Developmental Zinc Finger Protein, POGZ, in Genomic Stability, Breast Cancer Growth and Metastasis

John Heath
Division of Experimental Medicine

McGill University

Montreal, Quebec, Canada

2022

A Thesis submitted to McGill University in partial fulfillment of the requirements of the degree of Doctor of Philosophy.

Abstract

The neurodevelopmental-associated zinc finger protein POGZ was first described in its role in the maintenance of mitotic chromosomes and chromosomal stability. Mutations in POGZ are notably associated with the onset of autism-like or intellectual disabilities through dysregulation of gene transcription and genome maintenance. Many proteins necessary for development and genome stability are often aberrantly expressed or dysregulated in cancer, however, it is unknown if POGZ possesses any cancer-associated functions. Thus, we investigated the molecular functions of this protein in genomic integrity and examined its putative role in the growth and progression of breast cancer. We have identified a novel function for POGZ, in the repair of DNA double-stranded breaks (DSBs) by the homologous recombination (HR) pathway, which may be independent of its previously described role in regulating gene expression. Specifically, we have shown POGZ, through its interaction with the heterochromatin protein HP1, promotes the recruitment of the BRCA1/BARD1 complex to sites of DNA damage, a critical step in the subsequent resolution of DSBs by HR. Developing and utilizing an in vivo mouse model of constitutive POGZ loss, we have shown that haploinsufficient POGZ levels result in radio-sensitivity, the spontaneous generation of DSBs in a multiple tissues and compromised antibody diversification. Furthermore, with the importance of POGZ in controlling gene expression and DNA repair, we predicted that deregulated expression of this protein may further contribute to cancer development. To test the functional significance of POGZ in the pathobiology of breast cancer (BC), we generated POGZ-deficient (4T1-sg*Pogz)* and POGZ-overexpressing (4T1-sc*Pogz*) basal-like mammary carcinoma systems and monitored impacts on cellular and tumor growth. While overexpression of POGZ was dispensable for cell and tumor growth, loss of POGZ results in impaired cell proliferation and yielded a dramatic loss of tumor growth in vivo. Transcriptionally, an aberrant TGF-b signaling signature was observed in 4T1-sg*Pogz* cells, in vitro, and an upregulated epithelial-mesenchymal transition signature, *in vivo*. Surprisingly, loss of POGZ, despite a primary growth defect, elicited an increased metastatic burden, while overexpression of POGZ completely abrogated pulmonary

metastases. Basally, 4T1-sg*Pogz* cells possessed higher expression of TGFBR2, accompanied by increased levels of phosphorylated SMAD2/3. Furthermore, 4T1-sg*Pogz* cells display significantly higher migratory activity, which can be inhibited through genetic and pharmacological inhibition of TGFBR1/2. We have established a novel role for the neurodevelopmental protein, POGZ, in homologous recombination and the growth and progression of basal-like breast cancer. However, when exploring metastatic potential, despite overt growth defects, we uncovered additional roles for POGZ in suppressing metastasis, exemplifying how certain regulatory proteins impact multiple steps of breast cancer pathology. Overall, we have provided a foundation of data supporting POGZ in the regulation of DNA repair and provided novel insight into its regulation of TGF-b signaling and impacts on cancer growth and metastasis.

Resume

La protéine à doigt de zinc associée au développement neurologique POGZ a été décrite pour la première fois dans son rôle dans le maintien des chromosomes mitotiques et la stabilité chromosomique. Les mutations de POGZ sont notamment associées à l'apparition de déficiences autistiques ou intellectuelles par dérégulation de la transcription des gènes et de la maintenance du génome. De nombreuses protéines nécessaires au développement et à la stabilité du génome sont souvent exprimées de manière aberrante ou dérégulées dans le cancer, cependant, on ne sait pas si POGZ possède des fonctions associées au cancer. Ainsi, nous avons étudié les fonctions moléculaires de cette protéine dans l'intégrité génomique et examiné son rôle putatif dans la croissance et la progression du cancer du sein. Nous avons identifié une nouvelle fonction pour POGZ, dans la réparation des cassures double brin (DSB) de l'ADN par la voie de la recombinaison homologue (RH), qui peut être indépendante de son rôle précédemment décrit dans la régulation de l'expression génique. Plus précisément, nous avons montré que POGZ, par son interaction avec la protéine hétérochromatine, HP1, favorise le recrutement du complexe BRCA1/BARD1 sur les sites de dommages à l'ADN, une étape critique dans la résolution ultérieure des DSB par HR. En développant et en utilisant un modèle murin in vivo de perte constitutive de POGZ, nous avons montré que des niveaux de POGZ haplo-insuffisant entraînent une radiosensibilité, la génération spontanée de DSB de manière multi-tissulaire et une diversification des anticorps compromise. De plus, compte tenu de l'importance de POGZ dans le contrôle de l'expression des gènes et la réparation de l'ADN, nous avons prédit que l'expression dérégulée de cette protéine pourrait contribuer davantage au développement du cancer. Pour tester l'importance fonctionnelle de POGZ dans la pathologie de la BC nous avons généré un système de carcinome mammaire de type basal déficient (4T1-sg*Pogz*) en POGZ et sur exprimant POGZ (4T1) et surveiller les impacts sur la croissance cellulaire et tumorale. Alors que la surexpression de POGZ était dispensable pour la croissance cellulaire et tumorale, la perte de POGZ entraîne une altération de la prolifération cellulaire et a entraîné une perte spectaculaire de croissance tumorale, in vivo. Sur le plan transcriptionnel, une signature de signalisation aberrante du TGF-b a été observée dans les cellules 4T1 déficientes en POGZ, in vitro, et une signature de transition

épithéliale-mésenchymateuse régulée positivement, in vivo. Étonnamment, la perte de POGZ, malgré un défaut de croissance primaire, a provoqué une charge métastatique accrue, tandis que la surexpression de POGZ a complètement abrogé les métastases pulmonaires. Essentiellement, les cellules POGZ-KO 4T1 possédaient une expression plus élevée de TGFBR2, accompagnée d'une augmentation de SMAD2/3 phosphorylé. De plus, les cellules POGZ-KO présentent une activité migratoire significativement plus élevée, qui peut être inhibée par l'inhibition génétique et pharmacologique de TGFBR1/2. Nous avons établi un nouveau rôle pour la protéine neuro-développementale, POGZ, dans la recombinaison homologue et la croissance et la progression du cancer du sein de type basal. Cependant, lors de l'exploration du potentiel métastatique, malgré des défauts de croissance manifestes, nous avons découvert des rôles supplémentaires pour POGZ dans la suppression des métastases, illustrant l'impact de certaines protéines régulatrices sur plusieurs étapes de la pathologie du cancer du sein. Dans l'ensemble, nous avons fourni une base de données soutenant POGZ dans la régulation de la réparation de l'ADN et fourni un nouvel aperçu de sa régulation de la signalisation TGF et de ses impacts sur la croissance du cancer et les métastases.

Acknowledgements

I want to express the highest gratitude to Dr. Josie Ursini-Siegel for giving me absolutely unconditional kindness and acceptance throughout the years. She has continuously and whole-heartedly believed in me and has supported me in every endeavor.

I would like to thank Dr. Alex Orthwein for his leadership over the years. I will walk away from this Ph.D. with a much larger appreciation for scientific rigor.

I am grateful for the feedback on my project(s) from members of my advisory committee, Michael Witcher, Frederick Mallette, and Jorg Fritz. I am indebted to the wonderful collaboration with Dr. Claudia Kleinman, who, with Steven Hebert, helped move this project forward. I am indebted to the members of the LDI Animal Quarters and the Flow Cytometry facility, as they have provided support and assistance throughout the years.

I would like to thank my personal friends, Haley Kenny, Kelly Leblanc, Maria DiCarlo, for the support from far away for all these years. I'll be back out East eventually!

I would like to thank all of the members of both Ursini-Siegel and Orthwein labs, past and present for all the help and advice. I would like to thank Stephanie Totten and Angela Ahn for their seemingly unlimited patience while teaching me over the years. Lastly, I would like to thank Steven Findlay for the mutual support throughout the years. We finally made it.

Original Contributions to Knowledge

1. POGZ is required for template dependant DNA repair (HR/SSA)

2. POGZ deficiency results in lack of recruitment of HP1-γ and subsequent BRCA1/BARD1 complex to sites of damage.

3. Heterozygous loss of POGZ results in a growth defects, abnormal behavioural, and aberrant DSBs in multiple tissues.

4. *Pogz*$^{+/-}$ B cells possess reduced proficiency to undergo successful class switch recombination

5. Loss of POGZ in murine basal breast cancer inhibits primary tumor growth, however, enhances cellular migration

6. POGZ overexpression protects against experimental pulmonary metastasis *in vivo*

7. POGZ downregulates TGFBR2 and decreases TGF-b signalling, a critical signalling cascade in breast tumor progression

Contributions of the Authors

Chapter 1: Introduction

JH wrote the complete chapter under the guidance and editorial supervision of AO and JUS.

Chapter 2: POGZ promotes homology-directed DNA repair in an HP1-dependent manner

Chapter 2 was published as an original research article. JH designed, performed most of the experiments presented in this manuscript and analyzed the data. ESC, HB, and DG performed the MS experiments and analyzed the data under the supervision of JFC. SF performed the quantification of DNA damage in *ex vivo* stimulated B-cells. VML completed the ELISA for the different serum isotypes. EPC performed the phospho-blots analysis on POGZ-depleted cells. JL and XC performed the mouse perfusion, isolation of the murine brain, and prepared sections of brain. BD and TM performed laser micro-irradiation immunofluorescence experiments and AM designed the experiments and analyzed the data. BL performed micrococcal nuclease studies and MW designed the experiments and analyzed the data. MK optimized and performed initial GFP-reporter experiments. AO conceived the study, designed the research, provided supervision with JUS and wrote the manuscript with input from all the other authors.

Chapter 3: The developmental protein POGZ suppresses TGF-b mediated metastasis in Triple Negative Breast Cancer

Chapter 3 contains material to be included in a manuscript in preparation for publication as an original research article. Conception and design of this work by AO, JUS, and JH was based on the published work of JH and SF. Most of the experiments in this study were designed, executed and analyzed by JH under the guidance of my supervisors AO and JUS. The composition of this manuscript and the design of the experimental figures were accomplished with the supervision of JUS. VS provided animals for the *in vivo* studies. Mammary fat pad injections and surgical resections were assisted by ST. Immunohistochemistry of breast tumor samples were assisted by VS. Biostatistics and computational analysis of bioinformatics data was performed by SH and CLK.

Chapter 4: Discussion
JH wrote the complete chapter under the guidance and editorial supervision of AO and JUS.

Publications that include work performed by John Heath, but not included in this dissertation:

Dahabieh MS, Huang F, Goncalves C, Flores González RE, Prabhu S, Bolt A, Di Pietro E, Khoury E, **Heath J**, Xu ZY, Rémy-Sarrazin J, Mann KK, Orthwein A, Boisvert FM, Braverman N, Miller WH, Del Rincón SV. (2021) Silencing PEX26 as an unconventional mode to kill drug-resistant cancer cells and forestall drug resistance. *Autophagy*

Bazinet A, **Heath J,** Chong AS, Simo-Cheyou ER, Worme S, Rivera Polo B, Foulkes WD, Caplan S, Johnson NA, Orthwein A, Mercier FE (2021) Common clonal origin of chronic myelomonocytic leukemia and B-cell acute lymphoblastic leukemia in a patient with a germline *CHEK2* variant. *Cold Spring Harb Mol Case Stud*

Findlay S (co-author), **Heath J (co-author)**, Luo V, Malina A, Morin T, Coulombe C, Djerir B, Li Z, Samiei A, Simo-Cheyou E, Karam M, Bagci H, Rahat D, Grapton D, Lavoie EG, Dove C, Khaled H, Kuasne H, Mann KK, Klein KO, Greenwood CM, Tabach Y, Park M, Côté JF, Masson JY, Maréchal A, Orthwein A. (2018) SHLD2/FAM35A co-operates with REV7 to coordinate DNA double-strand break repair pathway choice. *EMBO J.*

Table of Contents

List of Figures

Abbreviations

Term	Abbreviation
53BP1	TP53 binding protein 1
ACVR	activin a receptor
ANKRD	ankyrin repeat domain
APC	anaphase-promoting complex
ATM	ataxia telangiectasia mutated
ATR	ataxia telangiectasia related
BARD1	BRCA1 Associated RING Domain 1
BCL	B cell lymphoma
BER	base excision repair
BIR	break-induced repair
BMPR	bone morphogenetic protein
BRCA1	Breast cancer type 1 susceptibility protein
CAF1	chromatin assembly factor 1
CDC	cell division cycle
CDK	cyclin-dependant kinase
CENP	centromere protein
CHK	checkpoint kinase
CRISPR	clustered regularly interspaced short palindromic repeats
DNA-PK	DNA-dependant protein kinase
DSB	double stranded DNA break
ECM	extracellular matrix
EMT	epithelial to mesenchymal transition
ER	estrogen receptor
FEN1	flap-structure specific endonuclease 1
FHA	forkhead-associated
GADD	growth arrest and DNA damage
H2AX	H2A.X Variant Histone
HDGFRP2	hepatoma-derived growth factor-related protein 2
HER2	human epidermal growth factor receptor 2
HMT	histone methyltransferase
HP1	heterochromatin protein 1
HR	homologous recombination
hTERT	human telomerase reverse transcriptase
JAG	jagged
KRAB	Kruppel associated box
LAP	latency associated protein
LINE	long interspersed nuclear elements

MAD2L2/REV7	Mitotic Arrest Deficient 2 Like 2
MCM	Mini-chromosome maintenance
MET	mesenchymal to epithelial transition
MH	Mad homology
MMP	matrix metalloproteases
MMTV	mouse mammary tumor virus
MRN	Mre11-RAD52-NBS1
mTOR	mammalian target of rapamycin
NER	nucleotide excision repair
NHEJ	non-homologous end-joining
PALB	Partner and localizer of BRCA2
PAR	poly-(ADP) ribose- polymerase
PARP	poly-(ADP) ribose- polymerase
PI3K	phosphoinositide 3-kinase
POGZ	Pogo transposable element derived with ZNF domain protein
PR	progesterone receptor
RAD51	recombinase protein 51
RIF1	Replication time factor 1
RNF	ring finger
RPA	replication associated protein A
RUNX	Runt-related transcription factor
SBE	Smad binding element
SHLD	Shieldin
SINE	short interspersed nuclear elements
SMAD	Mothers Against Decapentaplegic homologue
SSA	single-stranded annealing
SSB	single stranded DNA break
SUV	suppressor of variegation
TGF	transforming growth factor
TGFBR	transforming growth factor receptor
TLDU	terminal duct lobular units
TNBC	triple negative breast cancer
TRIM	tripartite motif-containing
TSC	tuberous sclerosis protein
UV	ultraviolet
WHSUS	White Sutton syndrome
WRN	Werner syndrome protein
XRCC	X-ray cross complementary

Chapter 1: Introduction

1.1. DNA damage and repair

Cells are continuously exposed to sources of DNA damage, which compromise genomic stability. Persistent genetic instability is linked to immunodeficiency syndromes, neurological disorders, premature aging, developmental abnormalities, infertility and cancer. DNA damage is generated due to a wide variety of endogenous and exogenous sources. Endogenous sources such as replication stress and reactive oxygen species often lead to single stranded DNA breaks (SSB). However, with only a single damaged DNA strand, these insults are efficiently repaired in a competent cell via an array of repair pathways, including base excision repair (BER) and nucleotide excision repair (NER). Exogenous sources, such as irradiation or UV damage, often lead to the formation of double stranded DNA breaks (DSB). DSBs, being the most lethal, are cytotoxic DNA lesions that, if left unrepaired, lead to major genomic rearrangements and cell death. Therefore, cells have evolved complex molecular signaling pathways to avoid such outcomes and orchestrate DNA repair. Regulation of DSB repair is multi-layered, composed of systematic processing of DNA physically, through topological and epigenetic alterations, and the initiation of larger cellular changes, such as altered gene transcription and activation of cell cycle arrest.

DSB repair is a deeply complex, multi-faceted, and step-wise process, as exemplified in Figure 1-1. First, the DSB is recognized by sensor proteins, which then recruit and stabilize key signal transducing kinases. Secondly, these kinases recruit and activate signal amplifying enzymes which work to generate chromatin modifications, adaptor protein recruitment sites, and complex formation surrounding the DSB. Following the signalling of the DSB, the recruitment of dedicated effector proteins and subsequent repair machinery resolve the DSB. While these proteins work in tandem to locally repair DNA, following the detection of a DSB, another signalling cascade concomitantly initiates cellular responses that promote cell cycle arrest. Activation of these cell cycle

checkpoints provides essential and resources to ensure effective DNA repair. Each of these steps, and their regulation, with particular attention to the HR pathway, will be discussed further.

1.1.1. Detection and signalling of DSBs

Molecular recognition of DNA damage is largely characterized by sensor proteins, the MRN (Mre11-Rad50-Nbs1) complex for DSBs[1–3]. The MRN complex is composed of mitotic recombination 11 homolog 1 (MRE11), ATP-binding cassette (ABC)-ATPase (RAD50), and Nijmegen breakage syndrome protein 1 (NBS1). The MRN complex serves as the first enzyme that reaches the DSB and facilitates the initiation of the DNA damage response[1]. DNA damage surveillance proteins are often stress kinases that get activated during DSB responses to not only trigger the signalling responsible for the local modifications and initial stages of DSB repair but also signalling cascades responsible for cell cycle checkpoint activation or apoptosis[3]. Serine-threonine kinases belonging to the class IV phosphoinositide 3-kinase (PI3K) family, including ataxia telangiectasia mutated (ATM), ataxia telangiectasia related (ATR), and the DNA-dependent protein kinase catalytic subunit (DNA-PKcs), are induced by genotoxic stress to initiate DNA repair[4,5]. DSBs can also be recognized by the Ku proteins, which is a heterodimer of Ku70/80[6]. These proteins are bound together in a ring conformation which can bind non-covalently to the end of an open DSB. The two sides of the protein structure are for protection of the DSB and also act as a scaffold for signal transducer kinases, specifically DNA-PK, and subsequent DNA repair enzymes[4].

After the MRN complex is recruited to the site of damage, ATM binds the MRN complex and auto-phosphorylate itself to initiate its kinase activity. Importantly, it also phosphorylates histone H2AX at Ser139 (gamma (γ)-H2AX), representing a surrogate marker of DSBs that serves as a focal point for DSB repair[7]. Abundant nuclear concentrations of another kinase, casein kinase 2 (CK2), will trigger phosphorylation of another key protein involved in DSB signal amplification, mediator of DNA damage checkpoint protein 1 (MDC1)[8]. The MRN complex binds MDC1 through its forkhead-

associated (FHA) domain and stabilizes ATM through its ankyrin repeat domain (ANKRD)[9]. MDC1 also directly binds γH2AX, increasing the local concentration of ATM. This triggers further H2AX phosphorylation and MDC1 recruitment, thus amplifying and spreading the γH2AX modification, forming a focal region[10].

After DSBs are detected by the MRN complex, γH2AX spreading occurs through concordant interactions between activated ATM and MDC1. Phosphorylated MDC1 also serves as a binding site for the E3-ubiquitin ligase ring finger protein 8 (RNF8), which serves to poly-ubiquitinate H1 on Lys63, which triggers binding of ring finger protein 168 and mono-ubiquitination of histone H2A and Lys13-15[11–14]. These K13/15 mono-ubiquitin residues do not canonically serve as signals for the proteasome, but in fact, serve as docking sites for the receptor associated protein 80 (RAP80)-BRCA1 complex (BRCA1-A complex). While K63 chains do not serve as a direct binding site for 53BP1, histones proximal to DSBs possessing these modifications, expose a di-methylated H4K20 tail to which 53BP1 directly binds[15–17]. It is at this point, on the level of mutual antagonism between BRCA1 and 53BP1, and the protection of DNA ends, that a pathway decision emerges.

Additional DNA damage sensors include the poly-ADP-ribose (PAR) polymerases (PARPs), which catalyze the post-translational, covalent attachment of poly-ADP-ribose (PAR) to target proteins, a process called PAR-ylation. These PAR branches represent an accumulation of ribose sugar residues and, much like ubiquitin chains, serve as binding sites for other proteins to potentiate signal amplification. PARP1, and subsequent PAR-ylation, rapidly accumulates at both SSB and DSB within seconds of damage, however, its function is largely presumed to inhibit DNA end resection and promote NHEJ. However, in certain cell cycle contexts, PARP1 can compete with and even remove Ku70/80 from binding DSB ends[18–21]. In other contexts, PARP1 has been shown to influence other DNA repair pathways such as base excision repair, a SSB repair pathway that prevents toxic DSB accumulation[22].

1.1.2. Effector Pathways of DNA Repair

The canonical DSB response consists of 2 major pathways: homologous recombination (HR) and non-homologous end-joining (NHEJ). An important distinction between these pathways is the rate of error prone repair. HR is a template-mediated or "faithful" repair response, which is largely mediated by the BRCA1/CtIP signaling pathway and yields very low frequency of errors in repaired DNA. NHEJ-mediated repair of a DSB involves the direct ligation of strands and therefore lacks the requirement for a homologous template. While the NHEJ process allows for faster DSB resolution, it may often result in small sequence changes near the DSB site, leading to an error-prone repair in comparison to HR.[23,24]

1.1.3. Non-homologous End Joining (NHEJ)

The first defining events of NHEJ is the recognition of DSB ends by Ku70/80, which stabilize and protect the DSB ends to inhibit long range resection by the MRN complex[18]. DNA-PKcs binds Ku70/80, creating the holoenzyme DNA-PK. This triggers its kinase activity and the phosphorylation of the canonical Ser139 of H2AX, as well as key substrates such as the Ku proteins, end processing enzymes, ligases, and the DNA-PK complex itself[25]. While DNA ends largely cannot be ligated directly, there is a minor level of nucleolytic processing that is required prior to repair. Nucleases such as Artemis and the Werner syndrome protein (WRN), target any ssDNA overhangs which may form during Ku formation and stabilization[26–30]. However, it has been shown that within the MRN complex, Mre11 can perform extremely limited end resection or end processing (as few as 20 bp) that can contribute to NHEJ[31,32]. Once DSB ends are processed and stabilized, the X-ray cross complementary 4 (XRCC4) – DNA ligase IV (LIG4)- is loaded onto the Ku complex to facilitate end joining and ligation[33,34].

Through elegant exploration of the functional domains of both 53BP1 and BRCA1, the complicated regulation of resection of the DNA strands containing a DSB largely impacts the stability and affinity of DNA repair complexes at sites of damage. It is this length of

resection that influences which DNA repair machinery becomes stabilized at sites of damage. Short, prompt, limited resection favor NHEJ, therefore, proteins that inhibit extensive resection are required during cell phases when a homologous template is not available. 53BP1 can engage with DSB ends and limit the duration and length of resection of one of the complementary strands of DNA composing the DSB[14,35,36]. Replication time factor 1 (RIF1) interacts with 53BP1, through ATM-mediated phosphorylation of 53BP1, further blocking and antagonizing any 5' resection that may occur via the exonuclease activity of the BRCA1 interactor, CtBP-interacting protein (CtIP)[35–38]. 53BP1-RIF1 will then engage with REV7 in G1 cell cycle phases, which further antagonizes end resection by inhibiting the accumulation of BRCA1-CtIP at sites of damage[39,40]. It was recently identified by our group and other research studies that REV7 repressed HR in G1 by interacting with the shieldin complex (SHLD1/2/3) and further inhibiting end resection and by binding ssDNA, preventing exonuclease activity and RPA accumulation[41–47].

1.1.4. Homologous Recombination (HR)

In cells undergoing S/G2 phases, minor 5' DNA strand resection of the DSB is performed very early by MRE11 in the MRN complex[2]. This serves as the initial detection of the DSB by the host cell. S-phase cell cycle kinases phosphorylate the exonuclease, CtIP, reinforcing its interaction with BRCA1 and its binding partner BARD1, and their recruitment to the DSB[48,49]. The BRCA1/BARD1 can directly bind proximal nucleosomes (illustrated in Figure 1-1), through BARD1 mediated recognition and interaction with the unmethylated histone residue H4K20. This stabilizes CtIP in this location and in concert with the MRN complex, CtIP facilitates further resection of the 5' DNA strand of the DSB, exposing a long single strand of DNA (ssDNA). The exposed ssDNA is rapidly coated in replication associated protein A (RPA), which predominantly signals SSB through the activation of the sensor kinase, ATR[50–52]. In the context of HR, in local pockets surrounding the DSB, activated ATR phosphorylates PALB2, a DNA binding protein that forms a complex with BRCA2 and BRCA1[53]. Following the stabilization of BRCA1 at sites of damage, PALB2-BRCA2 complexes are recruited to sites of damage and interact with BRCA1 through the coiled-coil domain of PALB2[54,55]. BRCA2, through its 8 BRC repeats, can effectively remove and replace RPA on ssDNA with helical filaments composed of

the recombinase protein, RAD51[54,56]. This filament coated ssDNA is a nucleoprotein complex and is used in the process known as strand invasion and is critical for successful HR. Strand invasion involves the search for a complementary template that can be used for DNA synthesis. The search ends when either the sister chromatid or homologous chromosome interacts with the RAD51-ssDNA structure and forms a displacement loop (D-loop)[56–58]. This "nascent" D-loop composed of the homologous strand separated by the invaded strand serves as the DNA synthesis platform for functional HR.

While D loop formation is necessary for HR, homologous regions (i.e. repeat regions) can anneal and are often formed during other repair processes such as alternative end-joining (alt-EJ) or single-stranded annealing (SSA)[59,60]. In these processes, microhomologies on the 3' resected end bind regions of high similarity on the complementary strand (i.e. independent of a homologous chromosome)[61]. This process creates two 3' overhang flaps on either side of the , which eventually are trimmed by flap-structure specific endonuclease 1 (FEN1) and ligated[62–67]. These processes, while absolutely template dependent, are still considered error-prone due to this minor flap nucleotide deletions. The integrity of HR is further dependent on the error rate of the DNA polymerases responsible for catalyzing the complementary strand synthesis. DNA synthesis during HR is primarily controlled by DNA polymerase delta (Polδ), despite its primary function in lagging strand synthesis during S-phase DNA replication[68,69]. However, roles for DNA polymerase α and ε have been shown in studies of D-loop structures and stability in S. cerevisiae[70]. On a regulatory level, different subfamilies of DNA polymerases can be recruited, each having differences in both, processivity and D-loop resolution. Furthermore, another level of regulation of HR via D loop structure is that multiple modes of DNA synthesis can occur: first-end synthesis; second end synthesis; synthesis dependent strand-annealing (which is distinct from SSA); and break-induced repair (BIR). Many more mechanisms exist that dictate which polymerases get recruited and topological changes that must occur for successful synthesis[71]. While, HR arising from DNA synthesis can result in minor mutations[68], large-scale genomic rearrangements are protected against.

1.2. Cell cycle regulation

In most multicellular organisms, focusing on mammalian examples, the cell cycle has 2 major events, genome duplication and cellular division.[72] Complete replication of cellular DNA takes part in the synthesis phase (S phase), while condensation, organization, and separation of sister chromatids and the larger fission result of two daughter cells defines mitosis (M phase).[73] Given the large energy expenditures throughout M and S phase, these phases are separated by two growth phases (G1, G2, respectively), allowing time for nutrient storage and preparation for the next phase.[74,75] Non-proliferative cells reside in a G0 cell cycle phase and can be classified as reversible (quiescent) or irreversible (senescent, or differentiated (post-mitotic)).[73,76]

While many different proteins and transcriptional networks exist to coordinate efficient and successful cell division, the main mediators of cell cycle progression are the cyclin-dependent kinases (CDKs) and their cognate binding partners, cyclins (as exemplified in Figure 1-2). When CDKs interact and form a complex with respective cyclins, they create a holoenzyme, thereby activating the kinase domain of the respective CDK. These complexes are composed of: CDK1 and its partner cyclins A/B; CDK2 with cyclins A/E; and CDK4/6 with cyclin D isoforms. These enzymes are responsible for the multiple events required for cell cycle progression: (i) activation of specific transcription factors, like the E2 transcription factor (E2F) family[77]; (ii) directing ubiquitin ligases to complexes that may block progression, like the degradation of cyclin B[78]; (iii) activating or inactivating other kinases, like a cell cycle regulated phospho-switch. The CDK4/6: Cyclin D complex is engaged during G1 phase with a primary substrate being the tumor suppressor retinoblastoma (Rb)[79,80]. When unphosphorylated, Rb sustains a G1 phase by inhibiting E2F-family transcription targets required for S phase progression. S phase cyclin-CDK complexes specifically interact with and phosphorylate the pre-replication complexes (origin replication complex, MCM2-7, CDT1, CDC6) that coat the genome prior to the initiation of S phase[81]. Finally, M phase CDK-cyclin complexes are responsible for the

promotion of chromatin condensation and facilitate the binding of the anaphase promoting complex (APC) to CDC20 during mitosis[82].

1.2.1 DNA damage associated cell cycle checkpoints

As frequently as a somatic cell divides, each division requires tight regulation to ensure that necessary events occur and to decrease the risk of genomic errors and potential insults. Traditional cellular checkpoints, highlighted in Figure 1-2, exist at the cell cycle transitions between G1/S phases, where repair occurs prior to DNA synthesis, and at G2/M phases, where proper chromosomal duplication is assessed prior to mitosis. Evaluation and repair of DNA damage at these checkpoints reduce transmission of DNA damage during cell division, limiting genomic instability. These checkpoints allow sufficient time for the cell to evaluate damage, initiate repair activate death-associated pathways (apoptosis), or undergo senescence. NHEJ is active in all cell cycle phases, despite its suppression in G2/M, however, the G1/S checkpoint serves as an integral point for NHEJ to repair any DSBs acquired during interphase[83–85]. The activation of DNA damage-induced G2/M cell cycle arrest can correspond to multiple situations: DNA damage that was acquired through S/G2; any unrepaired DNA damage that persisted through a G1 checkpoint[86]; or in cancer cells that lack a functional p53 signalling cascade[87,88]. The G2/M checkpoint is intimately associated with DSB repair through the HR pathway, as this arrest takes place when the genome is duplicated and a homologous template is readily available.

This association between template independent or dependent repair and the activation of a cell cycle checkpoint highlights a concerted co-regulation of cell cycle dynamics and DSB repair. It is through the initiation of the same DSB signalling cascades that cell cycle checkpoints are mounted through regulation of the cyclin-CDK network. Activation of ATM/ATR directly initiates the DSB repair response, but it will also initiate a cell cycle arrest signaling cascade by phosphorylation of key substrates, the checkpoint kinases 1 and 2 (Chk1/Chk2)[89,90]. Chk1/Chk2 possess many substrates, like E2F transcription factors and BRCA1, however, the most notable in DNA repair and cell cycle regulation is

the tumor suppressor p53[91]. Activated p53 will homodimerize, forming tetramers, exposing DNA binding domains that will trigger transcription of downstream target genes, such as the CDK inhibitor, p21[91].

During the G1 phase, the main driving force behind progression to S phase is the activation of the E2F family transcription factors, which are largely repressed by activated Rb. As mentioned previously, CDK4/6-cyclin D and CDK2-Cyclin E complexes inactivate Rb by hyper-phosphorylation[92,93]. The CDK inhibitor, p21, can bind and inhibit both CDK4/6-cylin D and CDK2-Cyclin E complexes and inhibit the phosphorylation and inactivation of Rb, therefore driving and sustaining a G1 arrest[94]. The G1/S checkpoint, in steady state, ensures that prior to DNA synthesis, a cell has enough building blocks such as nutrients, nucleotides, and replication-associated enzymes. However, this checkpoint also serves as the first barrier against genomic instability, that is, to repair any damage prior to DNA replication. Failure to do so, would disseminate such toxic lesions to daughter cells if carried through to mitosis. If DNA damage is detected, normally p53-dependent G1 arrest will become active, however, in many cancers, mutated p53 results in inactivation of this checkpoint, leading to aberrant accumulation of mutations. Loss of p53 activity is now known to be a major contributor to the permissiveness of mutations and the heterogenous evolution of tumor clones[95].

As the cell transitions to G2, cyclin B-CDK1 complexes increase and trigger M phase progression. ATM activation and downstream Chk1/2 activation will trigger the phosphorylation and inhibition of CDC25A, a key phosphatase required for the dephosphorylation of the CDK1-cyclin B complex in mitosis[96,97]. As accumulation of active cyclin B is required for progression, it represents a single arm of the activation of the G2/M phase checkpoint. Activated Chk1 phosphorylates the regulator of mitosis, the kinase Wee1, which subsequently phosphorylates the CDK1-cyclin B complex, further sustaining the inhibition of M phase progression[98]. This cooperation between CDC25 inhibition and

Wee1 activation provides redundant roles in enforcing this checkpoint to safely ensure DNA repair prior to mitosis.

1.2.2 Epigenetic regulation of cell cycle control and DNA repair

The chromatin landscape of the genome consists of transcriptionally-active euchromatin and gene-repressive heterochromatin. Heterochromatin is canonically composed of methylated histones and possesses a highly compacted nucleosome structure, demarcated by H3K9me3 and H3K27me3, in contrast to acetylated histone marks observed in relaxed euchromatin[98]. This balance of chromatin compaction and accessibility represents the epigenetic basis of gene regulation. Furthermore, physical access of chromatin serves as a barrier that must be regulated such that certain proteins, such as transcription factors or DNA repair enzymes, can bind required regions. This accessibility is largely controlled by the amount of methylation, acetylation, and ubiquitination on histones or methylation of the DNA itself[99–102]. Fine regulation of chromatin structure is essential for gene expression, but also for DNA repair, DNA replication, cell growth and division.

During cell division, all regions of the genome are duplicated, including both euchromatic and heterochromatic regions. A key component of S phase is not only the replication of DNA, but the rapid dissociation of histones and removal of histone modifications, to allow relaxed accessible DNA for polymerase bubbles to move freely. After replication the re-facilitation of the histone code and the replacement of the histone modification to ensure exact duplication in sequence and in structure are required. Both active and repressive chromatin structures are required, mostly, for the regulation of gene expression and repression. This is exemplified by the fact that loss of regulation of H3K27ac marks, result in aberrant expression of repeat sequences such as repeat elements SINE/LINEs[103]. Uncontrolled transcription of genes also results in transcription-associated DNA damage[104]. However, in certain facultative regions of the genome, centromeres and telomeres, these repressive histone marks are required for structural elements that

preserve integrity of the chromosomes[104–106]. Loss of the H3K9me3 mark in telomeric regions destabilize compaction and activate the DNA damage response[107].

1.2.3 The emerging role of repressive epigenetic machinery in response to DNA damage

Pathways governing epigenetic gene regulation, such as histone methyltransferases (HMTs), are now increasingly shown to play direct and indirect roles in DSB repair. In euchromatin, DNA damage often occurs due to errors in transcriptional initiation and elongation, and in these instances, for successful repair, transcription must be transiently repressed. This can be done via the recruitment of HMTs and the temporary production of heterochromatic regions flanking DNA damage. Failure to temporarily repress transcription can result in further DNA damage and un-repaired DNA lesions[108–110]. Conversely in heterochromatin, repressive marks act as epigenetic barriers of transcription to aid in processes such as cell differentiation and lineage commitment[111,112]. However, this rigid structure also forms an obstacle during DNA damage. DNA damage that occurs in transcriptionally silent heterochromatin requires temporary epigenetic modifications to relax structurally inaccessible regions[113]. Furthermore, chromatin modifying enzymes, and the proteins that regulate their function, can serve dual roles in both DNA repair and transcriptional regulation[114,115].

The heterochromatin protein 1 (HP1) is a central component in the organization of heterochromatin by directly interacting with H3K9me3[116]. Three different HP1 isoforms are present in mammals (HP1-α, -β and –γ) and all possess an H3K9me3-binding chromodomain, a hinge region for homo-/hetero-dimerization, and chromo-shadow domain. Originally thought to be strictly required for additional physical integrity of heterochromatin, HP1 isoforms are now shown to serve as adaptors linking chromatin and chromatin modifying complexes, which regulate heterochromatin spreading[117]. HP1-mediated heterochromatin formation is a conserved cellular function, first identified in Drosophila as a mechanism of gene silencing. KRAB-associated protein 1 (KAP1)/tripartite motif-containing protein 28 (TRIM28) is an HP1-interactor and is widely

recognized as a repressor of gene transcription. KAP1 can be recruited to regulatory elements of genic regions, such a promoters or enhancers, via KRAB-domain containing proteins[106,118]. Acting as a scaffold for chromatin modifying enzymes, such as the chromatin assembly factor 1 (CAF1) complex, KAP1 promotes local heterochromatin formation (increased di- and tri-methylation of H3K9) which results in decreased gene transcription[119]. Furthermore, the interaction of KAP1 and HP1 is required for subsequent HP1 deposition, induction of repressive histone modifications, and subsequent KAP1-dependant transcriptional suppression[116]. These data indicate that HP1 and its interaction with KAP1 is required and represent an integral part of transcriptional repression.

HP1 isoforms and KAP1 have both recently emerged as key modulators of DNA repair[114,120–122]. The initial observation that KAP1, HP1-α, -β and –γ, are rapidly recruited to DSBs suggested an active role of these heterochromatin-promoting proteins during the signaling of DNA lesions. KAP1 potentiates the recruitment of the HP1-binding HMT, SUV39H1, whose enzymatic activity promotes H3K9-methylation, appearing as a histone methylation wave surrounding DSBs[123]. This methylation allows the binding of the histone acetyl transferase, TIP60, through an H3K9me3-binding chromodomain[124]. TIP60 can then acetylate ATM within its PI-3-K regulatory domain (PIKRD) which is critical for its kinase activity and subsequent autophosphorylation[125,126]. Furthermore, both KAP1 and the HP1 isoforms have been shown to be phosphorylated rapidly by ATM in response to DNA damage[121]. Importantly, cells lacking either HP1 isoforms, KAP1, SUV39H1, or TIP60 fail to undergo homologous recombination[104,114,121].

It was also determined via micro-irradiation experiments, that HP1 isoforms possess biphasic kinetics of DSB co-localization[120,127]. The first of which is HP1 removal at sites of damage, while the latter represents a recruitment and potential stabilization of DNA repair proteins. Within seconds of irradiation, HP1 becomes phosphorylated by the casein kinase 2 (CK2) at Thr51, decreasing affinity for H3K9me2/3 and its dissociation from H3 tails[128]. Furthermore, ATM mediated phosphorylation of KAP1 is required for HP1

mobilization from heterochromatin, and is required for DSB repair in heterochromatin[129]. Interestingly, the primary function of KAP1 is the regulation of transcriptional repression, i.e. the establishment of heterochromatin bodies in regulatory gene elements, like promoters, to silence gene expression. While representing a core component of both constitutive and facultative heterochromatin, HP1 isoforms and cognate H3K9 methylation needs to be removed to produce a less compact DNA structure[130]. This serves to allow access of DNA repair proteins and the formation of scaffolds necessary for enzymatic activity at sites of damage. The interplay between the repression machinery and regulation of chromatin structure in the context of DNA repair, is a field of limited knowledge.

In contrast, studies of later time points in DSB repair (in the order of hours post irradiation), HP1 isoforms are seen to be recruited to sites of damage. This later recruitment has been proposed to play multiple roles: serve as a platform for stabilization of the DNA repair machinery; co-operate with the gene repression machinery to suppress transcription in genes proximal to damaged DNA; and lastly, to facilitate the restructuring of the chromatin landscape post DSB repair. As mentioned previously, the BRCA1-BARD1 complex is stabilized at sites of damage through an interaction with histone marks, specifically H4K20 and additionally H3K9me2[131]. Interaction between the BRCA1-BARD1 complex and H3K9me2 is primarily mediated by the chromoshadow domain of HP1-γ [132,133]. Mutations in the chromoshadow domain in mammalian cells show loss of BRCA1-BARD1 at sites of damage and abolish their facilitation of CTIP recruitment, and downstream RAD51 filament formation, indicating there is a role for HP1 isoforms in the retention of HR factors at DSBs[133]. This interaction is dependent specifically on ATM phosphorylation of HP1 isoforms, rather than a histone modifying activity by RNF168, a key E3-ubiquitin ligase in DNA repair. Furthermore, while the canonical role of HP1 is binding methylated H3K9 through its CSD domain, elegant functional studies have elucidated that the CSD is not required for HP1 to accumulate at sites of damage via irradiation.[127] This indicates that the capacity of HP1 to bind heterochromatin, is not essential for HP1-mediated DSB repair. It is speculated that, that phosphorylated Thr51 residues on HP1 proteins may

represent a binding point for FHA containing proteins, which bind phosphorylated threonine residues, like MDC1, RNF8, and NBS1[128]. These two examples highlight the existence of a non-redundancy amongst mammalian HP1 isoforms and their individual regulation in the context of DNA repair. Largely, the network of proteins governing the activity of HP1 and its role in DNA repair, specifically HR, and how this is inclusive or exclusive of repressive chromatin structure or other protein stabilization, is unknown.

1.3. Cellular Transformation: Failures in HR and Chromatin

Through karyotyping experiments of HR-defective cancers, micronuclei production has been frequently observed. Micronuclei are extra nuclear structures that contain nuclear proteins and full or partial chromosomes that arise due to segregation defects, or errors in chromosomal duplication or alignment. Micronuclei can often be used as karyotypic evidence of DNA damage, as they are often γH2AX positive[134–136]. Often in cancer, chromosomal aberrations or loss can result in a lacking template during HR, therefore leaving cells exposed to larger and more lethal, genome-wide insults. Furthermore, mutations in BRCA1 represent one of the most well-studied examples of hereditary cancer, often in the breast and ovaries. Loss of BRCA1-mediated HR in this capacity renders cells sensitive to transformation and early neoplasia and expedited progression of cancer[137–139]. Interestingly, given the heavily regulated and stepwise nature of HR, loss of function mutations in any of the key proteins or regulatory components could potentially phenocopy the BRCA1 mutation. Therefore, defects such as mutations in BLM, NMS, PALB2, and ATM have been associated with large scale genomic rearrangements that either represent the transformation event during oncogenesis or an acquired event during tumor growth, much like the pathogenic mutations found in BRCA1/2[138].

Given the roles of epigenetic regulators in aiding in HR facilitation, it is possible that mutations or loss of function of such enzymes and proteins involved in heterochromatin stability, could recapitulate BRCA1 mutations. However, while these families of proteins play roles in HR, loss of these proteins results in loss of the diverse set of functions these

proteins play. HP1 proteins, in mouse models safeguard against tumorigenesis[140,141], however, increased expression of HP1 proteins in humans has been associated with cancer progression[142]. Loss of H3K27 methylation in individuals with H3K27M mutations often leads to glial cell transformation, predominantly early in life[103]. Deficiency of SUV39 proteins in various models also potentiate cellular transformation[143,144], while KAP1 overexpression is shown to advance cancer progression through KRAB-ZNF transcriptional promotion of proliferation and metastatic genes[145]. Therefore, while these proteins are crucial for HR and DNA repair, in the context of oncogenesis they may not exactly align with the BRCA1 hereditary cancer phenotype.

1.4. Breast Cancer Overview

Breast cancer is the most frequently diagnosed cancer in Canada comprising 25% of all cancer diagnoses in women.[146] Furthermore, 15% of all cancer-associated deaths positions breast cancer as the second most lethal cancer in women.[146] Despite these statistics, breast cancer has an exceptionally high survival rate, with a 5-year survival rate of 88%.[146] These cases are likely early staged breast cancer, described by its distribution to strictly the breast and close proximal lymph nodes (Stage I-II). Despite treatment providing a better quality of life, advanced (Stage III) and metastatic breast cancer, defined by spread to distant lymph nodes and organs (Stage IV), possess patient survival rates 2-10 times lower than early diagnosed breast cancer with a 5-year survival rate of 7-35%.[147]

1.4.1 Mammary Gland Architecture

The mammary gland is composed largely of luminal epithelial cells that comprise the ductwork of the tissue (Figure 1-3). These ducts line the breast, with one end composed of terminal duct lobular units (TLDUs), or lobules, and the other end draining to the areola. These lobules are pouches of cells that contain specialized cells that differentiate into the milk-forming cells during lactation. Milk will get secreted from the lobules, enter the ductwork, and exit through the areola. Luminal epithelial cells line the ducts and possess a cuboidal shape and a dense extracellular matrix (ECM), that binds each cell to the next,

composed of adherens- and tight junctions, to allow structural integrity of the gland network. The core aspect of this epithelial layer possesses polarity, with a specialized apical layer and an underlying basement membrane. While each cell remains static, this structure allows for a dedicated barrier and defense, but can serve other purposes like diffusion of bodily fluids (e.g. milk or sweat). Under the basement membrane of the luminal layer, lies the myoepithelium, which are contractile cells that control the luminal cell layer and aid in fluid flow through the branched ductwork within the gland. Mammary stem cells reside within the basal epithelial layer and replenish terminally differentiated lumen or myoepithelial cells through differentiation to luminal or basal progenitor cells, respectively.[148,149] Hormone receptors for progesterone (PR) and oestrogen (ER) are essential for differentiation, maintenance, and development of a functional gland. These receptors are ligand activated and throughout gland development, puberty, and pregnancy, signalling through regulated hormone secretion, these activated receptor complexes drive rapid growth and expansion of luminal epithelial cells through transcription factors that initiate gene programs governing ductal cell division and branching.[148,150–152]

The mammary gland tissue during pregnancy, lactation and involution (the resolution and return to a non-lactating state) is a rapidly changing microenvironment. Microenvironmental changes within the breast during puberty, menstruation, and pregnancy give rise to aberrant ductal cell growth and expansion through rapid cellular proliferation, which may drive accumulation of DNA damage[153]. Furthermore, these periods of growth are also defined by mammary tissue reconstruction, therefore the massive changes within the extracellular matrix and the influence of immune-mediated inflammation can contribute to the production of damaging agents such as reactive oxygen species that may poise cellular transformation[153–156]. The exact factors surrounding the exact initiation of breast cancer are unknown, which may contribute to the complex heterogeneity of the disease.

1.4.2 Breast Cancer Subtypes

There are two ways to classify breast tumors that aid in therapeutic strategy, histopathological and molecular subtypes (as seen in Figure 1-4). Histopathological classification utilizes the presence, or lack thereof, of hormone receptor and human epidermal growth factor 2 (HER2) expression levels. These molecules are responsible for providing hormone and growth factor driven oncogenic signalling, respectively, however, can also provide clinically relevant transmembrane targets for targeted therapy. While intrinsic molecular classification defines these subtypes based on their transcriptional profiles (luminal vs basal) and aggressiveness, which is demarcated by nuclear expression of a marker of cell division (Ki67)[157].

Luminal A is primarily composed of histologically ER+PR+ tumors with a low Ki67 index, while Luminal B tumors tend to be ER+PR+ but a higher Ki67 index, delineating a more aggressive growth pattern[158]. Luminal cancers, comprising the majority of ER+PR+HER2- have high 5-year survival of most cancers, when stratifying based on stage of diagnoses: Stage I:94.7%; Stage II:88.1%; Stage III:72.9%; Stage IV:24.0%[147]. Luminal A and B tumors, transcriptionally possess a gene signature of a more developed mature luminal cell[152]. Luminal subtypes largely possess signatures deriving from aberrant hormone receptor signalling complexes and respective signal transduction cascades[159].

The HER2+ subtype is defined by the amplification of the gene coding for HER2 (17q21) leading to high expression of HER2 and are largely ER-PR- with a high Ki67 index[158]. While HER2+ breast cancer is often associated with poor outcome breast cancer, recent survival rates position it as comparable with ER+PR+ breast cancer when stratifying based on stage of diagnoses: Stage I:96.5%; Stage II:87.5%; Stage III:79.9%; Stage IV:36.6%[146]. While these subtypes seem discrete, emerging evidence is suggesting another subtype of Luminal B breast cancer that possesses HER2 expression but retains its luminal hormone receptor expression and high Ki67 index[160].

Lastly, the basal molecular subtype is largely devoid of both ER/PR and HER2 expression, and therefore is often referred to as triple negative breast cancer, (TNBC, ER-PR-HER2-)[158]. Basal subtypes represent the breast cancer with the poorest patient survival rates based on stage: Stage I:93.3%; Stage II:78.9%; Stage III:47.2; Stage IV:7.4%[146]. The basal subtype is also heterogeneous and subsets of tumors contain a mesenchymal transcriptional signature, often associated with higher rate of metastasis and poor outcome in late stage diagnoses[161]. Furthermore, basal breast cancers are enriched in mammary stem cell transcriptional responses, governed largely by the SOX family of stem cell transcription factors, and markers such as cluster of differentiation 44 (CD44) or CD24[160,162–164]. These key findings support basal breast cancer aggressiveness and poor outcomes, as the stem cell hypothesis of cancer suggests that quiescent, metabolically flexible, repopulating cells are exquisitely resistant to therapy and can rapidly adapt or relapse.[165]

1.4.3 Therapeutic Targeting of Breast Cancer

While ER/PR/HER2 receptors may drive growth and pro-tumorigenic signalling, they also serve as therapeutic targets. When overexpressed, these receptors can uniquely identify tumor cells within the breast.

1.4.3.1 Standard of Care Treatment

Standard of care treatments for breast cancer include surgery in combination with a form of treatment such as hormone-based therapy or chemotherapy, depending on the breast cancer subtype. Therapy can be given before (neoadjuvant) surgery to shrink the tumor to reduce the invasiveness of the surgery in an attempt to save portions of the breast, or after (adjuvant) therapy to reduce the likelihood of recurrence. Cancer cells require oncogenic signalling from hormones or HER2 receptors to grow and divide, much more than normal tissue. Therefore, the principle behind hormone therapy is by blocking hormones from binding the cognate receptor, or inhibiting the signal transduction form the engaged receptor complexes, can inhibit tumor growth. If the breast tumor is hormone

receptor positive (ER/PR) then, hormone-based therapy can exploit these features: by degrading hormone receptors (selective estrogen receptor degrader, SERD); by blocking hormone binding to receptors (selective estrogen receptor modulator, SERM); and blocking the production of hormones (aromatase inhibitors, AI)[166]. Often tamoxifen (SERM) is used pre- and post-surgery in ER/PR+ breast cancer. If the tumor is HER2+, then kinase inhibitors like lapatinib or monoclonal antibodies directed against the HER2 receptor, trastuzumab, have been developed to specifically disengage the pro-tumorigenic receptor kinase domains downstream of hormone or HER2 receptor signalling complexes[165]. Similar to tamoxifen, trastuzumab is used pre- and post-surgery, as standard of care[167]. If individuals upon diagnoses possess lymph node invasion of the breast cancer, these individuals may additionally receive radiation therapy.

While these therapies specifically target the unique properties of the tumors, TNBC tumors lack specifically defined receptors, and by proxy, a targeted therapy. Individuals with TNBC often get neoadjuvant platinum, taxanes, or anthracycline based chemotherapies[168,169]. These therapies target essential pathways involved in cell division, such as crosslinking/intercalating DNA or by inhibiting the microtubules required for successful mitosis. In some cases, individuals with TNBC can be treated withan immune checkpoint inhibitor (ICI) based therapy, often pembrolizumab, to enhance immune activation within the solid tumor.[170] However, recent research has delved into the molecular underpinnings of the basal breast cancer subtype via transcriptomic and exome sequencing.

1.4.3.2. Emerging Treatments

Importantly, the basal subtype of breast is composed of mostly TNBC, within this group of tumors there is a disproportionately high rates of mutations in genes responsible for DNA repair, most notably those involved in HR. While only a very small portion of non-hereditary breast cancers contain a *BRCA1* mutation, a high distribution of about 20-30% is seen in basal/TNBC which lack targeted therapies[139] . The term “BRCAness” has emerged to describe tumors that share may features and phenotypic outcomes with

tumors arising from hereditary *BRCA1* mutations. BRCAness can now refer to epigenetic alterations, like methylation of HR gene promoters, or mutations in HR pathway proteins (extending far beyond just *BRCA1*, to other genes such as *PALB2* and *BRCA2*)[171]. Poly-(ADP) ribose- polymerase inhibitors (PARPi), such as olaparib and talazopirib (targeting PARP1/2 and PARP1/2/14, respectively) show promise in treating a subset of TNBC cases (individuals with germline BRCA1/2 mutations), which have compromised DNA double-strand break (DSB) responses.[172–174] PARP, traditionally, is a key component of the SSB repair pathway, BER, however, possesses many other cellular functions in addition to this role in DNA repair. Briefly, if cells lack PARP, or if PARP is inhibited, BER efficiency is greatly reduced, therefore increasing the likelihood of SSB becoming a lethal DSB.[175] Healthy cells can then initiate HR to repair such damages, however, cancer cells deficient in such repair machinery (e.g. *BRCA1* mutations) cannot readily repair such DSBs, resulting in cell death. It has recently been described that unresponsiveness or resistance to PARPi in BRCA1/2-mutant patients emerges in approximately 40-70% of patients.[176,177] Resistance to PARPi, on a molecular level, can emerge through loss of 53BP1 or RIF1. Furthermore, a downstream interactor of RIF1, the adaptor protein MAD2L2/REV7 has emerged as a central regulator of the DSB response and loss promotes PARPi resistance in DNA repair-deficient cells.[39,40] Lastly, predicting subtypic TNBC responses to PARPi and limiting tolerance remains a challenge, therefore, an emerging therapeutic strategy is to combine PARPi with currently utilized chemotherapies.[173,178]

As mentioned previously, the basis of many chemotherapies exploits cancer-specific attributes, differing from untransformed tissue. Established neoplasia acquire DNA damage to a much greater extent, possess aberrant cell cycle checkpoints, and have increased cell division, creating unique vulnerabilities of primary breast cancers, independent of subtype. However, despite utilizing broad and targeted therapy of a primary tumor, even with the addition of surgery, once breast cancers become advanced and spread to distant organs, long-term survival outcomes drastically decrease.[179]

1.4.4 Advanced Breast Cancer and Metastasis

During the development of metastatic breast cancer, colonization of the lymphatics (lymph nodes) and/or dissemination through the blood stream will occur first, followed by spread to the lung, liver, brain and bone.[179,180] The metastatic cascade is the process through which a primary tumor can grow beyond its primary microenvironment and migrate to distant organs and colonize (outlined in Figure 1-5). Metastasis begins with an initial molecular and phenotypic alteration in a subset of breast tumor cells endowing them with enhanced migratory and invasive properties. These cells, often in close proximity to stromal vasculature, enter proximal tissue and eventually into the hematogenous or lymphatic circulation, a process called intravasation. Once in circulation, cancer cells must survive physical stress and alterations in nutrient availability, until extravasating into other organs. Once infiltrated into distant tissue, these cancer cells must seed, re-enter the cell cycle and evade the immune system for form metastases. Given the many steps of the metastatic cascade, these cancer cells must overcome and survive many challenges to effectively form a clinically relevant lesion, therefore the overall efficiency of metastasis is extremely low.[181–183] However, primary tumors can effectively release thousands to millions of circulating tumor cells, often having already done so at time of diagnosis. Understanding how this process is initially triggered is of large importance, therefore the remainder of this review will focus on one aspect of the metastatic cascade, which increases the migratory and invasive properties of breast cancer cells, called the epithelial to mesenchymal transition (EMT).

1.4.5 The Epithelial to Mesenchymal transition

The EMT occurs naturally and systematically during organismal development, serving a critical role during various stages of early tissue growth during embryogenesis, such as gastrulation.[184,185] In brief, the EMT is a biological process through which a polarized epithelial cell with asymmetric membranes, loses such qualities and acquire a mesenchymal phenotype, losing its attachment to its basement membrane and gaining migratory and invasive features. These cells can then move along the vasculature and return to an epithelial state in attempts to expand tissue size, developing and dispersing layers of epithelial tissue, or repair and renew damaged epithelium through the generation

of mesenchymal cells. The main feature of epithelial cells is the pronounced cell-to-cell adhesion network, which link neighboring cells through adherens and tight junctions. The formation of adherens junctions is predominantly though the E-cadherin proteins, which link with catenin family proteins on neighboring cells, acting as anchors for the actin cytoskeleton. Through the occludin and claudin family proteins, the formation of tight junctions between epithelial cells allows for ion transfer and permeability between cells.[186–188] In addition to providing the physical network underlying the high physical integrity of epithelial tissue, these junction proteins can also trigger intracellular events through downstream transcriptional modulation.[189] Mesenchymal cells, in turn, are largely described by their loss of polarity and migratory nature. During the early stages, these cells secret proteins to degrade existing cell-to-cell networks such as matrix metalloproteases 2 and 9 (MMP2/9).[145,190] The loss of the adherens and tight junction structure between cells and the loss of actin cytoskeletal anchorage points leads to a transition from a cuboidal to a more spindle shape. Once free, these cells can upregulate fibronectin, vimentin, N-cadherin, which are all secreted or membrane bound proteins that can facilitate navigation through vasculature.[191,192] Importantly, it should be recognized that the EMT is an extremely transient process, and through the mesenchymal-to-epithelial transition (MET), is reversible.[193,194] Mesenchymal cells are not characterized by their extensive cell division or structural integrity and therefore can do little to increase tissue mass or physical strength. Thus, these cells, once in destination, can revert back to epithelial cells and begin to reconstruct polarity and cell-cell adhesions.

The initiation and development of the EMT is facilitated largely through transcription. Such orchestration is governed by the master transcription factor families: Snail, Zeb, and Twist.[195–199] The most well understood hallmark functions of these transcription factors are the repression of components of adherens junctions, namely E-cadherin.[200–203] Specifically, SNAIL1 and TWIST1 can bind the promoter of E-cadherin directly and repress expression though recruitment of Sp1 transcriptional repressor machinery, eliminating pro-epithelial signalling through this cell junction protein.[200,202,204] In addition to repression of epithelial adhesion proteins, these factors increase expression of ECM

components, MMPs, and anti-apoptotic proteins.[205–208] Therefore, EMT re-programing is defined not just by a repression of epithelial genes, but also the concordant upregulation of mesenchymal and survival genes.

Cues from the microenvironment such as hypoxia, inflammation, and growth factor receptor signaling, triggers an EMT.[185] Ligands for growth factor receptors are readily found systemically and are produced by various pro-tumorigenic sources such as tumor-associated macrophages and fibroblasts. Microenvironmental factors such as TGF-β, FGF, EGF, Wnt, Notch ligand, and even hormones such as estrogen, can induce pro-EMT signalling from respective activated receptors. EMT in gastrulation and the formation of mesoderm and endoderm is entirely dependent on Wnt signalling, mediated largely by Nodal.[209,210] The EMT that occurs during fibrosis and tissue healing is largely triggered by inflammation, leading to EMT induction by nuclear factor kappa b (NF-κb).[211,212] The establishment of inflammatory macrophages leads to production of MMPs and pro-inflammatory cytokines trigger epithelial cells to deconstruct damaged basement membranes. This produces a partial EMT which allows movement and reconstruction of the epithelial layer, heavily utilizing both the EMT and MET processes.[213]

In untransformed tissue, EMT largely drives development and homeostatic tissue regulated processes. Unsurprisingly, cancer cells can undergo and exploit the EMT process, utilizing such cell traits to promote tumor aggressiveness. EMT within cancer bestows transformed cell migratory behaviors, granting cancer cells the opportunity to escape primary tumor niches, therefore invading circulation, culminating in distant organ and lymph node colonization.[213–215] Utilizing the same pathways of EMT initiation as within developing tissue and wound healing, cancer cells can exploit inflammation and cytokine signalling, the most notable example being TGF-β, to drive the onset of an EMT.[191] While most luminal cancers retain cuboidal structure and epithelial qualities (as seen in luminal cells within the duct in Figure 1-3), histologically described basal-breast cancers, however, are associated with the greatest degree of mesenchymal

characteristics.[161,216] These characteristics are largely presumed to drive the increased metastatic colonization and poor survival outcomes seen within this subtype.[209] Identifying the drivers behind the initiation and potentiation of EMT, like TGF-β signalling, are essential in understanding the complex biology of basal tumors.

1.5. TGF-β signalling overview

TGF-β signalling can trigger: a cell cycle arrest within non-transformed epithelial cells; a differentiation and proliferation program, such as in haematopoietic cells; or both an arrest and differentiation, as observed in neurons; and lastly, triggering the EMT in both developing tissue and cancer.[217,218] These various and heterogenous effects witnessed depend highly on the signal transduction platforms present, pre-existing transcriptional profiles, and epigenetic landscape of the recipient cell.[219] Therefore, TGF-β signalling phenotypes may not be discretely conserved amongst all cell types in terms of specific gene targets or cellular fates, therefore this literature review will focus specifically on the TGF-β signalling cascade (Figure 1-4), its tumor suppressor effect and initiation of the EMT, within the mammary gland and specifically during breast cancer.

As mentioned previously, mammary gland development is predominantly orchestrated through tightly regulated secretion and signalling of estrogen and other hormones. TGF-β family members have been shown to control early gland formation during embryogenesis, ductal growth and maintenance through puberty and menstruation, as well as control alveologenesis and lactation during pregnancy[220–223]. Estrogen and progesterone differentially influence cell type and architecture during gland development, specifically utilizing TGF-β as a main driver in controlling these effects. Overexpression of TGFB1 within the mammary gland, via a transgenic MMTV promoter, suppresses tumorigeneses completely. However, when TGF-β is aberrantly expressed in luminal progenitor cells under control of the whey acidic protein promoter (WAP), the regenerative potential of the gland, itself, is inhibited and increased apoptosis is observed during gland involution.[224] Lower concentrations of TGF-β stimulate ductal branching and

alveologenesis in concert with progesterone, while higher concentrations inhibit these developmental programs through the initiation of cell cycle arrest and apoptosis.[225] Therefore, the concentration of stimulus adds another level of regulation of signalling, as gradients of TGF-β can further differentially regulate mammary cell growth. Furthermore, the overall effect of TGF-β is required to be constantly regulated to both support necessary mammary growth programs, while inhibiting any transformative potential.[221]

1.5.1 TGF-β Ligands

TGF-β family of cytokines comprise over 35 different molecules. TGF-β cytokines, ACTIVIN/NODAL families, developmental Lefty proteins, and the BMP/GDF subfamily compose the four major groups of the TGF-β superfamily of proteins. The TGF-β subfamily contains 3 proteins, TGF- β1, TGF- β2, and TGF-β3. Different TGF-β proteins have alternative affinity for cognate receptors which will directly impact downstream signalling.[226,227] Biological situations where minor, yet stimulatory, TGF-β signalling is required, like mammary ductal branching during pregnancy, often utilize the TGFB2 isoform, where high signalling isoforms TGF- β1/3 trigger growth arrest and apoptosis during mammary gland involution.[225]

To precisely regulate concentration and gradients of TGF-β isoform signalling, TGF-β is secreted in a latent complex (as seen in Figure 1-4) and through integrin and other ECM component engagement, TGF-β is rendered to its active form. TGF-β pro-peptides contain two regions, the C terminal mature TGF-β sequence and an N terminus containing the latent associated region. Pro-TGF-β proteins are translated in the endoplasmic reticulum where they form homo/heterodimers linked by disulphide bridges at sites Cys223/225. The latency associated region is post-translationally cleaved by the protease, furin, in the Golgi body. This will form the latency-associated protein (LAP), which remains non-covalently linked to the TGF-β dimer, thus inhibiting the dimers' receptor binding domains. Lastly, latent TGF-β is secreted with the latent TGF-β-binding protein 1 (LTBP1). These large proteins form disulfide bridges with the LAP monomers and stabilize the complex.[228] Furthermore, when secreted and bound to ECM

components, fibrillin and integrins, these interaction-induced conformational changes destabilizes the LAP-TGF-β complex, producing TGF-β in its active form.[229–231] This interaction with the ECM is thought to not only provide assistance in TGF-β activation but also the localization and anchoring to the ECM, as these complexes are often secreted in a paracrine manner to impact proximal cell fates.

1.5.2 TGF-β Receptors

Once TGF-β, and other family members, are present in active forms, they will bind to the TGF-β receptor (TGFBR) superfamily of receptors. The TGF-β subfamily exclusively binds to the TGFBR1 and TGFBR2, which represent the class I and class II receptors of the TGF-β specific subfamily. While other receptors within the family, i.e. ACVR1, ACVR2A/B, BMPR1A, BMPR2, work to signal activins, BMPs, and Nodal. Furthermore, different combinations of type I and type II engagements can adjust signalling strength or target gene expression.[219,226,227,231,232] Type I receptors transmit and propagate signals received from type II that are activated during ligand binding. Both type I and type II TGF-β receptors utilize serine-threonine kinase domains, unlike widespread receptor-tyrosine kinase (RTK) usage by most cytokine receptors. The overall TGFBR superfamily contains seven type I and five type II subfamilies. Type II receptors are constitutively phosphorylated and are the first receptor to engage with ligand. This triggers autophosphorylation and enhancement of its kinase activity, proximal type I receptors will then be activated by phosphorylation of the type I glycine-serine (GS) rich domain, gradually recruiting other type I and II receptors.[232] A complete signalling complex consists of two TGFBR2 and two TGFBR1 and a bound active TGF-β dimer (as seen in the membrane portion of **Figure 6**).

1.5.3. TGF-β signalling mediators: SMADs

An activated TGFBR complex will then phosphorylate the main substrates and mediators of the TGF-β superfamily signalling pathway, the SMAD proteins. Operating as signal transduction proteins and as transcriptional regulators, SMAD proteins converge as the fulcrum and crux of the TGF-β signaling.[232,233] The SMAD family is a conserved family of

proteins found in all metazoan organisms, with extremely high cross species homology.[234] The eight members of the SMAD family, organized in three groups: receptor-regulated (R-SMADs); a common partner (co-SMAD); and inhibitory (I-SMAD). The two main domains found in high conservation are the Mad homology 1 (MH1) and MH2, often separated by a semiconserved linker or hinge region. MH2 domains are conserved amongst all SMAD proteins and are required for oligomerization, receptor engagement and transactivation associated interactions. The MH1 domain, which is not present in I-SMADs, is primarily utilized for DNA binding, most notably to SMAD-binding elements (SBE) in regulatory regions of downstream target genes.

R-SMADs are the main substrates of engaged receptor complexes and consist of SMAD2 and SMAD3, which are phosphorylated by TGF-β, nodal and activin engaged receptor complexes, and SMAD1, SMAD5, SMAD8/9, which are downstream substrates of activated BMP-receptors. Once phosphorylated, R-SMADs will hetero- and homo-dimerize via MH2 domain engagement. The co-SMAD, SMAD4, does not directly interact with the various receptor complexes but will bind activated R-SMAD dimers to execute transcriptional functions (as seen in the signalling cascade in Figure 1-4).[232,235] This complex of two R-SMADs and a single co-SMAD are the principal signalling mediator for the TGFBR family signalling. I-SMADs, through the conserved MH2 domain, can compete with R-SMADs for protein-binding at virtually every step of R-SMAD activation. However, lacking an MH1 domain and therefore any downstream transcriptional activity, these proteins can sequester signalling by binding activated receptor complexes, co-SMADs, and even inhibit heteromerization with co-SMADs by binding R-SMADs directly.[235]

Once R-SMADS are phosphorylated they dimerize to create binding partners for the co-SMAD (SMAD4). These R-SMAD/co-SMAD complexes will translocate to the nucleus acting as transcription factors for genes containing SMAD-binding elements (SBE) sites within their promoter proximal gene body. Once in the nucleus SMAD2/3 complexes can interact with a multitude of transcriptional modulators. Forming greater complexes with

both co-repressors and co-activators expands the downstream transcriptional effects of the SMAD complexes beyond the stringency of an SBE element. The R-SMAD complex can also directly interact and modulate transcriptional activity of E2F family members, RUNX family transcription factors (RUNX3), activating transcription factor 3 (ATF3), and Sp1 transcription factors (SP1).[236–238]

1.5.4. TGF-β signalling and gene transcription: Cytostatic

TGF-β, canonically, is a tumor suppressor, that inhibits the growth of a potentially transformed and oncogenic cell, preventing the establishment of malignancy. This effect culminates as a G1 cell cycle arrest and is mediated through both the transcriptional silencing of the proto-oncogene, MYC, and the indirect inhibition of Rb-phosphorylation.[192,239] SMAD3/4 can interact with E2F4 and the Rb pocket protein, p107, upon translocation to the nucleus.[240–242] This complex can trigger silencing of Myc via an E2F4 binding side that resides in a negative regulatory region of the Myc gene.[241,243] Myc, itself, is a master transcriptional regulator of cell proliferation, whose downstream target genes, such as CDC25, are required to push cells past the G1-S checkpoint.[243] This complex also sequesters p107 and prevents its interaction with Rb, inhibiting the Rb complex phosphorylation by CDK4-Cyclin D, further promoting a G1 cell cycle arrest.[244]

SMAD complexes can also directly interact with signalling proteins that regulate cell growth and division. Loss of tuberous sclerosis protein 1 and 2 (TSC1/2) effectively diminished SMAD2/3 phosphorylation, indicating that TSC complex formation with SMAD2 regulates the interaction between the TGFBR1 and the r-SMADs.[245] TSC1/2 negatively regulate the metabolic and stress induced pathways of the mammalian target of rapamycin (mTOR), which represents a fundamental mitogenic signalling pathway. Furthermore, SMAD2 can bind TSC2, which can both enhance SMAD mediated repression of cell cycle inhibitors p21 and p27.[244] In contrast, TGF-β ligand can induce mTOR phosphorylation within developing podocytes, however, this phosphorylation is only triggered during chronic exposure to the ligand.[246,247] Therefore, complex signalling

interplay exists between TGF-β pathway stability, and amplification, with required negative regulators of cell growth.

In addition to inhibiting cell division of transformed cells, TGF-β signalling possesses the tumor suppressive capacity to initiate apoptosis. R-SMAD complex transcriptionally activates many apoptotic genes, such as the growth arrest and DNA damage 45 family, (GADD45), B cell lymphoma 2-like protein 11 (BIM), and the tumor necrosis family member Fas ligand (FasL).[248–250] It has been displayed in a variety of cell tissues, like neurons, hepatocytes, and mammary epithelium, that TGF-β signalling can transcriptionally upregulate GADD45 proteins, triggering p38 mitogen activated protein kinase (p38MAPK) triggered apoptosis.[248,251] However, apoptosis initiation was exhibited to much higher extent in non-transformed cells in comparison Ras transformed isogenic cell lines, indicating aberrant signalling crosstalk in cancer cells may rewire TGF-β signalling cascades.[250] Furthermore, in primary B lymphocytes, TGF-β induced pro-apoptotic BIM expression initiates programmed cell death during lymphocyte contraction in secondary lymphoid organs, as a way to clear white blood cells after pathogen clearance.[249] BIM expression sequestered anti-apoptotic BCL2 family members, triggering mitochondrial outer membrane polarization and the release of caspase-3 into the cytosol, there-by triggering the intrinsic apoptotic pathway. This TGF-β mediated programmed cell death in primary tissues also extends to B lymphocyte engagement of the Fas:FasL pathway. TGF-β in a SMAD3-dependent context, can trigger caspase-3 mediated apoptosis through the procaspase 8 pathway.[250] These examples illustrate that throughout tissue homeostasis, TGF-β can elicit a sensitive apoptosis induction, however, this sensitivity may be deregulated in cells that have been established and are resistant to TGF-β tumor suppression.

1.5.5. TGF-β signalling and gene transcription: EMT

The most notable example of cancer associated regulation of transcriptional networks is during the induction of EMT during chronic TGF-β exposure. While absolutely possessing tumor suppressive attributes in primary tissues, TGF-β plays a dual role in cancer and

transformed cells. Breast cancers are extremely responsive to TGF-β signalling, as this pathway is used in a regulatory capacity during development.[221] However, in transformed mammary epithelium TGF-β initiates an EMT after chronic exposure. During this large switch in transcriptional programming, the genome undergoes a global alteration in chromatin accessibility, elicited by histone and DNA demethylation.[250] Specifically, regions containing TGF-β responsive genes, such as ZEB1 or SNAIL (as seen as the outcome of signal transduction in Figure 1-4), become demethylated and accessible.[252,253] This global switch is in part due to a strong ERK2-Egr1-Sp1 mediated suppression of the HP1-interacting complex, CAF-1.[254] Furthermore, loss of CAF1 alone was sufficient to promote EMT in the untransformed mammary epithelial cell line, MCF10A, through the deregulation of ZEB1. [254] To further elicit and enhance transcriptional activity of R-SMAD complexes, specific coactivators are recruited to SBEs. The SMAD2/3/4 complex's engagement with by the CBP/p300 protein complex, which antagonize HP1-associated gene repression, further amplifies target gene expression.[254] These results indicate that HP1-associated chromatin effector complexes are required for tumor suppressive traits, such as antagonizing EMT. Finally, loss of expression or regulation of HP1 proteins, in various different types of cancer, is associated with transcriptional repression defects, however these alterations have had variable effects on invasiveness**.** Basal breast cancer cells can quickly promote the H3K27me3 mediated methylation of promoters for cell cycle inhibitors, such as p21, in response to long term TGF-β exposure.[255] Furthermore, TGF-β sensitive genes that promote the cytostatic effects in breast cancer, are often mutated, rendering these cells vulnerable to only the EMT-promoting and pro-metastatic TGF-β gene expression. Therefore, HP1 isoforms and their regulation may be tissue specific and depend on the concerted regulation of TGF-β receptor complexes and signal transduction machinery.

1.6. The Zinc Finger Protein, POGZ

HP1 isoforms, highly associated with transcriptional repression via interaction with KAP1 and recruitment of histone methyltransferases, have shown immediate recruitment at DSBs.[128] How chromatin architecture, particularly HP1 and associated interacting

proteins, and its dynamic nature, modulate DNA repair are largely unknown but represent a fundamental gap in the understanding of how transcriptional repression functions in the context of DSB repair. A number of HP1 interactors have been identified in recent years that may have functional roles in DNA repair. Studies by Baude et al, identified an HP1-β complex with pogo transposable element with zinc finger domain (POGZ) and the hepatoma-derived growth factor-related protein 2 (HDGFRP2).[256] This was the first implication that the HP1-interactor, POGZ, possessed any role in DNA repair, as it was suggested that this complex served to promote HR in heterochromatin. Furthermore, in studies generated by our group on the functional implication of the adaptor protein REV7 in NHEJ, POGZ was identified as REV7 interactor using both proximity labelling and immunoprecipitation mass-spectroscopy.[47] However, despite having shown POGZ loss to impact NHEJ, the exact function of POGZ in this context was not explored.

POGZ is a 155 kDa zinc finger protein with a C2HC-lyar and 8 C2H2 zinc finger domains. Interestingly, most HP1-binding proteins bind to the chromoshadow domain through a PxVxL domain, however, POGZ binds the hinge region through a proline rich domain, containing a C2H2 zinc finger.[257] In the C-terminus portion of the protein there is a putative transposase domain which may have a role in silencing transposable elements. Furthermore, it contains helix-turn-helix and CENP-B binding domains, both of which are required for DNA binding.[258] H3K9me3 immunoprecipitation mass spectroscopy by Vermeulen et al. identified POGZ in coordination with the HP1 isoforms, initially postulating POGZ to play a role in the regulation of repressive chromatin.[259] POGZ was first functionally described in the regulation of chromosomal stability during mitosis, specifically via its interaction with HP1-a. Depletion of POGZ in cervical cancer cells show decreased HP1-α ejection from chromosomal arms during mitosis, which resulted in decreased activation of the chromosomal passenger complex (CPC), chromosomal aberrations, and mitotic arrest.[257]

Pathologically, loss of function mutations in POGZ have been implicated in the development of a clinical syndrome, White Sutton Syndrome (WHSUS). Features of WHSUS include autism-like intellectual and social disabilities, developmental delay,

microcephaly, and in certain severe cases, recurrent infections. Several groups have shown that interruption of either the DNA-binding domain or the HP1-binding domain through de novo mutations are associated with WHSUS.[260,261] However, the severity of the clinical manifestation is variable and may depend on the location of the mutation. Mechanistic studies of WHSUS pathogenesis have shown that loss of POGZ, via genetic ablation or induction of loss of function mutations, render expression of genes whom repression is required for proper differentiation of neuronal stem cells, like JAG2.[258,261] Specifically, these studies have shown that POGZ accumulates at regulatory regions of such genes, however, suggesting that POGZ is directly involved in the required differentiation-associated repression of certain genes. Currently the only information we have about the role of POGZ and its interaction with HP1 in human pathology is restricted to neurological development, therefore, its specific role in other pathologies, such as cancer, are left unknown.

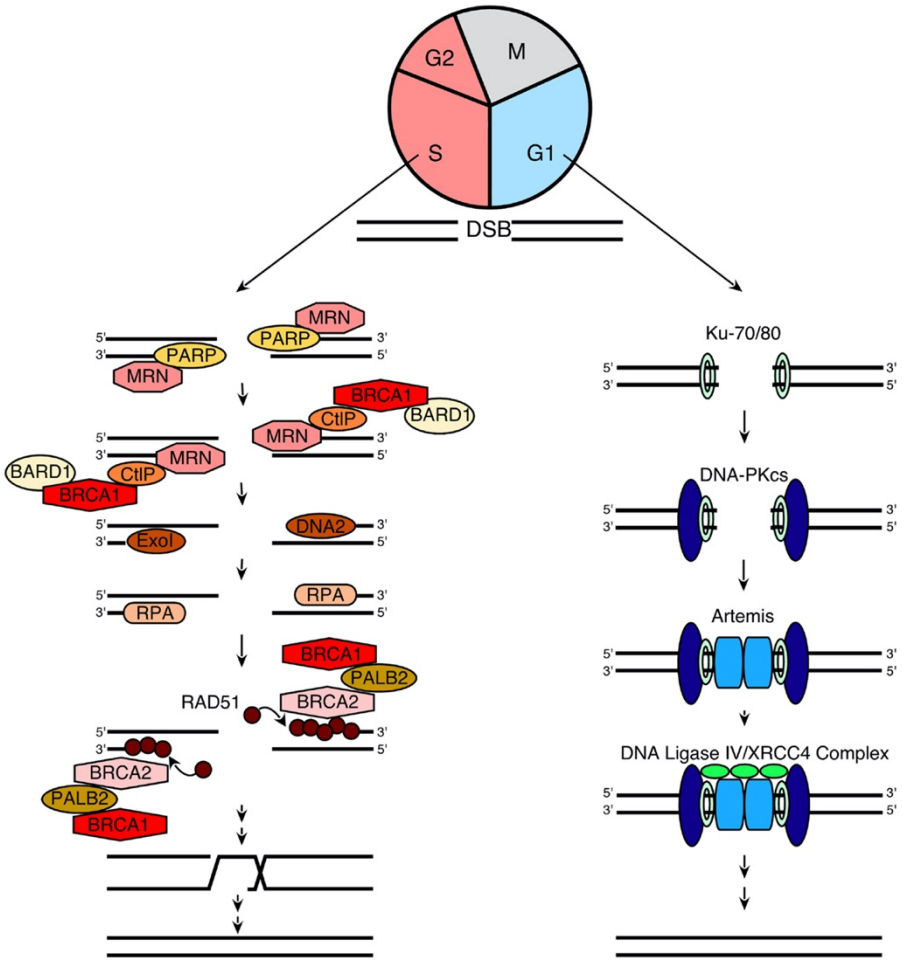

FIGURE 1-1 OVERVIEW OF DSB BREAK RESPONSE AND PATHWAY DECISION. ADAPTED FROM DE LORENZO ET AL. FRONT ONCOL. (2013)

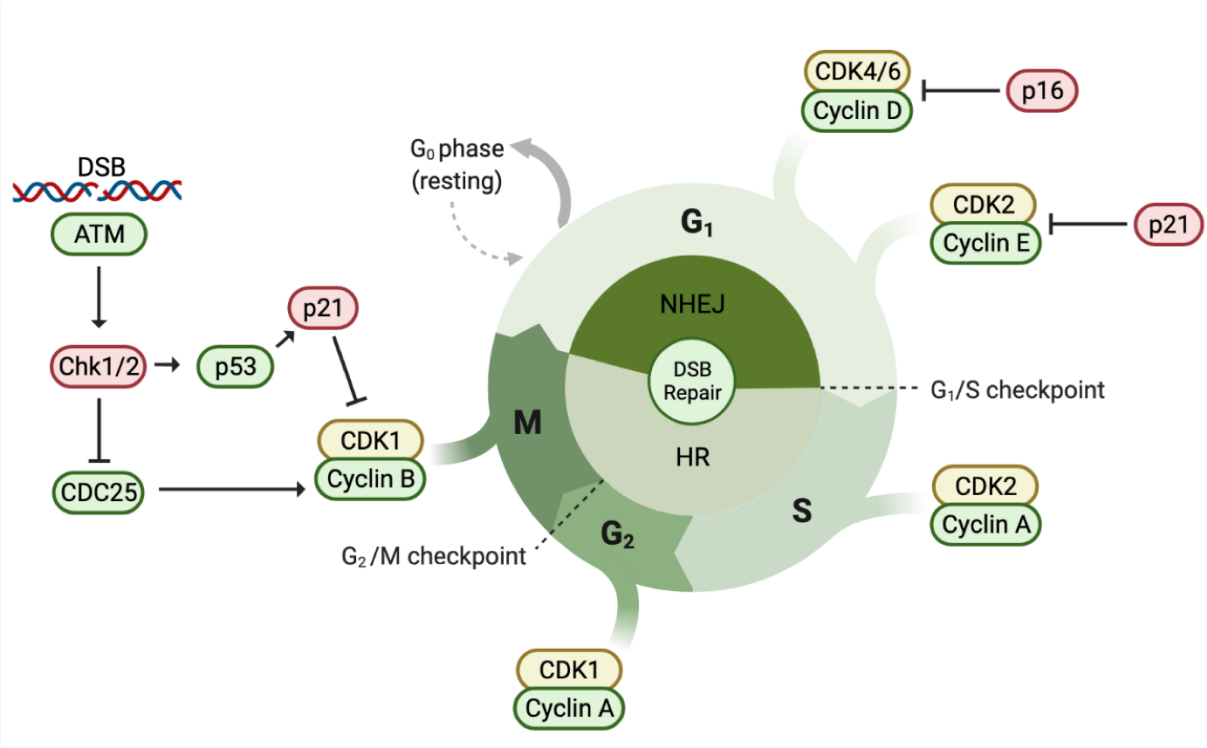

FIGURE 1-2 CDK-CYCLIN REGULATION OF CELL CYCLE AND DNA DAMAGE ASSOCIATED CHECKPOINTS. MADE IN BIORENDER

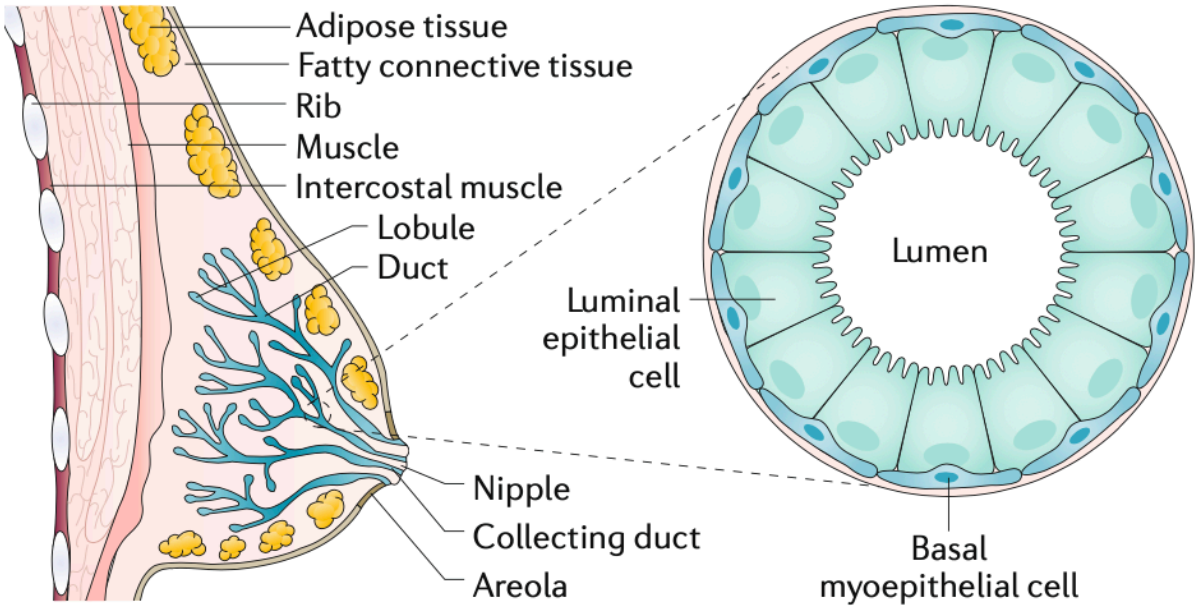

FIGURE 1-3 MAMMARY GLAND ARCHITECTURE AND LUMEN STRUCTURE. ADAPTED FROM HARBECK ET AL. BREAST CANCER. NAT REV DIS PRIMERS. (2019)

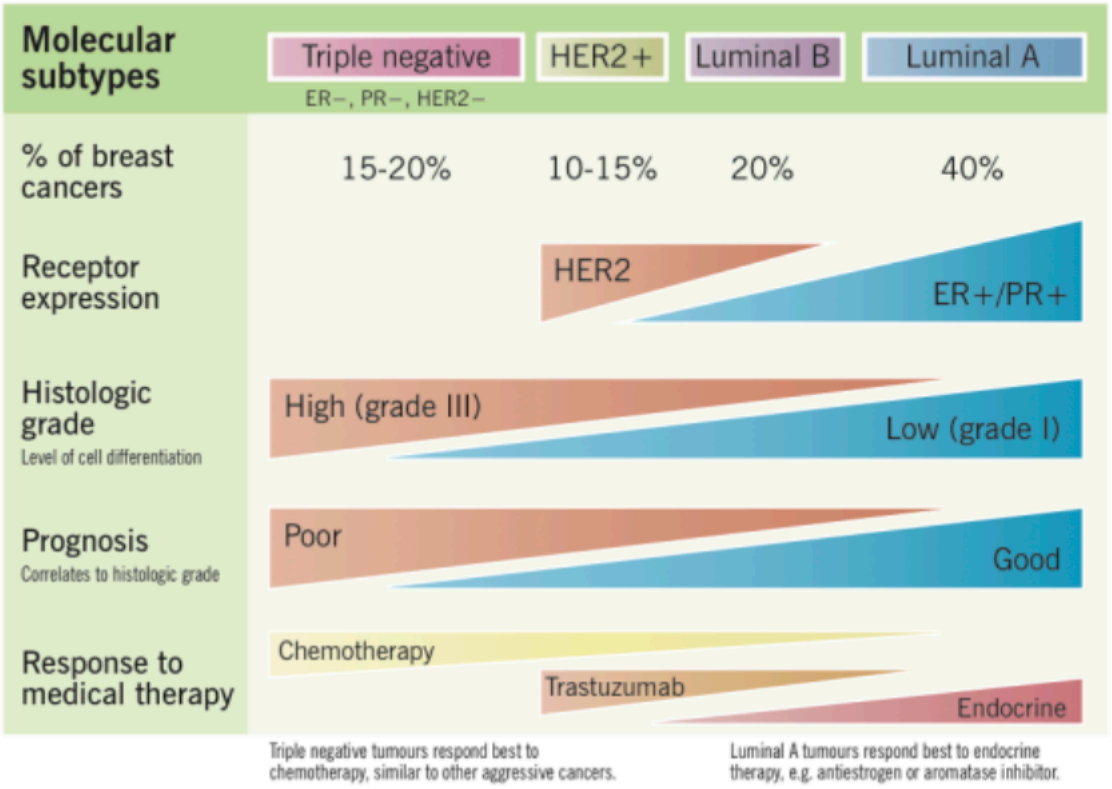

FIGURE 1-4 MOLECULAR SUBTYPES OF BREAST CANCER. ADAPTED FROM WONG ET AL (2012)

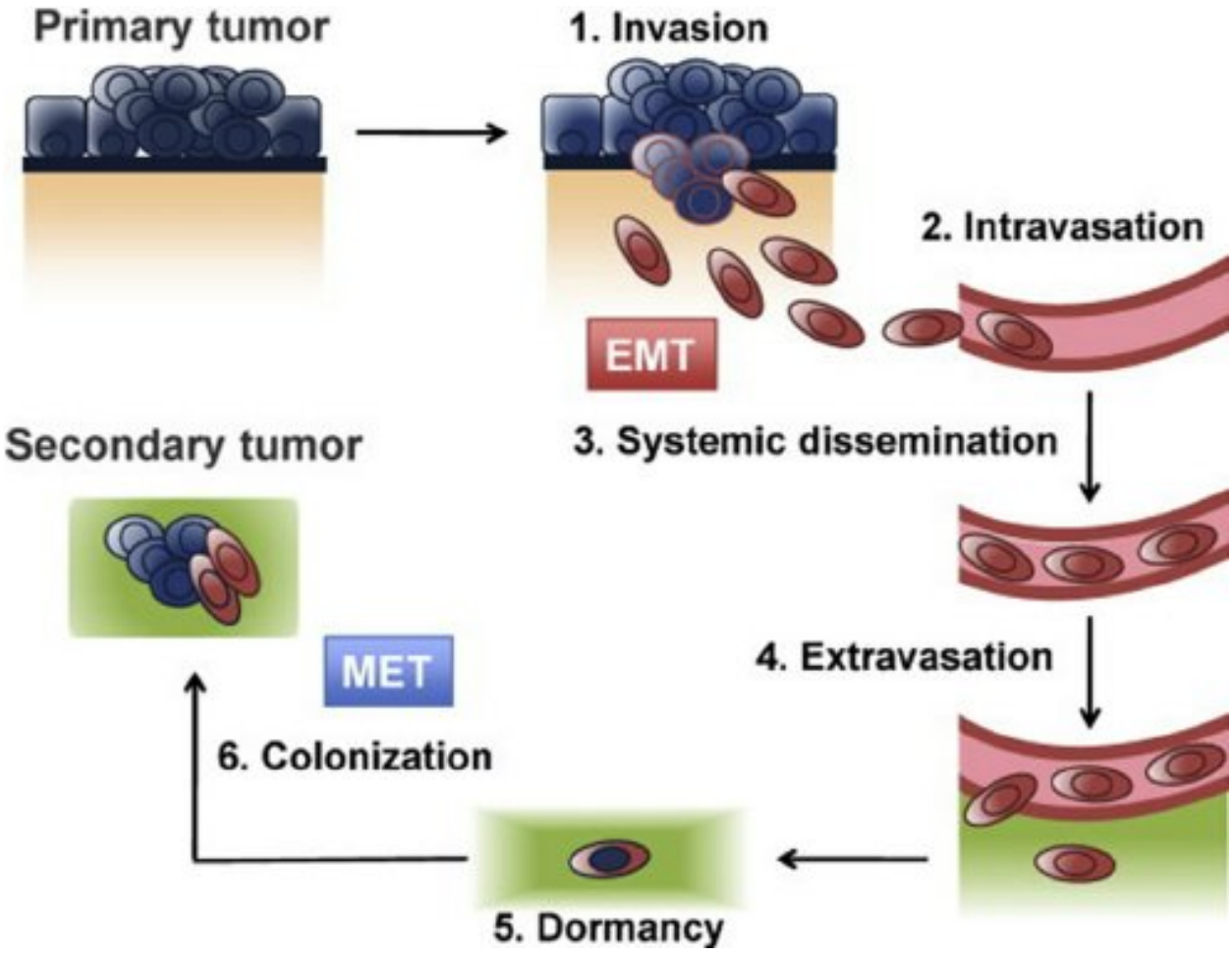

FIGURE 1-5 THE METASTATIC CASCADE, HIGHLIGHTING SPECIFICALLY THE REQUIRED EMT AND MET PROCESSES. ADAPTED FROM BEURAN ET AL. (2015)

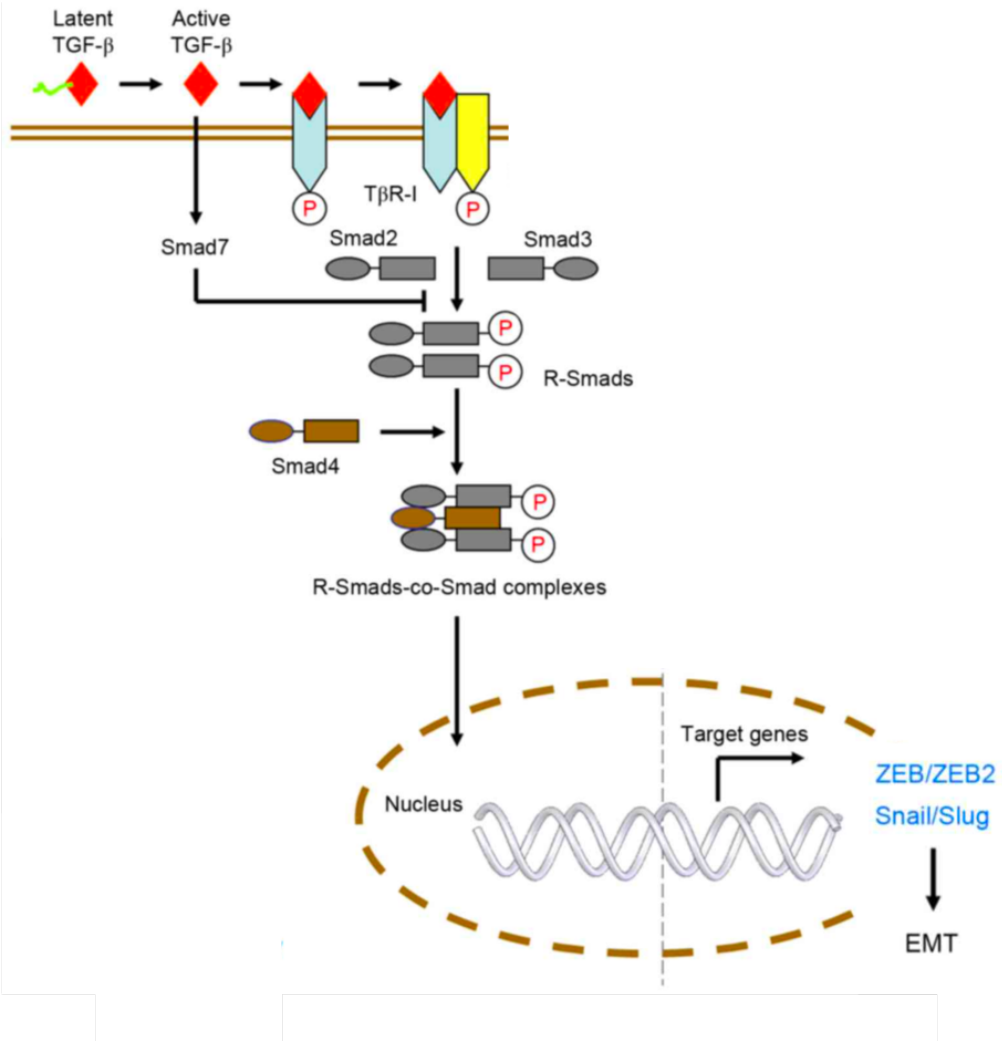

FIGURE 1-6 TGF-Β-TGFBR1/2-SMAD SIGNALLING CASCADE TRIGGERS THE EMT. ADAPTED FROM LIU ET AL. MOL MED REP. (2018)

Chapter 2: POGZ modulates the DNA damage response in a HP1-dependent manner

John Heath, Estelle Simo Cheyou, Steven Findlay, Vincent M Luo, Edgar Pinedo Carpio, Jeesan Lee, Billel Djerir, Xiaoru Chen, Théo Morin, Benjamin Lebeau, Martin Karam, Halil Bagci, Damien Grapton, Josie Ursini-Siegel, Jean-Francois Côté, Michael Witcher, Stéphane Richard, Alexandre Maréchal, and Alexandre Orthwein

2.1 Abstract

The heterochromatin protein HP1 plays a central role in the maintenance of genome stability. However, little is still known about how HP1 is controlled during this process. Here, we describe a novel function of the zinc finger protein POGZ in the regulation of HP1 during the DNA damage response *in vitro*. POGZ depletion delays the resolution of DNA double-strand breaks (DSBs) and sensitizes cells to different DNA damaging agents, including cisplatin and talazoparib. Mechanistically, POGZ promotes homology-directed DNA repair pathways by retaining the BRCA1/BARD1 complex at DSBs, in a HP1-dependent manner. *In vivo* CRISPR inactivation of *Pogz* is embryonically lethal and *Pogz* haplo-insufficiency ($Pogz^{+/\Delta}$) results in a developmental delay, impaired intellectual abilities, a hyperactive behaviour as well as a compromised humoral immune response in mice, recapitulating the main clinical features of the White Sutton syndrome (WHSUS). Importantly, $Pogz^{+/\Delta}$ mice are radiosensitive and accumulate DSBs in diverse tissues, including the spleen and the brain. Altogether, our findings identify POGZ as an important player in homology-directed DNA repair both *in vitro* and *in vivo.*

2.2. Introduction

DNA double-strand breaks (DSBs) are among the most cytotoxic DNA lesions, in part due to their highly recombinogenic and pro-apoptotic potential (Iyama & Wilson, 2013). Inaccurate resolution of DSBs can result in gross genomic rearrangements that drive genomic instability, a characteristic feature of several human genetic disorders and cancer subtypes.[1] To avoid this deleterious outcome, cells have deployed a complex network of proteins that detect and signal these DNA lesions for subsequent repair.[2] Ultimately, two major pathways can be mobilized to repair these DNA lesions: non-homologous end-joining (NHEJ) and homologous recombination (HR).[3] While NHEJ is active throughout the cell cycle, HR is only active in the S/G2 phases, as it requires a sister chromatid as a template for the faithful repair of these DNA lesions. Importantly, several additional elements influence DNA repair pathway choice, including the complexity of the DNA ends and the epigenetic context.[4]

One key step in the "decision-making" process underpinning DNA repair pathway choice relies on the antagonism between 53BP1 and BRCA1.[5] On one hand, 53BP1 relies on both H4K20me^{2}/me^{3} and RNF168-mediated ubiquitination of H2A variants for its recruitment to DSBs.[6–8] On the other hand, BRCA1, which exists as an obligate heterodimer with BARD1, is known to be rapidly recruited to DNA damage sites in a poly-ADP-ribose (PAR)- and ATM-dependent manner.[9–11]Importantly, the identification of BARD1 as a reader of unmethylated histone H4 at lysine 20 (H4K20me^{0})[12], a post-replicative chromatin mark, shed new light on how the BRCA1/BARD1 complex counteracts 53BP1 at sites of DNA damage in the S/G2 phases of the cell cycle [13–17], thereby initiating DNA end resection and favoring homology-directed DNA repair.

Several additional factors can influence the localization of the BRCA1/BARD1 complex.[18] For instance, the rapid accumulation of the heterochromatin protein HP1 at DNA damage sites,[19–23] and the specific recognition of its γ isoform (HP1-γ) by BARD1 through a consensus PxVxL motif[24] have emerged as key pre-requisites for the presence of BRCA1 at DSBs[25], and the commitment towards homology-directed DNA repair.[24,26] Interestingly, the mobilization of HP1 correlates with dynamic waves of H3K9 methylation and

demethylation around these DNA lesions,[27–30] pointing towards a methylation-dependent mobilization of the HP1-BARD1-BRCA1 axis.[26] However, conflicting reports have suggested that HP1 could accumulate at DSBs by interacting with local DNA repair factors through its chromoshadow (CSD) domain,[22,31] thereby eliminating H3K9 methylation as a pre-requisite for the mobilization of the HP1-BARD1-BRCA1 axis. In both models, little is known about how this multiprotein complex is regulated during the DNA damage response and whether any additional factor may control the mobilization of the BRCA1/BARD1 complex to DSBs.

We therefore sought to gain further insight into the contribution of HP1 during genotoxic stress by using a biotin-based labelling approach, called BioID.[32] As mammals encode three distinct isoforms (-α, -β, and -γ), we mapped their respective proximal interactomes under normal and genotoxic stress conditions and identified the POGO transposable element derived with ZNF domain protein (POGZ) as one of the most abundant interactors of the different HP1 isoforms in both conditions, as previously described.[33] POGZ has been implicated in the dissociation of HP1-α from mitotic chromosomes, thereby influencing their proper segregation.[34] Still, its role in the maintenance of genome stability during interphase remains elusive,[35] prompting us to investigate its contribution to the DNA damage response. Interestingly, POGZ depletion delays the resolution of DSBs in S/G2 phases of the cell cycle, which correlates with a prolonged G2 DNA damage checkpoint. Using well-established GFP-based DNA repair assays, we established that POGZ regulates both HR and single-strand annealing (SSA) pathways. Importantly, we noted that POGZ is rapidly recruited to DNA damage sites where it allows the presence of both BRCA1 and BARD1 at DSBs in a HP1-dependent manner. Subsequent *in vivo* analysis demonstrated the critical role of Pogz in murine embryogenesis and *Pogz* haplo-insufficient (*Pogz*$^{+/\Delta}$) mice display a significant growth defect, a deficit in intellectual abilities, a hyperactive behaviour as well as a compromised humoral immune response, recapitulating the main clinical features of the White Sutton syndrome (WHSUS).[36–39] Strikingly, *Pogz*$^{+/\Delta}$ mice are hypersensitive to ionizing radiation (IR) and present constitutive DSBs in several tissues. Furthermore, *Pogz*$^{+/\Delta}$ B-cells have impaired survival capacities following the induction of programmed DSBs *ex vivo*.

Altogether, our data describe a novel role of POGZ in the regulation of homology-directed DNA repair pathways through the HP1-BRCA1-BARD1 axis, with new perspectives for the aetiology of the WHSUS.

2.3. Results

2.3.1. Identification of POGZ as a high confidence interactor of the HP1 isoforms

To gain better insight into the contribution of the different HP1 isoforms during the DNA damage response (Figure 1A), we used the BioID labelling technique, which allows the monitoring of proximal/transient interactions (Figure EV1A) [40]. Briefly, HP1 proteins were fused to a mutant of an *E. coli* biotin-conjugating enzyme (BirA*) and stably expressed in the human embryonic kidney 293 (HEK293) cell line using the Flp-In/T-REX system and validated for their ability to biotinylate proteins that come in close proximity or directly interact with them (Figure EV1B). Labelled proteins were subsequently purified by streptavidin affinity and identified by mass spectrometry. This approach was carried out in cells exposed to the radiomimetic DNA damaging drug neocarzinostatin (NCS) or the solvent control (Ctrl). For each HP1 isoform, we identified ~500 different high-confidence interactors that were common to both experimental conditions (Figure 1B and Figure EV1C). Gene set enrichment analysis (GSEA) demonstrated that proteins involved in cell cycle progression, in particular during M phase, epigenetic regulation of gene expression and DNA repair were commonly found in the interactome of HP1-α, -β and –γ in both Ctrl and NCS-treated conditions (Figure 1C, Figure EV1D and Dataset EV2). As expected, histone variants (HIST1H2BL, HIST3H2BB, H2AFY, H2AFZ), chromatin-associated proteins (CHAF1A, HMGN2), and histone methyltransferases (EHMT1, WIZ) emerged as the most abundant interactors of the different HP1 isoforms in both Ctrl and NCS-treated conditions (Figure 1D). Additionally, we identified POGZ as a high-confidence interactor of the three HP1 isoforms (Figure 1D), which tends to be more biotinylated upon NCS treatment compared to Ctrl conditions (Dataset EV1), particularly with the BirA-HP1-γ construct. This prompted us to investigate whether POGZ functions during the DNA damage response.

2.3.2. POGZ modulates DNA repair *in vitro*

POGZ is a well-documented interactor of both HP1 and REV7/MAD2L2,[33] and its contribution has been described during mitosis, [34] but its role to the maintenance of genome stability in interphase remains elusive.[35] To confirm the HP1-POGZ interaction,

we took advantage of a single-cell assay where the association of two proteins can be assessed at an integrated LacO array by tethering a mCherry-LacR tagged version of a bait of interest (Figure 1E). This approach has been successful in recapitulating both BRCA1-PALB2 and RAD51D-XRCC2 interactions *in cellulo.* [41,42] Targeting a mCherry-LacR-tagged version of POGZ resulted in a significant accumulation of endogenous HP1-α, -β and –γ to the LacO array compared to control conditions (empty vector; EV; Figure 1E and Figure EV1E). To ascertain whether POGZ is relevant for DNA repair, we monitored the presence of DSBs in POGZ-depleted cells using the neutral comet assay.[43] Interestingly, treatment of U2OS cells with two distinct small interfering RNAs (siRNAs) targeting POGZ (siPOGZ-1, and -2) resulted in a substantial increase of DSBs at steady-state (T0) compared to the control condition (siCtrl) (Figure 1F and Figure EV1F-G). Upon exposure to ionizing radiation (IR; 2 Gy), which generated a similar amount of DNA lesions in both siCtrl- and siPOGZ-treated cells (T=1hr), POGZ depletion caused a significant delay in the resolution of these DSBs at late time point (T=24hrs; Figure 1F), suggesting a role for POGZ during DNA repair. In parallel, we monitored the phosphorylation of the histone variant H2AX on serine 139 (γ-H2AX), which is a key step in the initiation of the response to DSBs and their subsequent repair. Using a well-established flow cytometry-based approach,[44] POGZ depletion correlated with persistent phleomycin-induced DSBs (Phleo; 50 μg/mL) in both U2OS and HeLa cells compared to control conditions (siCtrl; Figure 1G and Figure EV1H). Importantly, we noted that this phenotype is associated with a prolonged G2 phase DNA damage checkpoint (Figure 1H), as well as the formation of micronuclei (Figure EV1I-J), pointing towards an important role of POGZ in the maintenance of genome stability during genotoxic stress.

2.3.2. POGZ promotes homology-based DNA repair pathways

To gain further insight into the contribution of POGZ *in vitro,* we generated both shRNA-mediated POGZ-depleted RPE1-hTERT cells (shPOGZ-1 and -2) and CRISPR-mediated POGZ-deleted HeLa cells (POGZΔ-1 and -2) (Figure EV2A). Based on our preliminary data, we hypothesized that depletion of POGZ should correlate with an increased cytotoxicity to DNA damaging agents that produce DSBs. Using the sulforhodamine B

(SRB) assay to determine cell density by measuring cellular protein content,[45] we observed that POGZ-depleted cells were significantly more sensitive to the radiomimetic drug neocarzinostatin (NCS), irrespective of cell type (Figure 2A and Figure EV2B). Similar observations were made with the intercalating agent cisplatin (CIS) and the PARP inhibitor talazoparib (TZ) (Figure EV2B). Importantly, re-expression of a full-length mCherry-POGZ (FL) in POGZ-deleted HeLa cells (POGZΔ-1), ablated this hypersensitivity to both NCS and TZ (Figure 2B and Figure EV2C). Interestingly, dysregulated HR pathway has been linked to the cytotoxic potential of these drugs ([46–48], suggesting a potential contribution of POGZ in this DNA repair pathway.

To directly test this possibility, we employed a well-established GFP-based reporter assay that monitors DNA repair by HR, the DR-GFP assay, and evaluated the impact of POGZ depletion on restoring GFP expression (Figure 2C). As positive controls, we introduced siRNAs targeting key components of the HR pathway: CtIP and RAD51. In both U2OS and HeLa DR-GFP cells, POGZ depletion led to a significant decrease in HR using two distinct siRNAs (Figure 2D). Next, we evaluated whether POGZ could regulate another homology-based DNA repair pathway, SSA, using the SA-GFP assay (Figure 2C). We observed a similar phenotype in the SA-GFP reporter assay, where POGZ depletion resulted in a significant reduction of the GFP signal (Figure 2E), indicative of a reduced SSA efficiency. These results are consistent with a model where POGZ promotes homology-directed DNA repair pathways.

If our model is correct, loss of POGZ should impair the resolution of DSBs in S/G2 phases of the cell cycle, where HR is restricted. We therefore pulse-labelled our cell lines with 5-ethynyl-2'-deoxyuridine (EdU) and monitored the quantity of IR-induced γ-H2AX foci in EdU-positive (EdU+) cells by immunofluorescence. As predicted, the number of γ-H2AX+/EdU+ cells remained significantly higher upon partial (U2OS and RPE1-hTERT cells) or complete loss of POGZ (HeLa cells) at late time points (6 and 24hrs) compared to control conditions (Figure 2F-G, Figure EV2D). As previously observed, this phenotype correlated with a sustained G2-phase cell cycle checkpoint in POGZ-depleted cells upon exposure to IR (Figure EV2E), . Of note, upon exposure to IR, we noted a significantly

larger proportion of apoptotic cells in POGZ-depleted versus control conditions, as monitored by annexin V binding (Figure EV2F). Importantly, upon radiation-induced DNA damage, POGZ-deficient RPE1-hTERT cells likely possess sustained phosphorylation of ATM (Ser1981) and CHK1 (Ser345) (Figure EV3A-B). Interestingly, the lack of a sustained activation of ATR (pATR Ser1989) would suggest that POGZ promotes HR prior to the formation of ssDNA during DNA end resection (Figure EV3A-B). Our data indicate that POGZ plays a pivotal role in regulating both DNA repair by HR and the associated G2 DNA damage checkpoint, thereby modulating permanent cell fate such as apoptosis.

2.3.3. POGZ facilitates the accumulation of BRCA1 at DSBs

To pinpoint at which step(s) POGZ is regulating HR-mediated DNA repair, we monitored the impact of its depletion on the recruitment of well-established DSB signaling factors. Here, we used the LacO-LacR system where we expressed a mCherry-LacR-tagged version of the endonuclease FokI, allowing the formation of localized DSBs and the visualization of DNA repair factors at the LacO repeat by immunofluorescence.[49] As expected, we did not observe any significant impact on the recruitment of 53BP1 and RIF1 to FokI-induced DSBs upon depletion of POGZ (siPOGZ-1 and -2; Figure 3A and Figure EV3C). However, under the same conditions, the presence of BRCA1 and RAD51 at DSBs was significantly impaired (Figure 3A and Figure EV3C). In fact, we made similar observations when we monitored the formation of IR-induced BRCA1 foci in cells pulsed with EdU (Figure 3B-C), pointing towards a key role of POGZ in regulating BRCA1 accumulation at DNA damage sites.

POGZ is a 1410 amino-acid protein with multiple functional domains (Figure 3D): one atypical and 8 classical C_2H_2 zinc finger domains at its N-terminus, a proline-rich domain, a helix-turn-helix domain also identified as a centromere protein (CENP) B-like DNA binding domain, a putative DDE-1 transposase domain and a coiled-coil motif at its C-terminus. POGZ has been proposed to act as a negative regulator of gene expression in different biological processes, including hematopoiesis and neuronal development.[50–52] To exclude the possibility that POGZ may indirectly control DNA repair through its known

transcriptional function, we profiled by quantitative RT-PCR (qPCR) the expression of BRCA1 and BARD1 as well as downstream effectors in the HR pathway, including PALB2, BRCA2 and RAD51. However, we did not notice any substantial changes in their expression upon depletion of POGZ in both HeLa and RPE1-hTERT cells (Figure EV3D). We therefore explored the possibility that POGZ may have a more direct contribution to DNA repair by monitoring its recruitment to DNA damage sites. Interestingly, we observed that HA-tagged POGZ rapidly accumulates at laser micro-irradiation-induced DNA damage in U2OS cells, co-localizing with γ-H2AX (Figure EV3E). This recruitment is a transient event and POGZ accumulation disappears within 30 min after laser micro-irradiation, a dynamic reminiscent of what has been observed with HP1.[19,21,22,31]

2.3.4. POGZ allows the presence of the HP1-γ/BARD1/BRCA1 complex at DSBs

HP1 is a well-established factor in the response to DSBs[53] at least, in part through the retention of BRCA1 at DNA damage sites by HP1-γ.[26] We confirmed these observations in the U2OS mCherry-LacR-FokI cells where depletion of HP1-γ, but neither HP1-α or -β significantly impaired the accumulation of BRCA1 at the focal DNA damage site (Figure 3E and Figure EV4A-B, top panel). If POGZ facilitates BRCA1 retention at DSBs in a HP1-γ-dependent manner, co-depletion of both POGZ and HP1-γ should not impair further BRCA1 accumulation at DSBs any further. Indeed, we did not notice any significant decrease in the retention of BRCA1 in this condition compared to either HP1-γ or POGZ depletion alone (Figure 3E and Figure EV4A-B, bottom panel). Similar observations were made in the DR-GFP assay where co-depletion of both POGZ and HP1–γ did not further decrease HR-mediated DNA repair compared to the individual HP1–γ or POGZ depletion in the U2OS cell line (Figure 3F). Interestingly, POGZ depletion significantly impaired the recruitment of all HP1 isoforms to FokI-induced DSBs; however, we noted that it had the most drastic impact on HP1-γ (Figure 3G and Figure EV4C), pointing towards a model where POGZ promotes HR by allowing the accumulation of BRCA1 at DSBs in an HP1-γ-dependent manner.

To gain further insight into how POGZ promotes DNA repair, we performed a structure-function analysis by generating several truncation mutants (Figure 4A). First, we tested their sub-cellular localization by expressing a mCherry-tagged version of these mutants in HEK293T cells. Mutants lacking the proline-rich domain (amino acids 800-848; ΔHP1), which mediates HP1 binding,[34] were unable to accumulate in the nucleus (Figure EV4D), confirming a previous report linking the nuclear accumulation of POGZ to its ability to bind to HP1.[51] We first focused our attention on the POGZ$^{366-848}$ mutant, which contains the zinc finger region of POGZ as well as its HP1 binding domain and retains the capacity to localize to the nucleus (Figure EV4D). We expressed a Flag-tagged version in this mutant in POGZ-depleted U2OS cells containing the inducible LacR-FokI system and monitored its ability to restore BRCA1 recruitment to DSBs. Strikingly, POGZ$^{366-848}$ mutant restored BRCA1 accumulation to localized DSBs, at a level comparable to full-length (FL) POGZ (Figure 4B and Figure EV4E, left panel). Interestingly, this mutant allowed the recruitment of both BARD1 and HP1-γ to the localized DNA damage site (Figure 4B and Figure EV4E, right panel). To further dissect the critical domain(s) of POGZ promoting DNA repair, we generated a construct exclusively containing the HP1 binding domain (HPZ) and expressed it in HeLa POGZΔ cells. We pulse-labelled these cells with EdU and monitored their capacity to form IR-induced BRCA1 foci by immunofluorescence. Remarkably, the POGZ HPZ mutant restored BRCA1 foci in POGZ-deleted HeLa cells, to a similar extent as FL POGZ (FL; Figure 4C-D). Critically, we observed that HPZ-expressing cells display significantly less IR-induced γ-H2AX foci over time, compared to HeLa POGZΔ cells (Figure 4E-F and Figure EV4F), suggesting that this construct is able to restore DSB resolution. In light of these data, we conclude that the HP1 binding domain of POGZ is necessary and sufficient to promote BRCA1 recruitment to DSBs and HR-mediated DNA repair, primarily through HP1-γ.

2.3.5. Loss of *Pogz* impairs proper murine development *in vivo*

Heterozygous pathogenic variants in *POGZ* have been linked to a rare human disorder, known as the White-Sutton syndrome (WHSUS), characterized by craniofacial abnormalities such as microcephaly, a developmental delay, intellectual disabilities as

well as behavioural problems (e.g. hyperactivity, overly friendly behaviour), and in certain rare cases, recurrent infections.[36–39] These observations prompted us to define the relevance of POGZ *in vivo.*

Using the CRISPR/Cas9 technology, we targeted exons 9 and 10 of *Pogz* in embryonic stem (ES) cells derived from C57BL/6J mice in order to generate a *Pogz* knock-out mouse model (Figure 5A). Remarkably, we failed to obtain any viable constitutive *Pogz* knockout mice ($Pogz^{\Delta/\Delta}$) (Figure 5B). However, we were successful in deriving mouse embryonic fibroblasts (MEFs) from E12.5 embryos where we confirmed that CRISPR-mediated targeting of one or both alleles of *Pogz* resulted in its partial or complete ablation at the protein level, respectively (Figure 5C). Upon more systematic analysis, homozygous *Pogz* knock-out embryos died mid-gestation, starting between embryonic day E12.5 and E14.5 (Figure 5D), suggesting that *Pogz* is essential for mouse embryonic development. As heterozygous pathogenic mutations in *POGZ* lead to the WHSUS, we decided to investigate whether *Pogz* haplo-insufficiency ($Pogz^{+/\Delta}$) may have an overall impact on murine development. Indeed, $Pogz^{+/\Delta}$ mice have a significantly lower body weight compared to their wild-type counterparts as early as 3 weeks post-birth (Figure 5E). This growth defect correlated with smaller organs in $Pogz^{+/\Delta}$ mice, including the thymus, the spleen, the liver and the brain (Figure 5F), suggesting that Pogz levels need to be tightly regulated to allow proper murine development.

As microcephaly often correlates with impaired cognitive functions,[54] we performed a systematic behavioral analysis of our mouse model. Using the open field maze test, we noticed that $Pogz^{+/\Delta}$ mice have significantly more locomotor activity, with a substantially greater average speed, than their age-matched wild-type littermates (Figure 5G-H), indicative of a hyperactive behavior. Furthermore, *Pogz* haplo-insufficient mice spent more time in the center of the arena (inner zone of the maze), which is typically linked to a decreased level of anxiety (Figure 5G-I). To assess the intellectual capabilities of our $Pogz^{+/\Delta}$ mice, we performed a contextual and cued fear conditioning test (Figure 5J). In this procedure, a neutral conditioned stimulus (i.e. steady tone) is paired with an aversive unconditioned stimulus (mild foot shock) and the time during which animals present a lack

of mobility or reduced locomotor activity is a readout of learning/memory performances. Interestingly, *Pogz* haplo-insufficient mice exhibited decreased freezing behavior compared to control mice, in which the baseline behavior remains comparable (Figure 5K), indicative of a deficit in contextual learning and memory capacities.

Severe cases of the WHSUS are characterized by recurrent infections,[51] likely due to a dysfunctional immune system. For instance, reduced lymphoid organ weight, as observed in *Pogz*$^{+/\Delta}$ mice (Thymus, Spleen; Figure 5F), may be indicative of a compromised immune system. We evaluated whether *Pogz* haplo-insufficient mice have a compromised humoral immune response by measuring total immunoglobin (Ig) levels of IgM, IgG1, IgG2b, IgG3 and IgA in the serum. Interestingly, we found that serum IgG2b levels were almost 50% lower in *Pogz*$^{+/\Delta}$ mice compared to age-matched wild-type controls (Figure 5L), indicative of a defective antibody response. Importantly, patients with a selective IgG2 subclass deficiency usually suffer from recurrent upper and lower respiratory tract infections [55]which have also been reported in severe cases of WHSUS.[51] Altogether, our data indicate that *Pogz* haplo-insufficient mice present a developmental delay, a deficit in intellectual abilities, a hyperactive behaviour as well as a compromised humoral immune response, reminiscent of the clinical features reported in WHSUS patients.

2.3.5. *Pogz* haplo-insufficient mice display features of genomic instability

In light of our findings *in vitro*, we wondered whether *Pogz*$^{+/\Delta}$ mice present any DNA repair defect. To test this hypothesis, we exposed mice to IR (8 Gy) and monitored their survival over time. Interestingly, IR-induced mortality occurred significantly faster in *Pogz*$^{+/\Delta}$ mice than in wild-type controls (median survival: 7 days vs. 11 days; Figure 6A), suggesting that Pogz may also be relevant to promote DNA repair *in vivo*. We therefore tested whether *Pogz*$^{+/\Delta}$ mice spontaneously accumulate DSBs by monitoring both γ-H2AX levels and intensity in the spleen by flow cytometry. Strikingly, we observed significantly more γ-H2AX-positive splenocytes in *Pogz*$^{+/\Delta}$ mice compared to controls (WT; Figure 6B and Figure EV5A), and they display substantiality more γ-H2AX signal intensity than wild-type

(Figure 6B and Figure EV5A). We extended our analysis to the brain, where we stained sections of the cerebral cortex for γ-H2AX (Figure 6C and Figure EV5B). Again, we noted substantially more γ-H2AX-positive cells in *Pogz*$^{+/\Delta}$ mice vs. wild-type in this region of the brain (Figure 6C and Figure EV5B), pointing towards a global DNA repair defect *in vivo*.

To validate our observations *in vivo*, we took advantage of MEFs that we derived from our mouse model (Figure 5D) and we tested their sensitivity to two distinct DNA damaging drugs, phleomycin and camptothecin. As expected, *Pogz*$^{+/\Delta}$ MEFs were hypersensitive to both drugs compared to wild-type in the SRB assay (Figure 6D and Figure EV5C), confirming that partial loss of Pogz impairs DNA repair. *Ex vivo* stimulation of B-cells is another well-established system where the integrity of DNA repair pathways can be examined. Importantly, intact DNA repair pathways are required for the resolution of activation-induced deaminase (AID)-induced DSBs during class switch recombination (CSR; Figure EV5D). We therefore extracted primary splenic B-cells from both WT and *Pogz*$^{+/\Delta}$ mice and activated them *ex vivo* with a cocktail of cytokines (IL-4/LPS) to induce class switching from IgM to IgG1. Interestingly, we noted that partial loss of *Pogz* significantly impaired CSR at both 96h and 120h post-activation (Figure 6E and Figure EV5E). Importantly, we confirmed that this phenotype was neither due to a proliferation defect (Figure EV5F), nor a lack of *Aicda* expression (Figure EV5G). As expected, we observed a significant reduction (~50%) of *Pogz* mRNA expression in *Pogz*$^{+/\Delta}$ mice compared to wild-type (Figure EV5G). Successful CSR relies on the capacity to resolve on-target DSBs by NHEJ and alternative end-joining (a-EJ) pathways in G1 phase of the cell cycle (Figure EV5D).[56] However, a functional HR pathway has been shown to be important in the repair of both on- and off-target DSBs, thereby promoting B-cell survival (Figure EV5D).[57] Based on our data *in vitro*, we wondered whether *Pogz*$^{+/\Delta}$ B-cells attempting CSR might be more prone to apoptosis, explaining the apparent deficit of CSR. In fact, we observed a substantial increase in the proportion of Annexin V-positive *Pogz*$^{+/\Delta}$ B-cells compared to control conditions upon activation with a cocktail of cytokines (Figure 6F and Figure EV5H). Of note, a significant fraction of non-activated (NA) *Pogz*$^{+/\Delta}$ B-cells were Annexin V-positive (Figure 5F), likely linked to the γ-H2AX signal that we observed previously in splenocytes (Figure 6B and Figure EV5A). If our model is right,

Pogz$^{+/\Delta}$ B-cells should accumulate a significant amount of DSBs upon induction of CSR. We therefore monitored γ-H2AX levels by flow cytometry and we noted that a significant increase in the proportion of γ-H2AX-positive *Pogz*$^{+/\Delta}$ B-cells compared to wild-type at 48h and 72h post-activation (Figure 6G). We also monitored the number of γ-H2AX foci/cell in both wild-type and *Pogz*$^{+/\Delta}$ B-cells upon induction of CSR. As expected, B-cell activation resulted in a significant increase in the proportion of cells displaying γ-H2AX foci (Figure EV5I). Interestingly, around half of these activated B-cells contain more than 2 γ-H2AX foci in a haplo-insufficient background compared to ~25% in a wild-type context (Figure 6H and Figure EV5J-K), suggesting that Pogz is critical for the repair of off-target DSBs during CSR. Altogether, our data are consistent with a model where POGZ promotes the repair of DSBs by homology-directed DNA repair pathways both *in vitro* and *in vivo*.

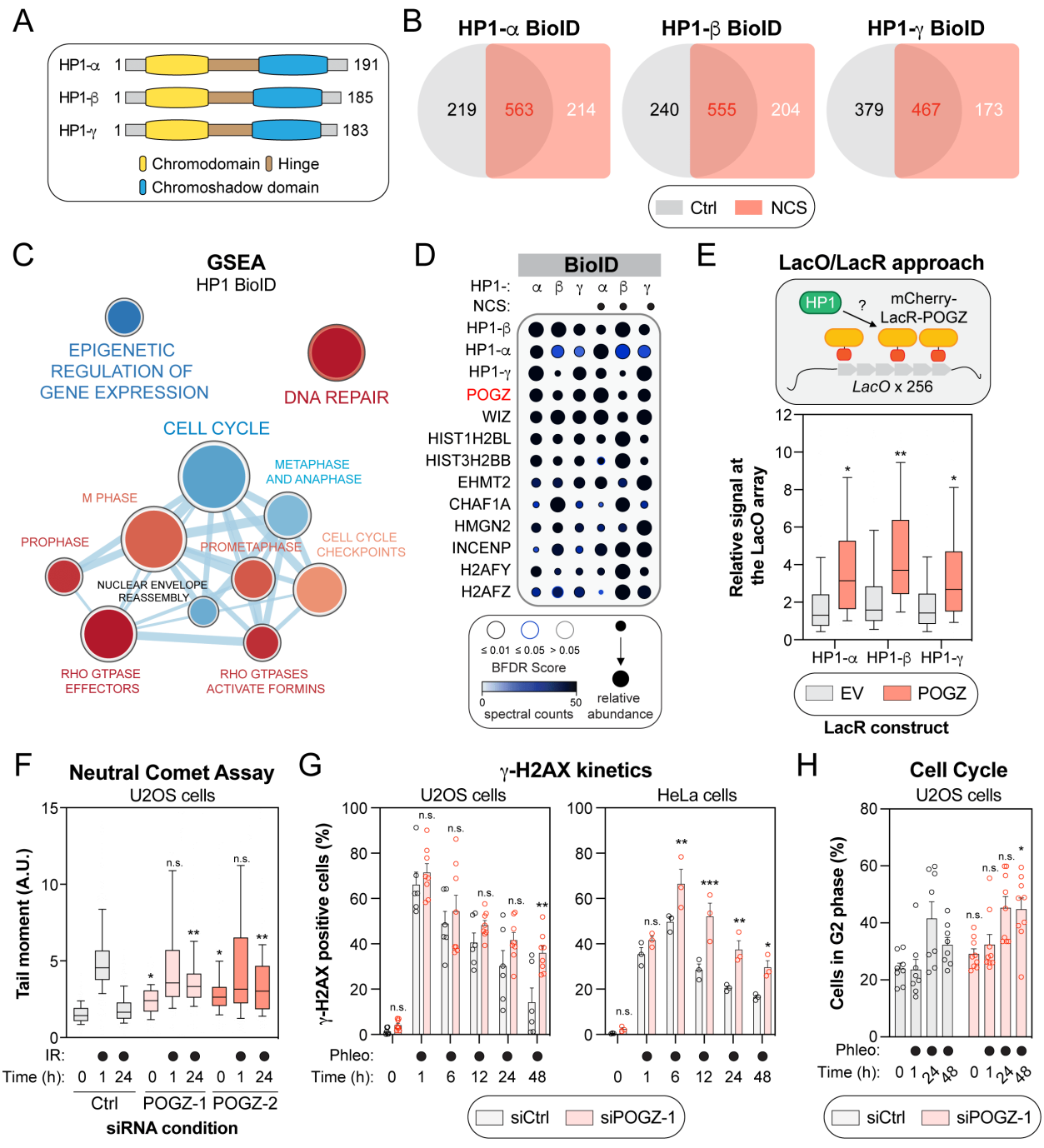

FIGURE 2- 1 THE HP1-INTERACTING PROTEIN POGZ PARTICIPATES IN DNA REPAIR.

Figure 1. The HP1-interacting protein POGZ participates in DNA repair.

(A) Schematic of the 3 human isoforms of the heterochromatin protein 1 (HP1). The N-terminal chromodomain of HP1 (in yellow) recognizes H3K9 methylation *in vitro*, with a preference for higher methylation states ($H3K9me^1$>$H3K9me^2$>$H3K9me^3$), while the chromoshadow domain at its C-terminus (in blue) is involved in homo-/hetero-dimerization as well as interaction with other proteins containing a PXVXL motif. Both domains are separated by a hinge region (in brown). (B) Venn diagram outlining the distribution of HP1-α, -β and -γ high-confidence interactors identified by the BioID approach, under control (Ctrl; DMSO) or genotoxic conditions (NCS). (C) Gene set enrichment analysis (GSEA) visualization of the common HP1 high-confidence interactors using Reactome pathways. Enrichment maps were developed2 with a ranked interaction network ($p < 0.2$, FDR < 0.5 and overlap coefficient = 0.75) and the cell cycle cluster is provided in this panel. The complete interaction network can be found in Expanded View Fig.1D. Pathways enriched in: *(i)* control conditions are represented in blue; *(ii)* NCS-treated conditions are represented in red. (D) Dot plot of selected HP1 high-confidence interactors identified by BioID. The node size displays the relative abundance of a given prey across the 6 conditions analyzed, the node color represents the absolute spectral count sum (capped at 50 for display purposes), and the node edge color corresponds to the Bayesian False Discovery Rate (BFDR). Proteins were selected based on a SAINT score of > 0.95, BFDR of < 0.05, and ≥ 10 peptide count. (E) Schematic representing the LacO/LacR tethering system in U2OS cells (top panel). Box Quantification of the endogenous HP1 signal at the mCherry focus upon expression and tethering of mCherry-LacR alone (EV) or a construct containing POGZ. Data are represented as a box-and-whisker (10-90 percentile; bottom panel). At least 100 cells per condition were counted. Significance was determined by one-way ANOVA followed by a Tukey test. **P<0.05*, ***P<0.0001*. (F) U2OS cells containing a non-targeting siRNA control (Ctrl), or one of two siRNA(s) against human POGZ (POGZ-1 or -2), were irradiated with 2 Gy before being collected at the indicated time points and assessed for comet tail migration in neutral conditions. Quantification of the neutral comet assay is represented as a box-and-whisker (10-90 percentile). At least 100 cells per condition were counted. Significance was determined by two-way ANOVA followed by a Dunnett's test. **P<0.05*, ***P<0.0001*. (G) U2OS (left panel, n=6 biological replicates) or HeLa cells (right panel, n = 3 biological replicates) were transfected with the indicated siRNA; 48 hours post-transfection, they were treated with the radiomimetic antibiotic, phleomycin (50 μg/mL), and collected at the indicated time points. Flow cytometry analysis of phosphorylated—H2AX signal was used to measure γ-H2AX endogenous signal. Data are represented as a bar graph showing the mean ± SEM, each replicate being represented by a round symbol. Significance was determined by two-way ANOVA followed by a Holm-Sidak's test. **P<0.05*, ***P<0.01*, ****P<0.0005.* (H) U2OS (n=8 biological replicates) were transfected with the indicated siRNA; 48 hours post-transfection, they were treated with the radiomimetic antibiotic, phleomycin (50 μg/mL), and collected at the indicated time points. Data are represented as a bar graph showing the mean ± SEM, each replicate being representing as a round symbol. Significance was determined by two-way ANOVA followed by a Sidak's test. **P<0.05*.

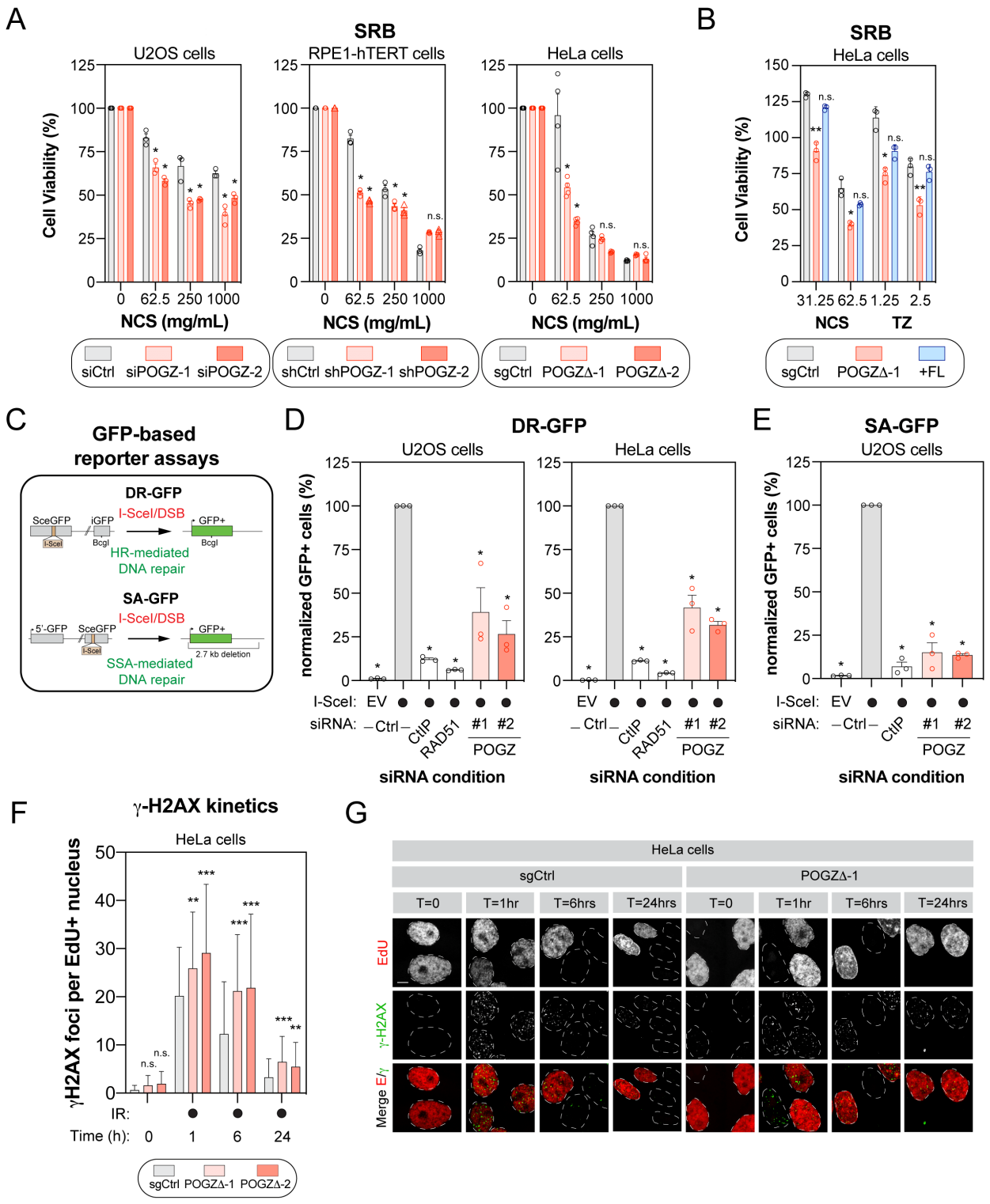

FIGURE 2- 2 POGZ PROMOTES HOMOLOGY-DIRECTED DNA REPAIR PATHWAYS

Figure 2. POGZ promotes homology-directed DNA repair pathways

(A) U2OS (left panel), RPE1-hTERT (middle panel), and HeLa cells (right panel) were monitored for their sensitivity to the radiomimetic drug NCS using the SRB assay. For each cell line, the following conditions were used: U2OS cells were transfected with a nontargeting siRNA (siCtrl) or an siRNA targeting human POGZ (siPOGZ-1 or -2); RPE1-hTERT cells were transduced a control shRNA (shCtrl) or a shRNA directed against human POGZ (shPOGZ-1 or -2); HeLa cells expressing a non-targeting sgRNA (sgCtrl) or a sgRNA targeting human POGZ and sub-cloned (POGZΔ-1 or -2). Cells were pulsed with NCS at the indicated concentrations for 1 hour, replenished with fresh medium and incubated for 4 days before being processed for SRB assays. Data are represented as a bar graph showing the relative mean $\pm$ SEM, each replicate being representing as a round symbol (3 biological replicates). Significance was determined by two-way ANOVA followed by a Bonferroni's test. *$P<0.01$. (B) HeLa cells with (+FL, blue), or without full length POGZ-cDNA supplementation (POGZΔ-1, red), as well as control HeLa cells (sgCtrl, grey), were treated with NCS (1hr) or TZ (24h) at the indicated concentrations and processed as in (A) for SRB assay. Data are represented as a bar graph showing the relative mean $\pm$ SEM, each replicate being representing as a round symbol (3 biological replicates). Significance was determined by two-way ANOVA followed by a Bonferroni's test. *$P<0.05$, **$P<0.005$. (C) Schematic diagram of the DR-GFP (top panel) and the SA-GFP (bottom panel) assays. (D) U2OS (left panel) and HeLa (right panel) cells containing the DR-GFP reporter construct were transfected with the indicated siRNA. 24h post-transfection. Cells were transfected with the I-SceI expression plasmid or an empty vector (EV), and the GFP+ population was analyzed 48h post-plasmid transfection. The percentage of GFP+ cells was determined for each individual condition and subsequently normalized to the non-targeting condition provided with I-SceI (siCtrl, I-SceI). Data are represented as the mean $\pm$ SEM, each replicate being representing as a round symbol (n=3 biological replicates). Significance was determined by one-way ANOVA followed by a Dunnett's test. *$P\leq0.0001$. (E) U2OS cells containing the SA-GFP reporter plasmid were processed and analyzed as in (D). Data are represented as the mean $\pm$ SEM, each replicate being representing as a round symbol (n=3 biological replicates). Significance was determined by one-way ANOVA followed by a Dunnett's test. *$P\leq0.0001$. (F) Quantification of γ-H2AX foci in HeLa cells where POGZ has been targeted by CRISPR technology (POGZΔ-1 or -2) and in control HeLa cells (sgCtrl). Cells were exposed to 1 Gy before being pulsed with Edu for 1hr and were recovered at the indicated time points. Cells were fixed, stained, and imaged via confocal microscopy. Data are the total number of γ-H2AX foci in EdU+ cells and represented as a bar graph showing the mean $\pm$ SD (n = 3 biological replicates, with at least 100 cells analyzed for each time point). Significance was determined by two-way ANOVA followed by a Dunnett's test. *$P<0.05$, **$P<0.0005$. (G) Representative images used for quantification in (F). Scale bar = 5 μm.

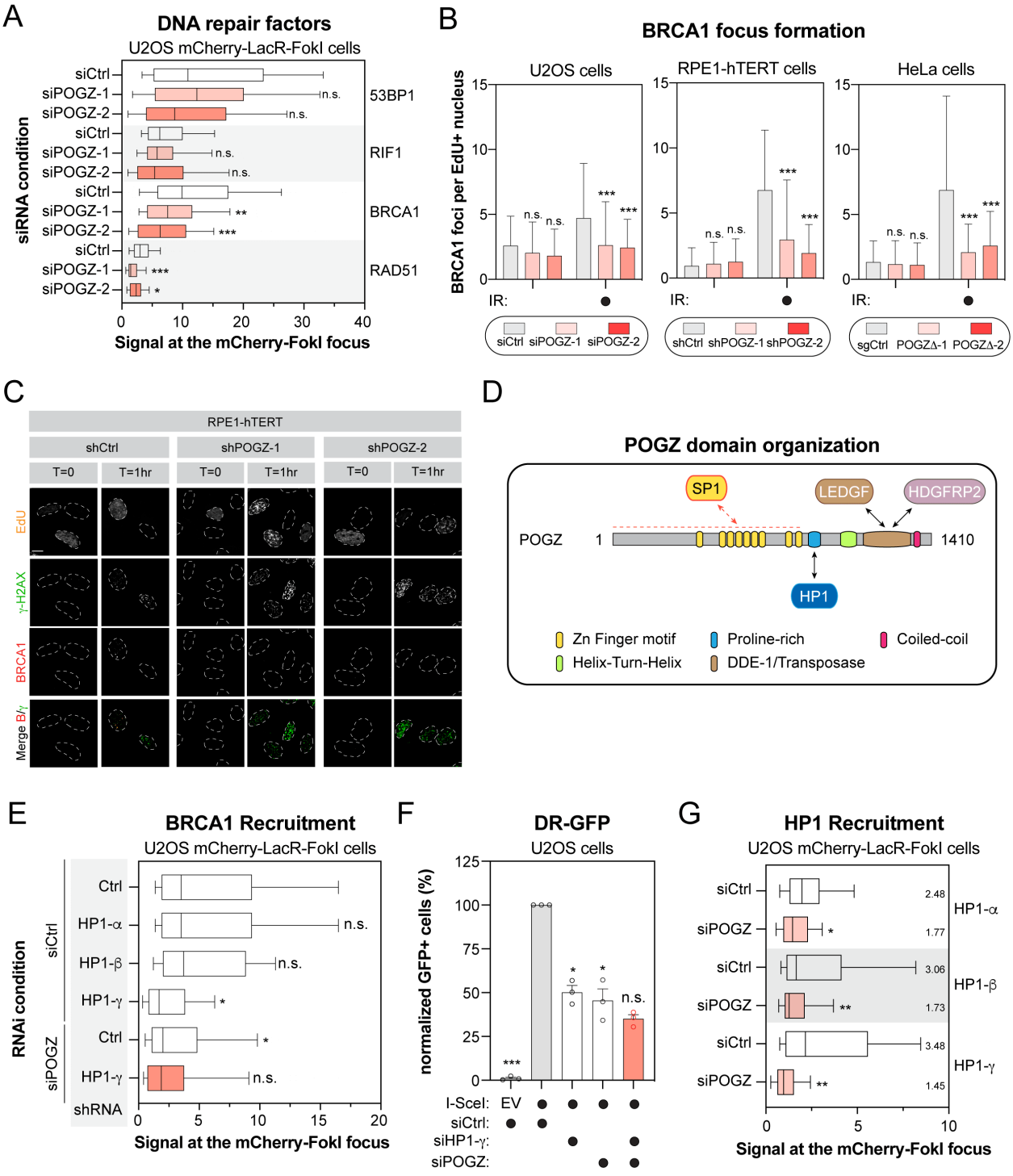

FIGURE 2- 3 POGZ MODULATES THE PRESENCE OF BRCA1 AT DNA DAMAGE SITES.

Figure 3. POGZ modulates the presence of BRCA1 at DNA damage sites.

(A) U2OS stably expressing mCherry-LacR-FokI were transfected with the indicated siRNA. 24h post-transfection, DNA damage was induced using Shield1 and 4-OHT. Immunofluorescence against the indicated DNA repair proteins was subsequently performed to monitor their accumulation at sites of DNA damage by confocal microscopy. Data are represented as a box-and-whisker (10-90 percentile) where the fluorescent signal at the mCherry focus was normalized to nuclear background. At least 100 cells per condition were counted (n=3 biological replicates). Significance was determined by two-way ANOVA followed by a Dunnett's test. *$P<0.05$, **$P<0.005$, **$P\leq0.0005$. (B) U2OS (left panel), RPE1-hTERT (middle panel), and HeLa cells (right panel) were monitored for their capacity to form IR-induced BRCA1 foci. For each cell line, the following conditions were used: U2OS cells were transfected with a nontargeting siRNA (siCtrl) or an siRNA targeting human POGZ (siPOGZ-1 or -2); RPE1-hTERT cells were transduced a control shRNA (shCtrl) or a shRNA directed against human POGZ (shPOGZ-1 or -2); HeLa cells were expressing a non-targeting sgRNA (sgCtrl) or a sgRNA targeting human POGZ and sub-cloned (POGZΔ-1 or -2). Cells were exposed to 1 Gy before being pulsed with Edu for 1hr and were recovered 1h post-exposure to IR. Cells were fixed, stained, and imaged via confocal microscopy. Data are the total number of BRCA1 foci in EdU+ cells and represented as a bar graph showing the mean $\pm$ SD (n = 3 biological replicates, with at least 100 cells analyzed for each time point). Significance was determined by two-way ANOVA followed by a Dunnett's test. *$P<0.005$, **$P<0.001$. (C) Representative images used for quantification in (B). Scale bar = 5 μm. (D) Schematic diagram outlining the different domains of human POGZ. Each structural domain and interacting partners are indicated. (E) U2OS stably expressing mCherry-LacR-FokI were transduced with the indicated shRNA and subsequently transfected with the indicated siRNA. 24h post-transfection, DNA damage was induced using Shield-1 and 4-OHT. Immunofluorescence against BRCA1 was subsequently performed to monitor its accumulation at sites of DNA damage by confocal microscopy. Data are represented as a box-and-whisker (10-90 percentile) where the fluorescent signal at the mCherry focus was normalized to nuclear background. At least 50 cells per condition were counted. Significance was determined by two-way ANOVA followed by a Dunnett's test. *$P<0.0001$. (F) U2OS cells containing the DR-GFP reporter construct were transfected with the indicated siRNA. 24h post-transfection. Cells were transfected with the I-SceI expression plasmid or an empty vector (EV), and the GFP+ population was analyzed 48h post-plasmid transfection. The percentage of GFP+ cells was determined for each individual condition and subsequently normalized to the non-targeting condition provided with I-SceI (siCtrl, I-SceI). Data are represented as a bar graph showing the relative mean $\pm$ SEM, each replicate being representing as a round symbol (n=3 biological replicates). Significance was determined by one-way ANOVA followed by a Dunnett's test. *$P\leq0.0001$. (G) U2OS stably expressing mCherry-LacR-FokI were transduced with the indicated siRNA. 24h post-transfection, DNA damage was induced using Shield-1 and 4-OHT. Immunofluorescence against the indicated HP1 isoform was subsequently performed to monitor its respective accumulation at sites of DNA damage by confocal microscopy. Data are represented as a box-and-whisker (10-90 percentile) where the fluorescent signal at the mCherry focus was normalized to nuclear background. At least 75 cells per condition were counted.

Significance was determined by two-way ANOVA followed by a Dunnett's test. *$P<0.005$, **$P<0.0001$.

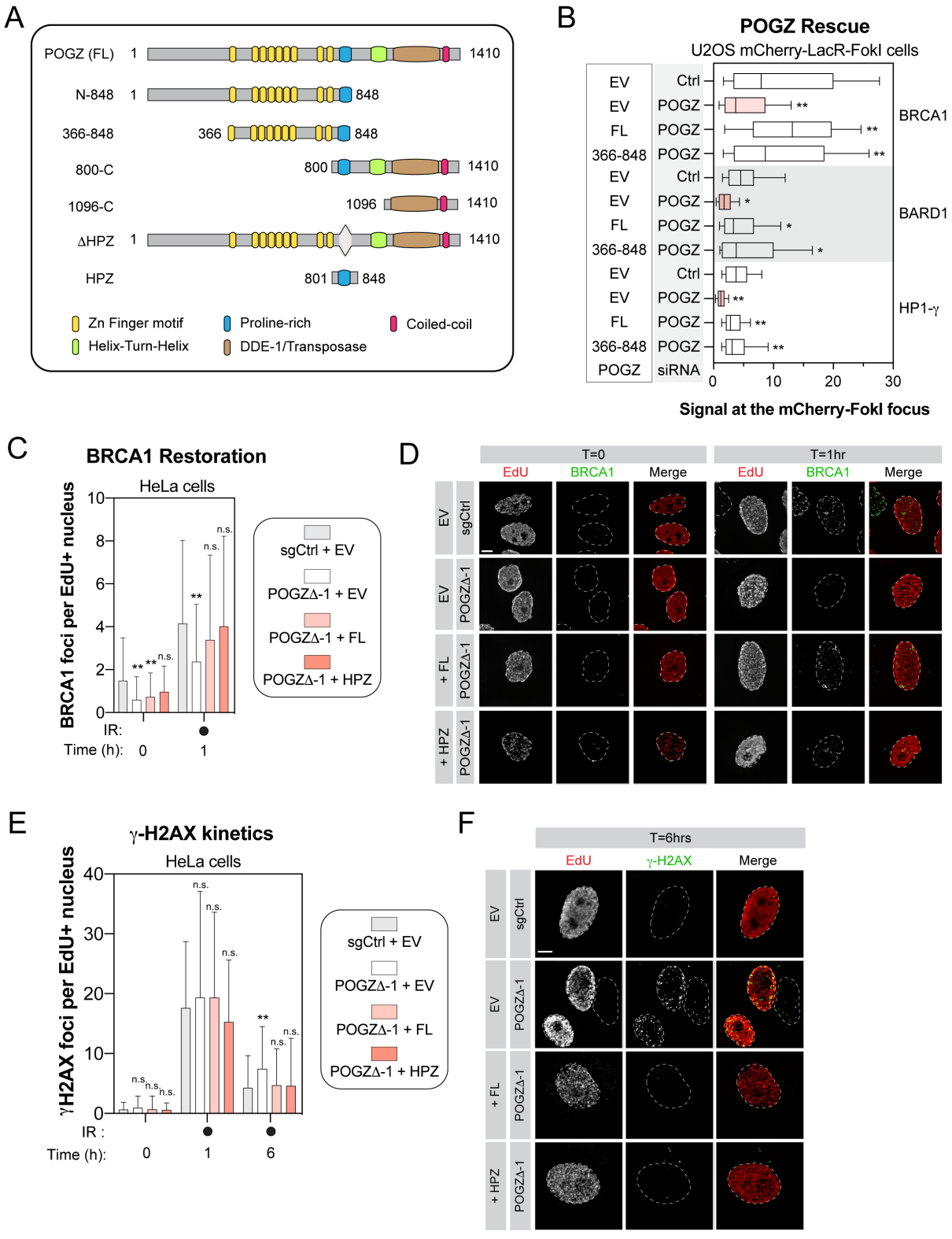

FIGURE 2- 4 POGZ MEDIATES BRCA1/BARD1 ACCUMULATION AT DSBS THROUGH ITS HP1-BINDING SITE.

Figure 4. POGZ mediates BRCA1/BARD1 accumulation at DSBs through its HP1-binding site.

(A) Schematic diagram outlining the different domains of human POGZ and the different deletion constructs of POGZ that we generated and analyzed. (B) U2OS stably expressing mCherry-LacR-FokI were transduced with the indicated siRNA. 24h post-transfection, cells were transfected with an empty Flag vector (EV) or a siRNA-resistant FLAG-tagged POGZ cDNA construct corresponding to indicated rescue mutant (full-length, FL; $POGZ^{366\text{-}848}$, 366-848). 24h after plasmid transfection, DNA damage was induced using Shield-1 and 4-OHT. Immunofluorescence against the indicated protein was subsequently performed to monitor its respective accumulation at sites of DNA damage by confocal microscopy. Data are represented as a box-and-whisker (10-90 percentile) where the fluorescent signal at the mCherry focus was normalized to nuclear background. At least 100 cells per condition were counted. Significance was determined by two-way ANOVA followed by a Dunnett's test. *$P<0.005$, **$P<0.0001$. (C) HeLa cells transfected with the indicated construct were monitored for their capacity to form IR-induced BRCA1 foci. HeLa cells where POGZ has been targeted by CRISPR technology (POGZΔ-1) and in control HeLa cells (sgCtrl) were transfected by an empty Flag vector (EV) or a sgRNA-resistant FLAG-tagged POGZ cDNA construct corresponding to indicated rescue mutant (full-length, FL; $POGZ^{801\text{-}848}$, HPZ). Cells were exposed to 1 Gy before being pulsed with Edu for 1hr and were recovered 1h post-exposure to IR. Cells were fixed, stained, and imaged via confocal microscopy. Data are the total number of BRCA1 foci in EdU+ cells and represented as a bar graph showing the mean $\pm$ SD (n = 3 biological replicates, with at least 100 cells analyzed for each time point). Significance was determined by two-way ANOVA followed by a Dunnett's test. *$P<0.05$, **$P<0.0001$. (D) Representative images used for quantification in (C). Scale bar = 5 μm. (E) Similar as in (C) except that γ-H2AX foci were monitored at the indicated time points by confocal microscopy. Data are the total number of γ-H2AX foci in EdU+ cells and represented as a bar graph showing the mean $\pm$ SD (n = 3 biological replicates, with at least 100 cells analyzed for each time point). Significance was determined by two-way ANOVA followed by a Dunnett's test. *$P<0.05$. (F) Representative images used for quantification in (E). Scale bar = 5 μm.

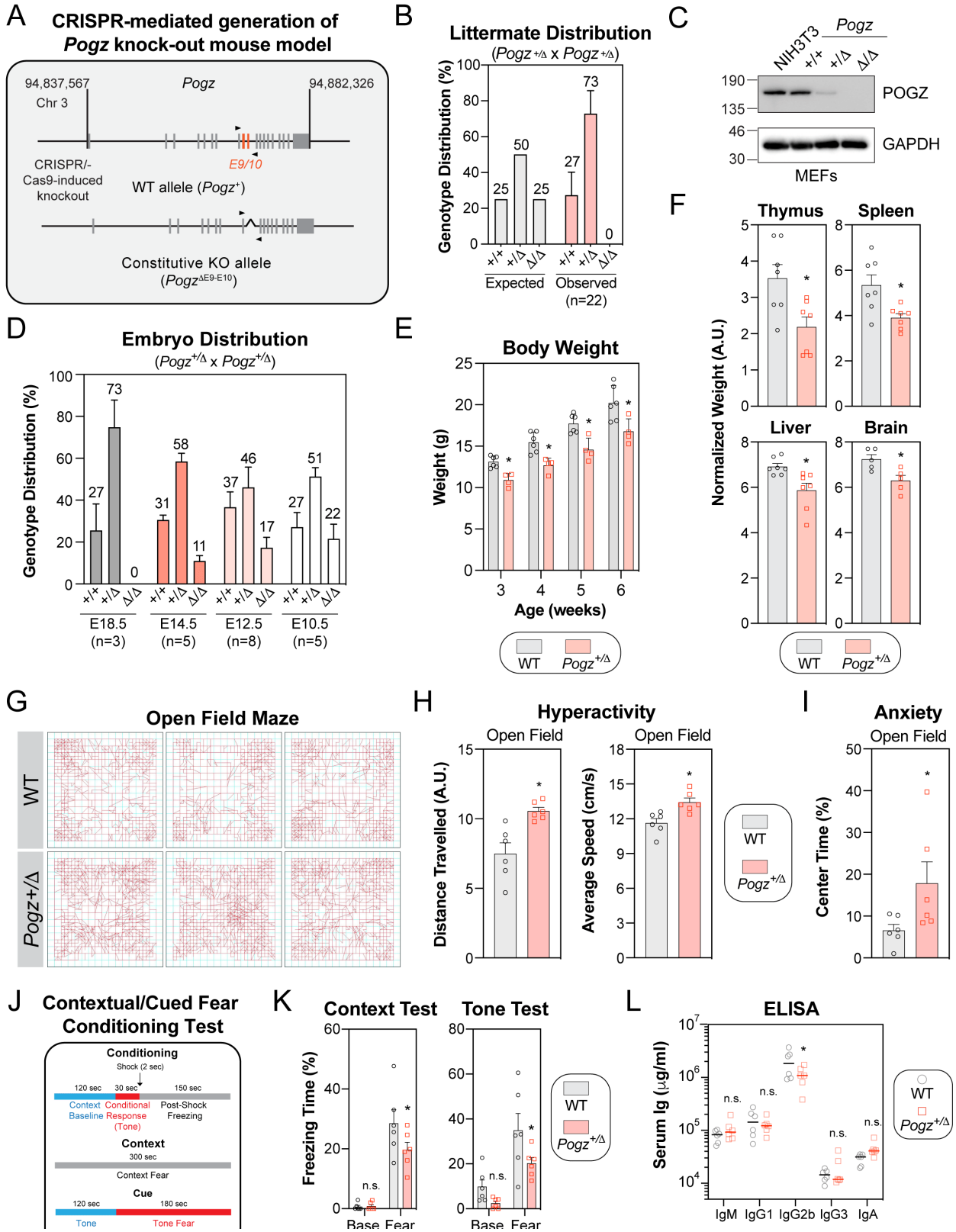

FIGURE 2- 5 POGZ HAPLO-INSUFFICIENCY IN MICE RECAPITULATES THE CLINICAL FEATURES OBSERVED IN PATIENTS AFFECTED BY THE WHSUS

Figure 5. Pogz haplo-insufficiency in mice recapitulates the clinical features observed in patients affected by the WHSUS.

(A) Schematic diagram outlining the generation of CRISPR/Cas9-mediated *Pogz*$^{+/\Delta}$ mouse model. A region spanning critical exons 9 and 10 of the murine *Pogz* gene on chromosome 3 was deleted using dual sgRNA CRISPR. (B) Expected and observed genotypic distribution of offspring of heterozygous *Pogz*$^{+/\Delta}$ crosses. Genotype was determined by PCR at time of weaning (3 weeks). Data are represented as a bar graph showing the mean ± SEM (n=22 individual litters, across 5 different breeding pairs). (C) Observed genotypic distribution of offspring of heterozygous *Pogz*$^{+/\Delta}$ crosses at specified embryonic day. Each litter is considered a biological replicate. Data are represented as a bar graph showing the mean ± SEM (n for each embryonic day is specified). (D) Expression analysis of Pogz by western blot in mouse embryonic fibroblasts (MEFs) generated from E12.5 embryos with the indicated genotype. NIH3T3 cells were used as a comparison. Gadph was used a loading control. (E) The body mass of male wild-type (WT) or *Pogz*$^{+/\Delta}$ mice was monitored weekly for 4 weeks post-weaning. Data are represented as a bar graph showing the mean ± SEM and each mouse is represented by a round dot (WT) or a square (*Pogz*$^{+/\Delta}$). At least 4 mice per genotype was monitored. Significance was determined by two-way ANOVA followed by a Sidak's test. **P<0.05.* (F) The indicated organ mass of male wild-type (WT) or *Pogz*$^{+/\Delta}$ mice were calculated relative to total body mass. Data are represented as a bar graph showing the mean ± SEM and each mouse is represented by a round dot (WT) or a square (*Pogz*$^{+/\Delta}$) (n=6-7 mice per genotype). Significance was determined by unpaired two-tailed t-test. **P<0.05.* (G) Representative movement traces of the indicated mice used for quantification in (H) and (I). (H) Quantification of the distance travelled (left panel) and the average speed (right panel) of each mouse (n=6 mice per genotype) in the open field. Data are represented as a bar graph showing the mean ± SEM and each mouse is represented by a round dot (WT) or a square (*Pogz*$^{+/\Delta}$). Significance was determined by unpaired two-tailed t-test. **P<0.005.* (I) The percentage of time that each mouse spent in the middle of the open field was quantified and represented as the mean ± SEM, each mouse being represented by a round dot (WT) or a square (*Pogz*$^{+/\Delta}$) (n = 6 mice per genotype). Significance was determined by unpaired two-tailed t-test. **P<0.005.* (J) Schematic diagram outlining the conditioning/experimental set up quantified in (K) of the contextual fear tests. (K) The percentage of freezing time in the different experimental conditions (context test, left panel; cue (tone) test, right panel) was monitored for each mouse and is represented as the mean ± SEM, each mouse being represented by a round dot (WT) or a square (*Pogz*$^{+/\Delta}$) (n=6 mice per genotype). Significance was determined by two-way ANOVA followed by a Sidak's test. **P<0.05.* (L) Plasma was isolated from cardiac punctures of wild-type (WT) or *Pogz*$^{+/\Delta}$ mice (8 weeks) and assessed for circulating levels of specified immunoglobulin isotypes. Each mouse is represented by a round dot (WT) or a square (*Pogz*$^{+/\Delta}$) (n=6 mice per genotype). Significance was determined by two-way ANOVA followed by a Bonferroni's test. **P<0.005.*

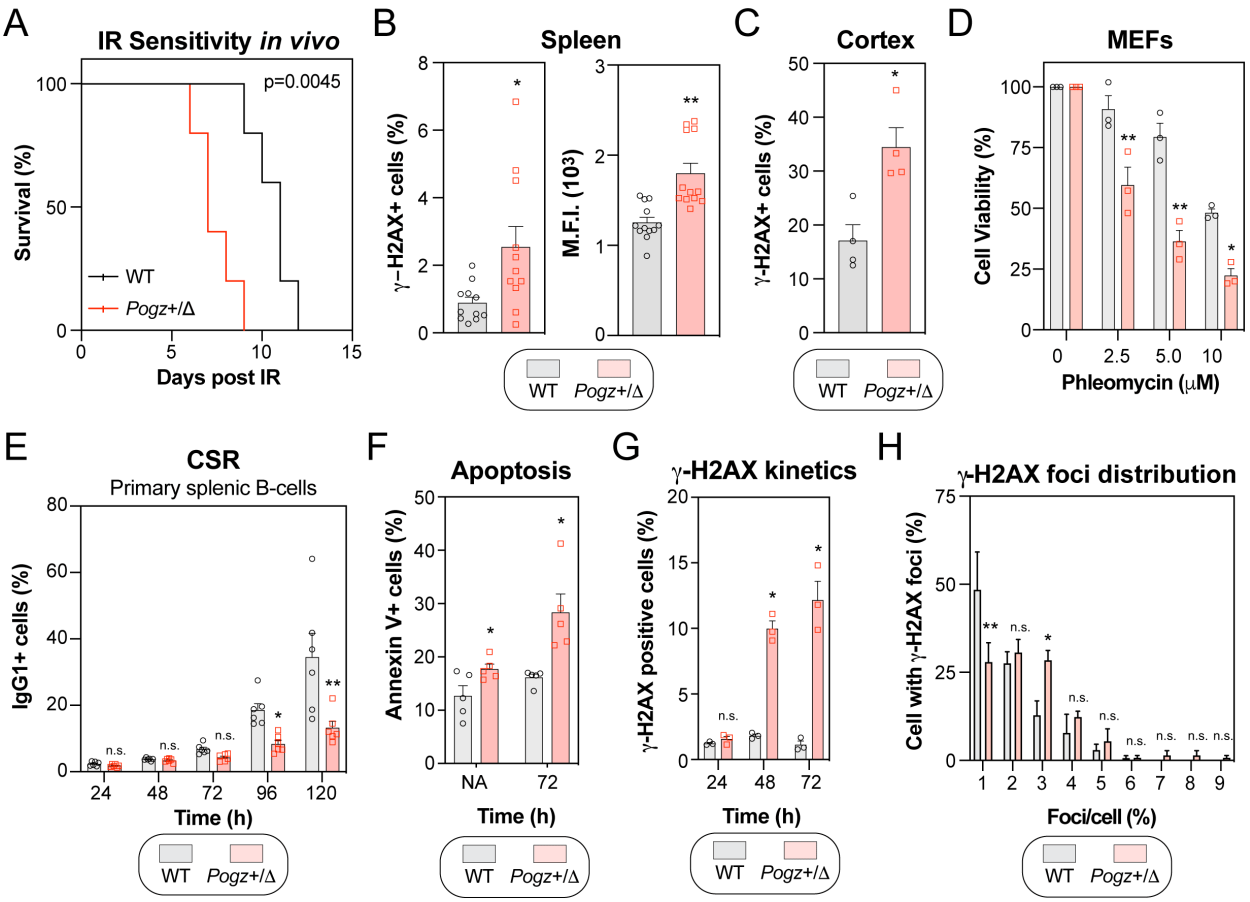

FIGURE 2- 6 POGZ HAPLOINSUFFICIENCY CORRELATES WITH FEATURES OF IMPAIRED DNA REPAIR IN MICE.

Figure 6. Pogz haploinsufficiency correlates with features of impaired DNA repair in mice.

(A) Wild-type (WT) and *Pogz*$^{+/\Delta}$ mice were subjected to a lethal dose of ionizing radiation (8.5 Gy) before recovering in sterile conditions and being assessed for their sensitivity to IR. Data are represented as a Kaplan-Meier survival curve of each genotype ((n=6 mice per genotype). Significance was determined by log-rank (Mantel-Cox) test. *$P<0.005$. (B) Quantification of phosphorylated-H2AX (γ-H2AX) levels by flow cytometry. Splenocytes isolated from 8-week-old wild-type (WT) and *Pogz*$^{+/\Delta}$ mice were processed for γ-H2AX staining and data are represented as bar graph showing the mean percentage of cells that were γ-H2AX-positive $\pm$ SEM (left panel) or the mean fluorescence intensity (M.F.I.) of the γ-H2AX signal $\pm$ SEM (right panel), each mouse being represented by a round dot (WT) or a square (*Pogz*$^{+/\Delta}$) (n = 11 mice for each genotype). Significance was determined by unpaired two-tailed t-test. *$P<0.05$, **$P<0.0005$. (C) Brain slices were sectioned from 6-week-old wild-type (WT) and *Pogz*$^{+/\Delta}$ mice, followed by immunostaining for phosphorylated H2AX (γ-H2AX). Data are the percentage of cells with γ-H2AX signal present in the nucleus per field of view and are represented as a bar graph showing the mean $\pm$ SEM, each mouse being represented by a round dot (WT) or a square (*Pogz*$^{+/\Delta}$)(n= 4 for each genotype with three distinct fields quantified for each mouse). (D) MEFs were monitored for their sensitivity to the radiomimetic drug phleomycin using the SRB assay. Immortalized MEFS obtained from the indicated genotype were treated with increasing concentrations of phleomycin for 1hr, replenished with fresh medium and incubated for 4 days efore being processed for SRB assays. Data are represented as a bar graph showing the relative mean $\pm$ SEM, each replicate being representing as a round dot (WT) or square (*Pogz*$^{+/\Delta}$). Significance was determined by two-way ANOVA followed by a Bonferroni's test. *$P<0.005$, **$P<0.0005$. (E) CD43-negative primary splenocytes from 8-week-old wild-type (WT) and *Pogz*$^{+/\Delta}$ mice were stimulated *ex vivo* with IL-4 (50 ng/mL) and LPS (25 μg/mL). Cells were harvested at the indicated time points and assessed for their surface expression of IgG1 by flow cytometry. Data are represented as a bar graph showing the mean $\pm$ SEM, each mouse being represented by a round dot (WT) or a square (*Pogz*$^{+/\Delta}$) (n=6 mice per genotype). Significance was determined by two-way ANOVA followed by a Bonferroni's test. *$P<0.05$, **$P<0.0001$. (F) Similar as in (E), except those cells were monitored for apoptosis by Annexin V staining. Data are represented as a bar graph showing the mean $\pm$ SEM, each mouse being represented by a round dot (WT) or a square (*Pogz*$^{+/\Delta}$) (n=5 mice per genotype). Significance was determined by two-way ANOVA followed by a Bonferroni's test. *$P<0.05$. (G) Similar as in (E), except that cells were monitored for phosphorylated H2AX (γ-H2AX) levels by flow cytometry at the indicate time points post-stimulation with IL-4/LPS. Data are represented as a bar graph showing the mean $\pm$ SEM, each mouse being represented by a round dot (WT) or square (*Pogz*$^{+/\Delta}$) (n=3 mice per genotype). Significance was determined by two-way ANOVA followed by a Bonferroni's test. *$P<0.05$. (H) Stimulated CD43-negative splenocytes were loaded on slides via Cytospin and processed for γ-H2AX immunofluorescence. Cells were fixed, stained, and imaged via confocal microscopy. Data are the percentage of cells in a field of view with indicated γ-H2AX foci and are represented as a bar graph showing the mean $\pm$ SEM. At least 100 cells per genotype

were counted. Significance was determined by two-way ANOVA followed by a Sidak's test. *$P<0.05$, **$P<0.005$.

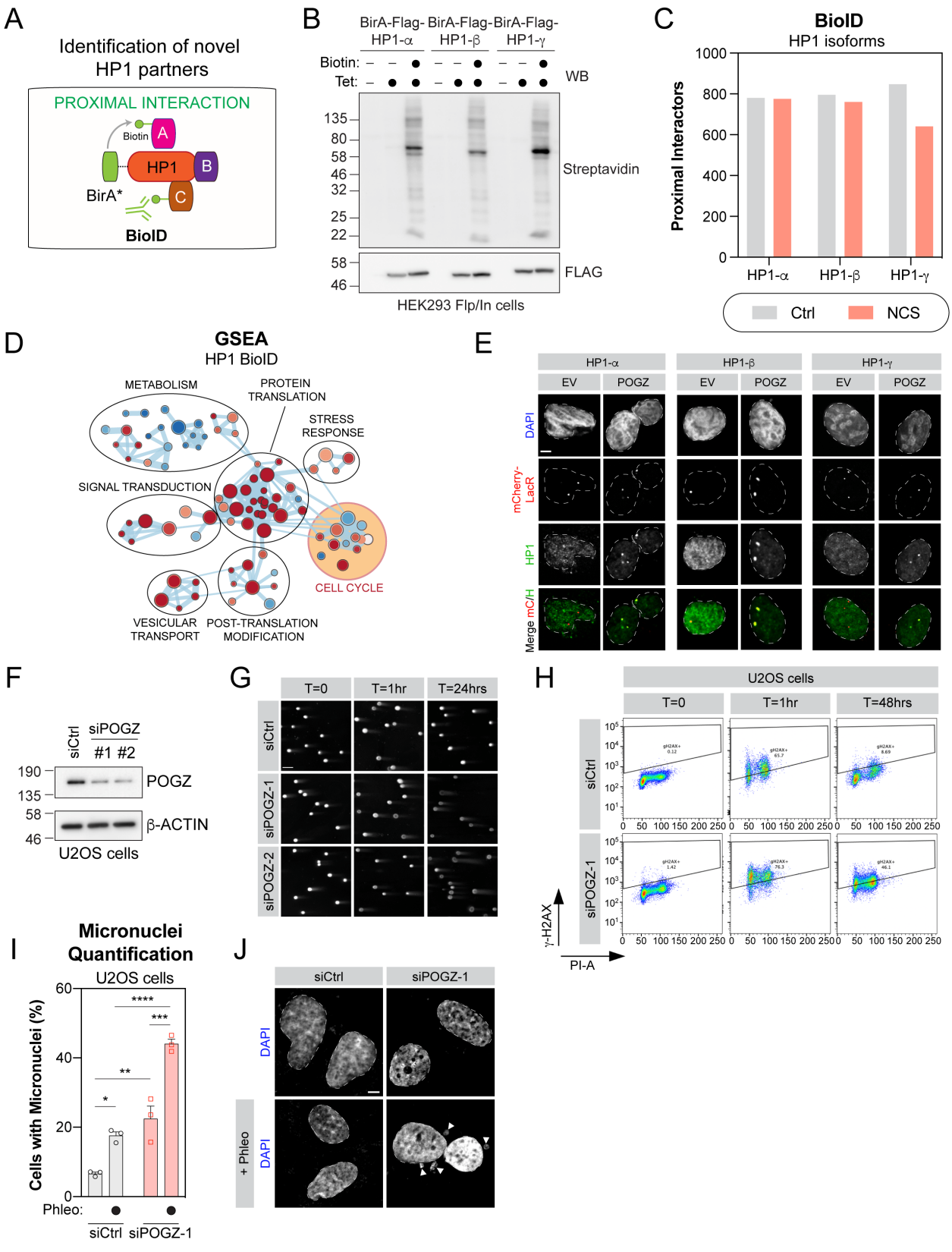

SUPPLEMENTAL FIGURE 2- 1 DEFINING THE PROXIMAL INTERACTOME OF THE DIFFERENT HP1 ISOFORMS.

Figure EV1. Defining the proximal interactome of the different HP1 isoforms.

(A) Schematic diagram representing the BioID approach applied to HP1 and the mapping of its proximal interactome by biotinylation. (B) HEK293 Flp-In cells stably expressing each BirA*-Flag-HP1 isoform were tested for expression and biotinylation following induction with tetracycline and incubation with biotin as indicated. After induction, cells were lysed and subjected to immunoblot for Flag and Streptavidin. (C) High-confidence proximal interactors of the different HP1 isoforms identified by BioID, in presence (NCS) or absence of DNA damage (Ctrl) (n=3 biological replicates). (D) GSEA enrichment map of HP1-isoform interactome identifying annotated Reactome pathways. Enrichment maps from GSEA were developed with a ranked interaction network ($p < 0.2$, FDR < 0.5 and overlap coefficient = 0.75). Individual pathways in "Cell Cycle", highlighted in yellow, are further examined in Fig.1C. (E) U2OS cells with a stable LacO sequence integration were transfected either with mCherry-LacR (EV) or a mCherry-LacR-tagged version of POGZ (POGZ). Immunofluorescent labeling of endogenous HP1 isoforms colocalizing with the mCherry-LacR signal were quantified and normalized to nuclear background fluorescence. Representative images of cells quantified in Fig.1E. Scale bar = 5 μm. (F) U2OS cells treated with the indicated siRNA were lysed 48hrs post-transfected and processed for POGZ western blot. β-actin was used a loading control. (G) Representative images used for quantification plotted in Fig.1F. U2OS cells treated with the indicated siRNA were irradiated, 48 hours post-transfection, with 1 Gy and run in low melting agarose under neutral conditions. DNA was stained with SYBR Gold to measure the tail moment. Scale bar = 10 μm. (H) Representative flow cytometry plots of g-H2AX levels analyzed in Fig.1G. (I) U2OS cells were transfected with indicated siRNA were stained with DAPI to visualize micronuclei by confocal microscopy. Data are number of cells per field of view displaying a micronucleus and are represented as a bar graph showing the mean ± SEM (n = 3 biological replicates, with a minimum of 3 fields taken per replicate). Significance was determined by two-way ANOVA followed by a Tukey's test. *$P<0.05$, **$P<0.005$, ***$P<0.0005$, ****$P<0.0001$. (J) Representative images used for quantification in (H). Scale bar is 10 μm.

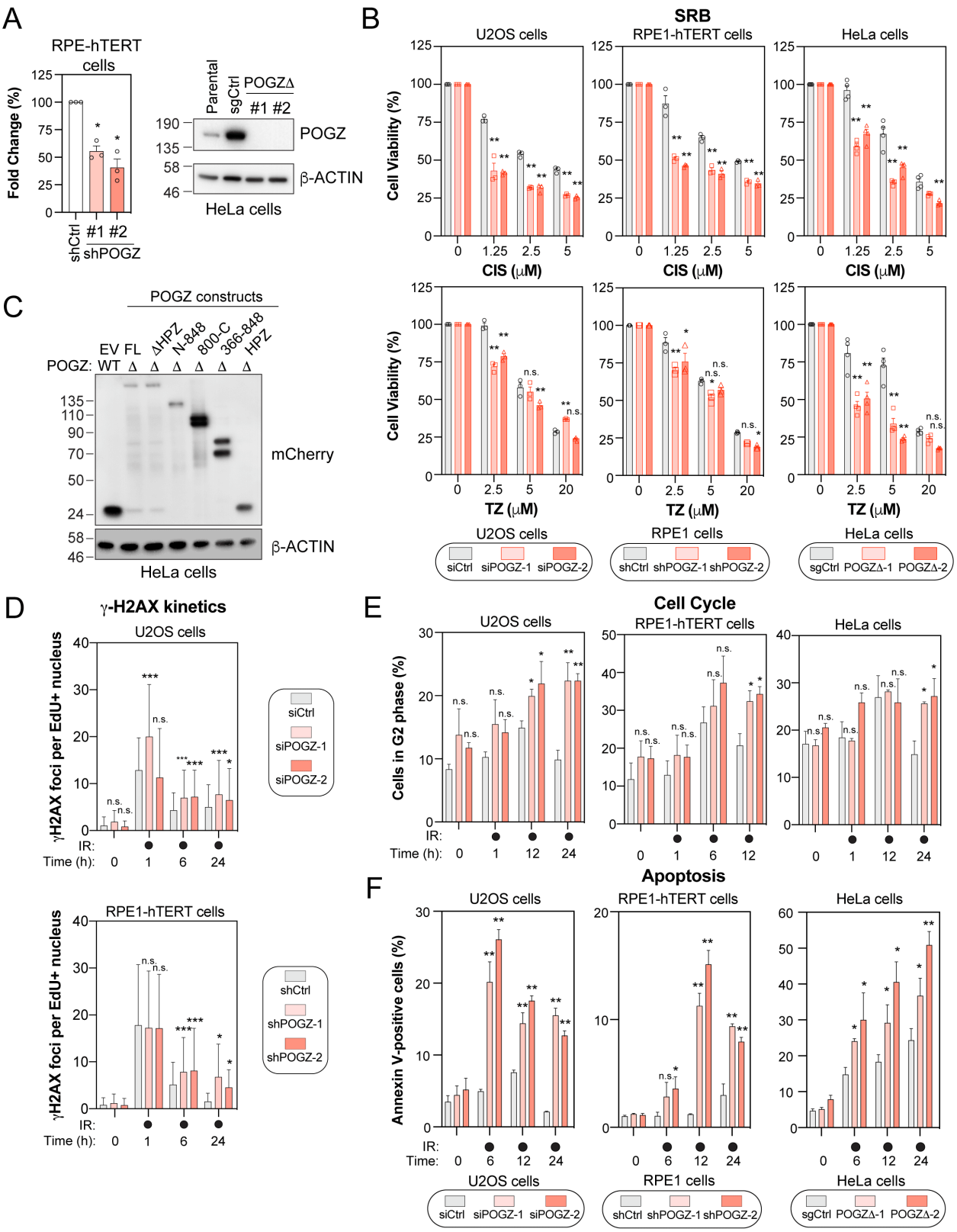

SUPPLEMENTAL FIGURE 2- 2 IMPACT OF ALTERING POGZ LEVELS ON DNA REPAIR, CELL CYCLE PROGRESSION, AND APOPTOSIS.

Figure EV2. Impact of altering POGZ levels on DNA repair, cell cycle progression, and apoptosis.

(A) RPE1-hTERT cells (right panel) transduced with a scramble shRNA (shCtrl) or with a shRNA directed against POGZ (shPOGZ-1 or -2) were processed for RNA extraction. Total RNA was isolated and cDNA was generated before POGZ RNA levels were quantified by qPCR and normalized to GAPDH RNA levels. Data are represented as a graph bar showing the mean ± SEM (n=3 independent transductions for each condition). Significance was determined by one-way ANOVA followed by a Dunnett's test. *$P<0.005$. HeLa sub-clones (left panel) where POGZ was targeted by CRISPR technology (POGZΔ-1 or -2) -or expressing a non-targeting sgRNA control (sgCtrl), were lysed and POGZ levels were monitored by western blot. The parental HeLa cell line was added for comparison. β-Actin was used as a loading control. (B) U2OS (left panel), RPE1-hTERT (middle panel), and HeLa cells (right panel) were monitored for their sensitivities to the intercalating agent cisplatin (CIS, top panel) and the PARPi talazopirib (TZ, bottom panel) using the SRB assay. For each cell line, the following conditions were used: U2OS cells were transfected with a nontargeting siRNA (siCtrl) or an siRNA targeting human POGZ (siPOGZ-1 or -2); RPE1-hTERT cells were transduced a control shRNA (shCtrl) or a shRNA directed against human POGZ (shPOGZ-1 or -2); HeLa cells were expressing a non-targeting sgRNA (sgCtrl) or a sgRNA targeting human POGZ and sub-cloned (POGZΔ-1 or -2). Cells were pulsed with CIS or TZ at the indicated concentrations for 16 hours, or 24h, respectively, and replenished with fresh medium and incubated for 4 days. Data are represented as a bar graph showing the relative mean ± SEM, each replicate being representing as a round (Ctrl condition), square (condition #1) or triangle (condition #2) symbol (n=3 biological replicates). Significance was determined by two-way ANOVA followed by a Bonferroni's test. *$P<0.05$, **$P<0.0001$. (C) HeLa clones where POGZ was targeted by CRISPR technology (POGZΔ) or expressing a non-targeting sgRNA control (WT), were transfected with the indicated mCherry-tagged POGZ constructs or a mCherry empty vector (EV) and lysed 48hrs post-transfection. mCherry expression was monitored by western blot. β-Actin was used as a loading control. (D) Quantification of γH2AX foci in U2OS cells transfected with the indicated siRNA (top panel), or in RPE1-hTERT cells stably expressing the indicated shRNA (bottom panel). Cells were treated with 1 Gy before being pulsed with Edu for 1hr and recovered at the indicated times. Data are the total number of γ-H2AX foci in EdU+ cells and represented as a bar graph showing the mean ± SD (n = 3 biological replicates, with at least 100 cells analyzed for each time point). Significance was determined by two-way ANOVA followed by a Dunnett's test. *$P<0.05$. (E) Cell cycle distribution was monitored in U2OS (left panel), RPE1-hTERT (middle panel) and HeLa cells (right panel), transfected or transduced with the indicated condition. Cells were pulsed with BrdU for 1hr treated before being treated with 1 Gy and recovered at the indicated time points for fixation and propidium iodide staining. Data are the percentage of cells in G2 phase of the cell cycle for each indicated condition and are represented as a bar graph showing the relative mean ± SEM (n=3 biological replicates). Significance was determined by two-way ANOVA followed by a Dunnett's test. *$P<0.05$, **$P<0.005$. (F) Apoptosis was assessed by Annexin V staining in U2OS (left panel), RPE1-hTERT (middle panel), and HeLa cells (right panel) transfected or transduced with the indicated condition, before being treated with 10 Gy

and harvested at the indicated time points for flow cytometry analysis. Data are represented as a graph bar ± SEM (n=3 biological replicates). Significance was determined by two-way ANOVA followed by a Dunnett's test. *$P<0.05$, **$P<0.005$.

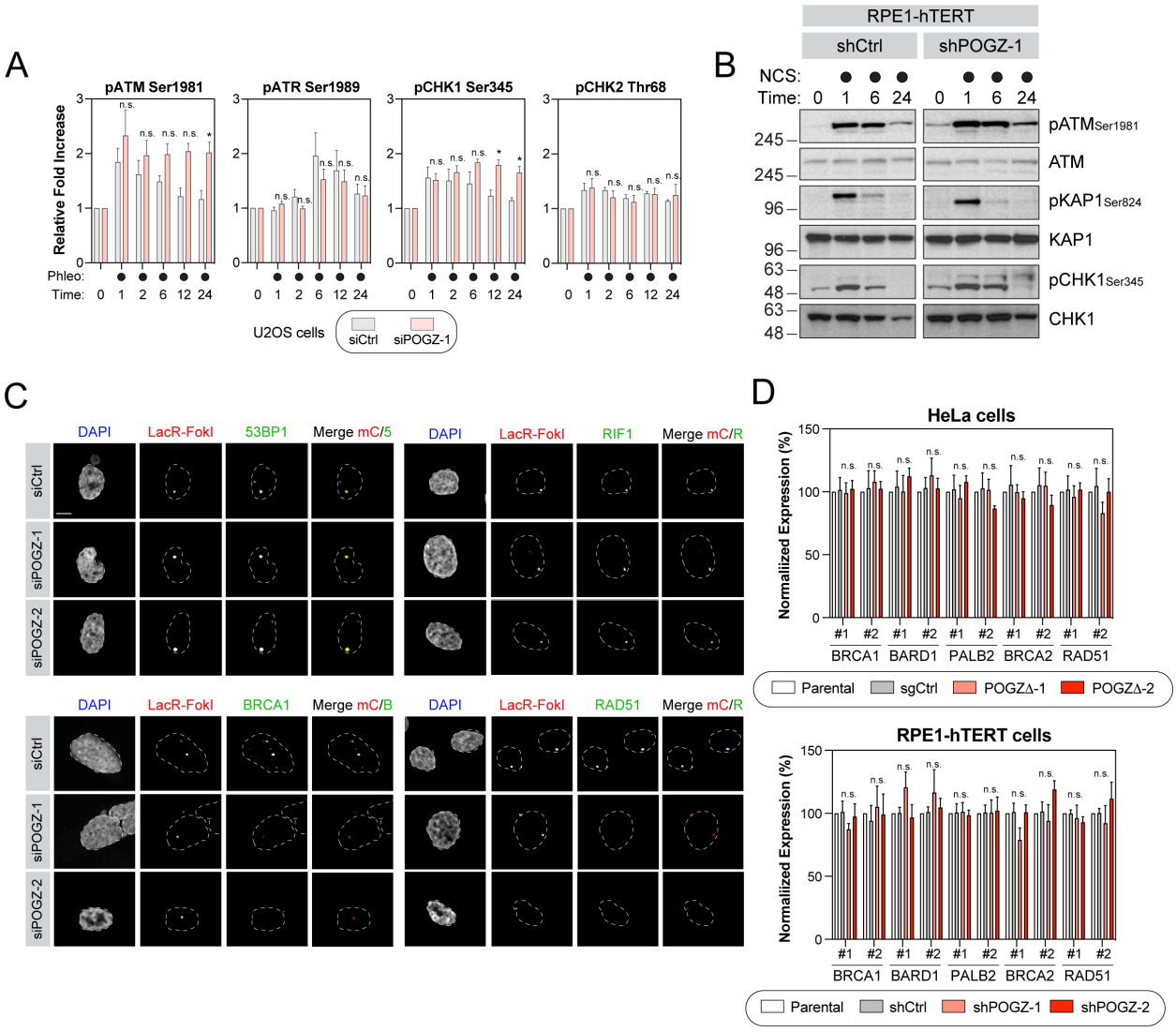

SUPPLEMENTAL FIGURE 2- 3 POGZ AND ITS CONTRIBUTION TO DNA DAMAGE CHECKPOINT SIGNALING AND CELL FATE.

Figure EV3. POGZ and its contribution to DNA damage checkpoint signaling and cell fate.

(A) U2OS cells were transfected the indicated siRNA. 48h post-transfection, cells were pulsed with phleomycin (50 μg/mL) for 1hr before being fixed, permeabilized, and subjected to flow cytometry analysis for the indicated phospho-proteins. Data are represented as a graph bar ± SEM (n=6 biological replicates) where the fold increase relative to untreated samples of the respective siRNA treatment is plotted. Significance was determined by two-way ANOVA followed by a Sidak's test. *$P<0.05$. (B) RPE1-hTERT cells transduced with the indicated shRNA were pulsed with NCS (500 μg/mL) for 1hr and harvested at the indicated time points for lysate. Western blot for the indicated phospho- and total proteins were performed. Representative images are displayed in this panel. (C) Representative images from the U2OS-FokI data summarized in Fig.3A. U2OS-LacR-FokI cells were transfected with the indicated siRNA. The following day, DSB induction was performed with 4-OHT and Shield-1. Cells were processed for immunofluorescence microscopy using primary antibodies directed against 53BP1, RIF1, BRCA1 and RAD51. Scale bar = 2.5 μm. (D) RNA was extracted from HeLa cells where POGZ was targeted by CRISPR technology (left panel) or from RPE1-hTERT cells transduced with the indicated shRNA (right panel). cDNA was produced and RNA levels of the indicated HR factors were monitored by qPCR and normalized to GAPDH RNA levels. Data are represented as a graph bar ± SEM (n=3 biological replicates). (E) U2OS cells stably expressing a HA-tagged version of POGZ were pre-sensitized with 10 μg/ml Hoescht 33342 before being exposed to UV micro-irradiation. Immunofluorescence against HA epitope and endogenous γ-H2AX was subsequently performed to monitor POGZ accumulation at sites of DNA damage. Shown are representative micrographs of cells displaying for HA and γ-H2AX staining (left, scale bar = 5 μm) and quantification of U2OS cells expressing HA-POGZ (right). Data are represented as a graph bar ± SEM (n=6 biological replicates) where the percentage of cells with HA-POGZ signal co-localizing with γ-H2AX at the indicated time points is plotted.

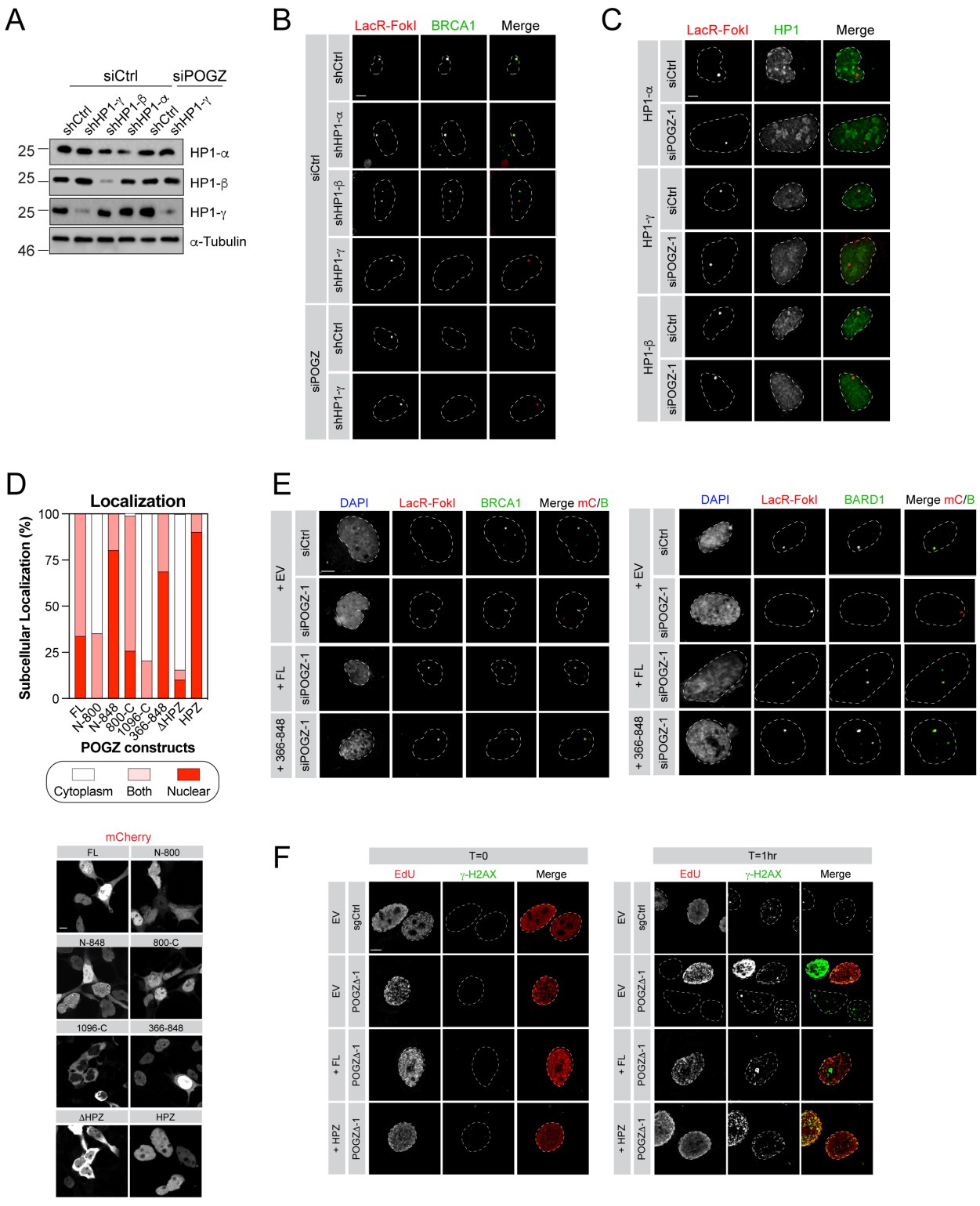

SUPPLEMENTAL FIGURE 2- 4 INTERACTION OF POGZ AND HP1 ISOFORMS IS NECESSARY FOR NUCLEAR LOCALIZATION AND SUFFICIENT TO RESTORE DNA REPAIR IN POGZ-DEPLETED CELLS.

Figure EV4. Interaction of POGZ and HP1 isoforms is necessary for nuclear localization and sufficient to restore DNA repair in POGZ-depleted cells.

(A) U2OS-FokI cells stably expressing the indicated shRNA and transfected with the indicated siRNA were analyzed by western blot. 48hrs post-transfection, cells were harvested for lysate and probed for the indicated HP1 isoforms. α-Tubulin was used as a loading control. (B) Representative images of BRCA1 accumulation in U2OS-mCherry-LacR-FokI cells transduced with the indicated shRNA and transfected with the indicated siRNA. Quantification of the BRCA1 signal at the mCherry dot is represented in Fig.3E. Scale bar = 5 μm. (C) Representative images of the different HP1 isoforms accumulating at FokI-induced DSB in U2OS-mCherry-LacR-FokI cells transfected with the indicated siRNA. Quantification of the HP1 signal at the mCherry dot is represented in Fig.3G. Scale bar = 5 μm. (D) HEK293T cells were transfected with mCherry-tagged truncation constructs of POGZ or full-length mCherry-POGZ (FL). Cells were harvested 24hrs post-transfection and re-plated on to coverslips. 48 hrs post-transfection, cells were fixed, permeabilized and stained with DAPI. Cells were subsequently visualized by confocal microscopy and quantified for the presence of mCherry signal in the nucleus, the cytoplasm or both, per field of view. A minimum of 5 fields of view were sampled per biological replicate (n=3 biological replicates). Data are represented as a bar graph (top) where the proportion of each sub-cellular localization is represented for each indicated construct. Representative images are shown in bottom panel (scale bar = 5 μm). (E) U2OS-mCherry-LacR-FokI cells were transfected with the indicated siRNA. 24h post-transfection, cells were transfected with a Flag empty vector (EV) or a siRNA-resistant Flag-tagged POGZ construct corresponding to indicated rescue mutant. DNA damage was induced, 24h post-transfection, with Shield1 and 4-OHT. Cells were stained for BRCA1 (left panel) or BARD1 (right panel) and imaged via confocal microscopy. Representative images of the data quantified in Fig.4B. Scale bar = 5 μm. (F) HeLa cells where POGZ has been targeted by CRISPR (POGZΔ-1) or a control sgRNA (sgCtrl) were transfected with a mCherry empty vector (EV) or a mCherry-tagged POGZ construct corresponding to indicated rescue mutant. Cells were treated with 1 Gy and were recovered at the 1hr post-IR exposure. Cells were fixed, stained for γ-H2AX, and imaged via confocal microscopy. Representative images of the data quantified in Fig.4E. Scale bar = 5 μm.

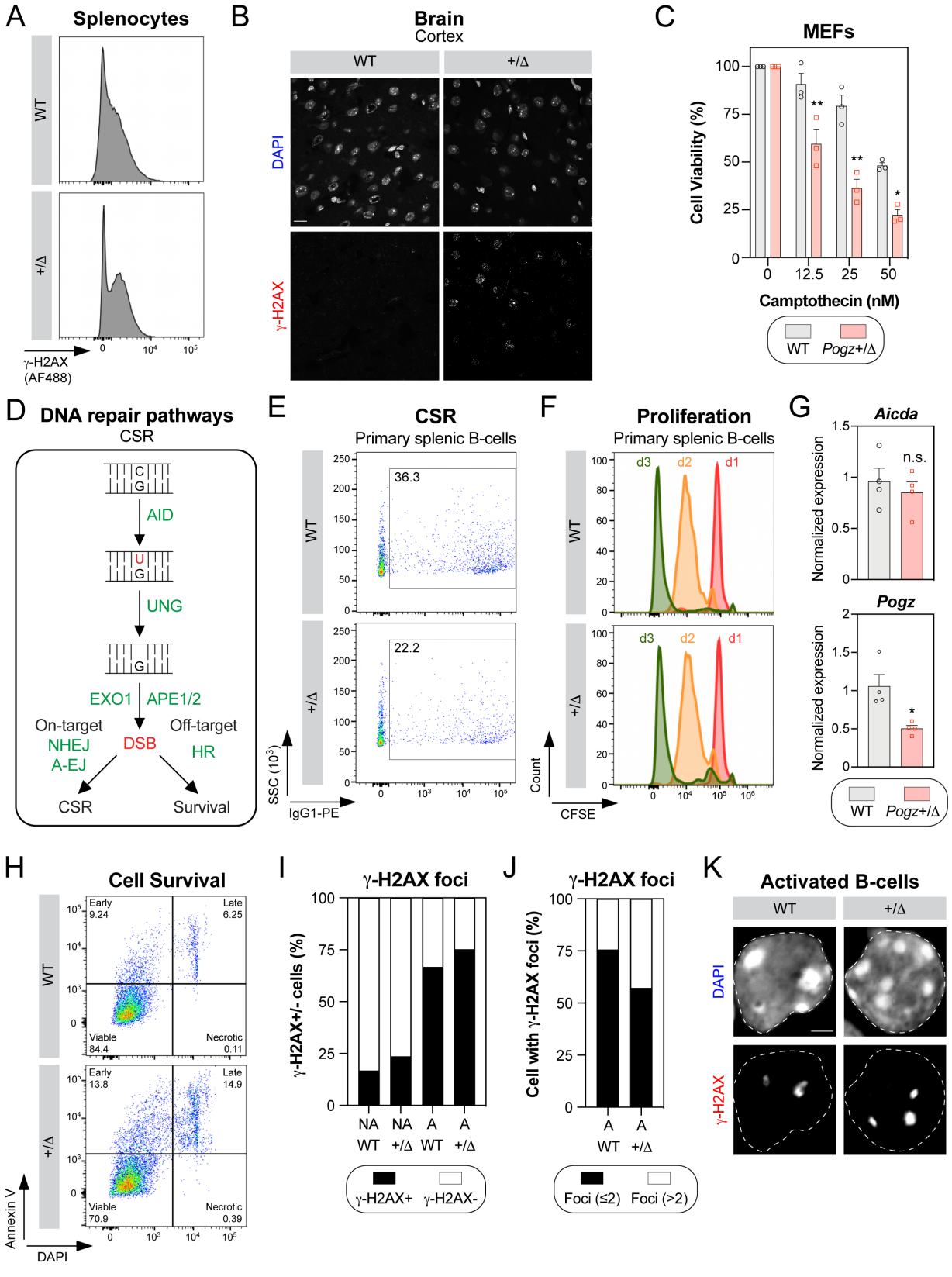

SUPPLEMENTAL FIGURE 2- 5 IMPACT OF POGZ HAPLO-INSUFFICIENCY IN VIVO.

Figure EV5. Impact of Pogz haplo-insufficiency *in vivo*.

(A) Representative flow cytometry plots of γ-H2AX staining performed in splenocytes isolated from 8-week-old *Pogz* wild-type (WT) and *Pogz*$^{+/\Delta}$ mice. (B) Representative micrographs of phosphorylated H2AX (γ-H2AX) from cortex tissue isolated from 6-week-old *Pogz* wild-type (WT) and *Pogz*$^{+/\Delta}$ mice. Scale Bar = 20 μm. (C) MEFs obtained from the indicated genotype were treated with increasing doses of camptothecin for 1hr, before being replenished with fresh medium and incubated for 4 days. Cells were fixed and processed for SRB assay at day 4. Stained cellular content was detected by absorbance and normalized to solvent-treated conditions. Data are represented as a bar graph showing the relative mean ± SEM, each replicate being representing as a round symbol (n=3 biological replicates). Significance was determined by two-way ANOVA followed by a Bonferroni's test. **P<0.005*, ***P<0.0005.* (D) Schematic diagram depicting the formation and the subsequent repair of programmed DSBs in B-cells during class switch recombination (CSR) as well as the requirement for different DNA repair pathways. (E) CD43-negative primary splenocytes from 8-week-old *Pogz* wild-type (WT) and *Pogz*$^{+/\Delta}$ mice were stimulated with IL-4 (50 ng/mL) and LPS (25 μg/mL). Representative flow cytometry plots monitoring surface expression of IgG1 120 hrs post-stimulation. (F) similar as in (E) except that proliferation is monitored over time by CFSE dilution. (G) 48 hrs of stimulation, total RNA was isolated from *Pogz* wild-type (WT) and *Pogz*$^{+/\Delta}$ B-cells and cDNA was generated. *Aicda* and *Pogz* RNA levels were monitored by qPCR and normalized to *Gapdh*. Data are represented as mean ± SEM (n=4 biological replicates). Significance was determined by unpaired two-tailed t-test. **P<0.05.* (H) similar as in (E) except that apoptosis is monitored by Annexin V/DAPI staining. (I) Stimulated CD43-negative splenocytes were loaded on to slides via Cytospin and processed for γ-H2AX immunofluorescence. Cells were fixed, stained, and imaged via confocal microscopy. Data are represented as the percentage of cells in a field of view displaying at least one γ-H2AX focus (γ-H2AX+) (n=3 biological replicates). (J) similar as in (I) except that cells displaying at least two γ-H2AX foci (black) are represented for the indicated genotype. (K) Representative images used for the quantification plotted in (I), (J) and Fig.6H.

2.4. Discussion

DNA repair by HR is an essential process for both the maintenance of genome stability and the generation of genetic diversity. A major factor influencing the commitment of a DSB to HR relates to its cell cycle positioning and the availability of a donor template. However, several additional elements participate in this "decision-making" process, including the presence of the BRCA1/BARD1 complex at DSBs, which is influenced by the epigenetic context. For instance, the direct recognition of H4K20me^0 by the ankyrin repeat domain of BARD1 allows BRCA1 to be present on newly synthesized chromatin, independently of any DNA damage, thereby antagonizing 53BP1 upon formation of DSBs. The retention of the BRCA1/BARD1 complex at DSBs has been proposed to rely, at least in part, on the recruitment of HP1 proteins to DSBs. While the requirement for H3K9 methylation remains a topic of debate,[22,31] recent evidence have shown that BARD1 can directly bind to HP1 through a PxVxL motif present in its BRCT domain, and this process retains BRCA1 at DSBs while allowing the initiation of DNA end resection.[24] However, the underlying mechanism regulating this step remained unknown. In this study, we identified POGZ as an important regulator of the HP1-BRCA1-BARD1 axis and a novel player in homology-directed DNA repair pathways. Importantly, our data may reconcile the two conflicting models proposed for HP1 in the repair of DSBs and POGZ may be the missing factor promoting the methylation-independent recruitment of HP1 at DNA damage sites while allowing methyltransferases (e.g. EHMT1/EHMT2), two known interactors of POGZ (Suliman-Lavie et al., 2020), to alter local methylation pattern and retain the HP1-BARD1-BRCA1 complex at DSBs.

POGZ has been initially proposed to promote genome stability during mitosis, by interacting with HP1-α, thus facilitating its ejection from chromosomes, a necessary step for their accurate segregation.[34] The identification of POGZ as a partner of the adaptor protein REV7/MAD2L2,[58] a key player in the faithful seggregation of chromosomes, was initially proposed to participate in the mitotic-related role of POGZ. Interestingly, the authors noted that POGZ depletion had limited impact on the steady-state localization of HP1-α in interphase.[34] Subsequent analysis of the role of POGZ during interphase showed that its depletion correlates with a defect in the phosphorylation of replication

protein A (RPA; Ser4/Ser8) upon camptothecin treatment,[35] a late marker of DNA end resection. The confirmation that POGZ is part of the proximal interactome of REV7/MAD2L2,[59] with direct relevance for DNA repair pathway choice, suggested a possible contribution of this zinc finger protein during the DNA damage response. Still, whether POGZ may directly impact DNA repair remained, until now, unknown. The recent identification of ZNF280C/ZPET, another member of the ZNF280 subfamily, in the proximal interactome of RAD18 during genotoxic stress[60] and its characterization as a novel inhibitor of DNA end resection further argued for a role of POGZ/ZNF280E during the repair of DSBs.

Here, we elucidated the role of POGZ in homology-directed DNA repair during interphase. Notably, our findings recapitulated several key features of HP1 during the DNA damage response. For instance, HP1 proteins dynamically accumulate and subsequently dissociate from DNA damage sites,[19–22,31] alike what we observed with POGZ, which can be detected within minutes at laser micro-irradiation before disappearing less than an hour after induction of DNA damage. Moreover, targeting HP1 has been shown to impair HR, thereby leading to a sustained G2 DNA damage checkpoint,[25] resembling what we noted in POGZ-depleted cells. Importantly, we did not observe any substantial impact on the phosphorylation status and dynamics of KAP1 in POGZ-depleted RPE1-hTERT cells, unlike what has been reported with HP1,[21,61,62] likely reflecting the non-redundant contribution of the different HP1 isoforms.[63] Along the same lines, loss of POGZ preferentially impaired the recruitment of HP1-γ to DNA damage sites, corroborating our BioID data where we observed an increased presence of POGZ in the vicinity of HP1-γ under genotoxic stress conditions. Importantly, POGZ depletion correlated with a drastic reduction of both BRCA1 and BARD1 at DSBs, confirming previous reports linking HP1-γ and the BRCA1/BARD1 complex to DNA repair by HR.[24–26]

Several groups have recently endeavored to better understand the role of POGZ *in vivo.*[50–52] *Pogz* ablation by conventional gene targeting has highlighted its essentiality for normal murine embryogenesis, [50] a phenotype that we confirmed in our CRISPR-mediated mouse model. Interestingly, conditional ablation of *Pogz* led to transcriptional

dysregulation in hematopoietic, neural and embryonic stem cells.[50–52] We tested whether POGZ could influence the DNA damage response at the transcriptional level; however, our targeted expression analysis suggests that POGZ depletion has limited impact on the expression of established HR factors. Systematic transcriptomic analysis noted that *Brca2* is downregulated in *Pogz*-/- murine fetal liver cells compared to wild-type controls (~1.8 fold change),[50] an observation that we did not witness in RPE1-hTERT and HeLa cells. While it is possible that POGZ regulates DNA repair at multiple levels, including transcriptional repression, its rapid accumulation at laser micro-irradiation argues for a more direct contribution during DNA repair. Importantly, our data re-enforce the tight interdependency between POGZ and HP1 protein, highlighted by our structure-function analysis that confirmed the reliance for POGZ on its HP1-binding site for its nuclear accumulation.[51]

The recent identification of *de novo POGZ* mutations in patients affected by a rare neurocognitive disorder,[36–39] further demonstrated the central role of this zinc finger protein *in vivo*. Interestingly, the characterization of a patient-derived mutation of POGZ in a mouse model recapitulated the main clinical features observed in the WHSUS and correlated with transcriptional dysregulation.[51] Our *in vivo* data suggest a more complex framework, where its impact on DNA repair may contribute to the clinical features observed in WHSUS patients, suggesting that the WHSUS may be multi-factorial, with a potential “genome instability” component.

2.5. Materials and Methods

Cell Lines and Transfection

HEK293T, RPE1-hTERT, and HeLa cells were cultured in Dulbecco's Modified Eagle medium (DMEM; Wisent) supplemented with 10 % fetal bovine serum (FBS, Sigma) and 1% Penicillin-Streptomycin (P/S, Wisent). U2OS cells were cultured in McCoy's 5A Modified medium (Wisent) supplemented with 10% FBS and 1% P/S. Primary murine B cells were maintained in Roswell Park Memorial Institute (RPMI) 1640 medium (Wisent) supplemented with 10% FBS, 5% NCTC-109 media (Thermofisher), 50 μM 2-mercaptoethanol (Sigma) and 1% P/S. All cell lines were regularly tested for mycoplasma contamination and STR DNA authenticated. Plasmid transfections were carried out using Lipofectamine 2000 Transfection Reagent (Invitrogen) following the manufacturer's protocol. Lentivirus production was done in HEK293T by co-transfection of sgRNA or shRNA constructs, envelope protein VSV-g, and packaging plasmid psPAX2. Supernatants harvested 48- and 72-hours post-transfection and concentrated whenever possible. The U2OS cell line stably expressing an inducible mCherry-LacR-FokI was a gift of R. Greenberg (University of Pennsylvania). The DNA-repair reporter cell lines DR-GFP and SA-GFP were a gift of Dr. Jeremy Stark (City of Hope National Medical Center). The U2OS-LacO cell line was a gift from Dr. Daniel Durocher (Lunenfeld-Tanenbaum Research Institute). HeLa-POGZ-VC and HeLa-POGZ-KO cell lines were generated using pLentiCRISPRv2-puro plasmids containing sgRNA outlined in Table 2B. Cell lines were selected with 2ug/mL puromycin (Tocris) 48 hours after infection with lentivirus. Cell lines were derived from single cells, expanded and screened by immunoblotting.

RNA Interference

All siRNAs employed in this study were siGENOME Human siRNAs purchased from Dharmacon (Horizon Discovery). RNAi transfections were performed using Lipofectamine RNAiMax (Invitrogen) using forward transfections. Except when stated otherwise, siRNAs were transfected 48 h prior to experimental procedures. The individual siRNA duplexes used are: siCTRL, D-001810-03; POGZ, D-006953-01,-18; CTIP, M-011376-00; RAD51,

M-003530-04; HP1-β, M-009716-00; HP1-γ, M-010033-01; HP1-α, M-004296-02. The pLKO-puro shRNA plasmids from against POGZ (TRCN0000005707-11), HP1-α (TRCN0000062240/1), HP1-β (TRCN0000062222/3), HP1-γ (TRCN0000021916/7) were obtained from the McGill Platform for Cellular Perturbation (MPCP) as part of the MISSION® shRNA library (RNAi Consortium, Broad Institute) and the nontargeting control was a gift from Dr. Marc Fabian (McGill University).

Plasmids

The cDNAs of human POGZ, HP1-α, HP1-β, HP1-γ were obtained from the McGill Platform for Cellular Perturbation (MPCP) as part of the MISSION® TRC3 human ORF collection. Quikchange site directed mutagenesis (Agilent) was performed using primers (listed in Table 2C) as per manufacturers guidelines to obtain selected POGZ mutants, furthermore, all mutant plasmids were transiently transfected into the HeLa cell line and validated by western blot. All constructs were transferred from pENTR vectors into pDEST-based constructs using LR Clonase II according to manufacturer's instructions (ThermoFisher, 11791020). The pDEST-CMV-N-mCherry was a gift from Robin Ketteler (Addgene plasmid # 123215) (Agrotis, Pengo et al., 2019). The pDEST-mCherry-NLS-LacR plasmid was a gift from Dr. Daniel Durocher (Lunenfeld-Tanenbaum Research Institute). The pDEST-pcDNA5-BirA-FLAG N-term plasmid was a gift from Anne-Claude Gingras (Lunenfeld-Tanenbaum Research Institute). For laser micro-irradiation experiments, pDONR221 POGZ was LR recombined into a pHAGE EF1α 3xHA-tag destination vector. Plasmids encoding, I-SceI or pDEST-FRT-FLAG for the different GFP reporter assays, were kindly provided by Dr. Daniel Durocher (Lunenfeld-Tanenbaum Research Institute). Oligonucleotides containing sgRNA were phosphorylated, annealed and ligated into gel-extracted BsmbI-digested linear lentiCRISPRv2. All constructs were validated by Sanger sequencing.

Drugs

The following drugs were used in this study: phleomycin (InvivoGen, ant-ph-1); neocarzinostatin (NCS; Sigma-Aldrich); cisplatin (Tocris); and talazoparib (BMN673; Selleckchem). Cells were pulsed with phleomycin (50 μg/ml) or NCS (100 μg/mL) for 1

hour, unless otherwise indicated, and replaced with fresh media and recovered for indicated times. Similarly, cisplatin and talazopirib were treated for 16 and 24 hours, unless otherwise indicated.

Immunoblotting

Selected cell lines were treated as indicated prior to trypsinization, collection and PBS washes. Cells were placed in 1x LDS loading buffer (10 mM Tris–HCl, 140 mM Tris-base, 0.5 mM EDTA, 1% lithium dodecyl sulfate, 10% glycerol) with 1X protease (Roche) and phosphatase (Sigma) inhibitors. Following sonication, cell lysates were cleared by centrifugation at maximum speed for 15 min at 4ºC. After the addition of loading dye and 2-mercaptoethanol, cleared lysate was placed at 70ºC for 10 mins. Protein lysates were subjected to immunoblotting as previously described (Findlay, Heath et al., 2018). For phospho-protein western blots, RPE1-hTERT cells were irradiated with 1 Gy and recovered for indicated time periods. Proteins from cell lysates were obtained as previously described (Loignon, Amrein et al., 2007, Xu, Loignon et al., 2005). Protein concentration were determined using the PierceTM Micro BCA protein assay kit (ThermoFisher). 35 μg of protein was resolved on 4-12% polyacrylamide gradient Criterion XT Bis-Tris Precast Gels (Biorad Laboratories) and transferred to a nitrocellulose membrane (Sigma). Membranes were blocked with BSA 5% in Tween 20 (0.015%)-TBS for 3 hours at 4˚C and probed overnight with primary antibody at a dilution 1:1000 in T-TBS. Secondary antibodies were used at a dilution of 1:10000 in T-TBS. Signal was detected using Immobilon Western Chemiluminescent HRP substrate (GE Healthcare) and X-ray films (Progene). Antibodies used are outlined in Table 1.

BioID sample preparation for Mass Spectrometry

Samples were processed from HEK 293-T Flp-In cells stably expressing Flag-BirA*HP1-β, Flag-BirA*HP1-γ and Flag-BirA*HP1-α as previously described.[59] Briefly, at 70% confluency, induction of fusion protein expression was achieved by adding 1 μM tetracycline to the cells for 24 h. After induction, the media was supplemented with 50 μM biotin, together with 150 ng/ml neocarzinostatin (NCS) where indicated, for an additional 24 h. Cells were then harvested and washed twice with PBS. Pellets were subsequently

resuspended in cold RIPA buffer containing: 50 mM Tris–HCl pH 7.4, 150 mM NaCl, 1 mM EDTA, 1% NP-40, 0.1% SDS, 0.5% sodium deoxycholate, 1 mM PMSF, 1 mM dithiothreitol, 1:500 Sigma-Aldrich protease inhibitor cocktail (Sigma). Cell homogenates were sonicated and 250 U benzonase was added before high speed centrifugation (12,000 rpm, 30 min). Supernatants were incubated with pre-washed streptavidin-sepharose beads (GE) at 4°C with rotation for 3 h. Beads were collected by centrifugation (2000 rpm 1 min), washed twice with RIPA buffer and three times with 50 mM ammonium bicarbonate (ABC, pH 8.2). Beads were resuspended in 50 mM ABC and on-bead digestion was achieved by adding 1 µg trypsin (Sigma-Aldrich) to the suspension for overnight incubation at 37°C with rotation. Supernatant containing peptides was collected by centrifugation and pooled with supernatants from two following washes with HPLC-grade H_2O. Digestion was ended with the addition of formic acid to a final concentration of 5%. Samples were centrifuged (12000 rpm for 10 min), and the supernatants were dried in a SpeedVac for 3 hr at high rate. Peptides were resuspended in 5% formic acid and kept at −80°C for mass spectrometric analysis. MS processing and protein analysis were carried out as previously described (Findlay et al., 2018). Three biological replicates were performed for each condition. Spectral counts from each replicated were averaged and normalized to protein length, yielding a normalized spectral abundance factor (NSAF).[64] All gene set enrichment analyses (GSEA) were performed with NSAF values and the Reactome v7.2 gene sets using GSEA 4.0.3 (UCSD and Broad Institute).[65] Enriched pathways were then visualized using the EnrichmentMap 3.3 plugin (Bader Lab, University of Toronto) for Cytoscape v8.0 (Ideker Lab, UCSD). [66,67]

Immunofluorescence

U2OS cells were transfected at 60% confluency and re-plated onto #1.5 coverslips of 12-15mm diameter in 24 or 12 well plates, respectively. Cells were allowed to recover for 24h, followed by selected stimulations or treatments. U2OS-LacO cell lines were transfected with 1.25-2.5 μg per well of selected plasmids containing LacR-fusion proteins and recovered for 48 hours. U2OS-FokI cells were transfected with 0.5 nmoles of selected siRNA (Dharmacon) and allowed to recover for 24 hours. In selected experiments cells would be then transfected with a siRNA-resistant construct and recovered for 24 hours

prior to induction with 1 μM Shield1 (Takara Bio) and 1 μM 4-hydroxytamoxifen (Sigma) for 2 hours. Coverslips were then rinsed with PBS, twice, and fixed with 2% paraformaldehyde (PFA, Thermofisher)/PBS for 20 min at RT, washed twice with PBS, followed by a 20 min fixation in 0.3% Triton-100/PBS solution. Coverslips were washed twice with PBS and blocked for one hour in 5% BSA/0.1% Triton-100/PBS (PBSA-T) at room temperature (RT). Selected primary antibodies were then incubated for one hour at RT or overnight at 4ºC. Coverslips were washed twice with PBS and incubated with fluorescent secondary antibodies (Anti-Rat Goat Alexa Fluor 488 [A-11070], Anti-Mouse Goat Alexa Fluor 647, Thermofisher) in PBSA-T for one hour at RT. Coverslips were washed twice in PBS, once in ddH2O, and then mounted with Fluoromount-G (Thermofisher). Images were acquired with a LSM800 confocal microscope (Carl Zeiss AG) and analyzed as previously described (Findlay et al., 2018). Briefly, we monitored the mean fluorescence intensity (M.F.I.) of each specific protein accumulating at the mCherry foci to the background signal for the given protein within the nucleus. Each data point represents a normalized signal on a per cell basis. For the FokI system a minimum of 25 cells were counted per biological replicate, with a total of 3 biological replicates and no less than 100 cells being counted. For γ-H2AX and BRCA1 quantification, HeLa, RPE1-hTERT, and U2OS cell lines were grown on cover slips as mentioned above. These cell lines were subjected to 1 Gy of γ -irradiation (Faxitron, MultiRad 225) and recovered for the indicated times. Prior to cell collection, cells were incubated for one hour with 10 μM 5-Ethynyl-2'-deoxyuridine (EdU). Cells were washed twice with PBS, fixed and permeabilized, as outlined above, then subjected to EdU Click-iT labeling (Thermofisher). Cells were then processed as outlined above. Images were analyzed using the open source Java ImageJ/Fiji program. Nuclei were first identified, by thresholding on DAPI fluorescence followed by analyzing particles larger than 75 μm^2. These regions were then used to measure fluorescence of EdU signal to identify EdU+ cells. BRCA1 and γ-H2AX foci were counted using the Find Maxima feature and Measure function. Analyses are presented as a percent of cells containing EdU in a field of view containing more than 5 respective foci. A total of 5 fields of view with a total of least 200 cells analyzed per timepoint for each cell line. For immunofluorescence of γ-H2AX in primary B cells, 50000 stimulated B-cells were collected and loaded into the cytospin

chambers (ThermoScientific) following the manufacturer's instructions and centrifuged at 500 rpm for 3 min. Slides were fixed with 4% paraformaldehyde (PFA, Thermofisher)/PBS for 10 min at room temperature (RT), washed twice with PBS, followed by a 10-minute permeabilization in 0.5% Triton-100/PBS solution. Slides were washed twice with PBS, blocked for one hour in M.O.M. Mouse IgG blocking reagent (Vector Laboratories) and blocked for one hour in 1% BSA/PBS at RT, followed by incubation with primary antibodies overnight at 4°C. Slides were washed twice with PBS and incubated with fluorescent secondary antibodies and DAPI in blocking solution for 1hr at RT. Slides were washed twice in PBS and once in ddH2O, and then mounted with Fluoromount-G (Thermofisher). Images were acquired with a LSM800 confocal microscope (Carl Zeiss AG).

Neutral Comet Assay

A modified alkali comet assay procedure was followed as previously described[68]. Cells were trypsinized at the indicated time points post radiation and resuspended at 30000 cells/mL in PBS. Cells were combined with low meting agarose (1%) (Sigma) at 1:3 ratio and spread over the CometSlide (Trevigen). Slides were dried at room temperature for 2 minutes and immersed into neutral lysis buffer overnight at 4°C. The next day the slides were immersed into neutral electrophoresis buffer (two 15-minute washes) followed by electrophoresis for 20 minutes. Subsequently the slides were washed in water, followed by 5-minutes incubation in 70% ethanol. Slides were dried and stained with SYBR Gold (Invitrogen). Images were acquired with a LSM800 confocal microscope (Carl Zeiss AG) and the tail moments were quantified using ImageJ with the OpenComet plugin.[69] For each condition at least 75 cells were analyzed.

Laser micro-irradiation

U2OS stable cell populations expressing the POGZ HA-tagged was transferred to a 96-well plate with 170 μm glass bottom (Ibidi), presensitized with 10 μg/ml Hoescht 33342, and micro-irradiated using a FV-3000 Olympus confocal microscope equipped with a 405 nm laser line as described previously.[70] Immunofluorescence was performed as described previously.[70,71] Briefly, following micro-irradiation, cells were allowed to recover

before pre-extraction in PBS containing 0.5% Triton X-100 on ice for 15 min. Following washes with PBS, cells were fixed for 15 min in 3% paraformaldehyde, 2% sucrose PBS solution, permeabilized in PBS containing 0.5% Triton X-100 for 15 min, blocked in PBS containing 3% BSA and 0.05% Tween-20, and stained with the primary antibodies. After extensive washing, samples were incubated with 1:250 each of goat anti-mouse Alexa 488-conjugated and goat anti-rabbit Alexa 647-conjugated antibodies. DAPI staining was performed, and samples were imaged on a FV-3000 Olympus confocal microscope.

BrdU Cell Cycle Flow Cytometry

HeLa, RPE1-hTERT, or U2OS cell lines were sub-cultured to 60% confluency. Cell lines were irradiated with 1 Gy and recovered for indicated times. Prior to cell collection, cells were incubated for one hour with 10 μM 5-bromo-2'-deoxyuridine (BrdU). Cells were harvested and immediately processed with the Biolegend Phase-Flow Alexa Fluor 647 kit (BioLegend). Cells were counterstained with DAPI and at least 10 000 events were acquired on a BD Fortessa (Becton Dickinson).

Phosphorylation-coupled Flow Cytometry

U2OS cells were cultured until 60% confluency and, unless otherwise stated, pulsed with phleomycin were recovered for selected durations to assess recovery from DNA damage. To assess levels of phosphorylated histones or selected kinases, cells were prepared as previously described.[23] Cells were collected via trypsinization and washed twice in PBS. Cells were fixed at RT in 2% PFA/PBS, followed by two washes in PBS, and then permeabilized via the addition of 95% ethanol dropwise, while vortexing, to a final concentration of 70% and stored at -20 ºC until use. Cells were centrifuged at 900g and washed once with cold PBS, pelleted at 500g, and washed once with PBSA-T at RT. Cells were incubated in PBSA-T with indicated primary antibodies or isotype controls for one hour at room temperature. Cells were washed with PBS, and incubated with selected secondary antibodies for one hour at RT. Cells were washed with PBS, followed by resuspension in a PBSA-T solution containing propidium iodide (20 μg/mL, Sigma) and RNAse A (250 μg/mL, BioShop Canada). A minimum of 10,000 events were collected on a BD Fortessa (Becton Dickinson). Antibodies used are outlined in Table 1.

Drug Cytotoxicity Screening by Sulforhodamine B Assay

HeLa, RPE1-hTERT, or U2OS cell lines were plated at a concentration of 1000 cells/well in 96 well plates. Cells were treated with indicated drugs, washed with PBS and recovered in normal medium for the remaining duration of the experiment. Cells were left to grow for 4 days and then washed twice in PBS, followed by fixation with a 10% trichloroacetic acid (TCA; Bioshop Canada Inc) at 4°C for one hour. Cells were washed in room temperature water and left to air-dry overnight. Plates were incubated in 0.04% sulforhodamine B (SRB; Sigma-Aldrich) for 30 minutes at room temperature, and washed 3 times with 0.1% acetic acid and left to air-dry. Dyed protein content was solubilized in 10mM unbuffered Tris and slight agitation at room temperature for 30 minutes. Optical density of absorbance at 530nm was acquired with a FLUOstar Optima plate reader. Control wells were used for background subtraction. Treatments were done in triplicate, averaged and normalized to an untreated control. At least 3 biological replicates were done for each drug.

GFP-based DNA Repair Assays

For DR- and SA-GFP reporter assays, U2OS cells carrying the respective GFP expression cassette were transfected with the indicated siRNAs. Twenty-four hours after transfection, cells were transfected with empty vector (EV, pDEST-FRT-FLAG) or I-SceI plasmids. After 48 hours, cells were trypsinized, harvested, washed and resuspended in PBS. The percentage of GFP-positive cells were determined by flow cytometry. The data was analyzed using the FlowJo software and presented as previously described.[59]

Micronuclei Formation

U2OS cells were transfected and plated on coverslips as previously described. Transfected cells were then subjected to a sublethal pulse of phleomycin (10 μg/mL) for one hour. Treated cells were cultured for 48 hours until being fixed, permeabilized and stained with DAPI before images were acquired via immunofluorescence microscopy, as previously described[72] to identify DNA containing nuclear and extranuclear bodies.

Quantitative Real Time PCR

RNA was extracted using the RNeasy Mini kit (Qiagen). One μg of RNA was used to prepare cDNA using the *LunaScript RT SuperMix (New England Biolabs). cDNA was then diluted 10-fold and 1* μL *was used per qRT-PCR reaction. Reactions were performed in triplicate with the Luna Universal qPCR Master mix (New England Biolabs) in a total volume of 10* μ*L.* Primers for reactions are outlined in Table 2a.

Pogz Germline Mutant Mice

To produce null alleles, annotated transcripts (Ensembl Rnor v6.0) were examined to identify a critical region defined as one or more exons that when deleted or frame-shifted by internal deletions will put all known full-length protein-coding transcripts out of frame. Guide RNAs (gRNAs) were then designed in flanking intronic regions or within exon(s) using CRISPR (Haeussler *et al*., 2016) with specificity confirmed using Cas-OFFinder (Bae *et al*., 2014) with off-target PAM set to -NRG. Exons 9 (ENSMUSE00001286300) and 10 (ENSMUSE00001225367) were identified as being present in all potential coding transcripts of *Pogz* and gRNAs flanking these critical exons were designed by The Toronto Centre for Phenogenomics (TCP) (sgRNA sequences listed in Table 2B).

Single gRNAs (sgRNAs) were synthesized as described (Gertsenstein, Nutter 2018). Briefly, templates for *in vitro* primer extension and transcription were ordered from Integrated DNA Technologies at 100 μM in IDTE buffer. Primers were diluted to 1 μM in IDTE buffer and 5 μL was used with the EnGen sgRNA synthesis kit as described. When four sgRNAs were used, primers for upstream or downstream sgRNAs were pooled for synthesis with 2.5 μL of each 1 μM primer added to a single reaction to produce a sgRNA pool. Purified sgRNAs were analyzed on an Agilent Bioanalyzer at The Centre for Applied Genomics at The Hospital for Sick Children to assess integrity. Concentration was determined by Qubit with the Broad Range RNA Assay Kit (ThermoFisher Q10211).

Three-four weeks old C57BL/6J (Jackson) females were used as embryo donors. CD-1 (ICR) (Charles River) outbred albino stock was used as pseudo-pregnant recipients. Animals were maintained on 12 h light/dark cycle and provided with food and water *ad libitum* in individually ventilated units (Techniplast) in the specific-pathogen free facility at the TCP. All procedures involving animals were performed in compliance with the Animals

for Research Act of Ontario and the Guidelines of the Canadian Council on Animal Care. Animal Care Committee reviewed and approved all procedures conducted on animals at TCP.

Donor females were superovulated by intraperitoneal (IP) injection of 5 IU of pregnant mare's serum gonadotropin (PMSG, Prospec, HOR-272) at 10 am (room light cycle: 5 am/on, 5 pm/off) followed 48 hours later by an IP injection of 5 IU human chorionic gonadotrophin (hCG, EMD Millipore 230734) and mated overnight with proven breeder males. The next morning the females were checked for the presence of a vaginal copulation plug as evidence of successful mating. Oviducts were dissected at approximately 22 hours post hCG and cumulus oocyte complexes were released in M2 medium (Cytospring) and treated with 0.3 mg/ml hyaluronidase (Sigma H4272) as described (Behringer et al., 2014). Fertilized embryos were selected and kept at 37 C, 6% CO_2 in microdrops of KSOM media with amino acids ($KSOM^{AA}$, Cytospring) covered by embryo tested paraffin oil (Zenith Biotech, ZPOL-50) prior to pronuclear microinjection or electroporation. Embryos were briefly cultured in $KSOM^{AA}$ and transferred into the oviducts of 0.5 d.p.c. pseudo-pregnant CD-1(ICR) female recipients shortly after manipulations (Behringer et al., 2014).

Founder mice were screened by PCR to assess the deletion of E9/E10 and confirmed by Sanger sequencing, backcrossed and maintained on a C57BL/6J strain background. All experimental protocols with mice were performed under ethical approval from McGill Animal Care Committee. Mice were maintained under pathogen-free conditions at the Lady Davis Institute for Medical Research Animal Care Facility in accordance with institutional guidelines. Organs, tissues, plasma were collected from 8-12-week-old mice, unless otherwise stated. Mice were genotyped at weaning age (3 weeks), if required. When indicated, age-matched mice were subjected to lethal irradiation (8.5 Gy). Post-irradiation mice were given Baytril-supplemented drinking water (Bayer DVM, 2.27 mg/ml). Mice were euthanized at an established humane endpoint.

To assess kinetics of embryonic lethality and derive embryonic fibroblasts (MEFs), timed-mating experiments between *Pogz* heterozygotes were initiated. E0.5 was designated when vaginal plugs were visible. Pregnant female mice were euthanized, and embryos

were harvested from uterine horns under sterile conditions. Embryos were dissected and dissociated with 0.25% trypsin at 4°C overnight, followed by 30 minutes at 37°C. MEFs were passaged twice before use in SRB assays.

For behavioral tests, age and gender matched littermates (wild type or *Pogz*$^{+/\Delta}$) mice were transported to the TCP and assessed in the Fear Conditioning and Open Field tests as per the Standard Operating Protocols. For the open field test, each open field arena (43.5 cm^2) was composed of a peripheral zone (8 cm from the edge of the arena walls) and a central zone (40% of the total area of the arena). Mice were tested in the open field chamber for 20 mins, and activity was measured by IR laser beam break detection in the x, y, and z dimensions. Activity was analyzed for the duration of time spent in either zone in 5 minute time bins. For the contextual and cued fear conditioning test, mice were placed in the experimental environment for 120 seconds to establish the context baseline, then exposed to a cue (tone – conditional stimulus) for 30 seconds which co-terminated with a mild foot shock (unconditional stimulus) for the last 2 seconds, and finished by 150 seconds with no stimuli. Time spent freezing was measured throughout the test. The following day the mice were placed in the same contextual environment for 5 minutes and time spent freezing was measured. After a minimum of 2 hours mice were placed back in an altered contextual environment (different scent, floor, walls, ceiling, and lighting) for 2 minutes (Tone baseline) and then the cue (tone – conditional stimulus) was sounded for 3 minutes without the foot shock (unconditional stimulus) and freezing time was measured.

***Ex vivo* B cell Class Switch Recombination.**

To prepare primary B cells for *ex vivo* class switch recombination, splenocytes were harvested as from 8-12-week-old mice under sterile conditions and prepared, as previously described.[73] Splenocytes were layered on Ficoll-Paque (GE Healthcare) to isolate lymphocytes. CD43- splenocytes were isolated by negative selection with CD43-conjugated microbeads and LR magnetic columns (Miltenyi Biotec). Cells were labelled with 0.5 μM CFSE (Thermofisher) and plated at a concentration of $0.5x10^6$ cells/mL in medium containing 50 ng/mL mouse IL-4 (R&D Systems) and 25 μg/mL lipopolysaccharide (LPS; Sigma). Unstimulated controls were set up in parallel. At

indicated time points, cells were harvested to assess IgG1 expression, phosphorylated H2AX levels, and Annexin V surface expression (BD Pharmingen). Antibodies used are outlined in Table 1.

ELISA for Determination of Immunoglobulin levels

Sandwich ELISAs were done as previously described.[74] Briefly, sera from blood was collected via cardiac puncture from 8-12-week-old mice while fecal samples were weighed and resuspended at a ratio of 100 mg feces per ml of PBS/0.01% sodium azide/1% (v/v) 100x protease inhibitor cocktail (Sigma). 96 well EIA/RIA plates (Corning) were coated overnight at 4ºC with anti-isotype-specific antibodies (BD Pharmingen) in carbonate buffer, pH 9.6 to capture IgM, IgG1, IgG2b, IgG3 or IgA. Washing was done with PBS/T (0.01% Tween-20), blocking was with PBS/1% BSA, and serum and antibodies were diluted in PBS/1% BSA. Serum dilutions were incubated in the coated wells for 2h, and bound antibodies were detected using corresponding biotinylated rat anti-mouse IgM, IgG1, IgG2b, IgG3 or IgA (BD Pharmingen). This was followed by incubation with HRP-conjugated streptavidin (1:5000; Thermo Scientific) for 1h and subsequently developed using 2,2-azino-bis (3-ethylbenzothiazoline-6-sulfonic acid) substrate (Sigma). Absorbance was measured at 405nm in a BioTek Synergy HTX multi-mode reader. Standard curves and relative serum antibody concentrations were calculated using GraphPad Prism 8 software.

Statistics

All quantitative experiments are graphed with mean +/- SEM with data from the independent number of independent experiments in the figure legend. All data sets were tested for normal distribution by Shapiro-Wilk Test. Statistical significance was determined using the test indicated in the legend. All statistical analyses were performed in Prism v8 (GraphPad Software).

Data Availability

The mass spectrometry raw data and associated peak lists related to the BioID analysis of the different HP1 isoforms in both control and upon NCS treatment have been

deposited to the MassIVE repository database and assigned the reference code MSV000087687 (ftp://massive.ucsd.edu/MSV000087687/).

2.6 References

1. Bunting SF, Nussenzweig A. End-joining, translocations and cancer. Nat Rev Cancer [Internet]. 2013/06/14. 2013;13:443–54. Available from: https://www.ncbi.nlm.nih.gov/pubmed/23760025
2. Polo SE, Jackson SP. Dynamics of DNA damage response proteins at DNA breaks: a focus on protein modifications. Genes Dev [Internet]. 2011/03/03. 2011;25:409–33. Available from: https://www.ncbi.nlm.nih.gov/pubmed/21363960
3. Hustedt N, Durocher D. The control of DNA repair by the cell cycle. Nat Cell Biol [Internet]. 2016/12/23. 2016;19:1–9. Available from: https://www.ncbi.nlm.nih.gov/pubmed/28008184
4. Scully R, Panday A, Elango R, Willis NA. DNA double-strand break repair-pathway choice in somatic mammalian cells. Nat Rev Mol Cell Biol [Internet]. 2019/07/03. 2019;20:698–714. Available from: https://www.ncbi.nlm.nih.gov/pubmed/31263220
5. Densham RM, Morris JR. Moving Mountains-The BRCA1 Promotion of DNA Resection. Front Mol Biosci [Internet]. 2019/09/26. 2019;6:79. Available from: https://www.ncbi.nlm.nih.gov/pubmed/31552267
6. Botuyan M V, Lee J, Ward IM, Kim JE, Thompson JR, Chen J, et al. Structural basis for the methylation state-specific recognition of histone H4-K20 by 53BP1 and Crb2 in DNA repair. Cell [Internet]. 2006/12/28. 2006;127:1361–73. Available from: https://www.ncbi.nlm.nih.gov/pubmed/17190600
7. Fradet-Turcotte A, Canny MD, Escribano-Diaz C, Orthwein A, Leung CC, Huang H, et al. 53BP1 is a reader of the DNA-damage-induced H2A Lys 15 ubiquitin mark. Nature [Internet]. 2013/06/14. 2013;499:50–4. Available from:

https://www.ncbi.nlm.nih.gov/pubmed/23760478

8. Huyen Y, Zgheib O, Ditullio Jr. RA, Gorgoulis VG, Zacharatos P, Petty TJ, et al. Methylated lysine 79 of histone H3 targets 53BP1 to DNA double-strand breaks. Nature [Internet]. 2004/11/05. 2004;432:406–11. Available from: https://www.ncbi.nlm.nih.gov/pubmed/15525939
9. Li M, Yu X. Function of BRCA1 in the DNA damage response is mediated by ADP-ribosylation. Cancer Cell [Internet]. 2013/05/18. 2013;23:693–704. Available from: https://www.ncbi.nlm.nih.gov/pubmed/23680151
10. Manke IA, Lowery DM, Nguyen A, Yaffe MB. BRCT repeats as phosphopeptide-binding modules involved in protein targeting. Science (80-) [Internet]. 2003/10/25. 2003;302:636–9. Available from: https://www.ncbi.nlm.nih.gov/pubmed/14576432
11. Yu X, Chini CC, He M, Mer G, Chen J. The BRCT domain is a phospho-protein binding domain. Science (80-) [Internet]. 2003/10/25. 2003;302:639–42. Available from: https://www.ncbi.nlm.nih.gov/pubmed/14576433
12. Nakamura K, Saredi G, Becker JR, Foster BM, Nguyen N V, Beyer TE, et al. H4K20me0 recognition by BRCA1-BARD1 directs homologous recombination to sister chromatids. Nat Cell Biol [Internet]. 2019/02/26. 2019;21:311–8. Available from: https://www.ncbi.nlm.nih.gov/pubmed/30804502
13. Chapman JR, Barral P, Vannier JB, Borel V, Steger M, Tomas-Loba A, et al. RIF1 is essential for 53BP1-dependent nonhomologous end joining and suppression of DNA double-strand break resection. Mol Cell [Internet]. 2013/01/22. 2013;49:858–71. Available from: https://www.ncbi.nlm.nih.gov/pubmed/23333305
14. Chapman JR, Sossick AJ, Boulton SJ, Jackson SP. BRCA1-associated exclusion

of 53BP1 from DNA damage sites underlies temporal control of DNA repair. J Cell Sci [Internet]. 2012/05/04. 2012;125:3529–34. Available from: https://www.ncbi.nlm.nih.gov/pubmed/22553214

15. Escribano-Diaz C, Durocher D. DNA repair pathway choice--a PTIP of the hat to 53BP1. EMBO Rep [Internet]. 2013/07/13. 2013;14:665–6. Available from: https://www.ncbi.nlm.nih.gov/pubmed/23846307
16. Feng L, Fong KW, Wang J, Wang W, Chen J. RIF1 counteracts BRCA1-mediated end resection during DNA repair. J Biol Chem [Internet]. 2013/03/15. 2013;288:11135–43. Available from: https://www.ncbi.nlm.nih.gov/pubmed/23486525
17. Zimmermann M, Lottersberger F, Buonomo SB, Sfeir A, de Lange T. 53BP1 regulates DSB repair using Rif1 to control 5' end resection. Science (80-) [Internet]. 2013/01/12. 2013;339:700–4. Available from: https://www.ncbi.nlm.nih.gov/pubmed/23306437
18. Greenberg RA, Sobhian B, Pathania S, Cantor SB, Nakatani Y, Livingston DM. Multifactorial contributions to an acute DNA damage response by BRCA1/BARD1-containing complexes. Genes Dev [Internet]. 2006/01/05. 2006;20:34–46. Available from: https://www.ncbi.nlm.nih.gov/pubmed/16391231
19. Ayoub N, Jeyasekharan AD, Bernal JA, Venkitaraman AR. HP1-β mobilization promotes chromatin changes that initiate the DNA damage response. Nature. 2008;453:682–6.
20. Ayoub N, Jeyasekharan AD, Venkitaraman AR. Mobilization and recruitment of HP1β: A bimodal response to DNA breakage. http://dx.doi.org/104161/cc8189486

[Internet]. 2009 [cited 2022 Apr 16];8:2946–51. Available from: https://www.tandfonline.com/doi/abs/10.4161/cc.8.18.9486

21. Baldeyron C, Soria G, Roche D, Cook AJ, Almouzni G. HP1alpha recruitment to DNA damage by p150CAF-1 promotes homologous recombination repair. J Cell Biol [Internet]. 2011/04/06. 2011;193:81–95. Available from: https://www.ncbi.nlm.nih.gov/pubmed/21464229

22. Luijsterburg MS, Dinant C, Lans H, Stap J, Wiernasz E, Lagerwerf S, et al. Heterochromatin protein 1 is recruited to various types of DNA damage. J Cell Biol [Internet]. 2009/05/20. 2009;185:577–86. Available from: https://www.ncbi.nlm.nih.gov/pubmed/19451271

23. Iyama T, Wilson 3rd DM, Spencer NF, Norton SD, Harrison LL, Li GZ, et al. DNA double-strand breaks promote methylation of histone H3 on lysine 9 and transient formation of repressive chromatin. Philippa Marrack, editor. Nature [Internet]. 2019/01/22. 2013 [cited 2016 Nov 26];9:976–97. Available from: https://www.ncbi.nlm.nih.gov/pubmed/24927542

24. Wu W, Togashi Y, Johmura Y, Miyoshi Y, Nobuoka S, Nakanishi M, et al. HP1 regulates the localization of FANCJ at sites of DNA double-strand breaks. Cancer Sci [Internet]. 2016/10/30. 2016;107:1406–15. Available from: https://www.ncbi.nlm.nih.gov/pubmed/27399284

25. Lee YH, Kuo CY, Stark JM, Shih HM, Ann DK. HP1 promotes tumor suppressor BRCA1 functions during the DNA damage response. Nucleic Acids Res [Internet]. 2013/04/17. 2013;41:5784–98. Available from: https://www.ncbi.nlm.nih.gov/pubmed/23589625

26. Wu W, Nishikawa H, Fukuda T, Vittal V, Asano M, Miyoshi Y, et al. Interaction of BARD1 and HP1 Is Required for BRCA1 Retention at Sites of DNA Damage. Cancer Res [Internet]. 2015/01/31. 2015;75:1311–21. Available from: https://www.ncbi.nlm.nih.gov/pubmed/25634209

27. Ayrapetov MK, Gursoy-Yuzugullu O, Xu C, Xu Y, Price BD. DNA double-strand breaks promote methylation of histone H3 on lysine 9 and transient formation of repressive chromatin. Proc Natl Acad Sci U S A [Internet]. 2014/06/14. 2014;111:9169–74. Available from: https://www.ncbi.nlm.nih.gov/pubmed/24927542

28. Falk M, Lukasova E, Gabrielova B, Ondrej V, Kozubek S. Chromatin dynamics during DSB repair. Biochim Biophys Acta [Internet]. 2007/09/14. 2007;1773:1534–45. Available from: https://www.ncbi.nlm.nih.gov/pubmed/17850903

29. Fnu S, Williamson EA, De Haro LP, Brenneman M, Wray J, Shaheen M, et al. Methylation of histone H3 lysine 36 enhances DNA repair by nonhomologous end-joining. Proc Natl Acad Sci U S A [Internet]. 2010/12/29. 2011;108:540–5. Available from: https://www.ncbi.nlm.nih.gov/pubmed/21187428

30. Young LC, McDonald DW, Hendzel MJ. Kdm4b histone demethylase is a DNA damage response protein and confers a survival advantage following gamma-irradiation. J Biol Chem [Internet]. 2013/06/08. 2013;288:21376–88. Available from: https://www.ncbi.nlm.nih.gov/pubmed/23744078

31. Zarebski M, Wiernasz E, Dobrucki JW. Recruitment of heterochromatin protein 1 to DNA repair sites. Cytom A [Internet]. 2009/05/30. 2009;75:619–25. Available from: https://www.ncbi.nlm.nih.gov/pubmed/19479850

32. Roux KJ, Kim DI, Raida M, Burke B. A promiscuous biotin ligase fusion protein identifies proximal and interacting proteins in mammalian cells. J Cell Biol [Internet]. 2012/03/14. 2012;196:801–10. Available from: https://www.ncbi.nlm.nih.gov/pubmed/22412018

33. Vermeulen M, Eberl HC, Matarese F, Marks H, Denissov S, Butter F, et al. Quantitative Interaction Proteomics and Genome-wide Profiling of Epigenetic Histone Marks and Their Readers. Cell. 2010;142:967–80.

34. Nozawa RS, Nagao K, Masuda HT, Iwasaki O, Hirota T, Nozaki N, et al. Human POGZ modulates dissociation of HP1α from mitotic chromosome arms through Aurora B activation. Nat Cell Biol 2010 127 [Internet]. 2010 [cited 2022 May 24];12:719–27. Available from: https://www.nature.com/articles/ncb2075

35. Baude A, Aaes TL, Zhai B, Al-Nakouzi N, Oo HZ, Daugaard M, et al. Hepatoma-derived growth factor-related protein 2 promotes DNA repair by homologous recombination. Nucleic Acids Res. 2015;44:2214–26.

36. Ferretti A, Barresi S, Trivisano M, Ciolfi A, Dentici ML, Radio FC, et al. POGZ-related epilepsy: Case report and review of the literature. Am J Med Genet A [Internet]. 2019/05/29. 2019;179:1631–6. Available from: https://www.ncbi.nlm.nih.gov/pubmed/31136090

37. Samanta D, Ramakrishnaiah R, Schaefer B. The neurological aspects related to POGZ mutation: case report and review of CNS malformations and epilepsy. Acta Neurol Belg [Internet]. 2019/03/18. 2020;120:447–50. Available from: https://www.ncbi.nlm.nih.gov/pubmed/30879264

38. Hashimoto R, Nakazawa T, Tsurusaki Y, Yasuda Y, Nagayasu K, Matsumura K, et

al. Whole-exome sequencing and neurite outgrowth analysis in autism spectrum disorder. J Hum Genet [Internet]. 2015/11/20. 2016;61:199–206. Available from: https://www.ncbi.nlm.nih.gov/pubmed/26582266

39. Zhao W, Tan J, Zhu T, Ou J, Li Y, Shen L, et al. Rare inherited missense variants of POGZ associate with autism risk and disrupt neuronal development. J Genet Genomics [Internet]. 2019/06/15. 2019;46:247–57. Available from: https://www.ncbi.nlm.nih.gov/pubmed/31196716

40. Varnaite R, MacNeill SA. Meet the neighbors: Mapping local protein interactomes by proximity-dependent labeling with BioID. Proteomics [Internet]. 2016/06/23. 2016;16:2503–18. Available from: https://www.ncbi.nlm.nih.gov/pubmed/27329485

41. Orthwein A, Fradet-Turcotte A, Noordermeer SM, Canny MD, Brun CM, Strecker J, et al. Mitosis inhibits DNA double-strand break repair to guard against telomere fusions. Science (80-) [Internet]. 2014/03/22. 2014;344:189–93. Available from: https://www.ncbi.nlm.nih.gov/pubmed/24652939

42. Rivera B, Di Iorio M, Frankum J, Nadaf J, Fahiminiya S, Arcand SL, et al. Functionally Null RAD51D Missense Mutation Associates Strongly with Ovarian Carcinoma. Cancer Res [Internet]. 2017/06/25. 2017;77:4517–29. Available from: https://www.ncbi.nlm.nih.gov/pubmed/28646019

43. Lu Y, Liu Y, Yang C. Evaluating In Vitro DNA Damage Using Comet Assay. J Vis Exp [Internet]. 2017/10/21. 2017; Available from: https://www.ncbi.nlm.nih.gov/pubmed/29053680

44. Johansson P, Fasth A, Ek T, Hammarsten O. Validation of a flow cytometry-based detection of gamma-H2AX, to measure DNA damage for clinical applications.

Cytom B Clin Cytom [Internet]. 2016/04/10. 2017;92:534–40. Available from: https://www.ncbi.nlm.nih.gov/pubmed/27060560

45. Vichai V, Kirtikara K. Sulforhodamine B colorimetric assay for cytotoxicity screening. Nat Protoc [Internet]. 2007/04/05. 2006;1:1112–6. Available from: https://www.ncbi.nlm.nih.gov/pubmed/17406391

46. Bhattacharyya A, Ear US, Koller BH, Weichselbaum RR, Bishop DK. The breast cancer susceptibility gene BRCA1 is required for subnuclear assembly of Rad51 and survival following treatment with the DNA cross-linking agent cisplatin. J Biol Chem [Internet]. 2000/06/14. 2000;275:23899–903. Available from: https://www.ncbi.nlm.nih.gov/pubmed/10843985

47. Farmer H, McCabe N, Lord CJ, Tutt AN, Johnson DA, Richardson TB, et al. Targeting the DNA repair defect in BRCA mutant cells as a therapeutic strategy. Nature [Internet]. 2005/04/15. 2005;434:917–21. Available from: https://www.ncbi.nlm.nih.gov/pubmed/15829967

48. Yuan SS, Chang HL, Hou MF, Chan TF, Kao YH, Wu YC, et al. Neocarzinostatin induces Mre11 phosphorylation and focus formation through an ATM- and NBS1-dependent mechanism. Toxicology [Internet]. 2002/07/24. 2002;177:123–30. Available from: https://www.ncbi.nlm.nih.gov/pubmed/12135616

49. Shanbhag NM, Greenberg RA. The dynamics of DNA damage repair and transcription. Methods Mol Biol [Internet]. 2013/08/28. 2013;1042:227–35. Available from: https://www.ncbi.nlm.nih.gov/pubmed/23980011

50. Gudmundsdottir B, Gudmundsson KO, Klarmann KD, Singh SK, Sun L, Singh S, et al. POGZ Is Required for Silencing Mouse Embryonic beta-like Hemoglobin and

Human Fetal Hemoglobin Expression. Cell Rep [Internet]. 2018/06/14. 2018;23:3236–48. Available from: https://www.ncbi.nlm.nih.gov/pubmed/29898395

51. Matsumura K, Seiriki K, Okada S, Nagase M, Ayabe S, Yamada I, et al. Pathogenic POGZ mutation causes impaired cortical development and reversible autism-like phenotypes. Nat Commun 2020 111 [Internet]. 2020 [cited 2022 Jan 4];11:1–16. Available from: https://www.nature.com/articles/s41467-020-14697-z

52. Suliman-Lavie R, Title B, Cohen Y, Hamada N, Tal M, Tal N, et al. Pogz deficiency leads to transcription dysregulation and impaired cerebellar activity underlying autism-like behavior in mice. Nat Commun 2020 111 [Internet]. 2020 [cited 2022 Jan 4];11:1–15. Available from: https://www.nature.com/articles/s41467-020-19577-0

53. Bartova E, Malyskova B, Komurkova D, Legartova S, Suchankova J, Krejci J, et al. Function of heterochromatin protein 1 during DNA repair. Protoplasma [Internet]. 2017/02/27. 2017;254:1233–40. Available from: https://www.ncbi.nlm.nih.gov/pubmed/28236007

54. Pavone P, Pratico AD, Ruggieri M, Rizzo R, Falsaperla R. Resuming the obsolete term “small head”: when microcephaly occurs without cognitive impairment. Neurol Sci [Internet]. 2017/07/28. 2017;38:1723–5. Available from: https://www.ncbi.nlm.nih.gov/pubmed/28748276

55. Barton JC, Barton JC, Bertoli LF, Acton RT. Characterization of adult patients with IgG subclass deficiency and subnormal IgG2. PLoS One [Internet]. 2020/10/14. 2020;15:e0240522. Available from: https://www.ncbi.nlm.nih.gov/pubmed/33048985

56. Cortizas EM, Zahn A, Hajjar ME, Patenaude AM, Di Noia JM, Verdun RE. Alternative end-joining and classical nonhomologous end-joining pathways repair different types of double-strand breaks during class-switch recombination. J Immunol [Internet]. 2013/10/23. 2013;191:5751–63. Available from: https://www.ncbi.nlm.nih.gov/pubmed/24146042

57. Hasham MG, Donghia NM, Coffey E, Maynard J, Snow KJ, Ames J, et al. Widespread genomic breaks generated by activation-induced cytidine deaminase are prevented by homologous recombination. Nat Immunol [Internet]. 2010/07/27. 2010;11:820–6. Available from: https://www.ncbi.nlm.nih.gov/pubmed/20657597

58. Vermeulen M, Eberl HC, Matarese F, Marks H, Denissov S, Butter F, et al. Quantitative interaction proteomics and genome-wide profiling of epigenetic histone marks and their readers. Cell [Internet]. 2010/09/21. 2010;142:967–80. Available from: https://www.ncbi.nlm.nih.gov/pubmed/20850016

59. Findlay S, Heath J, Luo VM, Malina A, Morin T, Coulombe Y, et al. SHLD2/FAM35A co-operates with REV7 to coordinate DNA double-strand break repair pathway choice. Embo j [Internet]. 2018/08/30. 2018;37. Available from: https://www.ncbi.nlm.nih.gov/pubmed/30154076

60. Moquin DM, Genois MM, Zhang JM, Ouyang J, Yadav T, Buisson R, et al. Localized protein biotinylation at DNA damage sites identifies ZPET, a repressor of homologous recombination. Genes Dev [Internet]. 2018/12/21. 2019;33:75–89. Available from: https://www.ncbi.nlm.nih.gov/pubmed/30567999

61. Goodarzi AA, Jeggo P, Lobrich M. The influence of heterochromatin on DNA double-strand break repair: getting the strong, silent type to relax. DNA Repair

(Amst). 2010;9:1273–82.

62. White D, Rafalska-Metcalf IU, Ivanov A V, Corsinotti A, Peng H, Lee SC, et al. The ATM substrate KAP1 controls DNA repair in heterochromatin: regulation by HP1 proteins and serine 473/824 phosphorylation. Mol Cancer Res [Internet]. 2011/12/30. 2012;10:401–14. Available from: https://www.ncbi.nlm.nih.gov/pubmed/22205726

63. Bosch-Presegue L, Raurell-Vila H, Thackray JK, Gonzalez J, Casal C, Kane-Goldsmith N, et al. Mammalian HP1 Isoforms Have Specific Roles in Heterochromatin Structure and Organization. Cell Rep [Internet]. 2017/11/23. 2017;21:2048–57. Available from: https://www.ncbi.nlm.nih.gov/pubmed/29166597

64. McIlwain S, Mathews M, Bereman MS, Rubel EW, MacCoss MJ, Noble WS. Estimating relative abundances of proteins from shotgun proteomics data. BMC Bioinformatics [Internet]. 2012/11/21. 2012;13:308. Available from: https://www.ncbi.nlm.nih.gov/pubmed/23164367

65. Subramanian A, Tamayo P, Mootha VK, Mukherjee S, Ebert BL, Gillette MA, et al. Gene set enrichment analysis: a knowledge-based approach for interpreting genome-wide expression profiles. Proc Natl Acad Sci U S A [Internet]. 2005/10/04. 2005;102:15545–50. Available from: https://www.ncbi.nlm.nih.gov/pubmed/16199517

66. Merico D, Isserlin R, Stueker O, Emili A, Bader GD. Enrichment map: a network-based method for gene-set enrichment visualization and interpretation. PLoS One [Internet]. 2010/11/19. 2010;5:e13984. Available from: https://www.ncbi.nlm.nih.gov/pubmed/21085593

67. Shannon P, Markiel A, Ozier O, Baliga NS, Wang JT, Ramage D, et al. Cytoscape: a software environment for integrated models of biomolecular interaction networks. Genome Res [Internet]. 2003/11/05. 2003;13:2498–504. Available from: https://www.ncbi.nlm.nih.gov/pubmed/14597658

68. Olive PL, Banath JP. The comet assay: a method to measure DNA damage in individual cells. Nat Protoc [Internet]. 2007/04/05. 2006;1:23–9. Available from: https://www.ncbi.nlm.nih.gov/pubmed/17406208

69. Gyori BM, Venkatachalam G, Thiagarajan PS, Hsu D, Clement M V. OpenComet: an automated tool for comet assay image analysis. Redox Biol [Internet]. 2014/03/14. 2014;2:457–65. Available from: https://www.ncbi.nlm.nih.gov/pubmed/24624335

70. Gaudreau-Lapierre A, Garneau D, Djerir B, Coulombe F, Morin T, Marechal A. Investigation of Protein Recruitment to DNA Lesions Using 405 Nm Laser Micro-irradiation. J Vis Exp [Internet]. 2018/04/10. 2018; Available from: https://www.ncbi.nlm.nih.gov/pubmed/29630045

71. Gaudreau-Lapierre A et al. Investigation of Protein Recruitment to DNA Lesions Using 405 Nm Laser Micro-irradiation. - PubMed - NCBI. 2018; Available from: https://www.ncbi.nlm.nih.gov/pubmed/

72. Harding SM, Benci JL, Irianto J, Discher DE, Minn AJ, Greenberg RA. Mitotic progression following DNA damage enables pattern recognition within micronuclei. Nature [Internet]. 2017/08/02. 2017;548:466–70. Available from: https://www.ncbi.nlm.nih.gov/pubmed/28759889

73. Orthwein A, Patenaude AM, Affar el B, Lamarre A, Young JC, Di Noia JM.

Regulation of activation-induced deaminase stability and antibody gene diversification by Hsp90. J Exp Med [Internet]. 2010/11/03. 2010;207:2751–65. Available from: https://www.ncbi.nlm.nih.gov/pubmed/21041454

74. Heath JJ, Fudge NJ, Gallant ME, Grant MD. Proximity of Cytomegalovirus-Specific CD8(+) T Cells to Replicative Senescence in Human Immunodeficiency Virus-Infected Individuals. Front Immunol [Internet]. 2018/03/13. 2018;9:201. Available from: https://www.ncbi.nlm.nih.gov/pubmed/29527205

Chapter 3: The developmental protein POGZ suppresses TGF-β mediated metastasis in Triple Negative Breast Cancer

John Heath, Valerie Sabourin, Steven Hebert, Steven Findlay, Claudia Kleinman, Alexandre Orthwein & Josie Ursini-Siegel

3.1 Connecting Text

In Chapter 2, a new function of the HP1 binding protein, POGZ, in the DNA repair pathway of homologous recombination, was presented. We furthered the current knowledge of POGZ in DNA repair by implicating its association with the γ isoform of HP1 in the recruitment and stabilization of the essential HR factors BRCA1-BARD1. Furthermore, we show in a novel mouse model of WHSUS, and POGZ haploinsufficiency, that there is a radio-sensitivity, the presence of tissue DNA damage, as well as a compromised B cell diversification response.

POGZ has been recently identified to many roles, ranging from the aforementioned involvement in HR, in cell cycle regulation, and now, recently, in transcriptional regulation. Furthermore, very little is understood about POGZ in the context of a transformed tissue, in contrast to the developing tissue through which most recent studies utilized.

The third chapter of this thesis focuses on identifying what role POGZ plays in an oncogenic capacity. This goal of this study was to generate and characterize both POGZ-deficient and POGZ-overexpressing models. These models were characterized in a 4T1 murine model, which closely resembles a poor outcome human TNBC pathology. We examined the loss and overexpression of POGZ on primary tumor growth and metastasis, as well as the potential of any transcriptional impact loss of POGZ may have.

3.2 Abstract

The neurodevelopmental-associated zinc finger protein POGZ, was first described in its role in the maintenance of mitotic chromosomes. Mutations in POGZ are notably associated with the onset of autism-like or intellectual disabilities through dysregulation of gene transcription. Many proteins necessary for development are often aberrantly expressed in cancer, however, it is unknown if POGZ possesses any cancer-associated functions. Thus, we investigated the contribution of this protein in the growth and progression of breast cancer. Utilizing a basal-like murine breast carcinoma model, genetically depleted of POGZ via CRISPR-Cas9 (4T1-sg*Pogz*), we observed defective cellular proliferation and colony forming capacity in comparison to a vehicle control cell line (4T1-sg*Rosa*). Interestingly, 4T1-sg*Pogz* tumors, *in vivo*, undergo a reduced growth rate, despite possessing less apoptotic cells and a higher lung-specific metastatic potential than 4T1-sg*Rosa* tumors. Transcriptional profiling of 4T1-sg*Pogz* cell lines revealed elevated TGF-β target genes (e.g. CTGF, ITGB6, CCL2). In fact, basally 4T1-sg*Pogz* cells possess higher phosphorylated SMAD2/3. Furthermore, 4T1-sg*Pogz* cells display significantly higher migratory activities, supporting that weakly proliferative 4T1-sg*Pogz* cells more readily metastasize. Interestingly, p-SMAD levels can be eliminated with TGFBRI/II kinase inhibitors, minorly enhancing cell proliferation but eliminating migratory activity of 4T1-sg*Pogz* cells. We have established a novel role for the neurodevelopmental protein, POGZ, in the growth and progression of a basal-like breast cancer. However, when exploring metastatic potential, despite overt growth defects, we uncovered additional roles for POGZ in suppressing metastasis, exemplifying how certain regulatory proteins impact multiple steps of breast cancer pathology.

3.3 Introduction

Metastatic breast cancer is among the leading causes of death in women, with an overall survival rate of approximately 22% within the next 5 years following diagnosis.[1] Functionally, cancer metastasis is a complex and multi-faceted cellular process particularly the emergence of the epithelial-mesenchymal transition (EMT). Primary tumor cells can become migratory, lose cell polarity, cell-cell adhesion, and acquire mesenchymal properties, allowing them to become invasive.[2–4] An EMT endows breast cancer cells with an increased ability to intravasate into the bloodstream, an essential first step in the metastatic cascade. Upon survival in circulation, a tumor cell must also extravasate and colonize into distant tissues and escape dormancy to form a metastatic colony.[5,6] Development of metastatic lesions of breast cancer, often to the lungs, bone, liver and brain, can restrict blood vasculature and result in loss of necessary organ function.[7,8] Therefore, identifying mechanisms regulating the emergence of metastatic breast cancer are crucial to enhance overall survival in patients affected by this pathology.

Indeed, the transforming growth factor β (TGF-β) pathway plays a dual role in cancer development and progression, through its transcriptional regulation of cell cycle.[9] TGF-β signalling is canonically tumor suppressive, by inducing cell arrest and initiating apoptosis.[9,10] Stimulation with TGF-β ligands trigger the heterodimerization of TGF-β receptor 1 and 2 (TGFBR1/2), catalytically activating the Ser/Thr kinase activity of TGF-βR1, which phosphorylates Mothers Against Decapentaplegic homologue 2 and 3 (SMAD2/SMAD3). These SMAD proteins specifically homo- and hetero-dimerize with the co-SMAD, SMAD4, and translocate to the nucleus to engage with co-activator complexes to initiate specific transcriptional programs.[10–12] Acute TGF-β signalling reduces transformation and growth of cancer cells, by transcribing genes encoding cell cycle inhibitors, including p57 and p21.[10,13] However, cancer cells can overcome this cell cycle arrest by alternative downregulation of such growth suppressive TGF-β target genes.[14,15] Furthermore, this switch in gene transcription can collaterally contribute to cancer progression via oncogenic expression of migratory and invasive gene networks.[16] For instance, chronic TGF-β signalling is known to be an important node that controls expression of genes involved in the EMT promoting metastatic spread, through up

regulation of key pro-metastatic transcription factors like Snail and Twist.[17–19] Downregulation of pro-proliferative cellular processes and the resultant compensatory increases in migration within the tumor microenvironment, largely aid the initiation of the metastatic cascade, however the exact molecular mechanisms through which this is manifested in primary breast cancer remain unclear.

The zinc-finger protein POGZ is an emerging regulator of tissue development and cellular maturation. POGZ was first shown to directly interact with heterochromatin protein 1 (HP1) isoforms to regulate cell cycle progression and chromosomal integrity.[20] However, recently Pogz expression has been shown to be in highest in embryonic cortical tissue where it can, through its propensity to bind DNA, transcriptionally repress JAG2, suppressing Notch signalling to coordinate neuronal maturation.[21] Furthermore, Pogz has been shown through its interaction with HP1 isoforms to repress BCL11A expression a repressor of fetal hemoglobin. Therefore, loss of Pogz can deregulate hematopoietic cell development by indirectly upregulating fetal hemoglobin levels and is implicated as a therapeutic target in pathologies such as β-thalassemia.[22] We recently described unique roles for POGZ in directing successful homologous recombination during DNA repair of double stranded breaks while regulating cell cycle progression during DNA damage.[23] Given the role of POGZ in early tissue development and cell cycle regulation, it could be hypothesized that POGZ and its associated regulatory networks may be dysregulated in cancer.

Here we identify the contribution of Pogz in the suppression of pulmonary metastases in a murine model of basal breast cancer. Pogz deficient tumors possess more immunosuppressive and mesenchymal properties. Loss of Pogz, via CRISPR-Cas9 genome editing, elevates transient levels of phosphorylated SMAD proteins, concordant with upregulation of a TGF-β regulated transcriptional program. At baseline, POGZ deficient cancer cells upregulate TGF-β signaling and are exquisitely sensitive to TGF-β induced migration by upregulating the expression of EMT-related genes during TGF-β treatment. Mechanistically, Pogz deficient cells increase TGFBR2 expression and genetic and pharmacological ablation of this pathway inhibits aberrant TGF-β hyper-responsiveness. This data suggests that Pogz expression in a murine model of basal

breast cancer can negatively regulate TGF-β signalling via the destabilization of TGFBR2 expression, reducing downstream effects on EMT and metastases.

3.4 Results

3.4.1. Loss of POGZ inhibits cancer cell proliferation and primary tumor growth.

Our previous research showed that POGZ is a novel zinc finger protein that plays a dual role in regulating cell cycle progression and DNA repair. Given the importance of both processes to the malignant phenotype, we were interested in studying whether POGZ also contributed to breast cancer progression. We first examined *POGZ* expression levels in human breast cancer cell lines and clinical specimens, interrogating publicly available TCGA breast cancer dataset and monitored its expression in the different BC subtypes. Interestingly, we show that *POGZ* expression is elevated in basal and luminal A/B breast cancers compared to normal mammary epithelium (Supplemental Figure 1A). Furthermore, basal breast cancer cell lines possess higher POGZ protein levels when compared to other breast cancer subtypes (Supplemental Figure 1B). Finally, Kaplan Meier curves reveal that lower POGZ levels correlate with significantly poorer overall and relapse-free survival rates (Supplemental Figure 1C-F) independent of subtypic stratification.[23] However, this inverse correlation between *POGZ* levels and poor prognosis is retained if the analysis is restricted to the basal subtype. This suggests that POGZ loss may be associated with poor prognosis subtypes, including basal breast cancer.

To investigate the relevance of POGZ in the pathobiology of BC, we took advantage of an orthotopic basal murine breast cancer model, the syngeneic 4T1 model, which is highly immunogenic and metastatic. We utilized CRISPR-Cas9 genome editing to develop a Pogz-knockout (sg*Pogz*) using an sgRNA targeting exon 4, an exon common to all known mRNA transcript variants. To control for sgRNA/Cas9 cutting, a vector control was developed targeting the *Rosa26* gene locus (4T1-sg*Rosa,* Figure 1A). Interestingly, 4T1-sg*Pogz* cell lines grew at a slower rate, *in vitro*, than the cells containing the vector control, 4T1-sg*Rosa* (Figure 1B). In transformed cells, a feature that correlates with carcinogenesis and tumorgenicity is the capacity to grow in an anchorage independent capacity. 4T1-sg*Pogz* colonies formed in 0.36% agar revealed a significant deficit in colony size and number compared to 4T1-sg*Rosa* cells (Figure 1D). Expanding on these results, we injected both 4T1-sg*Rosa* and -sg*Pogz* cell lines, orthotopically, in BALB/c mice. Tumors were monitored until 4T1-sg*Rosa* tumors reached endpoint (750 mm^3). In

comparison to the 4T1-sg*Rosa* 4T1 tumors, 4T1-sg*Pogz* tumors grew at a 2-fold decreased rate (Figure 1C). In concert with *in vitro* proliferation and tumor growth curves, this data suggests that the growth defect seen in 4T1-sg*Pogz* tumors is cell-intrinsic. Therefore, Pogz is necessary for anchorage-dependent and -independent cell growth *in vitro* and tumor growth *in vivo*.

Upon characterization by immunohistochemistry, at end stage, 4T1-sg*Pogz* tumors possessed significantly lower amounts of cleaved caspase-3 expressing cells, in comparison to 4T1-sg*Rosa* tumors (Supplemental Figure 3A). This revealed the reduced growth rate in a 4T1-sg*Pogz* tumors is not due to apoptosis.

To explore the potential impact of POGZ overexpression on cell proliferation and tumorigenicity we utilized a CRISPR-dCas9 synergistic activation mediator (SAM) system using scaffold RNAs (scRNA) directing the *activator complex (MS2-p65-HSF1, MPH)* to regulatory regions upstream of the endogenous TSS of Pogz (4T1-sc*Pogz*), we tested over-expression of POGZ by western blot (Supplemental Figure 2A). This system contains a vehicle control which contains both the MPH complex and sgRNA are directed towards a noncoding pericentromeric region (*Mmu19*) which did not alter POGZ expression. Interestingly, Pogz overexpression did not change proliferation in the 4T1 cell line, *in vitro*, in comparison to 4T1-sc*Mmu19*. Consistently, 4T1-sc*Pogz* grew in soft agar and displayed no significant change in colony size or number in compared to 4T1-sc*Mmu19* (Supplemental Figure 2D). 4T1-sc*Pogz* cells did not possess any alterations in primary tumor growth (Supplemental Figure 2B), and expectedly, no difference in cleaved caspase expression (Supplemental Figure 3A). Altogether this data suggests that over-expression of Pogz is necessary but not sufficient to impair breast cancer cell proliferation in vitro and tumor growth in vivo.

3.4.2. Loss of POGZ increases basal activation of TGFB-SMAD2/3 signalling.

There is growing evidence that POGZ governs embryonic and neural cell and tissue development by regulating gene transcription.[22,24,25] Therefore, we investigated the contribution of Pogz in modulating breast cancer growth at the transcription level by performing RNA sequencing in 4T1-sg*Rosa* and -sg*Pogz* 4T1 cell lines, *in vitro*. Overall,

we identified 243 differentially expressed genes in the 4T1-sg*Pogz* cell line, *in vitro* (Figure 2A). Importantly, gene set enrichment analysis (GSEA) delineated pathways involved in cell cycle progression, such as E2F1 target genes, G2M checkpoint, MYC signalling were downregulated in 4T1-sg*Pogz* cells (Figure 2B). Interestingly, one of the emerging pathways differentially upregulated in 4T1-sg*Pogz* was TGF-β signalling. TGF-β signalling through TGFBRI/II promotes acute tumor suppression through cell cycle arrest and apoptosis.[9] Validating our RNA-seq results, we assessed mRNA levels of genes downstream of the TGF-β pathway. Indeed, canonical SMAD2/3 target genes (*Serpine1, Cdkn1c, Thbs1, Fn1, Itgb6*) were found to be significantly enriched in 4T1-sg*Pogz* cells (Figure 2E), independent of the addition of exogenous TGF-β. In addition, cell cycle genes known to be repressed by activated SMAD2/3 (*E2f1, Myc, Id2*), were found to be downregulated in 4T1-sg*Pogz* cells when compared to 4T1-sg*Rosa*. Furthermore, elevated levels, even in basal conditions, of pSMAD2 were observed in 4T1-sg*Pogz* cells relative to 4T1-sg*Rosa* cells (Figure 2D). These data suggest that persistent TGF-β signalling may contribute to the growth inhibition exhibited by 4T1-sg*Pogz* cells.

Cell cycle arrest by TGF-β is elicited by the transcription repression of *Myc*, expression of the cell cycle inhibitor p57, leading to the accumulation of cells in the G1 phase.[23] Basally, 4T1-sg*Pogz* possessed decreased cell proliferation, DNA synthesis (S phase), and anchorage independent colony formation and size in comparison to 4T1-sg*Rosa* (Supplemental Figure 4A-C). The addition of TGF-β1 ligand efficiently inhibited proliferation in 4T1-sg*Rosa,* exhibited by a decrease in all three parameters measured. In contrast, 4T1-sg*Pogz* cells were minimally affected by the addition of TGF-β1 ligand (Supplemental Figure 4A-C). Transcriptionally, levels of SMAD2 target genes are significantly enhanced upon addition of TGF-β1 in 4T1-sg*Rosa* cells, however, this effect is seen to a much higher extent in the POGZ-deficient 4T1 cells. Interestingly, changes in genes responsible for cell cycle regulation, were not significantly changed in 4T1-sg*Pogz* cells (Supplemental Figure 4D). These data suggest that 4T1-sg*Pogz* cells may have a proliferative defect due to persistent TGF-β1 induced cytostatic effects, but this effect is not exacerbated by exogenous TGF-β1 supplementation.

To ask whether higher basal levels of phosphorylated SMAD2 were responsible for the cytostatic effect observed in 4T1-sg*Pogz* cells, we utilized an ALK5 (TGFBR1) specific inhibitor (TP0427736). First, we validated that TP0427736 can inhibit TGF-β induced SMAD2 phosphorylation in a dose dependent manner (Supplemental Figure 5A). Furthermore, basal levels of pSMAD2 in 4T1-sg*Pogz* cells are also decreased by TP0427736 treatment, indicating that elevated pSMAD2 levels are due, in part, to TGFBR1/2 kinase activity. However, when assessing colony size and formation via soft agar, inhibition of TGFBR1 kinase activity has no impact on, or reversal of, the growth inhibition observed in the 4T1-sg*Pogz* cells compared to 4T1-sg*Rosa* cells (Supplemental Figure 5B), despite complete inhibition of SMAD2 phosphorylation. These data suggest that this decrease in cell growth due to the loss of POGZ may not be a direct product of TGFBRI/II activation.

3.4.3. POGZ-deficient tumors possess a mixed EMT state.

To uncover any transcriptional programs elicited *in vivo* that could explain the primary tumor growth defect, we performed RNA sequencing in our 4T1-sg*Rosa* and -sg*Pogz* tumors, in vivo. Surprisingly, we did not identify any specific pathways that were downregulated in 4T1-sg*Pogz* compared to 4T1-sg*Rosa* tumors. Rather, we noticed there were numerous significantly enriched pathways in comparison to 4T1-sg*Rosa* tumors (Figure 3A-B). Of note, genes involved in the EMT process were significantly elevated in the 4T1-sg*Pogz* tumors compared to the 4T1-sg*Rosa* tumors (Figure 3C). Furthermore, decreased expression of the epithelial marker, E-cadherin, was observed in the 4T1-sg*Pogz* tumors, in comparison to 4T1-sg*Rosa*, which sustained high expression (Figure 3D). This data indicates that POGZ-deficient tumors could potentially acquire more mesenchymal traits. Since acquisition of an EMT is transcriptionally downstream of TGF-β signalling, we assessed mRNA levels of epithelial (*Cdh1*) or mesenchymal markers (*Snai1*, *Hmga1*, *Timp2*) (Figure 3E). Furthermore, there was a significant number of immune-associated pathways emerging within the GSEA, however, these pathways are associated with immune suppression or pro-tumor inflammatory responses, such as IL-10 and IL6-signalling. Of note, cell cycle and proliferation pathways that were decreased in the 4T1-sg*Pogz* 4T1 cell lines (G2/M checkpoint and E2F targets, Figure 2B-3B) are now over-expressed in the 4T1-sg*Pogz* tumors.

3.4.4. POGZ suppresses pulmonary metastasis and migratory capacity.

Given the presence of an EMT signature in POGZ deficient tumors, we next investigated their metastatic potential. To achieve this, 4T1-sg*Rosa* and -sg*Pogz* cell lines were injected orthotopically into mammary fat pads of BALBc and resected at scheduled tumor volumes and animals were necropsied 28 days later to quantify the lung metastatic burden in H&E stained sections. With the limited growth of 4T1-sg*Pogz* an immune-competent model, we injected 4T1-sg*Rosa* and –sg*Pogz* in several groups: 4T1-sg*Rosa* (resected at 350mm3 on 21 days post injection); 4T1-sg$Pogz^{E}$ (early, resected at 150mm3 on 21 days post injection); and 4T1-sg$Pogz^{L}$ (late, resected at 350mm3 on 35 days post injection) (Figure 4A). Interestingly, 4T1-sg*Rosa* and -sg$Pogz^{E}$ tumors possessed no difference in pulmonary metastatic burden, despite 4T1-sg$Pogz^{E}$ tumors being 50% of the 4T1-sg*Rosa* tumor volume (Figure 4B). However, normalizing metastatic burden to primary tumor volume, it is clear that 4T1-sg*Rosa* and -sg*Pogz* tumors can effectively metastasize to the lung earlier or more efficiently than 4T1-sg*Rosa* tumors (Figure 4C). Furthermore, 4T1-sg$Pogz^{L}$ tumors possessed a significantly higher metastatic burden than 4T1-sg*Rosa* tumors, when resected at the same volume (Figure 4B).

In order for a breast cancer cell to escape the primary tumor and form macroscopic metastatic outgrowths, it must overcome multiple and complex processes.[5] By identifying a role for POGZ in preventing metastasis from primary tumor, we asked the question of which step in the metastatic cascade POGZ has a protective role. Firstly, we performed a chemotaxis migration assay using a transwell, to which 4T1-sg*Rosa* and -sg*Pogz* were seeded in the top chamber and allowed to migrate to the bottom chamber following a 10% serum gradient. After 24 hours, 4T1-sg*Pogz* migrated significantly more than 4T1-sg*Rosa*. Furthermore, TGF-β signaling is known to promote breast cancer cell migration by transcriptional activating an EMT. Remarkably, 4T1-sg*Pogz* cells were extremely sensitive to TGF-β enhanced migration in comparison to 4T1-sg*Rosa* cells (Figure 4E). Importantly, this increased migratory behavior in 4T1-sg*Pogz* cells is completely and efficiently ablated under TGFBRi treatment (Figure 4G). Altogether, this data indicates that elevated TGF-β signalling is not responsible for the primary tumor growth defect in 4T1-sg*Pogz* cells but increases metastatic potential of basal breast cancer cells.

Given that 4T1-sg*Pogz* tumors possess a higher metastatic burden, we performed a primary tumor resection with 4T1-sc*Pogz* and 4T1-sc*Mmu19*, to ask whether overexpression of POGZ would impact metastases. Indeed, mice with resected 4T1-sc*Pogz* tumors possessed a significantly decreased metastatic burden in the lung in comparison to mice with resected 4T1-sc*Mmu19* (Figure 4D), despite no difference in primary tumor outgrowth. Furthermore, when migration along a serum gradient was assessed in 4T1-sc*Pogz* cells, they showed a significant decrease in migratory potential compared to 4T1-sc*Mmu19* (Figure 4F). Addition of TGF-β ligand to 4T1-sc*Pogz* did not enhance their migratory potential (Figure 4F). Taken together, these data show that POGZ functions to suppress the migratory and metastatic potential of basal breast cancer cells.

3.4.5. POGZ deficient tumors require the primary tumor microenvironment for metastases.

Identifying a strong susceptibility to TGF-β induced migratory activity and an increased metastatic burden of 4T1-sg*Pogz*, suggests that POGZ regulates early stages of the metastatic cascade. To assess whether loss of POGZ affected later stages of metastasis we performed tail-vein injections of 4T1-sg*Rosa* and -sg*Pogz* cells and measured metastatic burden 30 days post injection. Interestingly, 4T1-sg*Rosa* had significantly higher pulmonary metastatic burden in comparison to the 4T1-sg*Pogz* bearing mice (Supplemental Figure 6A). Tail vein injection mainly recapitulates later stages of the metastatic cascade post-intravasation (extravasation, anoikis, colonization), therefore we can conclude that the anti-metastatic function POGZ possesses, is most likely in promoting EMT.

Furthermore, early timepoints during early tumor development, microenvironmental contributions, such as TGF-β production, can initiate EMT with the primary tumor and promote premature metastatic seeding. 4T1-sg*Pogz* tumors possess a decreased immune infiltrate when compared to 4T1-sg*Rosa*, denoted by decreased $CD45^+$ cells, assessed by flow cytometry (Supplemental Figure 6A). However, within the $CD45^+$ population, there were increased $F4/80^+$ macrophages and a dramatic increase in $Ly6G^+$ neutrophils (Figure 5B). Myeloid/granulocytic infiltrates have been shown to promote metastasis in the 4T1 model and other models of metastatic cancer, by both TGF-β

production and immune suppression.[26–28] Multiple TGF-β cytokines and chemokines (*Ccl2*, *Csf2*, *Cxcl12*) identified via RNAseq were overexpressed in the 4T1-sg*Pogz* cell line and tumors (Figure 2B, 3B) possibly aiding in the mobilization and recruitment of pro-metastatic immune cell subsets.

3.4.6. POGZ negatively regulates expression of TGFBR2.

SMAD2 phosphorylation is mainly due to the kinase activity of TGFBR1, which to become active, requires phosphorylation by TGFBR2.[11] Upon treatment with a TGFBR1 antagonist (TP0427736) there was an observable decrease in phosphorylated SMAD2 in the 4T1-sg*Pogz*, therefore this increase witnessed in the POGZ deficient cells is regulated on the level of TGFBR1/2 expression and activity. Therefore, we assessed cell membrane expression, by flow cytometry, of both TGFBR1 and TGFBR2 in 4T1-sg*Rosa* and -sg*Pogz* cell lines. Importantly, TGFBR2 was shown to be two-fold higher in the 4T1-sg*Pogz* (Figure 5A). To examine if the effect on migratory behavior is due to the enhanced expression of TGFBR2 and its downstream effect on SMAD2 phosphorylation, we silenced TGFBR2 expression via lentiviral short hairpin RNA. We confirmed loss of membrane expression via flow cytometry (Figure 5B) and showed the constitutive loss in SMAD2 phosphorylation in the 4T1-sg*Pogz* cell line (Figure 5C). Furthermore, 4T1-sg*Pogz* deficient in TGFBR2 expression, when assayed for migration along a serum gradient, showed a dramatic loss in migratory propensity (Figure 5D). Expectedly, the responsiveness of 4T1-sg*Pogz* shTgfbr2 cells to TGF-β induced chemotaxis was ablated, mimicking the effect seen with pharmacological inhibition of TGFBR1 kinase activity (TP0427736) (Figure 5D). Lastly, to assess whether this upregulation of TGFBR2 through loss of POGZ could be translated to human breast cancer, we probed publicly available datasets (METABRIC, TCGA, MSKCC). Indeed, samples with higher expression of POGZ possessed lower expression of TGFBR2, indicating that increased of POGZ could possibly negatively TGFBR2 expression. These data identify that the enhanced migration witnessed within POGZ-deficient 4T1 is mediated through upregulation of TGFBR2 and downstream signalling.

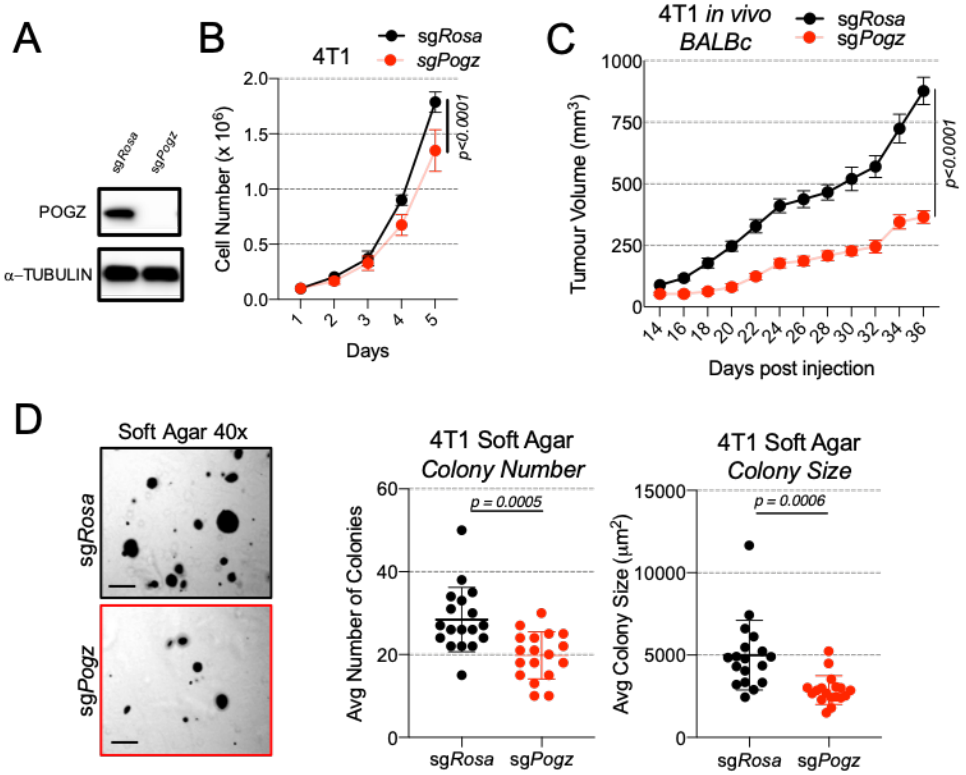

FIGURE 3- 1. LOSS OF POGZ INHIBITS CANCER CELL PROLIFERATION AND PRIMARY TUMOR GROWTH.

(A) Levels of POGZ and α tubulin were assessed in 4T1-sg*Rosa* and -sg*Pogz* cell lines cells via western blot. (B) 4T1-sg*Rosa* and -sg*Pogz* cell lines cell lines were plated at equal densities and were counted daily by trypan blue exclusion (n=3 independent experiments). (C) 4T1-sg*Rosa* and -sg*Pogz* cell lines cell lines were orthotopically injected into the MFP4 of BalbC. Tumors were measured every other day until humane endpoints were achieved. (n=20 per group). (D) 4T1-sg*Rosa* and -sg*Pogz* cell lines cell lines were cultured in 0.36% agar for 10 days and imaged (n=3 independent experiments, scale = 150um)

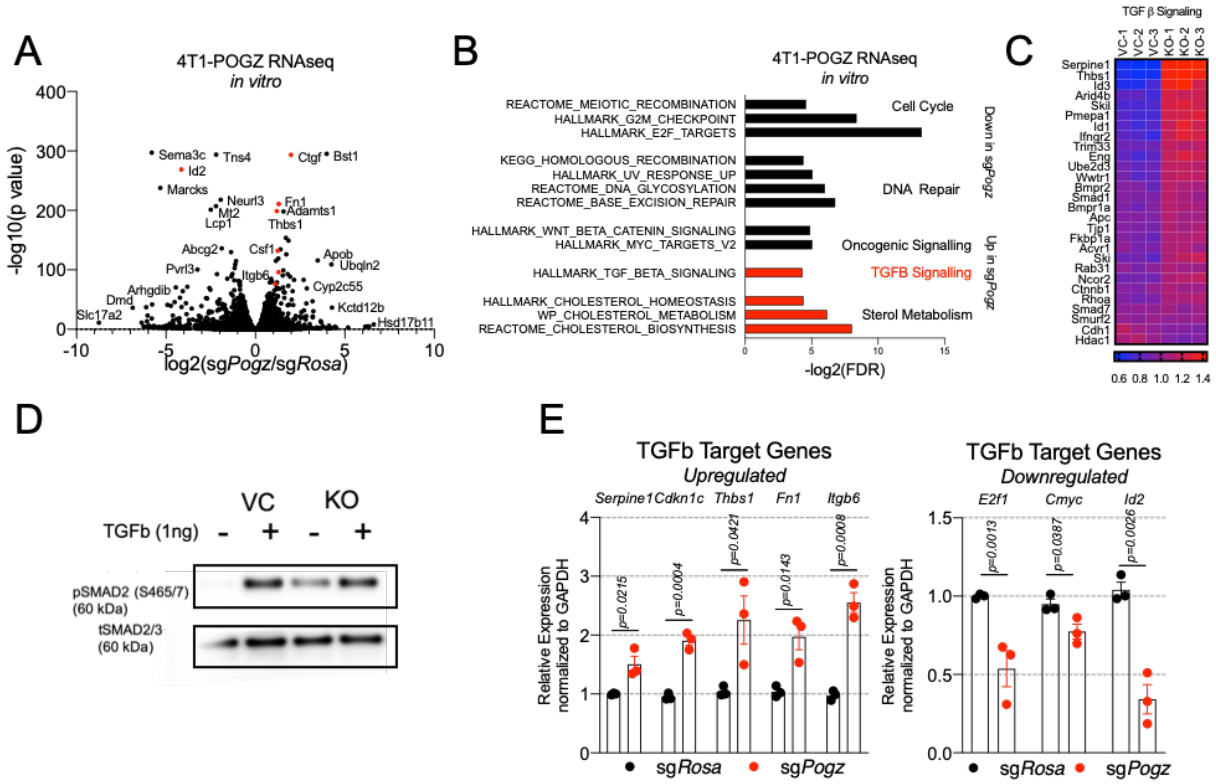

FIGURE 3- 2. LOSS OF POGZ INCREASES BASAL ACTIVATION OF TGFB-SMAD2/3 SIGNALING.

(A) Volcano plot of RNAseq analysis and GSEA differential pathway expression (B) performed on 4T1-sg*Rosa* and -sg*Pogz* cell lines. C) Leading edge gene expression heatmap from the TGF-b signaling pathway (3 replicates per group). (D) Phosphorylated and total levels of SMAD2 were screened in 4T1 cells with and without the addition of TGF-b via western blot. (E) mRNA levels of TGF-b target genes in 4T1-sg*Rosa* and -sg*Pogz* cell lines were quantified by RT-qPCR and normalized to GAPDH (n=3 independent experiments).

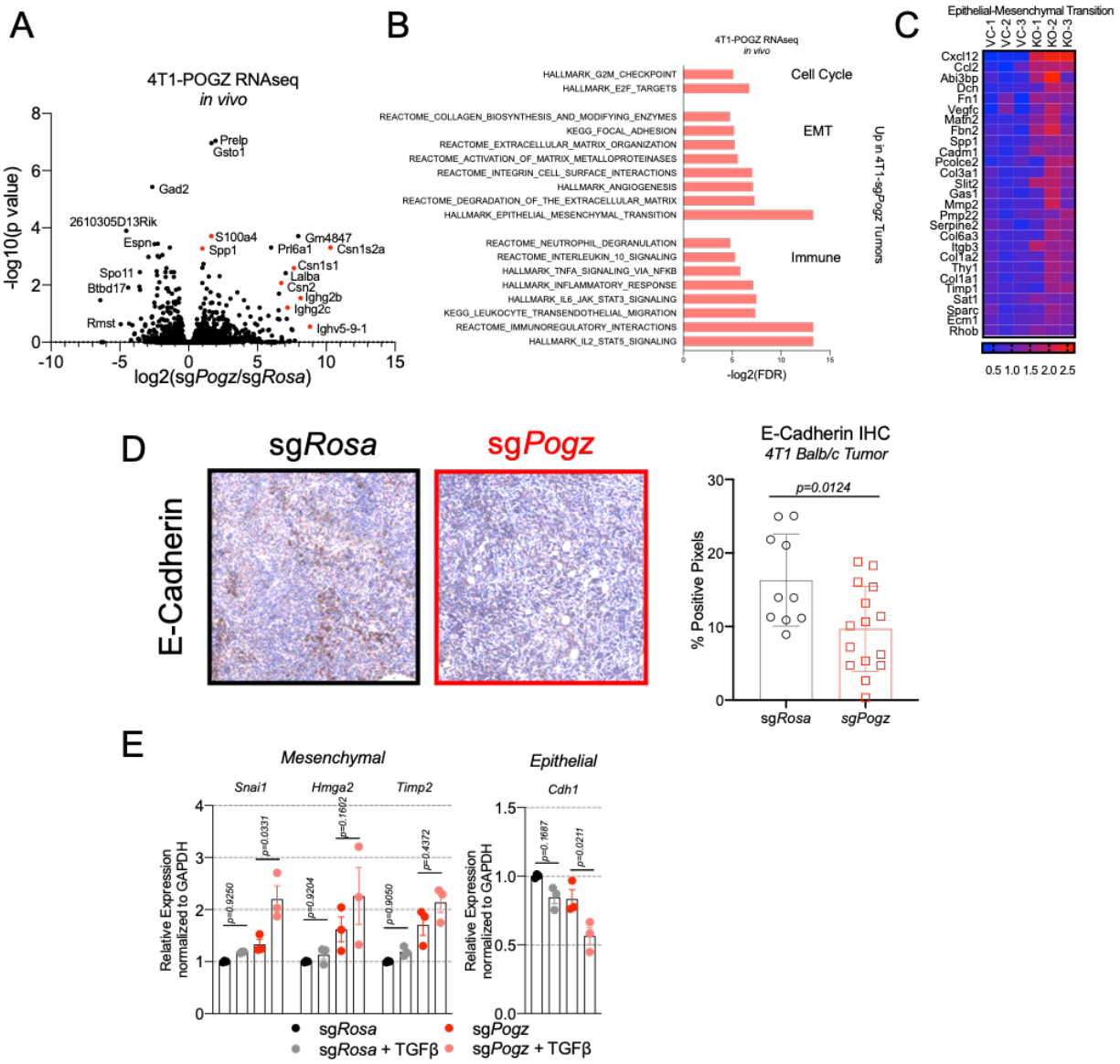

FIGURE 3- 3 POGZ-DEFICIENT TUMORS POSSESS A MIXED EMT STATE.

(A) Volcano plot of RNAseq analysis and GSEA differential pathway expression (B) performed on 4T1-sgRosa and -sgPogz 4T1 tumors. (C) Leading edge gene expression heatmap from the EMT signaling pathway. (D-E) E-Cadherin IHC of 4T1-sgRosa and -sgPogz 4T1 tumors. The data is shown as average percentage of positive cells ±SEM (*n* = 10-12 tumors/group). Representative images are shown. (F) mRNA levels of genes associated with EMT, with or without TGF-b for 24 hours, were quantified by RT-qPCR and normalized to GAPDH.

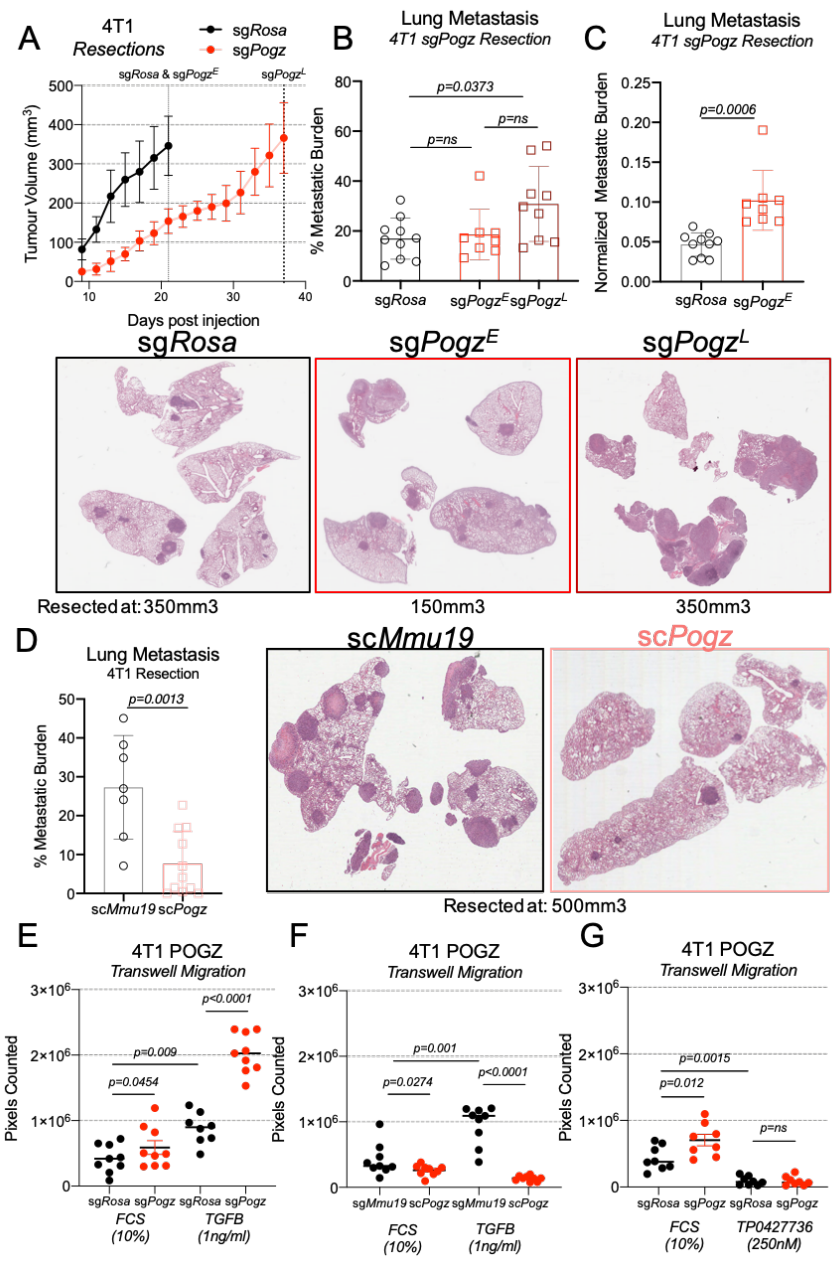

FIGURE 3- 4 POGZ SUPPRESSES PULMONARY METASTASIS AND MIGRATORY CAPACITY.

(A) 4T1 cell lines were orthotopically injected into the MFP4 of BALBc mice. Tumors were resected at 21 and 36 days post injection and lungs were harvested 28 days later. Growth curve and resection schedule is depicted (A, n= 8-10 per group) and quantification (B). (C) Percent of lung tissue containing metastases is normalized to primary tumor volume in 4T1-sg*Rosa* and -sg*Pogz* tumors. (D) MFP-resection experiment performed with 4T1-sc*Mmu19* and -sc*Pogz* tumors (n=7-10 per group). (E-G) Transwell migration experiments were performed with 4T1-sg*Rosa* and -sg*Pogz* cell lines (E, G) or 4T1-sc*Mmu19* and -sc*Pogz* (F) 4T1 cell lines with and without TGF-b (E, F) or TP0427736 (TGFBRi) (G) (all n=3 independent experiments).

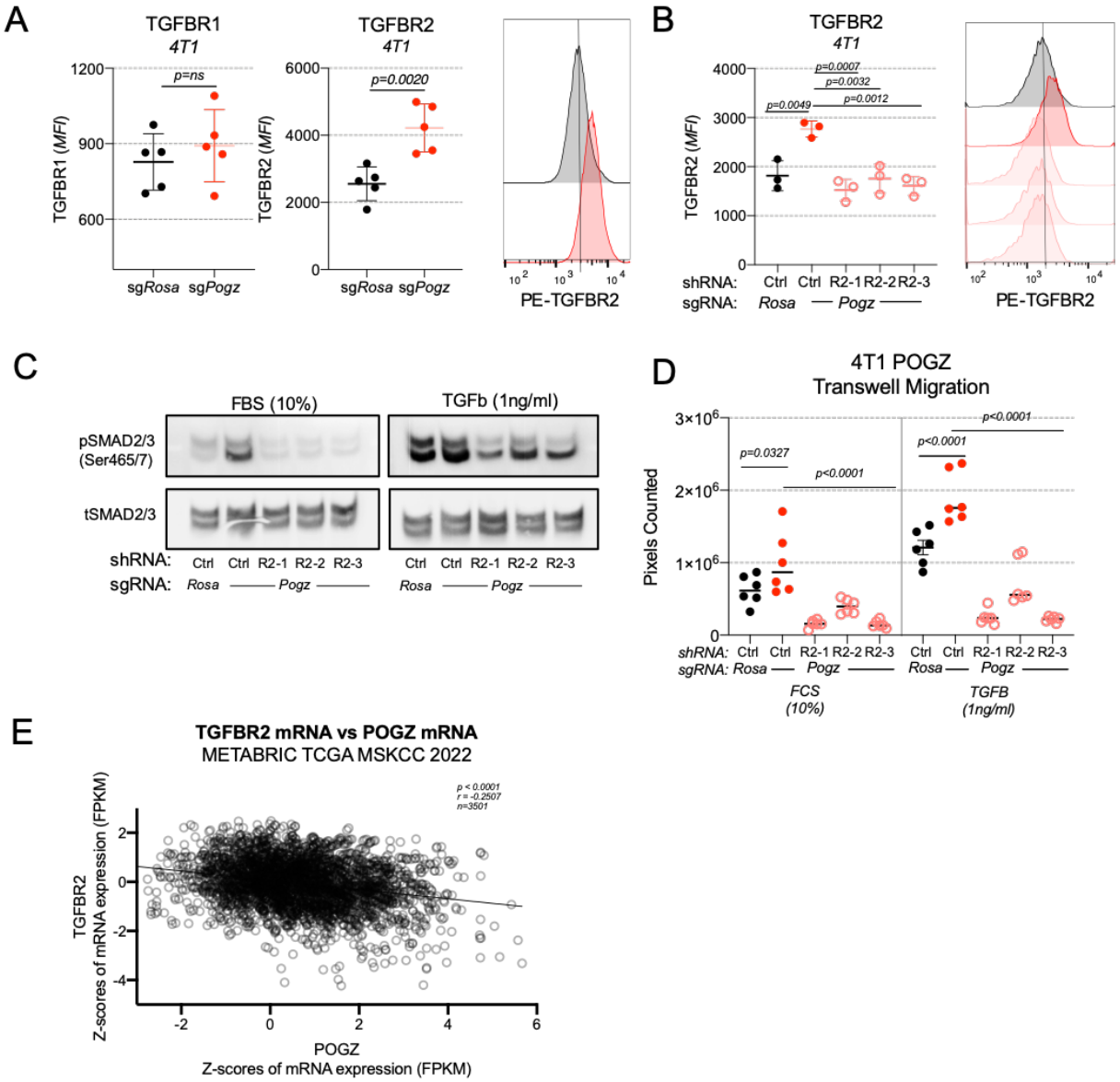

FIGURE 3- 5 LOSS OF POGZ ENHANCES PULMONARY METASTASIS VIA UPREGULATION OF TGFBR2.

(A) Membrane expression of TGFBR1/2 on 4T1-sg*Rosa* and 4T1-sg*Pogz* cells assessed by flow cytometry (n = 5 independent experiments). (B) Membrane expression of TGFBR1/2 on 4T1-sg*Rosa,* 4T1-sg*Pogz*, and 4T1-sg*Pogz* containing shRNA directed against TGFBR2 (R2-1, R2-2, R2-3) cells assessed by flow cytometry (n=3 independent experiments). (C) Phosphorylated and total levels of SMAD2 were screened in 4T1 cells with and without the addition of TGF-b via western blot. (D) Transwell migration experiments were performed with 4T1-sg*Rosa* and 4T1-sg*Pogz* cells with and without TGFB (n=3 independent experiments). (E) Correlation of POGZ mRNA expression level with TGFBR2 mRNA expression in METABRIC-TCGA-MSKCC breast cancer datasets (n=3501).

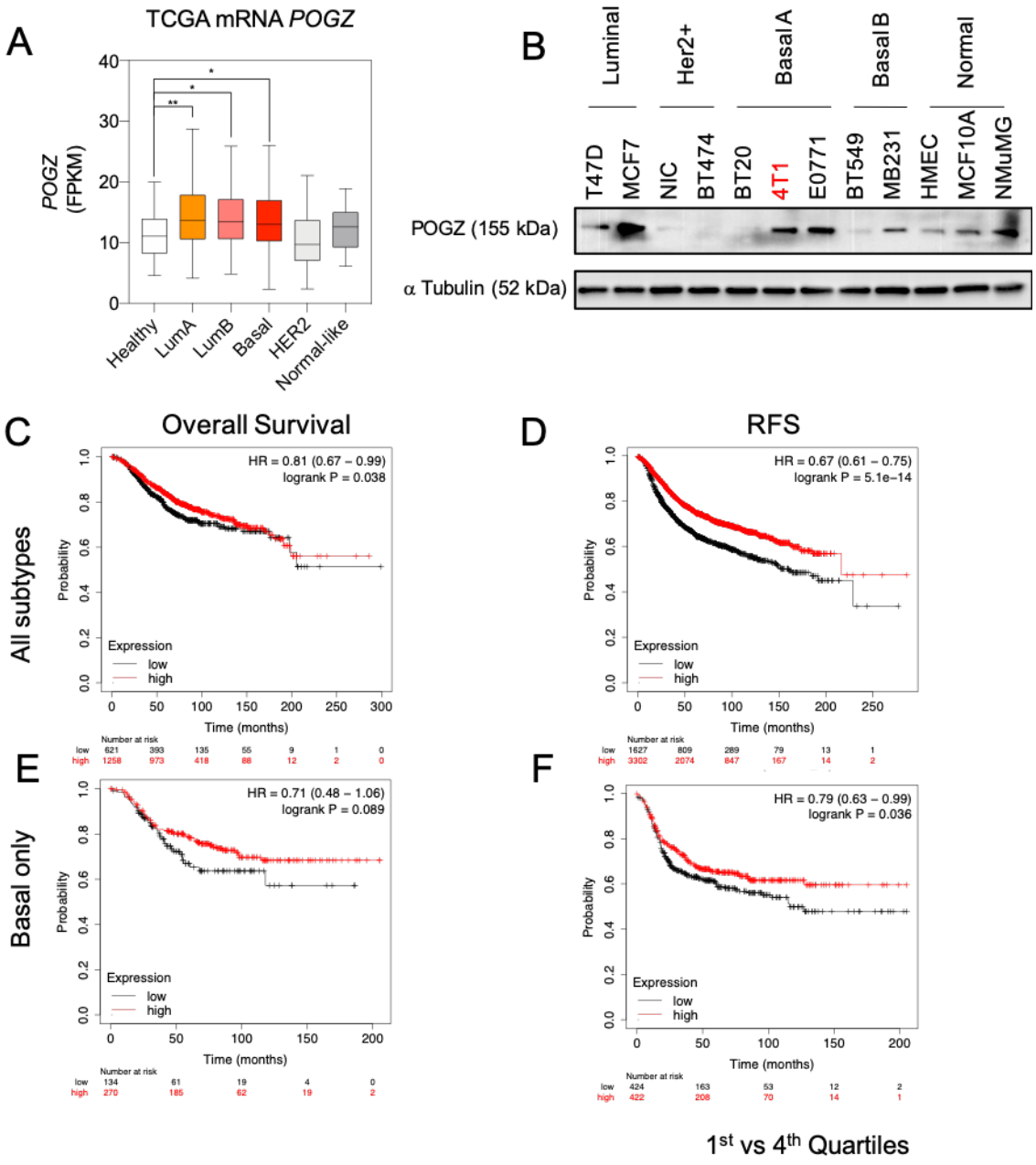

SUPPLEMENTAL FIGURE 3- 1 POGZ IS OVER-EXPRESSED AND PROTECTIVE IN BASAL BREAST CANCERS.

A) POGZ expression level in breast cancer subtypes according to PAM50 classification in TCGA breast cancer dataset. Healthy (n=83), Luminal A (n=480), Luminal B (n=197), Basal (n=157), HER2 (n=74), Normal-like(n=27). (B) Levels of POGZ and α tubulin were screened in breast cancer cell lines via western blot. (C-F) Association of clinical outcome vs POGZ expression using overall survival (C, E) and relapse-free survival (D, F) as endpoints. The breast cancer sample set was stratified into 4 quartiles based on DKK2 median expression, comparisons are between 1st and 4th quartiles. Overall OS (n=1879), Overall RFS (n=4929), Basal OS (n=404), Basal RFS (n=846).

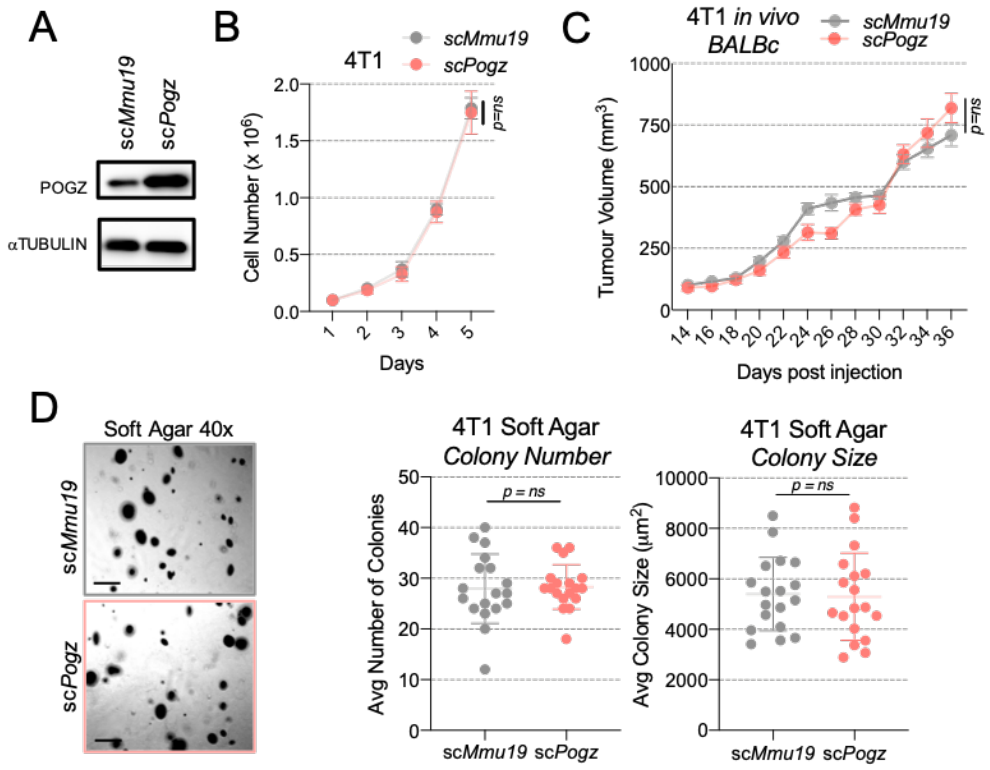

SUPPLEMENTAL FIGURE 3- 2 OVEREXPRESSION OF POGZ IS DISPENSABLE FOR CANCER CELL PROLIFERATION AND PRIMARY TUMOR GROWTH.

(A) Levels of POGZ and α -tubulin were screened in 4T1-sc*Mmu19* and -sc*Pogz* cells via western blot. (B) 4T1-sc*Mmu19* and -sc*Pogz* cell lines were plated at equal densities and were counted daily by trypan blue exclusion (n=3 independent experiments). (C) 4T1-sc*Mmu19* and -sc*Pogz* cell lines were orthotopically injected into the MFP4 of BALBc mice. Tumors were measured every other day until humane endpoints were achieved. (n=20 per group). (D) 4T1-sc*Mmu19* and -sc*Pogz* cell lines were cultured in 0.36% agar for 10 days and imaged (n=3 independent experiments, scale = 150um).

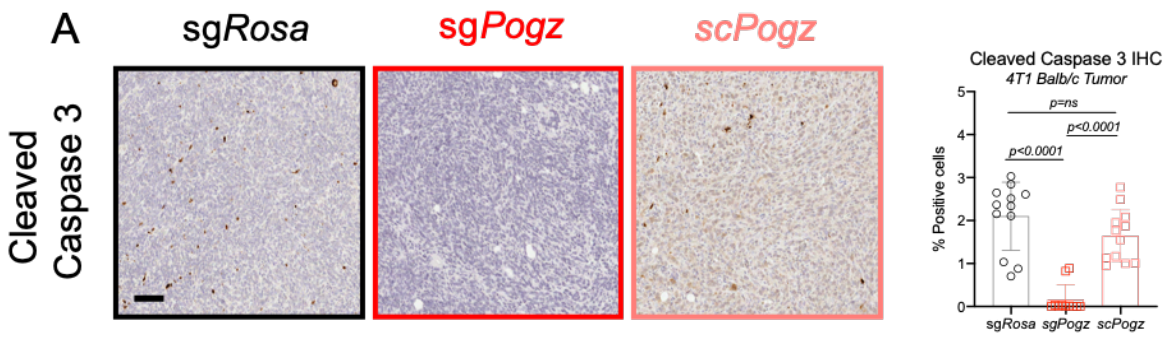

SUPPLEMENTAL FIGURE 3- 3 CHARACTERIZATION OF POGZ-NULL 4T1 PRIMARY TUMORS.

Cleaved caspase-3 IHC of 4T1-sg*Rosa,* -sg*Pogz,* and -*scPogz* 4T1 tumors. The data is shown as average percentage of positive cells ±SEM (*n* = 10-11 tumors/group). Representative images are shown.

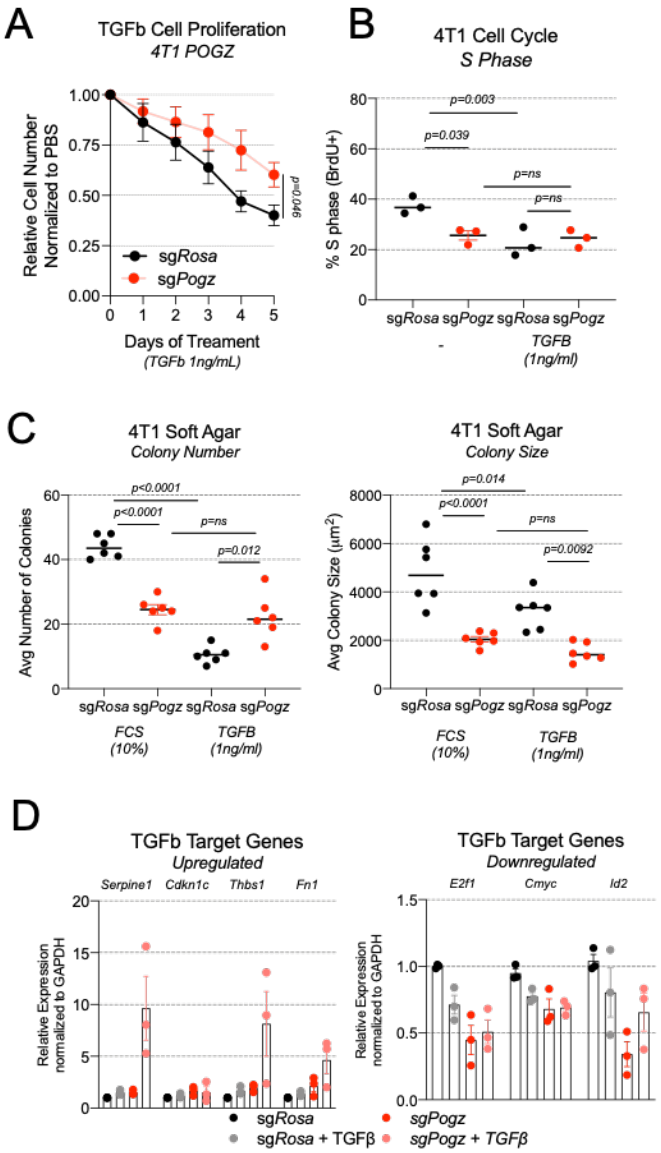

SUPPLEMENTAL FIGURE 3- 4 INCREASED TGFBR SIGNALING DOES NOT RESTRICT PROLIFERATION IN POGZ-DEFICIENT 4T1.

(A) 4T1-sg*Rosa* and -sg*Pogz* cell lines were plated at equal densities and treated with or without TGF-b for 5 days. Cells were counted daily by trypan blue exclusion and normalized to untreated/PBS control (n=3 independent experiments). (B) 4T1-sg*Rosa* and -sg*Pogz* cell cycle composition, with or without TGF-b, was assessed by flow cytometry. Data is presented as percent of cells in S phase +/- SEM. (C) 4T1-sg*Rosa* and -sg*Pogz* cell lines were cultured in 0.36% agar for 10 days with or without TFG-b. (n=3 independent experiments). (D) mRNA levels of genes associated with TGF-b, in 4T1-sg*Rosa* and -sg*Pogz* cell lines, with or without TGF-b, were quantified by RT-qPCR and normalized to GAPDH (n=3 independent experiments).

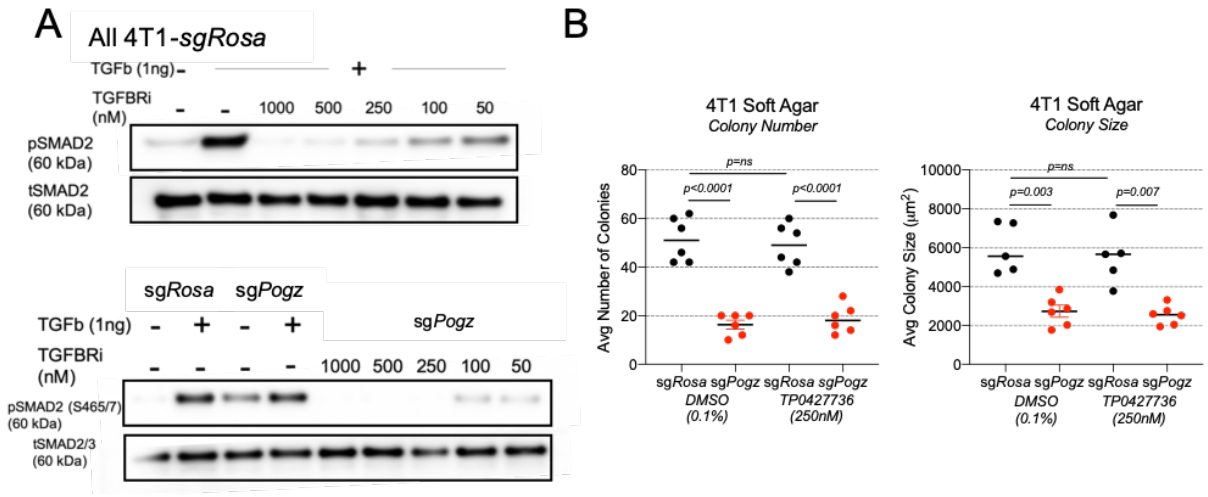

SUPPLEMENTAL FIGURE 3- 5 LOSS OF TGFBR SIGNALING DOES NOT RESTORE PROLIFERATIVE DEFECT IN POGZ-DEFICIENT 4T1 CELLS.

(A) Phosphorylated and total levels of SMAD2 were screened in 4T1-sg*Rosa* and -sg*Pogz* cell lines with/without TGF-b and TP0427736 (TGFBRi) via western blot. (B) 4T1-sg*Rosa* and -sg*Pogz* cell lines were cultured in 0.36% agar for 10 days with or without the addition of TP0427736 (TGFBRi) (n=3 independent experiments).

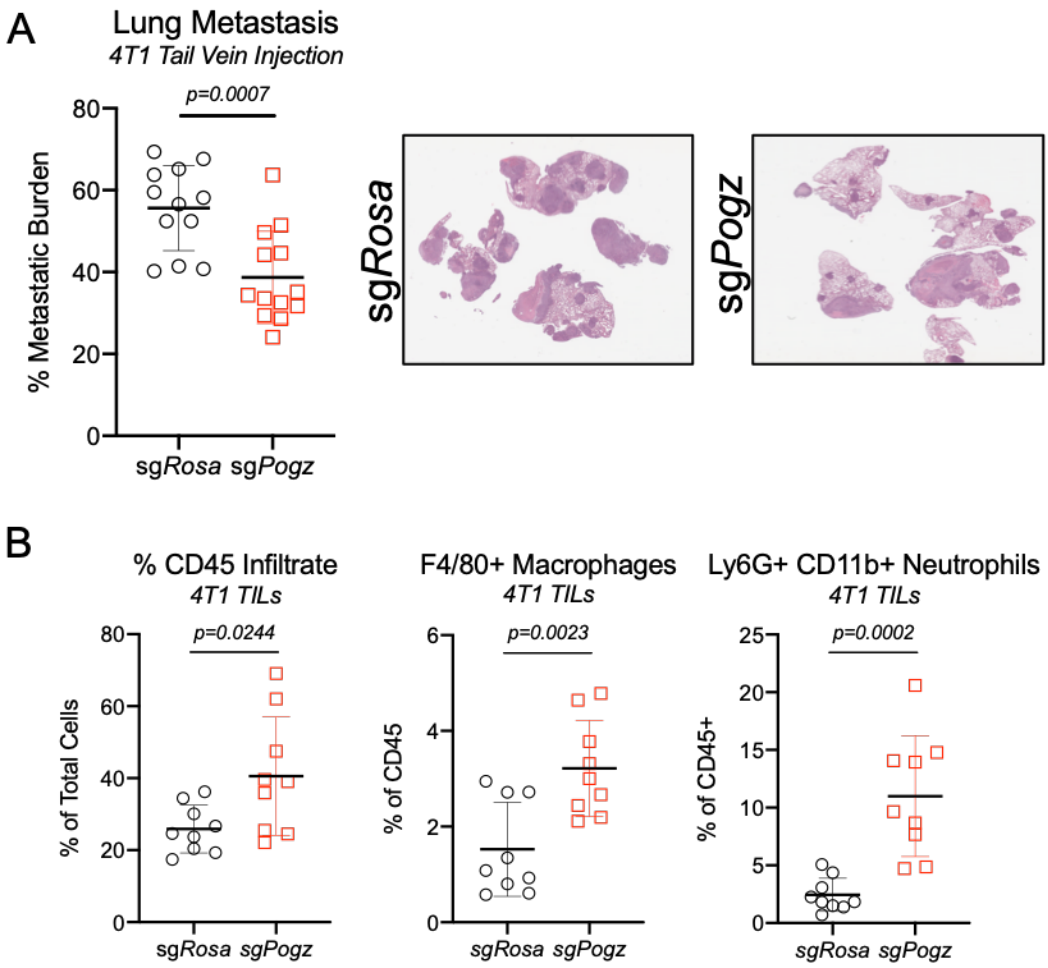

SUPPLEMENTAL FIGURE 3- 6 4T1-SGPOGZ 4T1 TUMORS REQUIRE THE PRIMARY TUMOR MICROENVIRONMENT.

(A) 4T1-sg*Rosa* and -sg*Pogz* cell lines were injected into the tail veins of BALBc mice and lungs were harvested 28 days later. (B) Immune profiling of tumor-infiltrating leukocytes was performed on 4T1-sg*Rosa* and -sg*Pogz* tumors via flow cytometry. Specific immune subsets are shown as percent of total CD45+ cells. (n=9 per group)

3.5. Discussion

The emerging roles for the zinc finger protein, POGZ, are only recently being identified. In particular, POGZ has been implicated in the development of multiple neurological conditions such as schizophrenia, epilepsy, autism and other intellectual disabilities.[29–32] However, the function of POGZ in non-neurological pathologies remain poorly described. Here, we report an important role for POGZ in basal breast cancer etiology. Our results indicate that while POGZ is required for sustained growth in the primary tumor microenvironment, this seemingly beneficial phenotype is negated with increased metastatic potential. We highlight the loss of POGZ results in a significant decrease in cell proliferation (both anchorage-dependent and -independent) and tumor growth in the 4T1 basal-like breast cancer model. POGZ was first described via its atypical interaction with HP1, playing a critical role in the regulation of cell division through the regulation of chromosomal arm stability and segregation. Recently, several studies identify a role for POGZ in maintaining proper gene transcription in neurological and embryonic tissue, suggesting a larger regulatory role for POGZ in the maintenance of cellular growth.[25,33] Consistent with other reports, we observe a dramatic decrease in gene expression of pathways involved in cell proliferation, including both Myc and the related E2F transcriptional targets.[22,33] In concert, with the decreased expression of pathways driving cell proliferation we observed an increase in expression of genes downstream of TGF-β signalling. The contradictory effects of TGF-β in cancer are widely studied, however, the exact switch between cytostatic gene expression and the promotion of EMT and metastases is unclear.[13,14,16,19] The loss of POGZ driving increases in gene expression associated with TGF-β signalling, in vitro, suggest that POGZ may play the role of a negative regulator. Furthermore, 4T1-sg*Pogz* cells possessed basally increased levels of phosphorylated SMAD2, however, were insensitive to the cytostatic effects of TGF-β1. 4T1-sg*Rosa* cells, when treated with exogenous TGF-β1, decreased in cell proliferation and S-phase, while 4T1-sg*Pogz* were unchanged in cell growth and S phase accumulation. These data likely suggest that the tumor suppressive activity of TGF-β was lost in the 4T1-sg*Pogz.* While this increase in TGF-β signalling could achieve persistent cytostatic effects in in POGZ deficient cells, pharmacological inhibition of the TGFBR1

kinase activity did not restore the growth rate despite reducing phosphorylated SMAD2/3 levels. Therefore, basal increases in TGF-β signalling appear to be dispensable in the context of growth inhibition in POGZ-deficient cells. We, therefore, explored the other arm of TGF-β signalling, the promotion of migratory potential and the initiation of the EMT. Loss of POGZ only modestly increased migration of 4T1 cells following a serum gradient, however, poised them to be remarkably sensitive to a TGF-β mediated migration. In further support of this finding, while TGF-β targets were, as a gene set, not significantly enriched within POGZ-deficient tumors, genes associated with the EMT were most enriched in comparison to the wild-type tumors. While TGF-β bore little impact on cell cycle and proliferation of 4T1-sg*Pogz*, the addition of TGFB1 drastically enhanced expression of EMT markers, such as the EMT transcription factor Snail. Furthermore, an increase in TGFBR2 expression witnessed in 4T1-sg*Pogz* cells, could allow for increased signalling from activated TGFBR1/2 complexes and result in increased SMAD phosphorylation and pro-migratory TGF-β target gene expression. Upregulation of this pathway prompted us to explore the how Pogz loss may affect metastasis.

We identify a protective role for POGZ in preventing pulmonary metastases in an established primary tumor-resection model.[34] This experimental model assesses the potential of a primary tumor to undergo all stages of the metastatic cascade. However, to control for the impact of the slow growth of the primary tumor, we utilized 2 different POGZ-deficient cohorts. Remarkably, POGZ-deficient 4T1 tumors, which grow at half the rate of POGZ-proficient tumors , metastasize to the lung with equal efficiency. However, when these POGZ-deficient tumors reach the same volume and are resected, the effective pulmonary metastatic burden was greatly enhanced compared to wild-type tumors. This data indicates that, *in vivo*, POGZ deficiency drastically enhances metastatic seeding. However, this enhanced metastatic potential is restricted to early stages of the metastatic cascade, as POGZ-deficient cells injected directly in to the circulation show decreased pulmonary outgrowth. The decreased metastatic burden exhibited in 4T1-sg*Pogz* cells, in this context, is likely due to the inherent cell growth defected exhibited in primary tumor. Importantly, over-expression of POGZ drastically reduces 4T1 migration and effectively inhibits pulmonary metastasis, highlighting the potential functional uncoupling of the roles POGZ may play in tumor cell proliferation and in metastasis.

In summary, we propose that loss of POGZ elicits a TGF-β-sensitive 4T1 tumor microenvironment, through upregulation of TGFBR2, that potentiates an early EMT and advances pulmonary metastasis. We identify amplified TGF-β signalling in POGZ-null 4T1 cells and link this to an increased migratory behavior. However, with this acquisition of aggressive traits, the loss of POGZ triggers an irreversible decrease in cell proliferation.

3.6. Materials and Methods

Cell Lines and Plasmids

4T1 cells were cultured in Dulbecco's modified Eagle's medium (DMEM; Wisent) and were supplemented with 10% fetal bovine serum (FBS) and 1% penicillin–streptavidin (P/S). LentiCRISPRv2, lentiSAMv2, lentiMPH were purchased from Addgene. sgRNA were cloned using an optimized Zhang lab protocol, as per Sanjana et al. (2014). Lentiviral infections were done as previously described (Findlay et al. 2018), with modifications listed below. Cell lines were infected with lentiviruses for 24 h in media containing 8 µg/ml polybrene, and 1 µg/ml puromycin selection or 5ug/mL of blasticidin was applied. TGF-B1 ligand (Peprotech) was dissolved in 4 mM HCl (Sigma) and 1 mg/mL bovine serum albumin V (Wisent) to final stock concentration of 10 ng/mL. TGF-B1 was aliquoted, stored at -80, and were not subject to any freeze-thaw cycles. TGFBR1 inhibitors TP0427736 and SB431542 (Selleckchem) were resuspended in DMSO to final concentrations of 250nM and stored at -20.

Cell Viability and Proliferation

4T1 cells were plated at a density of 100 000 per well in complete DMEM. Cells were treated with TGFB1 ligand or TP0427736 with indicated concentrations. Live cells were counted via trypan blue exclusion with a hemocytometer.

Anchorage Independent Growth Assay (Soft Agar)

In most experiments, 10 000 4T1 cells were grown in suspension in each well of a 6-well plate. The bottom layer was composed of 2% agar (Bioshop) in complete DMEM. The top layer was formed by mixing cells at desired density in complete DMEM with cooled 0.7% agar in complete DMEM, forming a cell containing layer of 0.35% agar. Agar containing wells were grown for 10 days and supplemented with 150uL of complete media every two days. Wells were stained with crystal violet (Sigma) at 37degC overnight and imaged at 4x. A minimum of 3 images were taken for each transwell. Images were analyzed using CellFinder feature with Qupath software. A total 3 images were per well with at least 2 independent experiments used for comparison.

Transwell Migration Assay

In most migration experiments, 12 well transwell inserts of 6.5mm diameter with 8.0um pore size was used (Falcon). Cultured 4T1 cells were collected with trypsin, washed with PBS and plated at a density of 100ul serum free DMEM in the top insert. Complete media with serum was placed in bottom of the well to contact with the insert. Cells were incubated for 24 hours. In some experiments TGF-b (1ng/mL) or SB100342 (250nM) was added to cells and serum free medium in top of transwell insert. Cells on the top of insert were removed with a cotton swap and inserts were fixed with formalin and stained with a crystal violet solution (Sigma). Once dried, transwells were imaged at 4x. A minimum of 3 images were taken for each transwell. Images were analyzed using CellFinder feature with Qupath software. A total 3 images were per well with at least 2 independent experiments used for comparison.

Cell Cycle

4T1 cells were plated at a density of 100 000 per well in complete DMEM. Cells were either subjected to treatment with TGF-b (1ng/mL) or SB100342 (250nM) for 48hrs. Cells were pulsed with BrdU (1ug/mL) for one hour and harvested using trypsin. Cells were subjected to fixation, permeabilization and DNase digest as per the Phase-flow™ BrdU-Alexa Fluor® 647 proliferation kit for Flow Cytometry (BioLegend). Cells were incubated with AF647 conjugated rabbit anti BrdU and counterstained with 7AAD. A minimum of 10 000 events were collected for each condition and cell line. A minimum of 3 independent experiments were performed.

Quantitative PCR/RNAseq

RNA extraction was performed using RNeasy columns (Qiagen). cDNA was generated with 0.5-1ng RNA using the Luna RT Master Mix (NEB). Lentiviral infections were done as previously described (Heath et al. 2021). with modifications listed below. RNA-seq was performed at the Universite de Montreal Institute for Research in Immunology and Cancer. RNA quality was assessed by Agilent 2100 Bioanalyzer (Agilent Technologies). Libraries for RNA-seq were prepared according to strand-specific Illumina TruSeq protocols. Samples were multiplexed at four samples per lane and sequenced on an Illumina HiSeq 2500 PE125 instrument.

Western Blot

Cells were cultured and treated as indicated in text. Cells were washed twice in PBS and scraped off plates in 1x LDS buffer and sonicated. Protein content was quantified using Bradford Assay (Thermofisher). Normalized concentrations of lysate were boiled. Equal amounts of protein were subjected to polyacrylamide electrophoresis as per Findlay et al. Membranes transferred in 1X Towbin Buffer with 5% methanol, blocked, and incubated overnight with primary antibodies in 5% BSA/TBS-T. Membranes were incubated HRP-conjugated secondary antibodies in 5% milk at room temperature for one hour. Membranes were washed and imaged using ECL. Primary antibodies used in this study were rabbit anti-POGZ (Abcam), mouse anti-Tubulin (CST), rabbit anti-SMAD2 (Ser465/476, CST), rabbit anti-SMAD2 (CST), rabbit antiSMAD3 (Ser423/425, CST), rabbit anti SMAD3.

Mice

BALBc mice (7-10 weeks old) used for mammary fat pad injections were purchased from Charles River Laboratories. All mice had ad libitum access to food and water and housed within the animal facilities of the Lady Davis Institute. These studies were approved by and follow the Animal Resource Centre at McGill University procedures (protocol: 2018-8003). These experiments comply with the guidelines set by the Canadian Council of Animal Care.

Mammary Fat-pad Injections

A total of 50 000 4T1 cells were injected in a 1:1 PBS:Matrigel mixture (Corning) into fourth mammary fat pads. Tumor size was determined by caliper measurements of two dimensions and volume calculated as follows: $4/3\pi \times \text{width} \times \text{length}^2$ (smaller measurement is always width). For lung colonization experiments, single fat pads were injected and tumors were resected at indicated tumor volume. For colonization experiments using tail vein injection, 500 000 4T1 cells were prepared as previously stated, washed twice with PBS, and injected intravenously via tail vein. Four weeks after primary tumor resection or tail vein injection, mice were euthanized and lungs subjected to paraffin embedding, sectioned, and stained for H&E. Images were analyzed using

Imagescope. Data is presented as the portion of the lung is metastatic colonies as a fraction of the whole lung.

Immunohistochemistry

Freshly isolated tumor materials were fixed in 10% neutral buffered formalin for 16-24h and stored in 70% ethanol until paraffin embedding. Embedded tumor pieces were sliced (5um) and subjected to IHC with sodium citrate-based antigen retrieval as per Totten et al (2021). Primary antibodies used are as follows: Cleaved caspase 3 (Cell Signaling Technologies), E-cadherin (EMD Millipore). Anti-mouse and -rabbit horseradish peroxidase-conjugated secondary antibodies were used. For mouse derived antibodies (E-cadherin), the Mouse-on-Mouse polymer kit (Abcam) was used as per manufacturer's instructions. Slides were scanned with Scan Scope XT Digital Slide Scanner (Aperio). Images were analyzed using Imagescope (Aperio). Specifically, cleaved caspase 3 and E-Cadherin were analyzed with signal thresholds for cellular staining (including membrane).

3.7 References

1. Fallahpour S, Navaneelan T, De P, Borgo A. Breast cancer survival by molecular subtype: a population-based analysis of cancer registry data. Can Med Assoc Open Access J [Internet]. 2017 [cited 2022 May 18];5:E734–9. Available from: https://www.cmajopen.ca/content/5/3/E734
2. Lima JF, Nofech-Mozes S, Bayani J, Bartlett JMS. EMT in Breast Carcinoma—A Review. J Clin Med [Internet]. 2016 [cited 2022 May 24];5. Available from: /pmc/articles/PMC4961996/
3. Prat A, Perou CM. Deconstructing the molecular portraits of breast cancer. Mol Oncol. 2011;5:5–23.
4. Lüönd F, Sugiyama N, Bill R, Bornes L, Hager C, Tang F, et al. Distinct contributions of partial and full EMT to breast cancer malignancy. Dev Cell. 2021;56:3203-3221.e11.
5. Strilic B, Offermanns S. Intravascular Survival and Extravasation of Tumor Cells. Cancer Cell [Internet]. 2017 [cited 2022 May 24];32:282–93. Available from: https://pubmed.ncbi.nlm.nih.gov/28898694/
6. Rejniak KA. Circulating tumor cells: When a solid tumormeets a fluid microenvironment. Adv Exp Med Biol. 2016;936:93–106.
7. Wang R, Zhu Y, Liu X, Liao X, He J, Niu L. The Clinicopathological features and survival outcomes of patients with different metastatic sites in stage IV breast cancer. BMC Cancer [Internet]. 2019 [cited 2022 May 24];19:1–12. Available from: https://bmccancer.biomedcentral.com/articles/10.1186/s12885-019-6311-z
8. Kennecke H, Yerushalmi R, Woods R, Cheang MCU, Voduc D, Speers CH, et al. Metastatic behavior of breast Cancer subtypes. J Clin Oncol. 2010;28:3271–7.
9. Zhang Y, Alexander PB, Wang XF. TGF-β Family Signaling in the Control of Cell Proliferation and Survival. Cold Spring Harb Perspect Biol [Internet]. 2017 [cited 2022 May 24];9. Available from: /pmc/articles/PMC5378054/
10. Yoo J, Ghiassi M, Jirmanova L, Balliet AG, Hoffman B, Fornace AJ, et al. Transforming Growth Factor-β-induced Apoptosis Is Mediated by Smad-dependent Expression of GADD45b through p38 Activation *. J Biol Chem [Internet]. 2003

[cited 2022 Apr 27];278:43001–7. Available from: http://www.jbc.org/article/S0021925820825733/fulltext

11. Kawabata M, Inoue H, Hanyu A, Imamura T, Miyazono K. Smad proteins exist as monomers in vivo and undergo homo- and hetero-oligomerization upon activation by serine/threonine kinase receptors. EMBO J. 1998;17:4056–65.
12. Yang H, Fan J, Cao Y, Gao R, Fan Z. Distal-less homeobox 5 promotes the osteo-/dentinogenic differentiation potential of stem cells from apical papilla by activating histone demethylase KDM4B through a positive feedback mechanism. Exp Cell Res [Internet]. 2018/12/07. 2019;374:221–30. Available from: https://www.ncbi.nlm.nih.gov/pubmed/30503866
13. Massagué J, Wotton D. Transcriptional control by the TGF-β/Smad signaling system. EMBO J [Internet]. 2000 [cited 2022 May 24];19:1745–54. Available from: https://onlinelibrary.wiley.com/doi/full/10.1093/emboj/19.8.1745
14. Gomis RR, Alarcón C, Nadal C, Van Poznak C, Massagué J. C/EBPβ at the core of the TGFβ cytostatic response and its evasion in metastatic breast cancer cells. Cancer Cell. 2006;10:203–14.
15. Seoane J. Escaping from the TGFb anti-proliferative control. [cited 2022 May 24]; Available from: https://academic.oup.com/carcin/article/27/11/2148/2391325
16. Pardali K, Moustakas A. Actions of TGF-β as tumor suppressor and pro-metastatic factor in human cancer. Biochim Biophys Acta - Rev Cancer. 2007;1775:21–62.
17. Peinado H, Olmeda D, Cano A. Snail, Zeb and bHLH factors in tumour progression: an alliance against the epithelial phenotype? Nat Rev Cancer 2007 76 [Internet]. 2007 [cited 2022 May 19];7:415–28. Available from: https://www.nature.com/articles/nrc2131
18. Taube JH, Herschkowitz JI, Komurov K, Zhou AY, Gupta S, Yang J, et al. Core epithelial-to-mesenchymal transition interactome gene-expression signature is associated with claudin-low and metaplastic breast cancer subtypes. Proc Natl Acad Sci U S A. 2010;107:15449–54.
19. Nawshad A, LaGamba D, Polad A, Hay ED. Transforming growth factor-beta signaling during epithelial-mesenchymal transformation: implications for embryogenesis and tumor metastasis. Cells Tissues Organs. 2005;179:11–23.

20. Nozawa RS, Nagao K, Masuda HT, Iwasaki O, Hirota T, Nozaki N, et al. Human POGZ modulates dissociation of HP1α from mitotic chromosome arms through Aurora B activation. Nat Cell Biol 2010 127 [Internet]. 2010 [cited 2022 May 24];12:719–27. Available from: https://www.nature.com/articles/ncb2075
21. Matsumura K, Seiriki K, Okada S, Nagase M, Ayabe S, Yamada I, et al. Pathogenic POGZ mutation causes impaired cortical development and reversible autism-like phenotypes. Nat Commun [Internet]. 2020/02/28. 2020;11:859. Available from: https://www.ncbi.nlm.nih.gov/pubmed/32103003
22. Gudmundsdottir B, Gudmundsson KO, Klarmann KD, Singh SK, Sun L, Singh S, et al. POGZ Is Required for Silencing Mouse Embryonic beta-like Hemoglobin and Human Fetal Hemoglobin Expression. Cell Rep [Internet]. 2018/06/14. 2018;23:3236–48. Available from: https://www.ncbi.nlm.nih.gov/pubmed/29898395
23. Heath J, Cheyou ES, Findlay S, Luo VM, Carpio EP, Lee J, et al. POGZ promotes homology-directed DNA repair in an HP1-dependent manner. EMBO Rep [Internet]. 2022 [cited 2022 May 24];23:e51041. Available from: https://onlinelibrary.wiley.com/doi/full/10.15252/embr.202051041
24. Suliman-Lavie R, Title B, Cohen Y, Hamada N, Tal M, Tal N, et al. Pogz deficiency leads to transcription dysregulation and impaired cerebellar activity underlying autism-like behavior in mice. Nat Commun [Internet]. 2020/11/19. 2020;11:5836. Available from: https://www.ncbi.nlm.nih.gov/pubmed/33203851
25. Markenscoff-Papadimitriou E, Binyameen F, Whalen S, Price J, Lim K, Ypsilanti AR, et al. Autism risk gene POGZ promotes chromatin accessibility and expression of clustered synaptic genes. Cell Rep [Internet]. 2021 [cited 2022 Jan 5];37:110089. Available from: https://linkinghub.elsevier.com/retrieve/pii/S2211124721015801
26. Hsu BE, Bastien Tabariè S, Johnson RM, Jones RG, St-Pierre J, Siegel Correspondence PM. Immature Low-Density Neutrophils Exhibit Metabolic Flexibility that Facilitates Breast Cancer Liver Metastasis. Cell Rep [Internet]. 2019 [cited 2022 May 24];27:3902–15. Available from: https://doi.org/10.1016/j.celrep.2019.05.091
27. Tabariès S, Ouellet V, Hsu BE, Annis MG, Rose AAN, Meunier L, et al. Granulocytic immune infiltrates are essential for the efficient formation of breast cancer liver

metastases. Breast Cancer Res [Internet]. 2015 [cited 2022 May 24];17:1–18. Available from: https://breast-cancer-research.biomedcentral.com/articles/10.1186/s13058-015-0558-3

28. Joyce JA, Pollard JW. Microenvironmental regulation of metastasis. Nat Rev Cancer. 2009;9:239–52.
29. Hashimoto R, Nakazawa T, Tsurusaki Y, Yasuda Y, Nagayasu K, Matsumura K, et al. Whole-exome sequencing and neurite outgrowth analysis in autism spectrum disorder. J Hum Genet [Internet]. 2015/11/20. 2016;61:199–206. Available from: https://www.ncbi.nlm.nih.gov/pubmed/26582266
30. Ferretti A, Barresi S, Trivisano M, Ciolfi A, Dentici ML, Radio FC, et al. POGZ-related epilepsy: Case report and review of the literature. Am J Med Genet A [Internet]. 2019/05/29. 2019;179:1631–6. Available from: https://www.ncbi.nlm.nih.gov/pubmed/31136090
31. Samanta D, Ramakrishnaiah R, Schaefer B. The neurological aspects related to POGZ mutation: case report and review of CNS malformations and epilepsy. Acta Neurol Belg [Internet]. 2019/03/18. 2020;120:447–50. Available from: https://www.ncbi.nlm.nih.gov/pubmed/30879264
32. Zhao W, Tan J, Zhu T, Ou J, Li Y, Shen L, et al. Rare inherited missense variants of POGZ associate with autism risk and disrupt neuronal development. J Genet Genomics [Internet]. 2019/06/15. 2019;46:247–57. Available from: https://www.ncbi.nlm.nih.gov/pubmed/31196716
33. Matsumura K, Seiriki K, Okada S, Nagase M, Ayabe S, Yamada I, et al. Pathogenic POGZ mutation causes impaired cortical development and reversible autism-like phenotypes. Nat Commun 2020 111 [Internet]. 2020 [cited 2022 Jan 4];11:1–16. Available from: https://www.nature.com/articles/s41467-020-14697-z
34. Lewis K, Kiepas A, Hudson J, Senecal J, Ha JR, Voorand E, et al. P66ShcA functions as a contextual promoter of breast cancer metastasis. Breast Cancer Res [Internet]. 2020 [cited 2022 May 24];22:1–19. Available from: https://breast-cancer-research.biomedcentral.com/articles/10.1186/s13058-020-1245-6

Chapter 4. Discussion and Future Directions

In these independent studies we focused on roles of the zinc finger protein POGZ, for which we and others have identified pleiotropic roles in embryogenesis and proper neurodevelopment, in DNA repair and breast cancer etiology. Our research has bridged POGZ's role in DNA repair and homologous recombination with its interaction with HP1-γ. This data also provides crucial information about the HP1-isoform specificity throughout the many putative functions of POGZ. Furthermore, we provide one of the first functional implications of POGZ in cancer. We largely focused on the loss of POGZ in the murine basal 4T1 breast cancer model, where we identify an essential role for primary tumor growth. However, through loss of POGZ we identified a modulatory activity of POGZ in the repression of TGF-β signalling, which in turn, suppresses metastatic burden.

4.1. POGZ in DNA Double Strand Break Repair

POGZ has been briefly implicated directly in homologous recombination in multiple studies.[256,262,263] Initially, we sought to identify novel interactors of HP1 that may impact DNA repair, as current models of HP1 in association in DNA repair are conflicting. Several key interactors were identified (histones, chromatin remodelling enzymes), however, no clear proteins currently associated with DNA repair emerged. Therefore, we chose to probe a high confidence interactor, the poorly described zinc finger protein POGZ, as it was previous identified by our group and others, to interact with the DSB repair protein, REV7.[42,45,47] We have furthered the understanding of POGZ by showing requirement of its interaction with HP1 isoforms in the context of DNA repair. Through this interaction with HP1, BARD1 and BRCA1, are efficiently recruited or stabilized at sites of damage to promote successful HR. However, mechanistically, the exact role of POGZ is unclear, as it appears in most studies as part of a larger functional complex.

The first POGZ complex identified by Baude et al, was in interaction with hepatoma-derived growth factor-related protein 2 (HDGFRP2) and HP1-β.[256,264] This complex was suggested to be responsible for the repair of DNA damage within transcriptionally silent genes through the binding of methylated histone marks. This binding would reside

through the PWWP domain of HDGFRP2 or the chromoshadow domain of HP1-β, as POGZ has not been shown to directly bind methylated histones. Specifically recruited to damage in heterochromatin, this complex is thought to bind CtIP directly and promote its localization and the DNA resection required for homologous recombination. Studies by Fujita et al. have furthered the mechanism by identifying another larger complex consisting of POGZ and another HP1 binding protein, chromosomal alignment maintenance phosphoprotein (CHAMP1).[262] CHAMP1, in this study, in complex with POGZ, antagonized the inhibitory effects of 53BP1-REV7 on DNA end resection, thus promoting homologous recombination. This finding positions the CHAMP1-POGZ complex, likely on the functional level of resection execution, via recruitment of exonucleases. Furthermore, this complex was shown to be dependent on HDGFRP2, as depletion of HDGFRP2 did not affect recruitment of CHAMP1 to DSB, however, hindered recruitment of CtIP to sites of damage. This suggests that CHAMP1, through POGZ, recruits CtIP to sites of damage, in a HDGFRP2 dependant manner. Interestingly, CHAMP1 and POGZ were shown as REV7 interactors in our previous study identifying REV7 and regulator of pathway decision for DSB repair.[47] When probed for recruitment of NHEJ effectors proteins 53BP1 and RIF1 to sites of damage during a depletion of POGZ or CHAMP1, no effect was seen.[262] However, similarly to POGZ depletion, the loss of CHAMP1 leads to defective recruitment of BRCA1. We furthered this by showing, in addition, there is a defect in HP1-isoform colocalization at sites of DSB in both POGZ and CHAMP1 depleted models. The data from these two studies support our model of POGZ driving homologous recombination through its interaction with HP1-γ. This interaction is required for stabilization of BRCA1-BARD1 at sites of damage and therefore seems likely that loss of this interaction would also affect CtIP recruitment and subsequent DNA end resection.

Furthermore, HP1 isoforms have been shown to be involved in DNA end resection, however, there is conflicting evidence regarding the exact nature of isoform specific contributions. One study, by Soria et al., showed that HP1-α and -β promoted HR, while HP1-γ was shown to suppress HR.[265] This study alluded that this too, was due to

differential effects on DNA end resection. However, another study by Wu et al., which aligns with our hypothesis of a POGZ-HP1 regulated impact on HR, identified that HP1-γ was specifically required for BARD1-BRCA1 recruitment to DNA damage and the promotion of successful HR.[133] We have shown that the interaction between POGZ and the HP1-γ isoform is specifically required for HR, while HP1-α and HP1-β seem dispensable for BRCA1 focus formation. REV7, CHAMP1, and POGZ, all bind each HP1 isoform through all phases of the cell cycle[263], however, the exact role, if any, for HP1 remains elusive in CtIP-recruitment. Interestingly, when performing the proximal-protein labelling BioID to identify interactors of HP1 and POGZ, upon analysis, CHAMP1 peptides were clearly found throughout all conditions (+/- DNA damage), however, REV7/MAD2L2, BRCA1, CtIP were not identified with high confidence. However, our biotin labelling was for an extensive duration (24 hours), meaning it could be that the interaction of POGZ/HP1 isoforms with REV7 and, potentially, the BRCA1-CtIP complex, could be much more regulated or interact for a very brief period. Furthermore, it would seem likely that these POGZ interactions would be context specific, i.e. in the presence of unrepaired DSBs.

4.2. The role of POGZ in cell cycle and gene regulation

We, and other groups, have clearly identified a functional role for POGZ in the regulation of DNA repair, in addition to its effects on cell cycle. However, this exact mechanism through which POGZ promotes HR, seems to be outside of its emerging role in gene transcription.[266,267] This is supported by the direct recruitment of POGZ to sites of damage, where by necessary and direct interactions with HP1 and CHAMP1 support the concerted recruitment of key HR factors, BRCA1 and BARD1. The majority of published reports of POGZ deficiency, while varying largely by pathology and tissue, there is consistent reports of decreased cell division and proliferation.[258,266,268] This phenotype is observed in both primary tissues derived from POGZ-mutant mice and in cell lines, indicating that across various models the requirement of POGZ for cell division is robust. Consistent with this hypothesis, we have further showed that decreased POGZ levels inhibited breast tumor growth *in vivo* and decreased anchorage independent growth of breast cancer cells *in vitro.* In agreeance with this, on a transcriptional level, the pathways

involving cell cycle (E2F, Myc targets, G2/M phase) were observed to be repressed in 4T1-sg*Pogz* cell lines. Overall, our data supports the concept of POGZ regulating a subset of genes responsible for growth promotion, in addition to its direct roles in DNA repair and cell cycle progression.

Across multiple different tissues and models, transcriptional profiling of POGZ-deficient cells reveals a conserved loss in expression of Myc target genes. Furthermore, in a recent study of the MYC interactome reveals distinct functional partners for concerted tumorigenic properties within Myc overexpression in breast cancer. Particularly, POGZ was identified as a novel interactor of Myc, via its MB0 domain.[268] The critical MB0 region is required for accelerated growth, however is dispensable for tumor initiation. The role of this specific binding domain of Myc, is to bind the general transcription factor TFIIF and supports its interactions with transcriptional elongation factors. Furthermore, the specific gene sets regulated by the MB0 domain were found to be similar to those lost in the POGZ deficient 4T1 cells (Myc signaling, cholesterol biosynthesis, fatty acid oxidation). It would be interesting to test if POGZ-deficient 4T1 cells could overcome the growth defect when Myc is overexpressed. If these cells did not regain efficient proliferation, the interaction between POGZ and MYC is required for tumor growth and could possibly explain the defect in primary tumor volumes. Furthermore, an important feature of TGF-β induced tumor suppression is the SMAD2/3 mediated repression of *Myc*.[239] If POGZ is required for Myc-dependent tumorigenesis, then TGF-β induced repression of Myc would yield little effect within POGZ deficient cells. While POGZ deficient cells possess lower mRNA expression of MYC at base line, the TGF-β induced decrease in *Myc* mRNA levels was more dramatic in treated 4T1 cells carrying wild type expression of POGZ. These studies, in addition to our characterization, identify a potential link for POGZ in effective transactivation of the transcriptional activity of MYC.

Multiple studies have now linked POGZ, through its interaction with HP1 isoforms, to incidences of transcriptional regulation of directed differentiation programs during

development of various tissues. Gudsmondottir et al. have shown that POGZ can bind regulatory elements of BAF Chromatin Remodeling Complex Subunit (BCL11A), a well-known suppressor of fetal globin production.[111] Loss of POGZ, in this context, was positioned as loss of a transcriptional activator regulation and decreased BCL11A expression and therefore increased globin expression. The same group published an additional finding of POGZ, specifically through the HP1 binding domain, could repress aberrant transcription of multiple pathways in developing neurons.[258] These aberrantly expressed pathways, many containing heavily annotated ASD associated protein networks, were also found in neural tissue derived from H3K9 demethylases (G9a/GLP). H3K9 modifying enzymes have been previously annotated as interactors of POGZ, by our group and others, highlighting a potential role of a complex centralized around H3K9-regulated transcriptional modulation. This complex relationship is furthered by study by Sun et al. in identifying the embryonic role of a POGZ-HP1-γ complex which maintains pluripotency in ESCs.[269] Loss of the functional capacity of this complex was shown to promote ESC differentiation, contrasting findings in neural stem cells, through upregulation of endodermal and mesodermal pathways. Unsurprisingly, many mesenchymal genes associated with EMT were also identified in the upregulated gene sets within the differentiating POGZ-mutant ESCs. Furthermore, occupancy of promoters of cell cycle genes, such as E2F proteins and cyclin D, were also downregulated by POGZ deficiency. These findings overlap significantly with our transcriptomic data in the POGZ-null 4T1 cell line. Interestingly, upon characterization of genomic positioning of HP1-γ/POGZ complexes, gene bodies were largely corresponding to gene sets governing RNA metabolism and processing. However, when looking at genomic regions bound exclusively by POGZ, the only significantly enriched gene sets were those involved in DNA repair, specifically DSB repair. This provides insight into the potential for non-HP1 associated regulation transcription by POGZ. Furthermore, while we concluded that the impact of POGZ on DSB repair was largely non-transcriptional, we showed a minimal impact of POGZ loss on the mRNA levels of a limited number of proteins that were critically required for HR (BRCA1/2, PALB2, RAD51). Therefore, larger POGZ-regulated transcriptional networks may exist that could be responsible for the transcriptional execution of DNA repair.

Loss of POGZ or incorporation of a clinically relevant mutation (Q1042R), which reduces DNA binding to CENP-B elements, inhibited correct neuronal migration and impaired neuronal stem cell (NSC) development.[261] Further characterization identified that POGZ was bound to the promoter and responsible for the repression of the Notch ligand, Jagged canonical Notch ligand (JAG2), a protein responsible for sustaining neural stem cells by negatively regulating differentiation. It should be noted that the dysfunctional migration was not due to a general lack of migration, rather than a loss of directed migration during nerve generation. Suliman-Lavie et al. utilized a neural stem cell specific conditional POGZ knock-out mouse and observed similar behavioural phenotypes.[258] This group identify an imbalance in inhibitory and activating synaptic firing, credited to a dysregulated neurogenesis. Importantly, in vitro the group suggests that heterochromatin dysregulation through loss of HP1 binding and aberrant transcriptional activation of depressed neuronal development factors, such as DACH2. These results suggest that transcriptional regulation of proper migration and stem cell function are governed by POGZ regulated repression of transcription factor or a secreted factor working in autocrine.

Mutations in POGZ, while quite heterogenous, result in a neurodevelopmental disorder, the White Sutton Syndrome (WHSUS).[260,270,271] This human syndrome has not been described to have any association with cancer, however, POGZ is widely amplified in most cancers. Specifically, POGZ, located in the human chromosomal region 1q21, is amplified in 20% of all human breast cancers, appearing to have oncogenic potential. While this could be resultant of the common 1q21 amplification, which is associated with poor outcomes, low expression of POGZ correlates with poorer patient survival, particularly in basal breast cancer. These conflicting observations, led us to develop both POGZ-deficient and over-expression models using the 4T1 basal breast carcinoma cell line, to explore, for the first time, the impact of POGZ in primary tumor growth and metastasis.

These identified POGZ-regulated networks all retain direct links to cellular proliferation and development, leading to loss of growth and increased differentiation. While our data in breast cancer tumor growth is in coordination with previously published phenotypes of POGZ loss and the effects on cell division,[111,112,261] we shed light on how POGZ may have additional roles in malignant tissue and the suppression of aggressive traits. The complex biology that underpins the potentiation and initiation of the metastatic cascade, via regulation of the EMT, is a multifactorial contribution of both microenvironment and tumor intrinsic attributes. Dormant metastases and lymph nodes bearing cancer are often found in advanced breast cancer and largely contribute to the poor survival rates, therefore, aspects of primary tumor biology that potentiate EMT and initiate metastasis is the greatest barrier to effective therapeutic outcomes of metastatic breast cancer. Understanding how POGZ contributes to tumor biology could shed light on an emerging concept of "grow or go" concept, in which alterations in the primary tumor microenvironment restrict growth despite costly increases in EMT and metastasis.[272]

4.3. POGZ in the regulation of the TGF-β signalling pathway

The enhanced TGF-β signalling, and its cumulative impact on metastasis, in our POGZ deficient system and the concerted defect on cell and tumor growth, pose the question if these phenotypes are mutually exclusive. The tumor suppressive, pro-apoptotic, cytostatic effects of TGF-β in transformed tissues are acute, as under chronic TGFBRI/II signalling, cancer cells adapt and overcome these effects and reposition SMAD2/3 transcriptional complexes at genes that promote the pro-tumorigenic TGF-β qualities such an EMT transcription factors. The increase in TGF-β associated genes is prevalent in POGZ deficient cell lines, the pathway is not significantly enriched in respective tumors. Therefore, the presumption would be that in the presence of exogenous TGF-β from contributing stroma or immune infiltrate could drive POGZ-deficient tumors to undergo EMT and initiate and early and extensive metastatic colonization. Furthermore, the enhanced migration and metastasis witnessed in 4T1-sgPOGZ cell lines is due to a reversible increase in TGFBRI/II signalling, as this phenotype can be pharmacologically and genetically rescued through inhibition of this signalling complex. As tumors downregulate and overcome the cytostatic effects of TGF-β signalling, it becomes an

efficient potentiator of in vivo metastasis, as over expression of TGF-β has been shown to increase *in vivo* metastasis in a wide variety of different cancer models. Therefore, it could be that POGZ loss epigenetically drives changes in only cytostatic gene regulation or facilitates the transcriptional switch, funnelling SMAD transcriptional complexes to only pro-tumorigenic TGF-β induced gene programs. It would be interesting to show SMAD2/3-SMAD4 genomic occupancy in POGZ-deficient systems, upon TGF-β stimulation, and assess the distribution of these sites as cytostatic or pro-metastatic/EMT.

Increased TGFBR1/2 levels are beneficial in precancerous tissue preventing cellular transformation through the tumor suppressive effects of TGF-β signalling. In addition, in order to by-pass this tumor suppressive pathway, TGFBR1/2 and SMAD2/3 proteins are often mutated in cancers. However, in cancerous tissue that successfully transform without the silencing of this pathway, ultimately utilize it to promote EMT and migration. It is well described that TGRBR2 levels directly correlate with phosphorylated SMAD2/3 and target gene transcription. Therefore, this increase in TGFBR2 expression witnessed in 4T1-sgPOGZ cells, may allow for increased signalling from activated TGFBR complexes and result in increased SMAD phosphorylation and TGF-β target gene expression. While the kinase domain of TGFBR1 is the target of most pharmacological inhibitors, activation of this kinase activity is initiated, solely, by the engagement of TGF-β ligand with TGFBR2. Whether POGZ can directly bind regulatory elements of *Tgfbr2* or other signalling modifying components, such as *Smurf2* or *Smad7*, and repress transcription through recruitment of silencing machinery, is unknown.

One study, by Zheng et al. recently showed that in addition to inhibited growth and colony formation, loss of POGZ yielded a decrease in transcription of key cell cycle mediating genes.[268] However, they also report a decrease in mesenchymal markers and migratory potential. Although the study does not speak to the propensity to undergo EMT during TGF-β treatment, they do show increased transcription of *TGFB1*. While in the transcriptomic profiling of the 4T1 POGZ-null cells, we did see a modest increase in

expression of TGF-β, it was not significantly enriched. Given the tight regulation of TGF-β ligand secretion and signalling, it is imperative that on the level of protein and secretion, if 4T1-sg*Pogz* possess any increases in TGF-β in comparison to 4T1-sg*Rosa*. Furthermore, this study utilized siRNA for POGZ-depletion, indicating that acute and short-term effects of POGZ depletion could represent a tumor suppressive phenotype, however, our results of pooled clones of POGZ-deficient 4T1 cell lines, show the long-term effects of POGZ loss and the sequential aggressive adaptation. Lastly, this study utilized the osteosarcoma, U2OS, which further complicates a direct comparison to our results. It should be be noted that, only utilizing one TNBC cell line is a limitation, as many cancer cell lines show different responses to TGF-β stimulation, some being completely resistant to cytostatic effects or the initiation of an EMT.

There may be a cell state that during an induction of a cell cycle arrest or inhibited growth, cancer cells may be poised to readily take on EMT qualities and are susceptible to EMT. These bifurcated and seemingly contradictory functions of an oncogene or tumor suppressor and their required roles in EMT/metastasis are not restricted to POGZ. The cell cycle inhibitor p21 reinforces a G1 arrest under the control of TGF-β signalling, the initiation of cellular senescence, and during the DNA damage response. Overexpression and sequestration of p21 in the cytoplasm promotes tumor acceleration and lung metastasis, indicating that even canonical tumor suppressors can contextually confer oncogenic potential.[273,274] Another example of duel or opposing roles in tumor progression is the case of Semaphorin 3B (SEMA3B). When overexpressed in TNBC, *Sema3b* inhibits the growth of primary tumors, however, drastically increases pulmonary metastases.[175] This is achieved through Sema3b induced activation of p38 MAPK and enhanced transcription of p21, inhibiting cell growth, however, the concordant increase in inflammatory interleukin 8 (IL-8), elicits a myeloid lineage driven pro-metastatic niche.

There is a larger question of how POGZ can play such concerted roles in mitotic stability, homologous recombination, and in the regulation of transcription. Initially, cell cycle

regulation by POGZ was identified through the direct interaction of HP1-α with the chromosomal passenger complex. Furthermore, the recruitment or retention of crucial HR complexes, i.e. BARD1-BRCA1, are potentiated through the engagement of POGZ and HP1-γ, particularly under conditions of DSB signalling. Despite this, there is growing evidence suggesting the POGZ-HP1-γ complex may also, basally, be largely responsible for its role in transcriptional regulation in tissue development. Lastly, POGZ may again directly be involved in DNA end resection, in part with CHAMP1-HDGFRP2, which may be largely through the HP1-β isoform, as this isoform has been identified to interact with REV7 and CHAMP1. It could be that POGZ through coordination with context driven specificity of HP1 isoforms may delineate differential functional capacities. Therefore, the specific regulation of the interaction between POGZ and HP1 isoforms may represent a more elegantly designed target to inhibit a relegated function of POGZ.

References

1. Paull TT, Lee JH. The Mre11/Rad50/Nbs1 complex and its role as a DNA double-strand break sensor for ATM. Cell Cycle [Internet]. 2005 [cited 2022 May 21];4:737–40. Available from: https://www.tandfonline.com/action/journalInformation?journalCode=kccy20

2. Bian L, Meng Y, Zhang M, Li D. MRE11-RAD50-NBS1 complex alterations and DNA damage response: Implications for cancer treatment. Mol Cancer. 2019;18.

3. Lee J, Dunphy WG. The Mre11-Rad50-Nbs1 (MRN) complex has a specific role in the activation of Chk1 in response to stalled replication forks. Mol Biol Cell. 2013;24:1343–53.

4. Burger K, Ketley RF, Gullerova M. Beyond the Trinity of ATM, ATR, and DNA-PK: Multiple Kinases Shape the DNA Damage Response in Concert With RNA Metabolism. Front Mol Biosci. 2019;6.

5. Menolfi D, Zha S. ATM, ATR and DNA-PKcs kinases-the lessons from the mouse models: Inhibition = deletion. Cell Biosci. 2020;10.

6. Zan H, Tat C, Qiu Z, Taylor JR, Guerrero JA, Shen T, et al. Rad52 competes with Ku70/Ku86 for binding to S-region DSB ends to modulate antibody class-switch DNA recombination. Nat Commun [Internet]. 2017/02/09. 2017;8:14244. Available from: https://www.ncbi.nlm.nih.gov/pubmed/28176781

7. Solier S, Pommier Y. The apoptotic ring: a novel entity with phosphorylated histones H2AX and H2B and activated DNA damage response kinases. Cell Cycle [Internet]. 2009/05/19. 2009;8:1853–9. Available from: https://www.ncbi.nlm.nih.gov/pubmed/19448405

8. Wu L, Luo K, Lou Z, Chen J. MDC1 regulates intra-S-phase checkpoint by targeting NBS1 to DNA double-strand breaks. Proc Natl Acad Sci U S A. 2008;105:11200–5.

9. Chapman JR, Jackson SP. Phospho-dependent interactions between NBS1 and

MDC1 mediate chromatin retention of the MRN complex at sites of DNA damage. EMBO Rep [Internet]. 2008 [cited 2022 May 23];9:795. Available from: /pmc/articles/PMC2442910/

10. Stucki M, Clapperton JA, Mohammad D, Yaffe MB, Smerdon SJ, Jackson SP. MDC1 directly binds phosphorylated histone H2AX to regulate cellular responses to DNA double-strand breaks. Cell [Internet]. 2005 [cited 2022 May 23];123:1213–26. Available from: https://pubmed.ncbi.nlm.nih.gov/16377563/

11. Bohgaki M, Bohgaki T, El Ghamrasni S, Srikumar T, Maire G, Panier S, et al. RNF168 ubiquitylates 53BP1 and controls its response to DNA double-strand breaks. Proc Natl Acad Sci U S A [Internet]. 2013/12/11. 2013;110:20982–7. Available from: https://www.ncbi.nlm.nih.gov/pubmed/24324146

12. Mallette FA, Mattiroli F, Cui G, Young LC, Hendzel MJ, Mer G, et al. RNF8- and RNF168-dependent degradation of KDM4A/JMJD2A triggers 53BP1 recruitment to DNA damage sites. EMBO J. 2012;31:1865–78.

13. Panier S, Ichijima Y, Fradet-Turcotte A, Leung CC, Kaustov L, Arrowsmith CH, et al. Tandem protein interaction modules organize the ubiquitin-dependent response to DNA double-strand breaks. Mol Cell [Internet]. 2012/06/30. 2012;47:383–95. Available from: https://www.ncbi.nlm.nih.gov/pubmed/22742833

14. Fradet-Turcotte A, Canny MD, Escribano-Diaz C, Orthwein A, Leung CC, Huang H, et al. 53BP1 is a reader of the DNA-damage-induced H2A Lys 15 ubiquitin mark. Nature [Internet]. 2013/06/14. 2013;499:50–4. Available from: https://www.ncbi.nlm.nih.gov/pubmed/23760478

15. Sobhian B, Shao G, Lilli DR, Culhane AC, Moreau LA, Xia B, et al. RAP80 targets BRCA1 to specific ubiquitin structures at DNA damage sites. Science (80-). 2007;316:1198–202.

16. Wu J, Liu C, Chen J, Yu X. RAP80 Protein Is Important for Genomic Stability and Is Required for Stabilizing BRCA1-A Complex at DNA Damage Sites in Vivo. J Biol Chem [Internet]. 2012 [cited 2022 May 23];287:22919. Available from:

/pmc/articles/PMC3391110/

17. Kim H, Chen J, Yu X. Ubiquitin-binding protein RAP80 mediates BRCA1-dependent DNA damage response. Science (80-) [Internet]. 2007 [cited 2022 May 23];316:1202–5. Available from: https://www.science.org/doi/abs/10.1126/science.1139621

18. Cheng Q, Barboule N, Frit P, Gomez D, Bombarde O, Couderc B, et al. Ku counteracts mobilization of PARP1 and MRN in chromatin damaged with DNA double-strand breaks. Nucleic Acids Res. 2011;39:9605–19.

19. Wang M, Wu W, Wu W, Rosidi B, Zhang L, Wang H, et al. PARP-1 and Ku compete for repair of DNA double strand breaks by distinct NHEJ pathways. Nucleic Acids Res. 2006;34:6170–82.

20. Anne-Marie Couto C, Hsu DW, Teo R, Rakhimova A, Lempidaki S, Pears CJ, et al. Nonhomologous end-joining promotes resistance to DNA damage in the absence of an ADP-ribosyltransferase that signals DNA single strand breaks. J Cell Sci. 2013;126:3452–61.

21. Couto CAM, Wang HY, Green JCA, Kiely R, Siddaway R, Borer C, et al. PARP regulates nonhomologous end joining through retention of Ku at double-strand breaks. J Cell Biol [Internet]. 2011 [cited 2022 May 23];194:367–75. Available from: https://pubmed.ncbi.nlm.nih.gov/21807880/

22. Rose M, Burgess JT, O'Byrne K, Richard DJ, Bolderson E. PARP Inhibitors: Clinical Relevance, Mechanisms of Action and Tumor Resistance. Front Cell Dev Biol. 2020;8:879.

23. Bétermier M, Bertrand P, Lopez BS. Is Non-Homologous End-Joining Really an Inherently Error-Prone Process? PLoS Genet [Internet]. 2014 [cited 2022 May 23];10. Available from: /pmc/articles/PMC3894167/

24. Rodgers K, Mcvey M. Error-prone repair of DNA double-strand breaks. J Cell Physiol [Internet]. 2016 [cited 2022 May 23];231:15. Available from: /pmc/articles/PMC4586358/

25. Mari PO, Florea BI, Persengiev SP, Verkaik NS, Brüggenwirth HT, Modesti M, et al. Dynamic assembly of end-joining complexes requires interaction between Ku70/80 and XRCC4. Proc Natl Acad Sci U S A [Internet]. 2006 [cited 2022 May 23];103:18597–602. Available from: www.pnas.orgcgidoi10.1073pnas.0609061103

26. Beucher A, Birraux J, Tchouandong L, Barton O, Shibata A, Conrad S, et al. ATM and Artemis promote homologous recombination of radiation-induced DNA double-strand breaks in G2. EMBO J. 2009;28:3413–27.

27. Chang HHY, Watanabe G, Gerodimos CA, Ochi T, Blundell TL, Jackson SP, et al. Different DNA end configurations dictate which NHEJ components are most important for joining efficiency. J Biol Chem. 2016;291:24377–89.

28. Ma Y, Pannicke U, Schwarz K, Lieber MR. Hairpin opening and overhang processing by an Artemis/DNA-dependent protein kinase complex in nonhomologous end joining and V(D)J recombination. Cell. 2002;108:781–94.

29. Pannunzio NR, Watanabe G, Lieber MR. Nonhomologous DNA end-joining for repair of DNA double-strand breaks. J Biol Chem [Internet]. 2018 [cited 2022 May 23];293:10512–23. Available from: http://www.jbc.org/article/S0021925820338096/fulltext

30. Davis AJ, Chen DJ. DNA double strand break repair via non-homologous end-joining. Transl Cancer Res [Internet]. 2013 [cited 2022 May 23];2. Available from: https://tcr.amegroups.com/article/view/1142/html

31. Dinkelmann M, Spehalski E, Stoneham T, Buis J, Wu Y, Sekiguchi JM, et al. Multiple functions of MRN in end-joining pathways during isotype class switching. Nat Struct Mol Biol. 2009;16:808–13.

32. Rass E, Grabarz A, Plo I, Gautier J, Bertrand P, Lopez BS. Role of Mre11 in chromosomal nonhomologous end joining in mammalian cells. Nat Struct Mol Biol [Internet]. 2009 [cited 2022 May 23];16:819–24. Available from: https://pubmed.ncbi.nlm.nih.gov/19633668/

33. Liu S, Liu X, Kamdar RP, Wanotayan R, Sharma MK, Adachi N, et al. C-Terminal region of DNA ligase IV drives XRCC4/DNA ligase IV complex to chromatin. Biochem Biophys Res Commun [Internet]. 2013 [cited 2022 May 23];439:173–8. Available from: https://pubmed.ncbi.nlm.nih.gov/23994631/

34. Francis DB, Kozlov M, Chavez J, Chu J, Malu S, Hanna M, et al. DNA Ligase IV regulates XRCC4 nuclear localization. DNA Repair (Amst). 2014;21:36–42.

35. Feng L, Fong KW, Wang J, Wang W, Chen J. RIF1 counteracts BRCA1-mediated end resection during DNA repair. J Biol Chem [Internet]. 2013/03/15. 2013;288:11135–43. Available from: https://www.ncbi.nlm.nih.gov/pubmed/23486525

36. Escribano-Diaz C, Orthwein A, Fradet-Turcotte A, Xing M, Young JT, Tkac J, et al. A cell cycle-dependent regulatory circuit composed of 53BP1-RIF1 and BRCA1-CtIP controls DNA repair pathway choice. Mol Cell [Internet]. 2013/01/22. 2013;49:872–83. Available from: http://dx.doi.org/10.1016/j.molcel.2013.01.001

37. Chapman JR, Barral P, Vannier JB, Borel V, Steger M, Tomas-Loba A, et al. RIF1 is essential for 53BP1-dependent nonhomologous end joining and suppression of DNA double-strand break resection. Mol Cell [Internet]. 2013/01/22. 2013;49:858–71. Available from: https://www.ncbi.nlm.nih.gov/pubmed/23333305

38. Zimmermann M, Lottersberger F, Buonomo SB, Sfeir A, de Lange T. 53BP1 regulates DSB repair using Rif1 to control 5’ end resection. Science (80-) [Internet]. 2013/01/12. 2013;339:700–4. Available from: https://www.ncbi.nlm.nih.gov/pubmed/23306437

39. Boersma V, Moatti N, Segura-Bayona S, Peuscher MH, van der Torre J, Wevers BA, et al. MAD2L2 controls DNA repair at telomeres and DNA breaks by inhibiting 5’ end resection. Nature [Internet]. 2015/03/25. 2015;521:537–40. Available from: https://www.ncbi.nlm.nih.gov/pubmed/25799990

40. Xu G, Ross Chapman J, Brandsma I, Yuan J, Mistrik M, Bouwman P, et al. REV7 counteracts DNA double-strand break resection and impacts PARP inhibition.

Nature [Internet]. 2015 [cited 2022 May 23];521:541. Available from: /pmc/articles/PMC4671316/

41. Gupta R, Somyajit K, Narita T, Nussenzweig A, Lukas J. DNA Repair Network Analysis Reveals Shieldin as a Key Regulator of NHEJ and PARP Inhibitor Sensitivity. 2018 [cited 2022 May 23]; Available from: https://doi.org/10.1016/j.cell.2018.03.050

42. Dev H, Chiang TWW, Lescale C, de Krijger I, Martin AG, Pilger D, et al. Shieldin complex promotes DNA end-joining and counters homologous recombination in BRCA1-null cells. Nat Cell Biol [Internet]. 2018 [cited 2022 May 23];20:954. Available from: /pmc/articles/PMC6145444/

43. Zimmermann M, Lottersberger F, Buonomo SB, Sfeir A, De Lange T. 53BP1 regulates DSB repair using Rif1 to control 5′ end resection. Science (80-). 2013;339:700–4.

44. Feng L, Fong KW, Wang J, Wang W, Chen J. RIF1 counteracts BRCA1-mediated end resection during DNA repair. J Biol Chem. 2013;288:11135–43.

45. Noordermeer SM, Adam S, Setiaputra D, Barazas M, Pettitt SJ, Ling AK, et al. The shieldin complex mediates 53BP1-dependent DNA repair. Nat 2018 5607716 [Internet]. 2018 [cited 2022 May 23];560:117–21. Available from: https://www.nature.com/articles/s41586-018-0340-7

46. Mirman Z, Lottersberger F, Takai H, Kibe T, Gong Y, Takai K, et al. 53BP1–RIF1–shieldin counteracts DSB resection through CST- and Polα-dependent fill-in. Nat 2018 5607716 [Internet]. 2018 [cited 2022 May 23];560:112–6. Available from: https://www.nature.com/articles/s41586-018-0324-7

47. Findlay S, Heath J, Luo VM, Malina A, Morin T, Coulombe Y, et al. SHLD2/FAM35A co-operates with REV7 to coordinate DNA double-strand break repair pathway choice. Embo j [Internet]. 2018/08/30. 2018;37. Available from: https://www.ncbi.nlm.nih.gov/pubmed/30154076

48. Polato F, Callen E, Wong N, Faryabi R, Bunting S, Chen HT, et al. CtIP-mediated

resection is essential for viability and can operate independently of BRCA1. J Exp Med [Internet]. 2014 [cited 2022 May 18];211:1027. Available from: /pmc/articles/PMC4042650/

49. Huertas P, Jackson SP. Human CtIP Mediates Cell Cycle Control of DNA End Resection and Double Strand Break Repair * □ S. 2009 [cited 2022 May 23]; Available from: http://www.jbc.org

50. Abraham RT. Cell cycle checkpoint signaling through the ATM and ATR kinases. Genes Dev. 2001;15:2177–96.

51. Buisson R, Boisvert JL, Benes CH, Zou L. Distinct but Concerted Roles of ATR, DNA-PK, and Chk1 in Countering Replication Stress during S Phase. Mol Cell. 2015;59:1011–24.

52. Ashton NW, Bolderson E, Cubeddu L, O'Byrne KJ, Richard DJ. Human single-stranded DNA binding proteins are essential for maintaining genomic stability. BMC Mol Biol [Internet]. 2013 [cited 2022 May 23];14:1–20. Available from: https://bmcmolbiol.biomedcentral.com/articles/10.1186/1471-2199-14-9

53. Manke IA, Lowery DM, Nguyen A, Yaffe MB. BRCT repeats as phosphopeptide-binding modules involved in protein targeting. Science (80-) [Internet]. 2003/10/25. 2003;302:636–9. Available from: https://www.ncbi.nlm.nih.gov/pubmed/14576432

54. Sy SMH, Huen MSY, Chen J. PALB2 is an integral component of the BRCA complex required for homologous recombination repair. Proc Natl Acad Sci U S A [Internet]. 2009 [cited 2022 May 23];106:7155–60. Available from: https://pubmed.ncbi.nlm.nih.gov/19369211/

55. Simhadri S, Vincelli G, Huo Y, Misenko S, Foo TK, Ahlskog J, et al. PALB2 connects BRCA1 and BRCA2 in the G2/M checkpoint response. Oncogene. 2019;38:1585–96.

56. Dray E, Etchin J, Wiese C, Saro D, Williams GJ, Hammel M, et al. Enhancement of RAD51 recombinase activity by the tumor suppressor PALB2. Nat Struct Mol

Biol [Internet]. 2010 [cited 2022 May 23];17:1255–9. Available from: https://pubmed.ncbi.nlm.nih.gov/20871616/

57. Harami GM, Seol Y, In J, Ferencziová V, Martina M, Gyimesi M, et al. Shuttling along DNA and directed processing of D-loops by RecQ helicase support quality control of homologous recombination. Proc Natl Acad Sci U S A. 2017;114:E466–75.

58. Petukhova G, Sung P, Klein H. Promotion of Rad51-dependent D-loop formation by yeast recombination factor Rdh54/Tid1. Genes Dev [Internet]. 2000 [cited 2022 May 23];14:2206. Available from: /pmc/articles/PMC316899/

59. Bennardo N, Cheng A, Huang N, Stark JM. Alternative-NHEJ Is a Mechanistically Distinct Pathway of Mammalian Chromosome Break Repair. PLoS Genet [Internet]. 2008 [cited 2022 May 23];4:1000110. Available from: /pmc/articles/PMC2430616/

60. Han J, Ruan C, Huen MSY, Wang J, Xie A, Fu C, et al. BRCA2 antagonizes classical and alternative nonhomologous end-joining to prevent gross genomic instability. Nat Commun 2017 81 [Internet]. 2017 [cited 2022 May 23];8:1–16. Available from: https://www.nature.com/articles/s41467-017-01759-y

61. Cortizas EM, Zahn A, Hajjar ME, Patenaude AM, Di Noia JM, Verdun RE. Alternative end-joining and classical nonhomologous end-joining pathways repair different types of double-strand breaks during class-switch recombination. J Immunol [Internet]. 2013/10/23. 2013;191:5751–63. Available from: https://www.ncbi.nlm.nih.gov/pubmed/24146042

62. Chen CC, Kass EM, Yen WF, Ludwig T, Moynahan ME, Chaudhuri J, et al. ATM loss leads to synthetic lethality in BRCA1 BRCT mutant mice associated with exacerbated defects in homology-directed repair. Proc Natl Acad Sci U S A. 2017;114:7665–70.

63. Moynahan ME, Jasin M. Mitotic homologous recombination maintains genomic stability and suppresses tumorigenesis. Nat Rev Mol Cell Biol. 2010;11:196–207.

64. Reczek CR, Szabolcs M, Stark JM, Ludwig T, Baer R. The interaction between CtIP and BRCA1 is not essential for resection-mediated DNA repair or tumor suppression. J Cell Biol. 2013;201:693–707.

65. Tsutakawa SE, Classen S, Chapados BR, Arvai AS, Finger LD, Guenther G, et al. Human flap endonuclease structures, DNA double-base flipping, and a unified understanding of the FEN1 superfamily. Cell [Internet]. 2011 [cited 2022 May 23];145:198–211. Available from: http://www.cell.com/article/S0092867411002418/fulltext

66. Chapados BR, Hosfield DJ, Han S, Qiu J, Yelent B, Shen B, et al. Structural basis for FEN-1 substrate specificity and PCNA-mediated activation in DNA replication and repair. Cell. 2004;116:39–50.

67. Teasley DC, Parajuli S, Nguyen M, Moore HR, Alspach E, Lock YJ, et al. Flap Endonuclease 1 Limits Telomere Fragility on the Leading Strand. J Biol Chem [Internet]. 2015 [cited 2022 May 23];290:15133–45. Available from: https://pubmed.ncbi.nlm.nih.gov/25922071/

68. Maloisel L, Fabre F, Gangloff S. DNA polymerase delta is preferentially recruited during homologous recombination to promote heteroduplex DNA extension. Mol Cell Biol [Internet]. 2008 [cited 2022 May 23];28:1373–82. Available from: https://pubmed.ncbi.nlm.nih.gov/18086882/

69. Brocas C, Charbonnier JB, Dhérin C, Gangloff S, Maloisel L. Stable interactions between DNA polymerase δ catalytic and structural subunits are essential for efficient DNA repair. DNA Repair (Amst). 2010;9:1098–111.

70. McVey M, Khodaverdian VY, Meyer D, Cerqueira PG, Heyer WD. Eukaryotic DNA Polymerases in Homologous Recombination. Annu Rev Genet [Internet]. 2016 [cited 2022 May 23];50:393. Available from: /pmc/articles/PMC5295669/

71. Chen JM, Férec C, Cooper DN. Gene conversion in human genetic disease. Genes (Basel). 2010;1:550–63.

72. Tachibana KEK, Gonzalez MA, Coleman N. Cell-cycle-dependent regulation of

DNA replication and its relevance to cancer pathology. J Pathol [Internet]. 2005 [cited 2022 Sep 17];205:123–9. Available from: https://onlinelibrary.wiley.com/doi/full/10.1002/path.1708

73. Matthews HK, Bertoli C, de Bruin RAM. Cell cycle control in cancer. Nat Rev Mol Cell Biol 2021 231 [Internet]. 2021 [cited 2022 Sep 17];23:74–88. Available from: https://www.nature.com/articles/s41580-021-00404-3

74. Grant GD, Cook JG. The temporal regulation of s phase proteins during G1. Adv Exp Med Biol. 2017;1042:335–69.

75. Magiera MM, Gueydon E, Schwob E. DNA replication and spindle checkpoints cooperate during S phase to delay mitosis and preserve genome integrity. J Cell Biol [Internet]. 2014 [cited 2022 Sep 17];204:165–75. Available from: www.jcb.org/cgi/doi/10.1083/jcb.201306023JCB165

76. Pennycook BR, Barr AR. Restriction point regulation at the crossroads between quiescence and cell proliferation. FEBS Lett [Internet]. 2020 [cited 2022 Sep 17];594:2046–60. Available from: https://onlinelibrary.wiley.com/doi/full/10.1002/1873-3468.13867

77. Morris L, Allen KE, La Thangue NB. Regulation of E2F transcription by cyclin E-Cdk2 kinase mediated through p300/CBP co-activators. Nat Cell Biol [Internet]. 2000 [cited 2022 May 23];2:232–9. Available from: https://pubmed.ncbi.nlm.nih.gov/10783242/

78. De Boer L, Oakes V, Beamish H, Giles N, Stevens F, Somodevilla-Torres M, et al. Cyclin A/cdk2 coordinates centrosomal and nuclear mitotic events. Oncogene 2008 2731 [Internet]. 2008 [cited 2022 May 23];27:4261–8. Available from: https://www.nature.com/articles/onc200874

79. Narasimha AM, Kaulich M, Shapiro GS, Choi YJ, Sicinski P, Dowdy SF. Cyclin D activates the Rb tumor suppressor by mono-phosphorylation. Elife. 2014;3.

80. Milazzo L, Foschi A, Mazzali C, Viola A, Ridolfo A, Galli M, et al. Short communication: impact of hepatitis C viral clearance on CD4+ T-lymphocyte

course in HIV/HCV-coinfected patients treated with pegylated interferon plus ribavirin. AIDS Res Hum Retroviruses [Internet]. 2012 [cited 2017 May 18];28:989–93. Available from: http://www.ncbi.nlm.nih.gov/pubmed/22220723

81. Braden WA, McClendon AK, Knudsen ES. Cyclin-dependent kinase 4/6 activity is a critical determinant of pre-replication complex assembly. Oncogene 2008 2756 [Internet]. 2008 [cited 2022 May 23];27:7083–93. Available from: https://www.nature.com/articles/onc2008319

82. Qiao R, Weissmann F, Yamaguchi M, Brown NG, VanderLinden R, Imre R, et al. Mechanism of APC/CCDC20 activation by mitotic phosphorylation. Proc Natl Acad Sci U S A [Internet]. 2016 [cited 2022 May 23];113:E2570–8. Available from: www.pnas.org/cgi/doi/10.1073/pnas.1604929113

83. Löbrich M, Jeggo P. A Process of Resection-Dependent Nonhomologous End Joining Involving the Goddess Artemis. 2017 [cited 2022 May 23]; Available from: http://dx.doi.org/10.1016/j.tibs.2017.06.011

84. Zhao X, Wei C, Li J, Xing P, Li J, Zheng S, et al. Cell cycle-dependent control of homologous recombination. Acta Biochim Biophys Sin (Shanghai). 2017;49:655–68.

85. Mao Z, Bozzella M, Seluanov A, Gorbunova V. DNA repair by nonhomologous end joining and homologous recombination during cell cycle in human cells. Cell Cycle [Internet]. 2008 [cited 2022 May 23];7:2902–6. Available from: https://pubmed.ncbi.nlm.nih.gov/18769152/

86. Yu W, Lescale C, Babin L, Bedora-Faure M, Lenden-Hasse H, Baron L, et al. Repair of G1 induced DNA double-strand breaks in S-G2/M by alternative NHEJ. Nat Commun 2020 111 [Internet]. 2020 [cited 2022 May 23];11:1–15. Available from: https://www.nature.com/articles/s41467-020-19060-w

87. Prost S, Bellamy COC, Clarke AR, Wyllie AH, Harrison DJ. p53-independent DNA repair and cell cycle arrest in embryonic stem cells. FEBS Lett [Internet]. 1998 [cited 2022 May 23];425:499–504. Available from:

https://pubmed.ncbi.nlm.nih.gov/9563521/

88. Chung JH, Bunz F. Cdk2 Is Required for p53-Independent G2/M Checkpoint Control. PLOS Genet [Internet]. 2010 [cited 2022 May 23];6:e1000863. Available from: https://journals.plos.org/plosgenetics/article?id=10.1371/journal.pgen.1000863

89. Lossaint G, Besnard E, Fisher D, Piette J, Dulic V. Chk1 is dispensable for G2 arrest in response to sustained DNA damage when the ATM/p53/p21 pathway is functional. Oncogene [Internet]. 2011/05/03. 2011;30:4261–74. Available from: https://www.ncbi.nlm.nih.gov/pubmed/21532626

90. Zaugg K, Su YW, Reilly PT, Moolani Y, Cheung CC, Hakem R, et al. Cross-talk between Chk1 and Chk2 in double-mutant thymocytes. Proc Natl Acad Sci U S A [Internet]. 2007/03/16. 2007;104:3805–10. Available from: https://www.ncbi.nlm.nih.gov/pubmed/17360434

91. Bartek J, Lukas J. Chk1 and Chk2 kinases in checkpoint control and cancer. Cancer Cell. 2003;3:421–9.

92. Ezhevsky SA, Nagahara H, Vocero-Akbani AM, Gius DR, Wei MC, Dowdy SF. Hypo-phosphorylation of the retinoblastoma protein (pRb) by cyclin D:Cdk4/6 complexes results in active pRb. Proc Natl Acad Sci U S A. 1997;94:10699–704.

93. Yao G, Lee TJ, Mori S, Nevins JR, You L. A bistable Rb-E2F switch underlies the restriction point. Nat Cell Biol. 2008;10:476–82.

94. Brugarolas J, Moberg K, Boyd SD, Taya Y, Jacks T, Lees JA. Inhibition of cyclin-dependent kinase 2 by p21 is necessary for retinoblastoma protein-mediated G1 arrest after γ-irradiation. Proc Natl Acad Sci U S A. 1999;96:1002–7.

95. Chen S, Wang Q, Yu H, Capitano ML, Vemula S, Nabinger SC, et al. Mutant p53 drives clonal hematopoiesis through modulating epigenetic pathway. Nat Commun 2019 101 [Internet]. 2019 [cited 2022 May 23];10:1–14. Available from: https://www.nature.com/articles/s41467-019-13542-2

96. Liu K, Zheng M, Lu R, Du J, Zhao Q, Li Z, et al. The role of CDC25C in cell cycle regulation and clinical cancer therapy: a systematic review. Cancer Cell Int 2020 201 [Internet]. 2020 [cited 2022 May 23];20:1–16. Available from: https://cancerci.biomedcentral.com/articles/10.1186/s12935-020-01304-w

97. Falck J, Mailand N, Syljuåsen RG, Bartek J, Lukas J. The ATM-Chk2-Cdc25A checkpoint pathway guards against radioresistant DNA synthesis. Nature [Internet]. 2001 [cited 2022 May 23];410:842–7. Available from: https://pubmed.ncbi.nlm.nih.gov/11298456/

98. Sørensen CS, Syljuåsen RG. Safeguarding genome integrity: the checkpoint kinases ATR, CHK1 and WEE1 restrain CDK activity during normal DNA replication. Nucleic Acids Res [Internet]. 2012 [cited 2022 May 23];40:477–86. Available from: https://academic.oup.com/nar/article/40/2/477/2409009

99. Fenley AT, Anandakrishnan R, Kidane YH, Onufriev A V. Modulation of nucleosomal DNA accessibility via charge-altering post-translational modifications in histone core. Epigenetics and Chromatin [Internet]. 2018 [cited 2022 May 23];11:1–19. Available from: https://epigeneticsandchromatin.biomedcentral.com/articles/10.1186/s13072-018-0181-5

100. Strahl BD, Allis CD. The language of covalent histone modifications. Nature. 2000;403:41–5.

101. Arya G, Schlick T. Role of histone tails in chromatin folding revealed by a mesoscopic oligonucleosome model. Proc Natl Acad Sci. 2006;103:16236–41.

102. Zhang Y. Transcriptional regulation by histone ubiquitination and deubiquitination. Genes Dev. 2003;17:2733–40.

103. Krug B, De Jay N, Harutyunyan AS, Kleinman CL, Jabado N, Mack Correspondence SC. Pervasive H3K27 Acetylation Leads to ERV Expression and a Therapeutic Vulnerability in H3K27M Gliomas. Cancer Cell [Internet]. 2019 [cited 2022 May 23];35:782–97. Available from:

https://doi.org/10.1016/j.ccell.2019.04.004

104. Meyer B, Fabbrizi MR, Raj S, Zobel CL, Hallahan DE, Sharma GG. Stem Cell Reports Repor t Histone H3 Lysine 9 Acetylation Obstructs ATM Activation and Promotes Ionizing Radiation Sensitivity in Normal Stem Cells. 2016 [cited 2022 May 23]; Available from: http://dx.doi.org/10.1016/j.stemcr.2016.11.004

105. Rea S, Eisenhaber F, O'Carroll D, Strahl BD, Sun ZW, Schmid M, et al. Regulation of chromatin structure by site-specific histone H3 methyltransferases. Nature. 2000;406:593–9.

106. Matsui T, Leung D, Miyashita H, Maksakova IA, Miyachi H, Kimura H, et al. Proviral silencing in embryonic stem cells requires the histone methyltransferase ESET. Nature. 2010;464:927–31.

107. Montavon T, Shukeir N, Erikson G, Engist B, Onishi-Seebacher M, Ryan D, et al. Complete loss of H3K9 methylation dissolves mouse heterochromatin organization. Nat Commun 2021 121 [Internet]. 2021 [cited 2022 May 23];12:1–16. Available from: https://www.nature.com/articles/s41467-021-24532-8

108. Liakos A, Konstantopoulos D, Lavigne MD, Fousteri M. Continuous transcription initiation guarantees robust repair of all transcribed genes and regulatory regions. Nat Commun 2020 111 [Internet]. 2020 [cited 2022 May 23];11:1–16. Available from: https://www.nature.com/articles/s41467-020-14566-9

109. Bunch H. Role of genome guardian proteins in transcriptional elongation. FEBS Lett [Internet]. 2016 [cited 2022 May 23];590:1064–75. Available from: https://onlinelibrary.wiley.com/doi/full/10.1002/1873-3468.12152

110. Lans H, Hoeijmakers JHJ, Vermeulen W, Marteijn JA. The DNA damage response to transcription stress. Nat Rev Mol Cell Biol 2019 2012 [Internet]. 2019 [cited 2022 May 23];20:766–84. Available from: https://www.nature.com/articles/s41580-019-0169-4

111. Gudmundsdottir B, Gudmundsson KO, Klarmann KD, Singh SK, Sun L, Singh S, et al. POGZ Is Required for Silencing Mouse Embryonic beta-like Hemoglobin

and Human Fetal Hemoglobin Expression. Cell Rep [Internet]. 2018/06/14. 2018;23:3236–48. Available from: https://www.ncbi.nlm.nih.gov/pubmed/29898395

112. Suliman-Lavie R, Title B, Cohen Y, Hamada N, Tal M, Tal N, et al. Pogz deficiency leads to transcription dysregulation and impaired cerebellar activity underlying autism-like behavior in mice. Nat Commun [Internet]. 2020/11/19. 2020;11:5836. Available from: https://www.ncbi.nlm.nih.gov/pubmed/33203851

113. Palomera-Sanchez Z, Zurita M. Open, repair and close again: chromatin dynamics and the response to UV-induced DNA damage. DNA Repair [Internet]. 2010/12/07. 2011;10:119–25. Available from: https://www.ncbi.nlm.nih.gov/pubmed/21130713

114. Bartova E, Malyskova B, Komurkova D, Legartova S, Suchankova J, Krejci J, et al. Function of heterochromatin protein 1 during DNA repair. Protoplasma [Internet]. 2017/02/27. 2017;254:1233–40. Available from: https://www.ncbi.nlm.nih.gov/pubmed/28236007

115. Goodarzi AA, Jeggo P, Lobrich M. The influence of heterochromatin on DNA double-strand break repair: getting the strong, silent type to relax. DNA Repair (Amst). 2010;9:1273–82.

116. Bosch-Presegue L, Raurell-Vila H, Thackray JK, Gonzalez J, Casal C, Kane-Goldsmith N, et al. Mammalian HP1 Isoforms Have Specific Roles in Heterochromatin Structure and Organization. Cell Rep [Internet]. 2017/11/23. 2017;21:2048–57. Available from: https://www.ncbi.nlm.nih.gov/pubmed/29166597

117. Zeng W, Ball Jr. AR, Yokomori K. HP1: heterochromatin binding proteins working the genome. Epigenetics [Internet]. 2010/04/28. 2010;5:287–92. Available from: https://www.ncbi.nlm.nih.gov/pubmed/20421743

118. Kalousi A, Hoffbeck AS, Selemenakis PN, Pinder J, Savage KI, Khanna KK, et al. The nuclear oncogene SET controls DNA repair by KAP1 and HP1 retention to

chromatin. Cell Rep [Internet]. 2015 [cited 2022 Apr 16];11:149–63. Available from: http://www.cell.com/article/S2211124715002570/fulltext

119. Baldeyron C, Soria G, Roche D, Cook AJ, Almouzni G. HP1alpha recruitment to DNA damage by p150CAF-1 promotes homologous recombination repair. J Cell Biol [Internet]. 2011/04/06. 2011;193:81–95. Available from: https://www.ncbi.nlm.nih.gov/pubmed/21464229

120. Ayoub N, Jeyasekharan AD, Venkitaraman AR. Mobilization and recruitment of HP1β: A bimodal response to DNA breakage. http://dx.doi.org/104161/cc8189486 [Internet]. 2009 [cited 2022 Apr 16];8:2946–51. Available from: https://www.tandfonline.com/doi/abs/10.4161/cc.8.18.9486

121. Ayrapetov MK, Gursoy-Yuzugullu O, Xu C, Xu Y, Price BD. DNA double-strand breaks promote methylation of histone H3 on lysine 9 and transient formation of repressive chromatin. Proc Natl Acad Sci U S A [Internet]. 2014/06/14. 2014;111:9169–74. Available from: https://www.ncbi.nlm.nih.gov/pubmed/24927542

122. Goodarzi AA, Noon AT, Deckbar D, Ziv Y, Shiloh Y, Lobrich M, et al. ATM signaling facilitates repair of DNA double-strand breaks associated with heterochromatin. Mol Cell [Internet]. 2008/07/29. 2008;31:167–77. Available from: https://www.ncbi.nlm.nih.gov/pubmed/18657500

123. White D, Rafalska-Metcalf IU, Ivanov A V, Corsinotti A, Peng H, Lee SC, et al. The ATM substrate KAP1 controls DNA repair in heterochromatin: regulation by HP1 proteins and serine 473/824 phosphorylation. Mol Cancer Res [Internet]. 2011/12/30. 2012;10:401–14. Available from: https://www.ncbi.nlm.nih.gov/pubmed/22205726

124. Jacquet K, Fradet-Turcotte A, Avvakumov N, Lambert JP, Roques C, Pandita RK, et al. The TIP60 Complex Regulates Bivalent Chromatin Recognition by 53BP1 through Direct H4K20me Binding and H2AK15 Acetylation. Mol Cell [Internet]. 2016/05/08. 2016;62:409–21. Available from: https://www.ncbi.nlm.nih.gov/pubmed/27153538

125. Sun Y, Jiang X, Chen S, Fernandes N, Price BD. A role for the Tip60 histone acetyltransferase in the acetylation and activation of ATM. Proc Natl Acad Sci U S A. 2005;102:13182–7.

126. Sun Y, Jiang X, Price BD. Tip60: Connecting chromatin to DNA damage signaling. Cell Cycle [Internet]. 2010 [cited 2022 May 23];9:930. Available from: /pmc/articles/PMC2901859/

127. Luijsterburg MS, Dinant C, Lans H, Stap J, Wiernasz E, Lagerwerf S, et al. Heterochromatin protein 1 is recruited to various types of DNA damage. J Cell Biol [Internet]. 2009/05/20. 2009;185:577–86. Available from: https://www.ncbi.nlm.nih.gov/pubmed/19451271

128. Ayoub N, Jeyasekharan AD, Bernal JA, Venkitaraman AR. HP1-β mobilization promotes chromatin changes that initiate the DNA damage response. Nature. 2008;453:682–6.

129. Bolderson E, Savage KI, Mahen R, Pisupati V, Graham ME, Richard DJ, et al. Krüppel-associated box (KRAB)-associated co-repressor (KAP-1) Ser-473 phosphorylation regulates heterochromatin protein 1β (HP1-β) mobilization and DNA repair in heterochromatin. J Biol Chem [Internet]. 2012 [cited 2022 Apr 16];287:28122–31. Available from: http://www.jbc.org/article/S0021925820478342/fulltext

130. Young LC, McDonald DW, Hendzel MJ. Kdm4b histone demethylase is a DNA damage response protein and confers a survival advantage following gamma-irradiation. J Biol Chem [Internet]. 2013/06/08. 2013;288:21376–88. Available from: https://www.ncbi.nlm.nih.gov/pubmed/23744078

131. Nakamura K, Saredi G, Becker JR, Foster BM, Nguyen N V, Beyer TE, et al. H4K20me0 recognition by BRCA1-BARD1 directs homologous recombination to sister chromatids. Nat Cell Biol [Internet]. 2019/02/26. 2019;21:311–8. Available from: https://www.ncbi.nlm.nih.gov/pubmed/30804502

132. Lee YH, Kuo CY, Stark JM, Shih HM, Ann DK. HP1 promotes tumor suppressor

BRCA1 functions during the DNA damage response. Nucleic Acids Res [Internet]. 2013/04/17. 2013;41:5784–98. Available from: https://www.ncbi.nlm.nih.gov/pubmed/23589625

133. Wu W, Nishikawa H, Fukuda T, Vittal V, Asano M, Miyoshi Y, et al. Interaction of BARD1 and HP1 Is Required for BRCA1 Retention at Sites of DNA Damage. Cancer Res [Internet]. 2015/01/31. 2015;75:1311–21. Available from: https://www.ncbi.nlm.nih.gov/pubmed/25634209

134. Harding SM, Benci JL, Irianto J, Discher DE, Minn AJ, Greenberg RA. Mitotic progression following DNA damage enables pattern recognition within micronuclei. Nature [Internet]. 2017/08/02. 2017;548:466–70. Available from: https://www.ncbi.nlm.nih.gov/pubmed/28759889

135. Sabatinos SA, Ranatunga NS, Yuan J-P, Green MD, Forsburg SL. Replication stress in early S phase generates apparent micronuclei and chromosome rearrangement in fission yeast. Solomon MJ, editor. Mol Biol Cell [Internet]. 2015 [cited 2019 Jun 3];26:3439–50. Available from: http://www.ncbi.nlm.nih.gov/pubmed/26246602

136. cGAS Conducts Micronuclei DNA Surveillance. Trends Cell Biol [Internet]. 2017 [cited 2017 Nov 11];27:697–8. Available from: https://www.sciencedirect.com/science/article/pii/S0962892417301447

137. Chen J, Silver DP, Walpita D, Cantor SB, Gazdar AF, Tomlinson G, et al. Stable interaction between the products of the BRCA1 and BRCA2 tumor suppressor genes in mitotic and meiotic cells. Mol Cell. 1998;2:317–28.

138. Van Der Groep P, Van Der Wall E, Van Diest PJ. Pathology of hereditary breast cancer. Cell Oncol 2011 342 [Internet]. 2011 [cited 2022 May 23];34:71–88. Available from: https://link.springer.com/article/10.1007/s13402-011-0010-3

139. Petrucelli N, Daly MB, Pal T. BRCA1- and BRCA2-Associated Hereditary Breast and Ovarian Cancer. GeneReviews® [Internet]. 2022 [cited 2022 May 23]; Available from: https://www.ncbi.nlm.nih.gov/books/NBK1247/

140. Saksouk N, Hajdari S, Perez Y, Pratlong M, Barrachina C, Graber C, et al. The mouse HP1 proteins are essential for preventing liver tumorigenesis. Oncogene 2020 3913 [Internet]. 2020 [cited 2022 May 23];39:2676–91. Available from: https://www.nature.com/articles/s41388-020-1177-8

141. Koschmann C, Nunez FJ, Mendez F, Brosnan-Cashman JA, Meeker AK, Lowenstein PR, et al. Mutated chromatin regulatory factors as tumor drivers in cancer. Cancer Res. 2017;77:227–33.

142. Dialynas GK, Vitalini MW, Wallrath LL. Linking Heterochromatin Protein 1 (HP1) to cancer progression. Mutat Res [Internet]. 2008 [cited 2022 May 23];647:13. Available from: /pmc/articles/PMC2637788/

143. Watanabe H, Soejima K, Yasuda H, Kawada I, Nakachi I, Yoda S, et al. Deregulation of histone lysine methyltransferases contributes to oncogenic transformation of human bronchoepithelial cells. Cancer Cell Int [Internet]. 2008 [cited 2022 May 23];8:1–12. Available from: https://cancerci.biomedcentral.com/articles/10.1186/1475-2867-8-15

144. Soejima K, Fang W, Rollins BJ. DNA methyltransferase 3b contributes to oncogenic transformation induced by SV40T antigen and activated Ras. Oncogene. 2003;22:4723–33.

145. Addison JB, Koontz C, Fugett JH, Creighton CJ, Chen D, Farrugia MK, et al. KAP1 promotes proliferation and metastatic progression of breast cancer cells. Cancer Res [Internet]. 2015 [cited 2022 May 23];75:344–55. Available from: https://pubmed.ncbi.nlm.nih.gov/25421577/

146. Breast cancer statistics | Canadian Cancer Society [Internet]. [cited 2022 May 23]. Available from: https://cancer.ca/en/cancer-information/cancer-types/breast/statistics

147. Seung SJ, Traore AN, Pourmirza B, Fathers KE, Coombes M, Jerzak KJ. A population-based analysis of breast cancer incidence and survival by subtype in Ontario women. Curr Oncol [Internet]. 2020 [cited 2022 May 19];27:e191.

Available from: /pmc/articles/PMC7253754/

148. Akers RM. Functional Development of the Mammary Gland. Lact Mammary Gland. 2016;66–87.

149. Fu NY, Nolan E, Lindeman GJ, Visvader JE. Stem cells and the differentiation hierarchy in mammary gland development. Physiol Rev [Internet]. 2020 [cited 2022 Sep 17];100:489–523. Available from: https://journals.physiology.org/doi/10.1152/physrev.00040.2018

150. Fu NY, Nolan E, Lindeman GJ, Visvader JE. Stem cells and the differentiation hierarchy in mammary gland development. Physiol Rev [Internet]. 2020 [cited 2022 May 23];100:489–523. Available from: https://journals.physiology.org/doi/full/10.1152/physrev.00040.2018

151. Hassiotou F, Geddes D. Anatomy of the human mammary gland: Current status of knowledge. Clin Anat [Internet]. 2013 [cited 2022 May 23];26:29–48. Available from: https://onlinelibrary.wiley.com/doi/full/10.1002/ca.22165

152. Visvader JE. Keeping abreast of the mammary epithelial hierarchy and breast tumorigenesis. Genes Dev [Internet]. 2009 [cited 2022 May 23];23:2563–77. Available from: http://genesdev.cshlp.org/content/23/22/2563.full

153. Sau A, Lau R, Cabrita MA, Nolan E, Crooks PA, Visvader JE, et al. Persistent Activation of NF-κB in BRCA1-Deficient Mammary Progenitors Drives Aberrant Proliferation and Accumulation of DNA Damage. Cell Stem Cell. 2016;19:52–65.

154. Atabai K, Sheppard D, Werb Z. Roles of the innate immune system in mammary gland remodeling during involution. J Mammary Gland Biol Neoplasia. 2007;12:37–45.

155. Monks J, Geske FJ, Lehman L, Fadok VA. Do inflammatory cells participate in mammary gland involution? J Mammary Gland Biol Neoplasia [Internet]. 2002 [cited 2022 May 23];7:163–76. Available from: https://pubmed.ncbi.nlm.nih.gov/12463737/

156. Stein T, Morris JS, Davies CR, Weber-Hall SJ, Duffy MA, Heath VJ, et al. Involution of the mouse mammary gland is associated with an immune cascade and an acute-phase response, involving LBP, CD14 and STAT3. Breast Cancer Res [Internet]. 2004 [cited 2022 May 23];6:1–17. Available from: https://breast-cancer-research.biomedcentral.com/articles/10.1186/bcr753

157. Perou CM, Sørile T, Eisen MB, Van De Rijn M, Jeffrey SS, Ress CA, et al. Molecular portraits of human breast tumours. Nature. 2000;406:747–52.

158. Zaha DC. Significance of immunohistochemistry in breast cancer. World J Clin Oncol. 2014;5:382–92.

159. Gomes Do Nascimento R, Otoni KM. Histological and molecular classification of breast cancer: what do we know? Mastology. 2020;30:20200024.

160. Harbeck N, Penault-Llorca F, Cortes J, Gnant M, Houssami N, Poortmans P, et al. Breast cancer. Nat Rev Dis Prim 2019 51 [Internet]. 2019 [cited 2022 May 23];5:1–31. Available from: https://www.nature.com/articles/s41572-019-0111-2

161. Burstein MD, Tsimelzon A, Poage GM, Covington KR, Contreras A, Fuqua SAW, et al. Comprehensive Genomic Analysis Identifies Novel Subtypes and Targets of Triple-negative Breast Cancer. Clin Cancer Res [Internet]. 2015 [cited 2022 May 23];21:1688. Available from: /pmc/articles/PMC4362882/

162. Mehta GA, Khanna P, Gatza ML. Emerging role of SOX proteins in breast cancer development and maintenance. J Mammary Gland Biol Neoplasia [Internet]. 2019 [cited 2022 May 23];24:213. Available from: /pmc/articles/PMC6790170/

163. Tischkowitz MD, Foulkes WD. The basal phenotype of BRCA1-related breast cancer: Past, present and future. Cell Cycle. 2006;5:963–7.

164. Molyneux G, Geyer FC, Magnay FA, McCarthy A, Kendrick H, Natrajan R, et al. BRCA1 basal-like breast cancers originate from luminal epithelial progenitors and not from basal stem cells. Cell Stem Cell [Internet]. 2010 [cited 2022 May 23];7:403–17. Available from: https://pubmed.ncbi.nlm.nih.gov/20804975/

165. Kakarala M, Wicha MS. Implications of the Cancer Stem-Cell Hypothesis for Breast Cancer Prevention and Therapy. J Clin Oncol [Internet]. 2008 [cited 2022 May 23];26:2813. Available from: /pmc/articles/PMC2789399/

166. Patel HK, Bihani T. Selective estrogen receptor modulators (SERMs) and selective estrogen receptor degraders (SERDs) in cancer treatment. Pharmacol Ther. 2018;186:1–24.

167. Choong GM, Cullen GD, O'Sullivan CC. Evolving standards of care and new challenges in the management of HER2-positive breast cancer. CA Cancer J Clin [Internet]. 2020 [cited 2022 May 23];70:355–74. Available from: https://onlinelibrary.wiley.com/doi/full/10.3322/caac.21634

168. Bianchini G, De Angelis C, Licata L, Gianni L. Treatment landscape of triple-negative breast cancer — expanded options, evolving needs. Nat Rev Clin Oncol 2021 192 [Internet]. 2021 [cited 2022 May 23];19:91–113. Available from: https://www.nature.com/articles/s41571-021-00565-2

169. Wahba HA, El-Hadaad HA. Current approaches in treatment of triple-negative breast cancer. Cancer Biol Med [Internet]. 2015 [cited 2022 May 23];12:106. Available from: /pmc/articles/PMC4493381/

170. Vinayak S, Tolaney SM, Schwartzberg L, Mita M, McCann G, Tan AR, et al. Open-label Clinical Trial of Niraparib Combined With Pembrolizumab for Treatment of Advanced or Metastatic Triple-Negative Breast Cancer. JAMA Oncol [Internet]. 2019 [cited 2022 Sep 17];5:1132–40. Available from: https://jamanetwork.com/journals/jamaoncology/fullarticle/2735888

171. Lord CJ, Ashworth A. BRCAness revisited. Nat Rev Cancer 2016 162 [Internet]. 2016 [cited 2022 May 23];16:110–20. Available from: https://www.nature.com/articles/nrc.2015.21

172. Wang J, Zhang Y, Yuan L, Ren L, Zhang Y, Qi X. Comparative efficacy, safety, and acceptability of single-agent poly (ADP-ribose) polymerase (PARP) inhibitors in BRCA-mutated HER2-negative metastatic or advanced breast cancer: a

network meta-analysis. Aging (Albany NY) [Internet]. 2021 [cited 2022 May 23];13:450. Available from: /pmc/articles/PMC7834995/

173. Han Y, Yu X, Li S, Tian Y, Liu C. New Perspectives for Resistance to PARP Inhibitors in Triple-Negative Breast Cancer. Front Oncol [Internet]. 2020 [cited 2022 May 19];10. Available from: /pmc/articles/PMC7724080/

174. Farmer H, McCabe N, Lord CJ, Tutt AN, Johnson DA, Richardson TB, et al. Targeting the DNA repair defect in BRCA mutant cells as a therapeutic strategy. Nature [Internet]. 2005/04/15. 2005;434:917–21. Available from: https://www.ncbi.nlm.nih.gov/pubmed/15829967

175. Rolny C, Capparuccia L, Casazza A, Mazzone M, Vallario A, Cignetti A, et al. The tumor suppressor semaphorin 3B triggers a prometastatic program mediated by interleukin 8 and the tumor microenvironment. J Exp Med [Internet]. 2008 [cited 2022 May 24];205:1155. Available from: /pmc/articles/PMC2373847/

176. Gupta R, Somyajit K, Narita T, Maskey E, Stanlie A, Kremer M, et al. DNA Repair Network Analysis Reveals Shieldin as a Key Regulator of NHEJ and PARP Inhibitor Sensitivity. Cell [Internet]. 2018 [cited 2022 May 23];173:972. Available from: /pmc/articles/PMC8108093/

177. Rose M, Burgess JT, O'Byrne K, Richard DJ, Bolderson E. PARP Inhibitors: Clinical Relevance, Mechanisms of Action and Tumor Resistance. Front Cell Dev Biol [Internet]. 2020 [cited 2022 May 23];8. Available from: /pmc/articles/PMC7509090/

178. Koh SB. Signaling dynamics of DNA damage response invoked by combination therapy are dose-dependent. J Biol Chem [Internet]. 2019/02/10. 2019;294:2191. Available from: https://www.ncbi.nlm.nih.gov/pubmed/30737318

179. Wang R, Zhu Y, Liu X, Liao X, He J, Niu L. The Clinicopathological features and survival outcomes of patients with different metastatic sites in stage IV breast cancer. BMC Cancer [Internet]. 2019 [cited 2022 May 24];19:1–12. Available from: https://bmccancer.biomedcentral.com/articles/10.1186/s12885-019-6311-z

180. Kennecke H, Yerushalmi R, Woods R, Cheang MCU, Voduc D, Speers CH, et al. Metastatic behavior of breast Cancer subtypes. J Clin Oncol. 2010;28:3271–7.

181. GP Gupta JM. Cancer metastasis: building a framework. Cell. 2006;127:679–95.

182. Riggio AI, Varley KE, Welm AL. The lingering mysteries of metastatic recurrence in breast cancer. Br J Cancer 2020 1241 [Internet]. 2020 [cited 2022 May 24];124:13–26. Available from: https://www.nature.com/articles/s41416-020-01161-4

183. CL Chaffer RW. A perspective on cancer cell metastasis. Science (80-). 2011;331:1559–64.

184. Nakaya Y, Sheng G. EMT in developmental morphogenesis. Cancer Lett. 2013;341:9–15.

185. Kalluri R, Weinberg RA. The basics of epithelial-mesenchymal transition. J Clin Invest [Internet]. 2009 [cited 2022 May 24];119:1420. Available from: /pmc/articles/PMC2689101/

186. Anderson JM, Van Itallie CM. Physiology and function of the tight junction. Cold Spring Harb Perspect Biol. 2009;1.

187. Al-Sadi R, Khatib K, Guo S, Ye D, Youssef M, Ma T. Occludin regulates macromolecule flux across the intestinal epithelial tight junction barrier. Am J Physiol - Gastrointest Liver Physiol. 2011;300.

188. Bhat AA, Uppada S, Achkar IW, Hashem S, Yadav SK, Shanmugakonar M, et al. Tight junction proteins and signaling pathways in cancer and inflammation: A functional crosstalk. Front Physiol. 2019;10:1942.

189. Klezovitch O, Vasioukhin V. Cadherin signaling: keeping cells in touch. F1000Research [Internet]. 2015 [cited 2022 May 24];4. Available from: /pmc/articles/PMC4544379/

190. Tester AM, Ruangpanit N, Anderson RL, Thompson EW. MMP-9 secretion and MMP-2 activation distinguish invasive and metastatic sublines of a mouse

mammary carcinoma system showing epithelial-mesenchymal transition traits. Clin Exp Metastasis [Internet]. 2000 [cited 2022 May 24];18:553–60. Available from: https://pubmed.ncbi.nlm.nih.gov/11688960/

191. Nawshad A, LaGamba D, Polad A, Hay ED. Transforming growth factor-beta signaling during epithelial-mesenchymal transformation: implications for embryogenesis and tumor metastasis. Cells Tissues Organs. 2005;179:11–23.

192. Lee J, Choi JH, Joo CK. TGF-β1 regulates cell fate during epithelial–mesenchymal transition by upregulating survivin. Cell Death Dis 2013 47 [Internet]. 2013 [cited 2022 May 24];4:e714–e714. Available from: https://www.nature.com/articles/cddis2013244

193. Jolly MK, Ware KE, Gilja S, Somarelli JA, Levine H. EMT and MET: necessary or permissive for metastasis? Mol Oncol [Internet]. 2017 [cited 2022 May 24];11:755. Available from: /pmc/articles/PMC5496498/

194. Li R, Liang J, Ni S, Zhou T, Qing X, Li H, et al. A mesenchymal-to-epithelial transition initiates and is required for the nuclear reprogramming of mouse fibroblasts. Cell Stem Cell. 2010;7:51–63.

195. Peinado H, Olmeda D, Cano A. Snail, Zeb and bHLH factors in tumour progression: an alliance against the epithelial phenotype? Nat Rev Cancer 2007 76 [Internet]. 2007 [cited 2022 May 24];7:415–28. Available from: https://www.nature.com/articles/nrc2131

196. Thiery JP, Sleeman JP. Complex networks orchestrate epithelial-mesenchymal transitions. Nat Rev Mol Cell Biol. 2006;7:131–42.

197. Huber MA, Kraut N, Beug H. Molecular requirements for epithelial-mesenchymal transition during tumor progression. Curr Opin Cell Biol. 2005;17:548–58.

198. Yang J, Mani SA, Donaher JL, Ramaswamy S, Itzykson RA, Come C, et al. Twist, a master regulator of morphogenesis, plays an essential role in tumor metastasis. Cell. 2004;117:927–39.

199. Barberà MJ, Puig I, Domínguez D, Julien-Grille S, Guaita-Esteruelas S, Peiró S, et al. Regulation of Snail transcription during epithelial to mesenchymal transition of tumor cells. Oncogene. 2004;23:7345–54.

200. Bolós V, Peinado H, Pérez-Moreno MA, Fraga MF, Esteller M, Cano A. The transcription factor Slug represses E-cadherin expression and induces epithelial to mesenchymal transitions: a comparison with Snail and E47 repressors. J Cell Sci. 2003;116:499–511.

201. Comijn J, Berx G, Vermassen P, Verschueren K, Van Grunsven L, Bruyneel E, et al. The two-handed E box binding zinc finger protein SIP1 downregulates E-cadherin and induces invasion. Mol Cell. 2001;7:1267–78.

202. Batlle E, Sancho E, Francí C, Domínguez D, Monfar M, Baulida J, et al. The transcription factor snail is a repressor of E-cadherin gene expression in epithelial tumour cells. Nat Cell Biol. 2000;2:84–9.

203. Cano A, Pérez-Moreno MA, Rodrigo I, Locascio A, Blanco MJ, Del Barrio MG, et al. The transcription factor snail controls epithelial-mesenchymal transitions by repressing E-cadherin expression. Nat Cell Biol. 2000;2:76–83.

204. Gutarra S, Lex Frias A`, Beltran M, Peiró S, García De Herreros A. Functional Cooperation between Snail1 and Twist in the Regulation of ZEB1 Expression during Epithelial to Mesenchymal Transition * □ S Natà lia Dave ‡1 , Sandra Guaita-Esteruelas ‡2. 2011 [cited 2022 May 24]; Available from: http://www.jbc.org

205. Taube JH, Herschkowitz JI, Komurov K, Zhou AY, Gupta S, Yang J, et al. Core epithelial-to-mesenchymal transition interactome gene-expression signature is associated with claudin-low and metaplastic breast cancer subtypes. Proc Natl Acad Sci U S A. 2010;107:15449–54.

206. Aiello NM, Kang Y. Context-dependent EMT programs in cancer metastasis. J Exp Med. 2019;216:1016–26.

207. Peinado H, Olmeda D, Cano A. Snail, Zeb and bHLH factors in tumour

progression: an alliance against the epithelial phenotype? Nat Rev Cancer 2007 76 [Internet]. 2007 [cited 2022 May 19];7:415–28. Available from: https://www.nature.com/articles/nrc2131

208. Sayan AE, Griffiths TR, Pal R, Browne GJ, Ruddick A, Edwards R, et al. SIP1 protein protects cells from DNA damage-induced apoptosis and has independent prognostic value in bladder cancer. [cited 2022 May 24]; Available from: www.pnas.orgcgidoi10.1073pnas.0902042106

209. Scheibner K, Schirge S, Burtscher I, Büttner M, Sterr M, Yang D, et al. Epithelial cell plasticity drives endoderm formation during gastrulation. Nat Cell Biol 2021 237 [Internet]. 2021 [cited 2022 May 24];23:692–703. Available from: https://www.nature.com/articles/s41556-021-00694-x

210. Jong IY, Li XY, Ota I, Fearon ER, Weiss SJ. Wnt-dependent Regulation of the E-cadherin Repressor Snail. J Biol Chem. 2005;280:11740–8.

211. Marconi GD, Fonticoli L, Rajan TS, Pierdomenico SD, Trubiani O, Pizzicannella J, et al. Epithelial-Mesenchymal Transition (EMT): The Type-2 EMT in Wound Healing, Tissue Regeneration and Organ Fibrosis. Cells [Internet]. 2021 [cited 2022 May 24];10. Available from: https://pubmed.ncbi.nlm.nih.gov/34201858/

212. Acloque H, Adams MS, Fishwick K, Bronner-Fraser M, Nieto MA. Epithelial-mesenchymal transitions: the importance of changing cell state in development and disease. J Clin Invest [Internet]. 2009 [cited 2022 May 24];119:1438. Available from: /pmc/articles/PMC2689100/

213. Lüönd F, Sugiyama N, Bill R, Bornes L, Hager C, Tang F, et al. Distinct contributions of partial and full EMT to breast cancer malignancy. Dev Cell. 2021;56:3203-3221.e11.

214. Gotzmann J, Mikula M, Eger A, Schulte-Hermann R, Foisner R, Beug H, et al. Molecular aspects of epithelial cell plasticity: implications for local tumor invasion and metastasis. Mutat Res. 2004;566:9–20.

215. Moreno-Bueno G, Portillo F, Cano A. Transcriptional regulation of cell polarity in

EMT and cancer. Oncogene. 2008;27:6958–69.

216. Aiello NM, Maddipati R, Norgard RJ, Balli D, Li J, Yuan S, et al. EMT Subtype Influences Epithelial Plasticity and Mode of Cell Migration. Dev Cell. 2018;45:681-695.e4.

217. Massagué J, Wotton D. Transcriptional control by the TGF-β/Smad signaling system. EMBO J [Internet]. 2000 [cited 2022 May 24];19:1745–54. Available from: https://onlinelibrary.wiley.com/doi/full/10.1093/emboj/19.8.1745

218. Massagué J. How cells read TGF-β signals. Nat Rev Mol Cell Biol. 2000;1:169–78.

219. Forrester E, Chytil A, Bierie B, Aakre M, Gorska AE, Sharif-Afshar AR, et al. Effect of conditional knockout of the type II TGF-β receptor gene in mammary epithelia on mammary gland development and polyomavirus middle T antigen induced tumor formation and metastasis. Cancer Res. 2005;65:2296–302.

220. Forrester E, Chytil A, Bierie B, Aakre M, Gorska AE, Sharif-Afshar AR, et al. Effect of conditional knockout of the type II TGF-beta receptor gene in mammary epithelia on mammary gland development and polyomavirus middle T antigen induced tumor formation and metastasis. Cancer Res [Internet]. 2005 [cited 2022 May 24];65:2296–302. Available from: https://pubmed.ncbi.nlm.nih.gov/15781643/

221. Ingman W V., Robertson SA. Mammary Gland Development in Transforming Growth Factor Beta1 Null Mutant Mice: Systemic and Epithelial Effects. Biol Reprod [Internet]. 2008 [cited 2022 May 24];79:711–7. Available from: https://academic.oup.com/biolreprod/article/79/4/711/2557618

222. Fata JE, Chaudhary V, Khokha R. Cellular turnover in the mammary gland is correlated with systemic levels of progesterone and not 17β-estradiol during the estrous cycle. Biol Reprod. 2001;65:680–8.

223. Kahata K, Maturi V, Moustakas A. TGF-β Family Signaling in Ductal Differentiation and Branching Morphogenesis. Cold Spring Harb Perspect Biol [Internet]. 2018 [cited 2022 May 24];10:a031997. Available from:

http://cshperspectives.cshlp.org/content/10/3/a031997.full

224. Li M, Lewis B, Capuco A V., Laucirica R, Furth PA. WAP-TAg transgenic mice and the study of dysregulated cell survival, proliferation, and mutation during breast carcinogenesis. Oncogene. 2000;19:1010–9.

225. Moses H, Barcellos-Hoff MH. TGF-β Biology in Mammary Development and Breast Cancer. Cold Spring Harb Perspect Biol [Internet]. 2011 [cited 2022 May 24];3:1–14. Available from: /pmc/articles/PMC3003461/

226. Radaev S, Zou Z, Huang T, Lafer EM, Hinck AP, Sun PD. Ternary complex of transforming growth factor-β1 reveals isoform-specific ligand recognition and receptor recruitment in the superfamily. J Biol Chem. 2010;285:14806–14.

227. Qian SW, Burmester JK, Tsang MLS, Weatherbee JA, Hinck AP, Ohlsen DJ, et al. Binding affinity of transforming growth factor-beta for its type II receptor is determined by the C-terminal region of the molecule. J Biol Chem [Internet]. 1996 [cited 2022 May 24];271:30656–62. Available from: https://pubmed.ncbi.nlm.nih.gov/8940041/

228. Robertson IB, Rifkin DB. Regulation of the Bioavailability of TGF-β and TGF-β-Related Proteins. Cold Spring Harb Perspect Biol [Internet]. 2016 [cited 2022 May 24];8:a021907. Available from: http://cshperspectives.cshlp.org/content/8/6/a021907.full

229. Aluwihare P, Mu Z, Zhao Z, Yu D, Weinreb PH, Horan GS, et al. Mice that lack activity of αvβ6- and αvβ8-integrins reproduce the abnormalities of Tgfb1- and Tgfb3-null mice. J Cell Sci. 2009;122:227–32.

230. Bagarova J, Vonner AJ, Armstrong KA, Börgermann J, Lai CSC, Deng DY, et al. Constitutively Active ALK2 Receptor Mutants Require Type II Receptor Cooperation. Mol Cell Biol. 2013;33:2413–24.

231. Bandyopadhyay B, Han A, Dai J, Fan J, Li Y, Chen M, et al. TβRI/Alk5-independent TβRII signaling to ERK1/2 in human skin cells according to distinct levels of TβRII expression. J Cell Sci. 2011;124:19–24.

232. Heldin CH, Moustakas A. Signaling Receptors for TGF-β Family Members. Cold Spring Harb Perspect Biol [Internet]. 2016 [cited 2022 May 24];8:a022053. Available from: http://cshperspectives.cshlp.org/content/8/8/a022053.full

233. Kawabata M, Inoue H, Hanyu A, Imamura T, Miyazono K. Smad proteins exist as monomers in vivo and undergo homo- and hetero-oligomerization upon activation by serine/threonine kinase receptors. EMBO J. 1998;17:4056–65.

234. Newfeld SJ, Wisotzkey RG. Molecular Evolution of Smad Proteins. Smad Signal Transduct. 2007;15–35.

235. Lönn P, Morén A, Raja E, Dahl M, Moustakas A. Regulating the stability of TGFβ receptors and Smads. Cell Res 2009 191 [Internet]. 2008 [cited 2022 May 24];19:21–35. Available from: https://www.nature.com/articles/cr2008308

236. Shi Z, Zhang K, Chen T, Zhang Y, Du X, Zhao Y, et al. Transcriptional factor ATF3 promotes liver fibrosis via activating hepatic stellate cells. Cell Death Dis 2020 1112 [Internet]. 2020 [cited 2022 May 24];11:1–16. Available from: https://www.nature.com/articles/s41419-020-03271-6

237. Lang C, Dai Y, Wu Z, Yang Q, He S, Zhang X, et al. SMAD3/SP1 complex-mediated constitutive active loop between lncRNA PCAT7 and TGF-β signaling promotes prostate cancer bone metastasis. Mol Oncol [Internet]. 2020 [cited 2022 May 24];14:808–28. Available from: https://pubmed.ncbi.nlm.nih.gov/31925912/

238. Chi X-Z, Yang J-O, Lee K-Y, Ito K, Sakakura C, Li Q-L, et al. RUNX3 suppresses gastric epithelial cell growth by inducing p21(WAF1/Cip1) expression in cooperation with transforming growth factor {beta}-activated SMAD. Mol Cell Biol [Internet]. 2005 [cited 2022 May 24];25:8097–107. Available from: https://pubmed.ncbi.nlm.nih.gov/16135801/

239. Warner BJ, Blain SW, Seoane J, Massagué J. Myc Downregulation by Transforming Growth Factor β Required for Activation of the p15Ink4b G1 Arrest Pathway. Mol Cell Biol [Internet]. 1999 [cited 2022 May 24];19:5913. Available from: /pmc/articles/PMC84444/

240. Wirt SE, Sage J. p107 in the public eye: an Rb understudy and more. Cell Div 2010 51 [Internet]. 2010 [cited 2022 May 24];5:1–13. Available from: https://celldiv.biomedcentral.com/articles/10.1186/1747-1028-5-9

241. Chen CR, Kang Y, Siegel PM, Massagué J. E2F4/5 and p107 as Smad cofactors linking the TGFβ receptor to c-myc repression. Cell. 2002;110:19–32.

242. Kowalik TF. Smad About E2F: TGFβ Repressionof c-Myc via a Smad3/E2F/p107 Complex. Mol Cell. 2002;10:7–8.

243. Wu L, Goodwin EC, Naeger LK, Vigo E, Galaktionov K, Helin K, et al. E2F-Rb complexes assemble and inhibit cdc25A transcription in cervical carcinoma cells following repression of human papillomavirus oncogene expression. Mol Cell Biol [Internet]. 2000 [cited 2022 May 24];20:7059–67. Available from: https://pubmed.ncbi.nlm.nih.gov/10982822/

244. Frederick JP, Liberati NT, Waddell DS, Shi Y, Wang X-F. Transforming Growth Factor β-Mediated Transcriptional Repression of c-myc Is Dependent on Direct Binding of Smad3 to a Novel Repressive Smad Binding Element. Mol Cell Biol [Internet]. 2004 [cited 2022 May 24];24:2546. Available from: /pmc/articles/PMC355825/

245. Thien A, Prentzell MT, Holzwarth B, Kläsener K, Kuper I, Boehlke C, et al. TSC1 Activates TGF-β-Smad2/3 Signaling in Growth Arrest and Epithelial-to-Mesenchymal Transition. Dev Cell. 2015;32:617–30.

246. Das R, Xu S, Nguyen TT, Quan X, Choi SK, Kim SJ, et al. Transforming Growth Factor β1-induced Apoptosis in Podocytes via the Extracellular Signal-regulated Kinase-Mammalian Target of Rapamycin Complex 1-NADPH Oxidase 4 Axis *. J Biol Chem [Internet]. 2015 [cited 2022 May 24];290:30830–42. Available from: http://www.jbc.org/article/S0021925820392851/fulltext

247. Huang J, Dibble CC, Matsuzaki M, Manning BD. The TSC1-TSC2 complex is required for proper activation of mTOR complex 2. Mol Cell Biol [Internet]. 2008 [cited 2022 May 24];28:4104–15. Available from:

https://pubmed.ncbi.nlm.nih.gov/18411301/

248. Yoo J, Ghiassi M, Jirmanova L, Balliet AG, Hoffman B, Fornace AJ, et al. Transforming Growth Factor-β-induced Apoptosis Is Mediated by Smad-dependent Expression of GADD45b through p38 Activation *. J Biol Chem [Internet]. 2003 [cited 2022 Apr 27];278:43001–7. Available from: http://www.jbc.org/article/S0021925820825733/fulltext

249. Ramesh S, Wildey GM, Howe PH. Transforming growth factor β (TGFβ)-induced apoptosis: The rise & fall of Bim. Cell Cycle [Internet]. 2009 [cited 2022 Apr 27];8:11. Available from: /pmc/articles/PMC3191464/

250. Lebman DA, Edmiston JS. The role of TGF-[beta] in growth, differentiation, and maturation of B lymphocytes. Microbes Infect. 1999;1:1297–304.

251. Bakkebø M, Huse K, Hilden VI, Smeland EB, Oksvold MP. TGF-β-induced growth inhibition in B-cell lymphoma correlates with Smad1/5 signalling and constitutively active p38 MAPK. BMC Immunol [Internet]. 2010 [cited 2022 May 24];11:1–10. Available from: https://bmcimmunol.biomedcentral.com/articles/10.1186/1471-2172-11-57

252. Lin Y, Dong C, Zhou BP. Epigenetic Regulation of EMT: The Snail Story. Curr Pharm Des [Internet]. 2014 [cited 2022 May 24];20:1698. Available from: /pmc/articles/PMC4005722/

253. Tam WL, Weinberg RA. The epigenetics of epithelial-mesenchymal plasticity in cancer. Nat Med [Internet]. 2013 [cited 2022 May 24];19:1438. Available from: /pmc/articles/PMC4190672/

254. Gomes AP, Ilter D, Low V, Rosenzweig A, Shen ZJ, Schild T, et al. Dynamic incorporation of histone H3 variants into chromatin is essential for acquisition of aggressive traits and metastatic colonization. Cancer Cell [Internet]. 2019 [cited 2022 May 24];36:402. Available from: /pmc/articles/PMC6801101/

255. Zhang Y, Alexander PB, Wang XF. TGF-β Family Signaling in the Control of Cell Proliferation and Survival. Cold Spring Harb Perspect Biol [Internet]. 2017 [cited

2022 May 24];9. Available from: /pmc/articles/PMC5378054/

256. Baude A, Aaes TL, Zhai B, Al-Nakouzi N, Oo HZ, Daugaard M, et al. Hepatoma-derived growth factor-related protein 2 promotes DNA repair by homologous recombination. Nucleic Acids Res. 2015;44:2214–26.

257. Nozawa RS, Nagao K, Masuda HT, Iwasaki O, Hirota T, Nozaki N, et al. Human POGZ modulates dissociation of HP1α from mitotic chromosome arms through Aurora B activation. Nat Cell Biol 2010 127 [Internet]. 2010 [cited 2022 May 24];12:719–27. Available from: https://www.nature.com/articles/ncb2075

258. Suliman-Lavie R, Title B, Cohen Y, Hamada N, Tal M, Tal N, et al. Pogz deficiency leads to transcription dysregulation and impaired cerebellar activity underlying autism-like behavior in mice. Nat Commun 2020 111 [Internet]. 2020 [cited 2022 Jan 4];11:1–15. Available from: https://www.nature.com/articles/s41467-020-19577-0

259. Vermeulen M, Eberl HC, Matarese F, Marks H, Denissov S, Butter F, et al. Quantitative Interaction Proteomics and Genome-wide Profiling of Epigenetic Histone Marks and Their Readers. Cell. 2010;142:967–80.

260. Ferretti A, Barresi S, Trivisano M, Ciolfi A, Dentici ML, Radio FC, et al. POGZ-related epilepsy: Case report and review of the literature. Am J Med Genet A [Internet]. 2019/05/29. 2019;179:1631–6. Available from: https://www.ncbi.nlm.nih.gov/pubmed/31136090

261. Matsumura K, Seiriki K, Okada S, Nagase M, Ayabe S, Yamada I, et al. Pathogenic POGZ mutation causes impaired cortical development and reversible autism-like phenotypes. Nat Commun 2020 111 [Internet]. 2020 [cited 2022 Jan 4];11:1–16. Available from: https://www.nature.com/articles/s41467-020-14697-z

262. Fujita H, Ikeda M, Ui A, Ouchi Y, Mikami Y, Kanno S, et al. CHAMP1-POGZ counteracts the inhibitory effect of 53BP1 on homologous recombination and affects PARP inhibitor resistance. Oncogene [Internet]. 2022 [cited 2022 May 24];41:2706–18. Available from: https://pubmed.ncbi.nlm.nih.gov/35393543/

263. Li F, Sarangi P, Feng H, Moreau L, Nguyen H, Clairmont C, et al. REV7/FANCV Binds to CHAMP1 and Promotes Homologous Recombination Repair. bioRxiv [Internet]. 2021 [cited 2022 May 24];2021.10.04.463067. Available from: https://www.biorxiv.org/content/10.1101/2021.10.04.463067v1

264. Daugaard M, Baude A, Fugger K, Povlsen LK, Beck H, Sørensen CS, et al. LEDGF (p75) promotes DNA-end resection and homologous recombination. Nat Struct Mol Biol. 2012;19:803–10.

265. Soria G, Almouzni G. Differential contribution of HP1 proteins to DNA end resection and homology-directed repair. Cell Cycle [Internet]. 2013/01/05. 2013;12:422–9. Available from: https://www.ncbi.nlm.nih.gov/pubmed/23287531

266. Markenscoff-Papadimitriou E, Binyameen F, Whalen S, Price J, Lim K, Ypsilanti AR, et al. Autism risk gene POGZ promotes chromatin accessibility and expression of clustered synaptic genes. Cell Rep [Internet]. 2021 [cited 2022 Jan 5];37:110089. Available from: https://linkinghub.elsevier.com/retrieve/pii/S2211124721015801

267. Suliman-Lavie R, Title B, Cohen Y, Hamada N, Tal M, Tal N, et al. Pogz deficiency leads to transcription dysregulation and impaired cerebellar activity underlying autism-like behavior in mice. Nat Commun 2020 111 [Internet]. 2020 [cited 2022 Jan 5];11:1–15. Available from: https://www.nature.com/articles/s41467-020-19577-0

268. Zheng S, Liu Y, Sun H, Jia J, Wu T, Ding R, et al. Identification of abnormally high expression of POGZ as a new biomarker associated with a poor prognosis in osteosarcoma. Eur J Histochem [Internet]. 2021 [cited 2022 May 24];65:3264. Available from: /pmc/articles/PMC8431870/

269. Sun X, Cheng L, Sun Y. Autism-associated protein POGZ maintains embryonic stem cells by association with esBAF and HP1γ. bioRxiv [Internet]. 2021 [cited 2022 May 2];2021.02.07.430173. Available from: https://www.biorxiv.org/content/10.1101/2021.02.07.430173v2

270. Zhao W, Quan Y, Wu H, Han L, Bai T, Ma L, et al. POGZ de novo missense variants in neuropsychiatric disorders. Mol Genet Genomic Med [Internet]. 2019/07/28. 2019;7:e900. Available from: https://www.ncbi.nlm.nih.gov/pubmed/31347273

271. Hashimoto R, Nakazawa T, Tsurusaki Y, Yasuda Y, Nagayasu K, Matsumura K, et al. Whole-exome sequencing and neurite outgrowth analysis in autism spectrum disorder. J Hum Genet [Internet]. 2015/11/20. 2016;61:199–206. Available from: https://www.ncbi.nlm.nih.gov/pubmed/26582266

272. Shiwarski DJ, Shao C, Bill A, Kim J, Xiao D, Bertrand CA, et al. To “Grow” or “Go”: TMEM16A Expression as a Switch between Tumor Growth and Metastasis in SCCHN. Clin Cancer Res [Internet]. 2014 [cited 2022 Sep 17];20:4673. Available from: /pmc/articles/PMC4160843/

273. Xiao BD, Zhao YJ, Jia XY, Wu J, Wang YG, Huang F. Multifaceted p21 in carcinogenesis, stemness of tumor and tumor therapy. World J Stem Cells [Internet]. 2020 [cited 2022 May 24];12:481. Available from: /pmc/articles/PMC7360995/

274. Cheng X, Xia W, Yang JY, Hsu JL, Chou CK, Sun HL, et al. Activation of p21(CIP1/WAF1) in mammary epithelium accelerates mammary tumorigenesis and promotes lung metastasis. Biochem Biophys Res Commun [Internet]. 2010 [cited 2022 May 24];403:103–7. Available from: https://pubmed.ncbi.nlm.nih.gov/21040707/